Acoustic and Respiratory Pressure Control in Brass Instrument Performance

Vincent Fréour

Music Technology Area
Department of Music Research, Schulich School of Music
McGill University
Montreal, Quebec, Canada

December 2013

A thesis submitted to McGill University in partial fulfillment of the requirements for the degree of Doctor of Philosophy.

© 2013 Vincent Fréour

à Mélanie,

à mes parents et à ma soeur, Claire,

Abstract

This thesis presents experimental and numerical investigations on the control of aeroacoustic and quasi-static pressures within the air column constituted by the player-instrument system in trombone performance.

The core of this work tackles the nature of the interaction between a player's vibrating lips and his/her vocal tract. Firstly, a measurement method was developed in order to assess important characteristics of the acoustical coupling between the lips, the downstream resonator and the upstream airways. Subjects able to play over the full range demonstrated significant upstream influence in the higher register of the instrument. These players were categorized in two groups according to their ability to control the phase of the upstream impedance and their ability to generate powerful downstream acoustic energy.

In order to further investigate the influence of the vocal tract on the behaviour of the lips of a trombone player, different conditions of upstream coupling were simulated on an artificial player system. This experiment demonstrated the importance of phase tuning on the behaviour of the lips; results particularly suggest the ability of a vocal-tract resonance to displace the playing frequency close to a lip mechanical resonance, hence producing maximal efficiency of the lip-excitation system. Numerical simulations involving different physical models of the lips and various conditions of upstream coupling lend support to experimental results; an upstream coupling at the fundamental frequency influences the playing frequency and hence the combined effect of the varying total impedance loading the lips and lip mobility at the playing frequency. It then results in different degrees of efficiency of the sound production mechanism with respect to the acoustic energy produced.

Finally, a quantitative analysis of chest-wall dynamics was conducted on a trombone player. Different standard tasks where analyzed with respect to the pressure developed by rib-cage and abdominal muscles, diaphragmatic activity, as well as embouchure and glottal resistance. This study aims to address the characteristics of physiological control and its relation to the management of the quasi-static mouth pressure. It also intends to provide further material to the discussion on physiological factors involved in the acoustical control of the vocal-tract.

Résumé

Cette thèse présente une étude expérimentale et numérique sur le contrôle des pressions aéroacoustiques et quasi-statiques au sein de la colonne d'air formée par le musicien et son instrument dans le jeu du trombone.

L'axe principal de ce travail s'articule autour de l'étude de l'interaction entre les lèvres du musicien et son conduit vocal. En premier lieu, une méthode de mesure est développée dans le but de quantifier les caractéristiques de couplage acoustique entre les lèvres, le résonateur formé par l'instrument, et les voies respiratoires en amont. Chez les sujets pouvant jouer sur le registre complet de l'instrument, le conduit vocal contribue de façon significative à la production du son dans le registre aigu. Deux catégories de stratégies sont proposées en fonction des caractéristiques de phase de l'impédance du conduit vocal à la fréquence fondamentale, ainsi que de la capacité à générer un maximum d'énergie acoustique.

Afin d'étudier plus précisément l'influence du conduit vocal sur le comportement mécanique des lèvres d'un tromboniste, différentes conditions de couplage en amont sont simulées sur un système de bouche artificielle. Cette expérience permet de démontrer l'importance de l'ajustement de la phase de l'impédance en amont sur le comportement mécanique des lèvres. Les résultats obtenus mettent particulièrement en évidence les capacités d'une résonance de conduit vocal à déplacer la fréquence de jeu afin de potentiellement la rapprocher d'une fréquence de résonance mécanique des lèvres, produisant ainsi une efficacité maximale du système d'excitation. Des simulations numériques utilisant différents modèles physiques de lèvres et différentes conditions de couplage acoustique avec le conduit vocal confirment les hypothèses formulées; un couplage avec le conduit vocal à la fréquence fondamentale influence la fréquence de jeu. En conséquence, ces variations induisent des changements, d'une part de l'impédance acoustique chargeant les lèvres, et d'autre part de leur mobilité mécanique. Il en résulte différents degrés d'efficacité du mécanisme de production sonore en ce qui concerne l'énergie acoustique générée.

Pour terminer, une étude quantitative de la dynamique du thorax est conduite sur un tromboniste. Différentes tâche musicales sont analysées en termes de pression développée par les muscles intercostaux et abdominaux, de l'activité du diaphragme, ainsi que de la résistance des lèvres et de la glotte à l'écoulement pendant le jeu. Cette étude a ainsi pour but d'évaluer les caractéristiques physiologiques du contrôle de la production du son et leurs relations à la gestion de la pression quasi-statique dans la cavité buccale. Elle suggère également de nouveaux éléments quant à l'influence du contrôle respiratoire sur l'effet acoustique du conduit vocal.

Acknowledgments

I would firstly like to thank my supervisors Isabelle Cossette and Gary Scavone without whom this research would not have been possible. Thank you for allowing me to work on this fascinating project in this great research group, for your support, advice and encouragements. I am extremely thankful to the Schulich School of Music and CIRMMT for their financial support, as well as to Professors Philippe Depalle and Christophe Vergez for their work as internal and external examiners, and to Prof. Vincent Gracco for accepting to be part of my defense committee.

Part of this work was conducted in France and Italy. Therefore, I am greatly indebted to René Caussé, Thomas Hélie and Andrea Aliverti for allowing me to work at IRCAM and Politecnico di Milano on my PhD project. Special thanks to Nicolas Lopes, Barbara Uva, Thomas Hézard and Tommaso Bianco for their precious collaboration, as well as to Andrea for his advice, avaibility and to congratulate him on his new trombone skills. Many thanks also go to Prof. Marcelo Wanderley for his support and advice, and to Prof. Caroline Palmer for the collaborations.

I am most grateful to my colleagues, Antoine Lefebvre, Andrey da Silva, Charalampos Saitis, Shi Yong, Hossein Mansour, Bertrand Scherrer, François Germain, Pauline Eveno and Sylvain Le Beux for their friendship, enlightening discussions and crucial advice! Furthermore, this work would not have been possible without the support of McGill, CIRMMT and IRCAM staff. Sincere thanks to Darryl Cameron, Yves Méthot, Julien Boissinot, Harold Kilanski, Alain Terrier and Gérard Bertrand for their essential contribution.

Music is at the core of this work, hence I would like to sincerely acknowledge my musician friends for their talent, availability, and for motivating this research. Thank you to my friends and "test subjects" in France (Fabien, Richard, Fred, Hikmet, Jean Marc), to the Bone Ultimatum crew in Montreal and to Thierry Champs for accepting to try my weird sensors and play high F with a tube in the mouth! My sincerest appreciation goes to my French mentors, Phillippe Miegeville, Robert Astre and Guy Figlionlos for passing on their passion for music.

I would like to extend my gratitude to all my Music Tech' and CIRMMT fellows and friends for their good mood and for sharing this wonderful experience, those with whom the story began and those I was delighted to meet later. They are many and I am sure those I will forget will recognize themselves! Thanks to Boye, Vijay, Brian, Marlon, Yorgos, Mark, Vanessa, Fernando, Jaime, Erika, Alfonso, Sven, Nils, Sandra, Johannes, Bennett, Guillaume, Jason.

Thank you so much to my cousin Clotilde for her care, to my friends who have been around me during these years, Phillipe (Raz), Clémentine, Vincent V. and G., Yann, Stéphane, and to the Boude family, Olivia, Hélène and Patrick for their support and for making these five years in Montreal such an unforgettable experience.

This work and amazing experience would not have been the same without Mélanie. I am infinitely thankful for her love, her care and her patience. Thank you for having been by my side these past few years and for all the things you bring in my life every day.

Finally, a doctorate overseas is not an easy thing and I am extremely grateful to my family, my parents and my sister who supported me along the way. I am deeply thankful for their support, their attention and confidence, without which none of this would have been possible.

Contents

1 Introduction **1**

2 Brass Instrument Acoustics and Playing Respiratory Mechanics **7**

2.1 Brass instrument acoustics 8

2.1.1 The air column 8

2.1.2 The lip-reed excitation 10

2.1.3 Flow equation and condition of regeneration 18

2.1.4 Influence of an upstream resonator on the flow equation 21

2.1.5 The vocal-tract resonator 22

2.2 Brass instrument respiratory mechanics 24

2.2.1 Physiology and mechanisms of breathing 24

2.2.2 Static properties of the chest wall 25

2.2.3 Respiratory muscles 28

2.2.4 Respiratory pressure measurements 31

2.2.5 Respiratory volume measurements 32

2.2.6 Pressure developed by respiratory muscles 37

3 *In-vivo* Investigation on Vocal-Tract Influence in Trombone Players **39**

3.1 Theoretical approach 42

3.1.1 Upstream to downstream impedance ratio 42

3.1.2 Phase of upstream and downstream impedances 43

3.2 Experimental approach 45

3.2.1 P_d and P_u recordings 45

3.2.2 Electrical impedance measurement of the lips 46

3.2.3 Interpretation of the data 48

3.2.4 Player tests . . . 52
3.3 Results from experiments . . . 53
3.3.1 Arpeggios . . . 53
3.3.2 Influence of dynamics . . . 64
3.3.3 Pitch bending . . . 66
3.3.4 Tone transitions . . . 69
3.4 Summary . . . 72

4 *in-vitro* Simulation of Upstream Coupling on an Artificial Player System 75
4.1 Vocal-tract coupling in an artificial player system . . . 77
4.1.1 Presentation of the artificial player system . . . 77
4.1.2 Inherent acoustical influence of the mouth cavity . . . 79
4.1.3 Active control method . . . 81
4.1.4 Description of the experimental setup . . . 84
4.2 Investigation on the effects of the phase at f_0 . . . 86
4.2.1 Experimental protocol . . . 86
4.2.2 Constant acoustic upstream energy condition . . . 87
4.2.3 Constant P_u to P_d amplitude ratio condition . . . 92
4.2.4 Comparison between different upstream levels within the constant upstream energy condition . . . 96
4.2.5 Analysis of the results in light of the linear theory of oscillation . . . 98
4.2.6 Comparison between $\angle\hat{H}$ and $\angle H$ . . . 99
4.3 Summary . . . 104

5 Numerical Simulations of Vocal-Tract Influence on Physical Models of the Lips 107
5.1 Simple outward and inward striking models . . . 111
5.1.1 Mechanical equation . . . 111
5.1.2 Flow equation . . . 112
5.1.3 Downstream coupling . . . 113
5.1.4 Upstream coupling . . . 114
5.2 Time-domain simulations . . . 116
5.3 Results from simulation for the outward striking model . . . 117
5.3.1 Lip mobility . . . 118

5.3.2 Downstream and upstream input impedances 120
5.4 Results from simulation for the inward striking model 123
5.5 Two-dimensional lip model 126
5.5.1 Mechanical equation 127
5.5.2 Lip mobility calculation 129
5.5.3 Flow equations 132
5.5.4 Simulation results 132
5.6 Summary 137

6 Respiratory Control in Trombone Performance 141
6.1 Materials and methods 145
6.1.1 Opto-electronic measurement of chest-wall deformations: kinematics measurements 145
6.1.2 Respiratory pressure measurements 148
6.1.3 Radiated sound measurement 149
6.1.4 Flow measurement 149
6.1.5 Relaxation curves 150
6.1.6 Power and resistance 156
6.1.7 Data visualization 157
6.1.8 Protocol 157
6.2 Playing control parameters in stable pitch and loudness conditions 159
6.3 Chest-wall dynamics 163
6.3.1 Sustained tones 163
6.3.2 Varying loudness 166
6.3.3 Varying pitch 170
6.3.4 Chest-wall dynamics and playing control parameters 173
6.4 Discussion in light of previous studies 176
6.5 Summary 180

Conclusions and Future Work 183

A Respiratory Pressure-Volume and Time-Domain Curves During Musical Tasks 189

B Measurement of the Latency of the Electrolabiograph Signal Conditioner 195

References **197**

List of Figures

2.1 Different types of trumpet mouthpieces. 9
2.2 Amplitude and phase of the input impedance normalized to the characteristic impedance of a King 2B Silver Sonic tenor trombone and Kelly 6 1/2 AL mouthpiece with the slide in the closed position. 11
2.3 Mechanical response curves of artificial lips. 13
2.4 Mechanical response curves of human lips. 14
2.5 Two-dimensional model of the lips. 17
2.6 Spirometric tracings of static pulmonary volume subdivisions. 26
2.7 Static pressure-volume curves during relaxation in the sitting position. 27
2.8 Trans-nasal balloon-catheter systems. 31
2.9 Respiratory Inductive Plethysmograhy (RIP). 33
2.10 Principle of the Opto-Electronic Plethymosgraphy (OEP) method. 34
2.11 89-marker Opto-Electronic Plethysmography setup. 35
2.12 Pressure-volume curve during quiet breathing and exercise. 38

3.1 Kelly plastic mouthpiece 6 1/2 AL with two silver-plated electrodes mounted on the rim. 48
3.2 Lip mobility estimated for an F4. 51
3.3 Amplitude and phase of the input impedance of the King 2B Silver Sonic tenor trombone and Kelly 6 1/2 AL mouthpiece with the slide in the closed position. . . 53
3.4 Results for Subject A playing ascending and descending arpeggio series. 54
3.5 Results for Subject A, B, C and E playing ascending arpeggio series. 56
3.6 SPL ratio in dB of upstream to downstream pressure at f_0, downstream and upstream pressure magnitude at f_0 normalized to the quasi-static blowing mouth pressure as a function of arpeggio index for all subjects. 58

3.7 Estimated $\angle Z_d$, $\angle Z_u$ and $\angle Z$ as a function of arpeggio index for all subjects. 59
3.8 SPL ratio in dB of upstream to downstream pressure at f_0, downstream and upstream pressure magnitude at f_0 normalized to the quasi-static blowing mouth pressure, estimated $\angle Z_d$, $\angle Z_u$ and $\angle Z$ at f_0 as a function of arpeggio index for all subjects. 61
3.9 Evolution of the magnitude of the upstream input impedance during ascending arpeggios. 63
3.10 Vocal-tract tuning during sustained tones of varying dynamics. 65
3.11 Vocal-tract tuning during pitch bending. 67
3.12 Vocal-tract influence at tone transition between B♭4 and C5 for subjects B and C. 69
3.13 Vocal-tract influence at tone transition between D4 and F4 for subjects A and C. . 70
3.14 Vocal-tract influence at tone transition between F3 and B♭3 for subjects A and C. 71

4.1 IRCAM artificial player system. 78
4.2 Amplitude of the downstream input impedance and upstream input impedance in the default configuration. 80
4.3 Active control method. 82
4.4 Diagram description of the analyzer implemented in Max/MSP. 83
4.5 Diagram of the experimental setup. 85
4.6 Sustained A4♭ with linearly varying phase difference between P_u and P_d at f_0 and amplitude of P_u maintained constant. 88
4.7 Input impedance of the valve trombone. 89
4.8 Temporal evolution of Z_d, Z_u and Z in the constant upstream energy condition. . . 90
4.9 Z_d, Z_u and Z in the constant upstream energy condition. 91
4.10 Sustained A4♭ with linearly varying phase difference between P_u and P_d at f_0 and amplitude ratio of P_u to P_d maintained constant and equal to unity. 93
4.11 Temporal evolution of Z_d, Z_u and Z in the constant amplitude ratio condition . . . 94
4.12 Z_d, Z_u and Z in the constant amplitude ratio condition. 95
4.13 Constant acoustic upstream energy condition (upstream level: 59% of the maximum level). 96
4.14 Constant acoustic upstream energy condition (upstream level: 100% of the maximum level). 97

4.15 Variations of f_0, downstream acoustic energy, and p_0, during active control in three constant upstream energy condition. 97
4.16 $\angle Z_d$ (gray), $\angle \hat{H}$ (crosses), and $\angle H$ (diamonds) during 85 % constant acoustic upstream energy condition. 100
4.17 Normalized downstream acoustic volume flow U_d as as function of the playing frequency f_0 in the 85 % constant acoustic upstream energy condition. 100
4.18 Z_d, Z_u and Z without active control. 101
4.19 $\angle Z_d$, $\angle \hat{H}$, and $\angle H$ without active control. 102
4.20 $\angle Z_d$, $\angle \hat{H}$, and $\angle H$ during 59 % constant acoustic upstream energy condition. . . . 103

5.1 One-mass model of the lips. 111
5.2 Reflection function $r_c(t)$ of a 2B King tenor trombone. 114
5.3 Results from a 96000 sample simulation at 48 kHz for an outward striking lip model. 118
5.4 Calculated and simulated lip mobility for an outward striking model. 119
5.5 Z_d, Z_u and Z during simulations for an outward striking model. 120
5.6 Closer view at Fig. 5.5 between 352 Hz and 358 Hz. 122
5.7 Results from a 96000 sample simulation at 48 kHz for an inward striking lip model. 123
5.8 Calculated and simulated lip mobility for an inward striking model. 124
5.9 Z_d, Z_u and Z during simulations for an inward striking model. 125
5.10 Two-dimensional model of the lips. 127
5.11 Lip mobility for a two-dimensional lip model. 131
5.12 Results from a 96000 sample simulation at 48 kHz for a two-dimensional lip model. 133
5.13 Calculated and simulated lip mobility for a two-dimensional lip model. 134
5.14 Z_d, Z_u and Z during simulations for a two-dimensional lip model. 135
5.15 Phase difference between Z and $-G$ at the fundamental frequency f_0. 136
5.16 Influence of the upstream coupling on the two-dimensional lip motion. 138

6.1 Bouhuys experiment on a trombone player using a body plethysmograph. 143
6.2 Marker positions and chest-wall compartments for optical analysis in standing position. 145
6.3 Experimental setup for recording of the radiated sound. 146
6.4 Experimental setup. 147
6.5 Input impedance of a tenor trombone and modified instrument used for experiments. 148

6.6 Chest-wall volumes during quiet breathing and a relaxation maneuver. 151
6.7 Respiratory pressures during quiet breathing and a relaxation maneuver. 152
6.8 Rib-cage relaxation curve. 153
6.9 Abdominal relaxation curve. 153
6.10 Rib-cage and abdominal pressure-volume curves during a sustained B♭3 155
6.11 Time-domain data representation during a sustained B♭3 158
6.12 Averaged control parameters as function of the fundamental frequency. 160
6.13 Pressure-flow relationship during sustained tones with increasing and decreasing dynamic. 162
6.14 Pressure-volume loops during sustained B♭2, F3 and B♭3. 164
6.15 Time-domain parameters during sustained B♭2, F3 and B♭3. 165
6.16 Pressure-volume loops during sustained D4, F4 and B♭4 played with increasing and decreasing dynamics. 167
6.17 Time-domain parameters during sustained D4, F4 and B♭4 played with increasing and decreasing dynamics. 168
6.18 Pressure-volume loops during ascending and descending arpeggios. 171
6.19 Time-domain parameters during ascending and descending arpeggios. 172
6.20 Relationship between the mouth pressure P_m and the net expiratory pressure developed by respiratory muscles during sustained tones with varying dynamics. . . 174
6.21 Relationship between the mouth pressure P_m and the net expiratory pressure developed by respiratory muscles during ascending and descending arpeggios. . . . 175
6.22 Relationship between the mouth pressure f_0 and the net expiratory pressure developed by respiratory muscles during ascending and descending arpeggios. . . . 176

A.1 Pressure-volume loops during sustained D4, F4, B♭4 and D5. 190
A.2 Time-domain parameters during sustained D4, F4, B♭4 and D5. 191
A.3 Pressure-volume loops during sustained B♭2, F3 and B♭3 played with increasing and decreasing dynamics. 192
A.4 Time-domain parameters during sustained B♭2, F3 and B♭3 played with increasing and decreasing dynamics. 193

B.1 Circuit diagram for the measurement of the latency of the VoceVista signal conditioner. 195
B.2 Calibration measurements. 196

B.3 Phase difference between V_{out} and U_0 as function of the frequency of the driving tension. 196

Nomenclature

Acoustics

t	time
f	frequency
$\omega = 2\pi f$	angular frequency
m	mass
k	stiffness factor
ρ	air density
c	speed of sound in a free field
b	width of the lip channel
p	time-domain pressure
u	time-domain volume flow
v	time-domain air velocity
y	time-domain vertical lip position
s	time-domain cross sectional area
P	frequency-domain pressure
U	frequency-domain volume flow
S	frequency-domain cross sectional area
Y	frequency-domain vertical lip position

H	frequency response of the lips
Z	impedance
G	lip mobility
R	reflectance
r	reflection function
F	force
Q	quality factor
$\mu = \frac{m}{S}$	effective mass divided by effective surface
Φ	phase
ξ	lip extremity two-dimensional position
$\sigma = +1$ or -1	reed-type parameter
$\gamma = \frac{\lvert P(f_0)\rvert}{p_0}$	dimensionless efficiency parameter
ζ	electrical tension
e	error
K	PID coefficient
a	amplitude
ϵ	small phase offset
$\eta = \frac{f_s}{N}$	spectrum frequency resolution
$j = \sqrt{-1}$	imaginary number

Respiratory mechanics

t	time
f	frequency
ρ	air density
c	speed of sound

P	pressure
V	volume
R	resistance
P_w	sound power
Q	volume flow
ζ	electrical tension

Preface and Contribution of Authors

The document is formatted as a monograph dissertation and includes contents from the following publications.

Chapter 3:

Fréour, V., and Scavone, G.P. (2013). Acoustical interaction between vibrating lips, downstream air column, and upstream airways in trombone performance. *Journal of the Acoustical Society of America, 134*(5), 3887-3898.

Fréour, V., and Scavone, G.P. (2012). Investigation of the effect of upstream airways impedance on regeneration of lip oscillations in trombone performance. *In Proceedings of the Acoustics 2012 Nantes Conference, Nantes, France*, 2225-2230.

Fréour, V., and Scavone, G.P. (2011). Development of an electrolabiograph embedded in a trombone mouthpiece for the study of lip oscillation mechanisms in brass instrument performance. *Canadian Acoustics, 39*(2), 130-131.

Fréour, V., Scavone, G.P., Lefebvre, A., and Germain, F. (2011). Acoustical properties of the vocal tract in trombone performance. *In Proceedings of the 2011 Forum Acusticum Conference, Aalborg, Denmark*, 625-630.

Fréour, V., and Scavone, G.P. (2010). Vocal-tract influence in trombone performance. *In Proceedings of the 2010 International Symposium on Musical Acoustics, Sydney / Katoomba, Australia*.

Chapter 4:

Fréour, V., Lopes, N., Hélie, T., Caussé, R., and Scavone, G.P. (2013). Simulating different upstream coupling conditions on an artificial player system using an active sound control approach. *In Proceedings of the International Congress on Acoustics, Montreal, Canada*.

Chapter 5:

Fréour, V., and Scavone, G.P. (2013). Trombone sound simulation under varying upstream coupling conditions. *In Proceedings of the Stockholm Musical Acoustics Conference, Stockholm, Sweden*, 502-508.

Chapter 6:

Fréour, V., Caussé, R., and Cossette, I. (2010). Simultaneous measurements of pressure, flow and sound during trumpet playing. *In Proceedings of the 10ème Congrès Français d'Acoustique, Lyon, France*.

I was responsible for designing and carrying out all experiments, including the experimental design, data collection and analysis, as well as preparation of manuscripts of all the above listed publications. My co-advisors, Gary Scavone and Isabelle Cossette, provided necessary funding, laboratory equipment and space. Furthermore, they contributed guidance in the conception and interpretation of the conducted studies, as well as in the writing and editing of the thesis and articles. Nicolas Lopes provided support for the control of the artificial player system described in Chapter 4, as well as in the implementation of the PID controller. I developed and implemented the active control method on the mechanical player, including the phase detection algorithm, designed the experiments, and performed analysis of the collected data. Barbara Uva and Andrea Aliverti participated in the design and data collection for the experiments described in Chapter 6.

Chapter 1

Introduction

The mastery of the playing technique of an acoustic instrument (i.e. its control) is a difficult and lifelong pursuit. The quality and reproducibility of a musical performance depends on the level of the technique attained, and results from a learning and training process highly influenced by the pedagogic actors involved along the career of a musician. Unlike certain sport categories where technology has emerged as a fundamental tool for the analysis of body mechanics and optimization of the physical performance, music pedagogy is still mainly based on qualitative interpretations of the mechanisms underlying sound production. Furthermore, it is often cluttered by the weight of myths and doctrines whose foundations are sometimes far from any scientific evidence. Similarly to athletes, musicians are prone to physical injuries and brass players are not spared. In brass instruments, where the musician uses his/her lips to form an embouchure that acts as a vibrating reed, lip injuries are a frequent problem encountered by experienced and young musicians. Lucinda Lewis, principal horn of the New Jersey Symphony Orchestra comments on this issue as follows (Lewis, 2010):

> *Within the brass community, discussions about embouchure function tend to be, more often than not, steeped in stylistic dogma. It is, therefore, not surprising that*

> *ignorance has been the prevailing understanding about brass performance overuse injuries. Sadly, in some circles, these injuries are even dismissed as a weakness in the afflicted player rather than the bona fide byproduct of too much playing.*

Training this complex sound production process (from the control of respiratory muscles to the adjustment of the lip embouchure) with the view of a coherent and optimized "gesture" should hence be at the core of the concerns of any proficient player. Furthermore, the development of musical expression, underpinned by improvements and innovations in instrument making, have promoted the emergence of new soloist instruments like the trombone across musical genres. This evolution, together with musicians' sustained creativity, has stimulated the emergence of new sound aesthetics and playing techniques (fast playing, multiphonic technique, double sounds, "doodle" tonguing, etc.) which add to the already wide range of existing usages (brassy sounds, pitch bends, slurs, double and triple tonguing, etc.) commonly used in brass instruments. John Fordhman (the Guardian) depicts the playing of famous jazz trombonist Albert Mangelsdorff in these terms (Fordhman, 2005):

> *Albert Mangelsdorff, [...], allowed nothing to block his determination to expand this awkward instrument's eloquence [...]. His multiphonic approach - playing more than one note simultaneously, and humming or singing and playing at the same time - defied the limitations of the trombone's plumbing, and he also led some of the most distinctive bands in European jazz, applying a palette of startling sound effects and phrasing both to Europeanised mutations of American jazz practices and new developments.*

In the middle of this sound production chain, the vocal tract constitutes a central component whose acoustic and aerodynamic influences remain relatively unclear for some musicians, despite their potentially great importance. This thesis aims to provide a scientific characterization on

the control of acoustic and respiratory pressures in trombone performance, in order to better understand the nature of the interaction between a player and instrument in different playing tasks. Particularly, the goal of this thesis is to develop a method for the investigation of the acoustical influence of the vocal tract in trombone performance, and use scientific knowledge of brass instruments to measure, simulate and analyze the acoustical effect of the vocal tract on the vibrating lips. Lastly, we wish to provide some new quantitative elements regarding the action of respiratory muscles in the control of sound production in trombones, as well as the possible correlations between the acoustical control of the vocal tract and the breathing mechanics in brass performance.

A first objective of this research is to characterize the acoustical influence of the vocal tract in trombonists through the investigation of the input impedance of the upstream airways during playing. In wind instruments, the vocal tract can be considered as an auxiliary resonator placed in series with the downstream resonating system formed by the instrument air column (Benade & Hoekje, 1982; Benade, 1985). Because its geometry can be significantly varied (during speech production for instance), the "acoustical load" of the vocal tract perceived by the lips is subject to change and may produce different effects on the vibrating lips. Whether this influence can be significant or not, and whether this potential influence results from an intrinsic configuration or a strategical tuning from the player, are part of the questions we wish to answer.

Directly measuring the input impedance of the vocal tract in brass instruments can be challenging because of the potential high invasiveness of the experimental setup. For direct measurements, it requires generating and measuring an acoustical signal directly in the mouth cavity of the player under playing conditions. The related disturbance may significantly affect the player's control and abilities, making the results difficult to interpret. Alternatively, an indirect method can be used to infer vocal-tract influence and tuning strategies in brass performers. Although this method requires the ability to measure the acoustical pressure in the mouth, this approach

provides a less invasive setup and much higher temporal resolution, which makes it appropriate to investigate dynamic variations of vocal-tract support, as well as tricky tasks such as high register playing. Furthermore, contrary to woodwinds, the playing frequency in brass instruments is partly determined by the resonance frequencies of the labial reed, which must be close enough to a resonance of the air column. This "tuning" of the lips thus enables the player to select a resonance of the downstream bore that will determine the frequency of the radiated tone. Consequently, the question of vocal-tract influence may be quite complex because of the phase relationships imposed between the lip motion and the acoustic pressure generated across the lips, which constrains the ability of the system to oscillate. Therefore, one objective is to develop a method including non-invasive monitoring of lip motion on musicians in order to allow detailed investigations on the acoustical interactions with the upstream system.

As an alternative to musicians, researchers have developed artificial player systems allowing the behaviour of a real player to be reproduced in a controlled manner, while being able to extract a number of physical variables often not accessible during *in-vivo* measurements. Using this type of benchmark also reduces the number of unknown variables and allows the influence of an upstream coupling with lips to be examined in a more systematic way. After investigating vocal-tract influence in real players, we intend to simulate different conditions of upstream coupling on an artificial player system in order to inform the results obtained *in-vivo*. One step further in the minimization of unknown parameters, this approach can be extended to physical models of the lips through numerical simulations, including different characteristics of acoustical interactions with the upstream system. Consequently, the results obtained *in-vitro* and numerically are expected to contribute to a better understanding of the modalities of an efficient tuning of the vocal tract and provide further data for the analysis of the results obtained on human subjects.

While the vocal tract may have an influence on the control of acoustic pressures along the air column, it belongs to the respiratory system which provides the quasi-static mouth pressure

driving the vibrating lips. Investigating the modalities of the control of mouth pressure with respect to the mechanics of the chest wall will provide insights on the way this control parameter is generated by the respiratory system. It may also inform acoustical investigations with respect to the potential coupling between the management of breathing and of the acoustical control of the upstream airways.

In Chapter 2, the current state of scientific knowledge regarding the excitation mechanism and air columns of brass instruments is summarized. In a second section, fundamentals of respiratory mechanics are presented in the context of the analysis of breathing in wind instrument performers.

The question of vocal-tract influence in brass instruments first requires its potential influence to be evaluated on musicians. In Chapter 3, an experimental setup for the *in-vivo* characterization of vocal-tract influence in trombone players is presented. This approach required the development of a lip electrical impedance sensor embedded in a trombone mouthpiece and based on the principle of electroglottography. The proposed setup enables the amplitude ratio of vocal-tract and downstream air-column input impedance at the playing frequency to be recorded. Furthermore, it makes possible the evaluation of the phase of both downstream and upstream system input impedances at the fundamental frequency f_0. The influence of the upstream system is studied as a function of playing frequency (low vs. high register) and dynamic (soft vs. loud sound), and in particular playing tasks such as pitch bends and slurred transitions. Results from experiments on a pool of trombone players are discussed and some hypotheses formulated regarding plausible vocal-tract tuning strategies from the subjects.

In order to clarify the interaction between an upstream impedance and adjacent control parameters, it becomes necessary to work under stable and controlled experimental conditions, which is not possible with human subjects. In Chapter 4, an experimental protocol that simulates different conditions of vocal-tract coupling at f_0 on an automated artificial trombone player system is presented. An active sound control approach was adopted and applied to the adjustment

of the acoustic pressure in the mouth cavity. This experimental approach allows investigation of different upstream coupling configurations for the same lip-reed setting. Particular attention is paid to the influence of upstream "phase tuning" with respect to an optimal efficiency of the sound production system.

In Chapter 5, the hypotheses formulated from the *in-vitro* study are evaluated through numerical simulations involving different physical models of the lips and varying upstream coupling conditions. Results from simulations on simple outward and inward striking models, as well as on a two-dimensional lip model, are presented and analyzed with regard to maximization of the acoustic energy produced and optimization of the sound production process.

Finally, in Chapter 6, the dynamics of the chest wall are studied with respect to the regulation of internal pressures by respiratory muscles. The respiratory patterns of a trombone player are analyzed and potential correlations with the acoustical control of the vocal tract are discussed.

Chapter 2

Brass Instrument Acoustics and Playing Respiratory Mechanics

The control of sound production in brass instruments is a complex process which involves accurate respiratory and acoustical control of various playing parameters. In the last decades, growing research efforts have been devoted to the study of the mechanisms underlying the production and control of sound in musical instruments and singers. The fundamental energy at the basis of the sound production chain is provided by the respiratory system, particularly by the respiratory muscles that accurately control the pressure in the respiratory airways. Respiratory muscles, in conjunction with the elastic properties of the respiratory system, operate on the deformation of the different chest-wall subdivisions, which, in turn, regulate the pressure in the lungs. The pressure transmitted to the player's mouth cavity constitutes the driving source of energy converted into acoustic energy by the non-linear excitation mechanism.

In brass instruments, the excitation mechanism is formed by the lips of the player which behave as the mechanical valve. This non-linear mechanical system modulates the flow introduced at the input of the instrument and converts the static mouth pressure generated by the respiratory

system into an acoustic pressure wave. Due to its non-linear behaviour, the lip-valve oscillator generates a complex waveform containing frequency components harmonically related to the fundamental frequency of vibration. This wave travels back and forth from the input to the bell of the instrument, resulting in a feedback of acoustical energy at the input of the instrument. This regenerative effect from the downstream air column induces a strong acoustical coupling between the lips and the instrument bore. If particular amplitude and phase conditions are realized such that the feedback from the air column provides support to the lip oscillations, a condition referred to as auto-oscillations of the lips occurs.

Upstream from the lips, the player's vocal tract constitutes a second resonator likely to interact acoustically with the lips. Under certain hypotheses regarding the behaviour of the lip-valve system, the acoustic flow generated in the upstream direction has the same amplitude as the flow directed in the downstream direction. Depending on the shape of the vocal tract, significant acoustical feedback may arise from the upstream resonator. The question of its influence on the behaviour of the excitation mechanism is then open.

In this introductory chapter, we first present a review on the fundamental theories describing the acoustical behaviour of the instrument bore and vocal tract, as well as current knowledge on the mechanics and modeling of the lip-valve systems. In the second part, fundamental background on respiratory physiology and mechanics is presented in the context of the analysis of respiratory control in wind instrument performance.

2.1 Brass instrument acoustics

2.1.1 The air column

The air column of a brass instrument typically consists of three components: a cup shaped mouthpiece, a cylindrical or conical section waveguide, and a rapidly flaring bell termination.

The mouthpiece constitutes a “key element” at the interface between the instrument and musician. The physical contact between the lips and the mouthpiece occurs on the rim which delimits the contour of the input section of the cup. The cup constitutes a bowl-shaped volume which connects to a conical section called the backbore. The input of the conical section at the junction of the cup and backbore is referred to as the mouthpiece throat. Alongside with the development of manufacturing tools and a growing music instrument market, instrument makers and musicians have investigated and developed various types of mouthpieces, proposing different alternatives to metal for the material (wood, plastic), as well as new geometries for the rim, cup, throat, etc. This wide range of products is particularly illustrated by the growing assortment of trumpet mouthpieces. An example of a traditional Bach trumpet mouthpiece, as well as three examples of “new generation” mouthpieces are presented in Fig. 2.1.

Figure 2.1 Different types of trumpet mouthpieces. From left to right: Bach 1-1/2 C trumpet mouthpiece, Schilke Heavyweight series trumpet mouthpiece, asymmetric cup trumpet mouthpiece, Bob Reeves plastic rim trumpet mouthpiece.

Acoustically, the mouthpiece behaves as a Helmholtz resonator (Campbell, 2004). Connected to the instrument bore, the mouthpiece tends to strengthen the amplitude of some of the resonances around its center frequency, while decreasing the frequencies of the higher modes (Benade, 1976).

Brass instrument bores are formed by a tubing section, cylindrical in some instruments (trumpet, trombone) or conical in others (French horn), which behaves as a waveguide in which longitudinal acoustic waves propagate and standing waves can be established. It terminates in a flaring

bell section showing a dominant radiator effect; the bell acts as a high-pass filter and hence tends to amplify high frequency components.

A physical quantity relevant to the description of the acoustical behaviour of wind instruments in the frequency domain is the acoustic impedance $Z(\omega)$, where ω denotes the angular frequency ($\omega = 2\pi f$). At a given location in the instrument air column, it relates the acoustic pressure $P(\omega)$ to the acoustic volume flow $U(\omega)$ in the following way:

$$Z(\omega) = \frac{P(\omega)}{U(\omega)} \tag{2.1}$$

The acoustic impedance can be particularly measured at the input of the instrument by different methods (Macaluso & Dalmont, 2011; Lefebvre & Scavone, 2011). We then refer to the input impedance of the instrument bore or downstream input impedance Z_d. Figure 2.2 represents the amplitude and phase of the acoustic impedance measured at the input of a tenor trombone and mouthpiece with the slide in the closed position. In Fig. 2.2, Z_d is normalized by the characteristic wave impedance $Z_c = \rho c / s_{cup}$ of a cylindrical tube of section area s_{cup}, where s_{cup} is the section area of the mouthpiece entry, ρ is the average air density and c is the speed of sound.

Consequently, at a given frequency, the relationships in amplitude and phase between the acoustic flow injected into the downstream air column and the acoustic pressure produced at the input of the instrument and resulting from the interaction with the resonator, can be derived from the complex value of Z_d.

2.1.2 The lip-reed excitation

The excitation mechanism is a crucial determinant of sound quality in musical instruments. In woodwind instruments, the natural frequency of a cane or synthetic reed is usually much higher than the main resonances of the instrument. The playing frequency is then predominantly con-

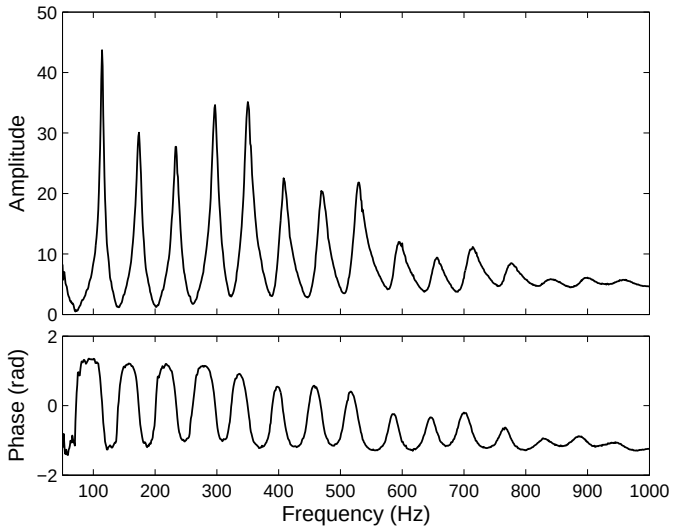

Figure 2.2 Amplitude and phase of the input impedance normalized to the characteristic impedance of a King 2B Silver Sonic tenor trombone and Kelly 6 1/2 AL mouthpiece with the slide in the closed position (the first resonance located below 80 Hz is not measured).

trolled by the natural frequencies of the air column. In brass instruments, the excitation mechanism is particularly complex since it consists of the lips of the player themselves, positioned against the mouthpiece. The resulting lip-valve system is often referred to as the "embouchure". Embouchure adjustments result from the synergy between lip shape, muscular tension of the facial muscles around the lips and the mechanical constraints arising from the physical contact with the mouthpiece. These parameters hence control the vibrating mass, stiffness and damping of the lip oscillator. Contrary to woodwind instruments where the resonant frequency of the reed is much higher than the bore resonances, the natural frequency of the lips lays within the range of the instrument resonances and has an important role in determining the playing frequency. Slight variations of the lip mechanical parameters may therefore significantly affect the mechanical behaviour of the lip-valve system and result in non-negligible changes in tone quality.

Different models have been proposed to represent the behaviour of brass players' lips. Ac-

cording to Helmholtz (1954), the reed excitation in wind instrument can be represented by two mechanisms: an "inward" striking model in which an increase in static upstream pressure results in closing the valve, and an "outward" striking mechanism in which an increase in upstream pressure results in opening the valve. Following this classification, single and double reed excitation mechanisms in woodwind instruments can be represented according to the inward striking model; a slow increase of the blowing pressure tends to close the valve opening. On the contrary, the lips of a brass player are more likely to behave according to an outward striking mechanism; increasing the static mouth pressure results in forcing the lips to move away from each other, increasing the lip-valve opening. This classification was later extended by Fletcher (1993) who proposed four different mechanisms according to the effect of the upstream and downstream static pressures on the reed. Reed mechanisms are represented by the (σ_1, σ_2) couple; σ_1 takes the value $+1$ if the upstream static pressure tends to open the valve and -1 if it tends to close it. Analogously, σ_2 takes the value $+1$ if an increase in downstream static pressure tends to open the valve, and -1 if it tends to close it. An inward striking valve is therefore represented by a (-1,+1) valve, while an outward striking valve is represented by the (+1,-1) type. The (+1,+1) valve therefore opens in reaction to both an increase in upstream and downstream pressure and is referred to as a sideway-striking valve or syrinx-type valve. The (-1,-1) valve does not appear to show practical applications according to Fletcher.

Although the mechanical behaviour of woodwind instrument reeds appears to be well represented by the inward striking reed type, the outward striking model partly fails to accurately represent lip-valve systems across the whole playing range (Yoshikawa, 1995; F. C. Chen & Weinreich, 1996). Visualization of lip motion (Copley & Strong, 1996; Yoshikawa & Muto, 2003; Bromage, 2007) as well as studies conducted on artificial player systems (Gilbert, Ponthus, & Petiot, 1998; Cullen, Gilbert, & Campbell, 2000; Newton, Campbell, & Gilbert, 2008) have shown that the lips of a brass player show both outward and inward (or upward) striking

characteristics.

The mechanical response of the lips $H(\omega)$ can be calculated as the ratio of the vertical lip displacement $Y(\omega)$ to a driving upstream acoustic signal $P_u(\omega)$:

$$H(\omega) = \frac{Y(\omega)}{P_u(\omega)} \tag{2.2}$$

Using an artificial player system, the mechanical response of the lips can be computed by acoustically driving the lips with a sine wave chirp generated by a loudspeaker coupled to the mouth cavity. Mechanical response curves of artificial lips using a transmission light method are shown in Fig. 2.3 for different embouchure settings (Newton et al., 2008). These curves highlight the presence of a pair of resonances showing an outward striking behaviour (-90° phase value) for the lower one, and an inward striking character (+90° phase value) for the highest resonance.

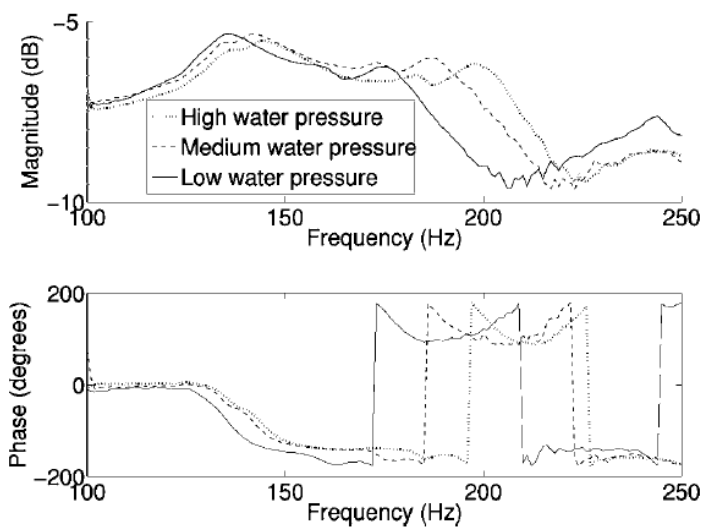

Figure 2.3 Mechanical response curves of artificial lips: obtained using a light transmission method (reprinted from (Newton et al., 2008)).

Using an adapted setup and high speed video capture of the lip opening area, mechanical

response measurements can be performed on a real player's lips (Newton et al., 2008). The results displayed in Fig. 2.4 show similar resonance pairs as observed in artificial lips with respect to the phase. The quality factor of real lips appear to be smaller than in artificial lips, which is most likely due to a higher internal damping of real lips as it was previously estimated (Yoshikawa & Muto, 2003).

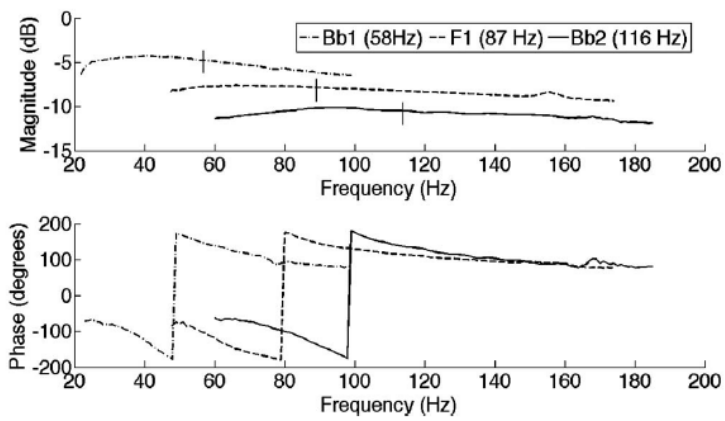

Figure 2.4 Mechanical response curves of human lips: obtained using a video method. The played frequencies for each tone are indicated by vertical lines (reprinted from (Newton et al., 2008)).

Locally, the mechanical response of the lips can be approximated by a parametric one-mass one-dimensional model allowing the lips to strike according to either an outward or inward mechanism. Assuming that the two lips are identical and placed symmetrically on the mouthpiece, a simple way to model the lip excitation mechanism is to consider that their movement is unidirectional and that their dynamic can be represented by a simple second-order oscillator. The transverse position of one lip $y(t)$ is therefore given by the following equation (Chaigne & Kergomard, 2008):

$$\frac{d^2y}{dt^2} + \frac{\omega_{lip}}{Q_{lip}}\frac{dy}{dt} + \omega_{lip}^2(y - y_0) = \frac{F}{m_{lip}}, \tag{2.3}$$

where ω_{lip} is the lip angular frequency ($\omega_{lip} = 2\pi f_{lip}$), Q_{lip} the lip quality factor, m_{lip} the mass of one lip and y_0 the vertical equilibrium position of the lip. F is the vertical component of the force acting on the lip and is therefore a function of the pressure difference between mouth and mouthpiece. The expression of F is determined by the geometry of the lip model. The effective area of the internal face of the lips s_u is loaded by the upstream mouth pressure p_m, the effective area of the external face of the lips s_d is loaded by the downstream mouthpiece pressure at the input of the instrument p_i. Finally, the effective area of the lip channel face (parallel to the flow direction) $s_{channel}$ is loaded by the pressure in the lip channel p_{ch}, F is then expressed as the sum of three force components:

$$F = F_u + F_d + F_l, \tag{2.4}$$

where:

$$\begin{cases} F_u = \sigma_1 \cdot s_u \cdot p_m \\ F_d = \sigma_2 \cdot s_d \cdot p_i \\ F_l = s_{channel} \cdot p_{ch}, \end{cases} \tag{2.5}$$

where σ_1 and σ_2 take the values +1 or -1 depending on the geometry of the model. Substituting Eq. 2.5 into Eq. 2.3, the following mechanical equation is derived:

$$\frac{d^2y}{dt^2} + \frac{\omega_{lip}}{Q_{lip}}\frac{dy}{dt} + \omega_{lip}^2(y - y_0) = \sigma_1\frac{p_m}{\mu_u} + \sigma_2\frac{p_i}{\mu_d} + \frac{p_{ch}}{\mu_l}, \tag{2.6}$$

where $\mu_u = m_{lip}/s_u$, $\mu_d = m_{lip}/s_d$, and $\mu_l = m_{lip}/s_{channel}$.

From Eq. 2.6, we observe that the oscillator may behave according to different valve categories depending on the parameterization of the model. For instance, if we assume $(\sigma_1, \sigma_2) = (+1, -1)$, $s_u = s_d$, and that the force component F_{ch} applied to the lip channel face negligible in

front of F_u and F_d, the model described by Eq. 2.6 will induce an outward striking behaviour. In this particular situation, Eq. 2.6 can be written in the Fourier domain as follows:

$$Y(\omega) = \frac{-\Delta P(\omega)/\mu}{(\omega_{lip}^2 - \omega^2) + j\frac{\omega_{lip}}{Q_{lip}}\omega}, \tag{2.7}$$

where $\Delta P(\omega)$ is the frequency-domain representation of the pressure difference across the valve ($\delta p = p_i - p_m$), and μ is positive and such as $\mu = \mu_u = \mu_d$.

From Eq. 2.7, the phase difference ϕ between the Y and ΔP at $\omega = \omega_{lip}$ is such that:

$$\phi = \angle Y(\omega_{lip}) - \angle \Delta P(\omega_{lip}) = \frac{\pi}{2}, \tag{2.8}$$

where $\angle X(\omega)$ designates phase of a quantity X at frequency ω.

For an inward striking reed, according to this model:

$$\phi = \angle Y(\omega_{lip}) - \angle \Delta P(\omega_{lip}) = -\frac{\pi}{2}. \tag{2.9}$$

Therefore, at the mechanical resonance, the valve motion is ahead of ΔP by 90° for an outward striking reed, whereas it lags behind ΔP by 90° for an inward striking valve mechanism. In practice, for a given geometry characterized by constant values σ_1 and σ_2, the outward or inward character of the lip model is determined by the relative values of μ_u, μ_d and μ_l.

A two-dimensional model that displays both an outward and inward striking character was proposed by Adachi and Sato (1996). In this representation (Fig. 2.5), the lips are allowed to move in both transverse and longitudinal directions, showing a movement closer to the motion of human lips. The combination of a swinging-door and sliding-door motion hence results in the ability of the reed to simulate the transition from a dominant outward striking to a dominant inward (or upward) striking behaviour with increase in playing frequency, as reported by Yoshikawa (1995).

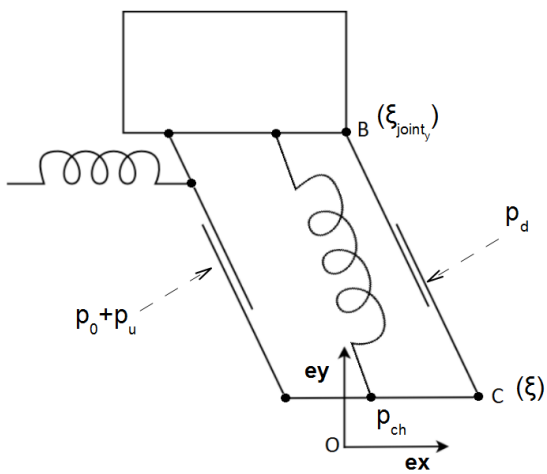

Figure 2.5 Two-dimensional model of the lips: $p_m = p_0 + p_u$ and the quasi-static component of p_i is neglected: $p_i = p_d$. p_{ch} designates the pressure in the lip channel.

Calling ξ the two-dimensional vector defined by the position of the lower tip of the lip (C), the mechanical equation governing ξ is given by the following expression:

$$\frac{d^2\xi}{dt^2} + \frac{\omega_{lip}}{Q_{lip}}\frac{d\xi}{dt} + \omega_{lip}^2\xi = \frac{s}{m_{lip}}(p_m - p_i) + \frac{s_{channel}}{m_{lip}}p_{ch}, \tag{2.10}$$

where s is the effective area of the internal and external face of the lips. In this model, s is time dependent as described by the geometry of the model in Fig. 2.5.

The lip movement hence regulates the input air flow injected into the instrument. In this latter model, a component of the volume flow u_{lip} induced by the longitudinal motion of the lip may be taken into account. This component is equivalent to the volume swept by the lips per unit of time and is given by the following equation:

$$u_{lip}(t) = b\left[\xi_x\frac{d\xi_y}{dt} - (\xi_y - OB)\frac{d\xi_x}{dt}\right], \tag{2.11}$$

where b is the width of the lip channel and OB designates the vertical position of point B

in Fig. 2.5.

2.1.3 Flow equation and condition of regeneration

The main component of the air flow entering the instrument is controlled by the vertical (or transverse) motion of the lips $y(t)$. The lip channel is assumed to have constant width b so that the time-varying lip opening area $s_{lip}(t)$ is estimated by the expression $s_{lip}(t) = 2b \cdot (y(t) + y_0)$. The volume flow through this channel is assumed to be quasi-stationary, frictionless and incompressible. Therefore, under the hypothesis that the jet cross section s_{ch} is much smaller than the mouth cross-section area, the air velocity in the mouth $v_m(t)$ can be neglected ($v_m(t)$=0) and the Bernoulli flow equation applied on the upstream side of the lips results in the following equation:

$$p_m(t) = p_{ch}(t) + \frac{1}{2}\rho v_{ch}(t)^2, \tag{2.12}$$

where $v_{ch}(t)$ is the time varying air velocity of the jet in the lip channel. We can then assume that the jet cross section s_{ch} is proportional to the time-varying lip opening area s_{lip} so that $s_{ch} = \alpha s_{lip}$ and $\alpha = 1$. Therefore, the volume flow at the entrance of the downstream resonator $u(t)$ is such as $u(t) = s_{lip}(t)v_{ch}(t)$, and Eq. 2.12 becomes:

$$p_m(t) = p_{ch}(t) + \frac{1}{2}\rho\left(\frac{u(t)}{s_{lip}}\right)^2. \tag{2.13}$$

It is assumed that the flow separates precisely at the exit of the lip channel to form a jet of velocity v_{ch} and pressure p_{ch}. The jet expands rapidly into a turbulent mix which dissipates the kinetic energy (Hirschberg, 1995). Therefore, no pressure recovery occurs in the mouthpiece and the pressure at the input of the instrument is considered equal to the pressure in the lip channel: $p_i(t) = p_{ch}(t)$. Eq. 2.12 then becomes:

$$u(t) = \mathrm{sgn}\Big(p_m(t) - p_i(t)\Big)\sqrt{\frac{2|p_m(t) - p_i(t)|}{\rho}} \cdot 2b \cdot \Big(y(t) + y_0\Big), \tag{2.14}$$

where $\mathrm{sgn}(x) = -1$ if x is negative and $\mathrm{sgn}(x) = +1$ if x otherwise.

By definition, p_m and p_i can be decomposed into their quasi-static and acoustic components:

$$p_m(t) = p_0 + p_u(t), \tag{2.15}$$

where p_0 is the quasi-static blowing pressure and p_u is the acoustic pressure resulting from the acoustical interaction with the upstream airway.

Similarly,

$$p_i(t) = \overline{p_i} + p_d(t), \tag{2.16}$$

where $\overline{p_i}$ is the static pressure component in the mouthpiece and p_d is the acoustic pressure resulting from the acoustical interaction with the downstream air column.

If no significant interaction with the upstream system is considered, it is assumed that the upstream acoustic pressure p_u is negligible in front of p_d. Furthermore, the quasi-static pressure component in the mouthpiece $\overline{p}_i$ can be neglected compared to p_0. Following these assumptions, Eq. 2.14 can be simplified to:

$$u(t) = \mathrm{sgn}\Big(p_0 - p_d(t)\Big)\sqrt{\frac{2|p_0 - p_d(t)|}{\rho}} \cdot 2b \cdot \Big(y(t) + y_0\Big). \tag{2.17}$$

Assuming $p_0 \gg p_d$ and p_0 positive, Eq. 2.17 can be further linearized to the following equation:

$$u(t) = \sqrt{\frac{2p_0}{\rho}} \cdot 2b \cdot \Big(y(t) + y_0\Big). \tag{2.18}$$

Considering only the oscillating component of Eq. 2.18 along with 2.1, the following Helmholtz condition of regeneration can be derived in the frequency domain (Elliot & Bowsher, 1982):

$$\frac{1}{Z_d(\omega)} = \sqrt{\frac{2p_0}{\rho}} \cdot 2b \cdot G_d(\omega), \tag{2.19}$$

where $Z_d(\omega) = P_d(\omega)/U(\omega)$ is the input impedance of the downstream air column, and $G_d(\omega) = Y(\omega)/P_d(\omega)$ is the downstream lip mobility.

Eq. 2.18 then infers that:

$$\angle Z_d + \angle G_d = 0. \tag{2.20}$$

In the case of an outward striking valve, the phase condition of regeneration (Eq. 2.20), along with the positive character of $\angle G_d$ for this reed type according to Eq. 2.8, suggests that the reed is able to operate for negative values of $\angle Z$, that is on the right side of the corresponding input impedance peak, and above the resonance frequency of the reed. On the contrary, an inward striking reed will oscillate on the left side of the corresponding input impedance resonance at frequencies below the natural frequency of the reed.

Expanding the square root of Eq. 2.17 up to the first two terms of the Taylor expansion leads to the following expression:

$$u(t) = C\left(y_0 + y(t) - \frac{y_0 p_d(t)}{2p_0} - \frac{y(t)p_d(t)}{2p_0}\right), \tag{2.21}$$

where $C = 2b\sqrt{2p_0/\rho}$, and the introduced non-linear term $\frac{y(t)p_d(t)}{2p_0}$ takes into account the acoustical interaction with the downstream air column.

Taking into considerations the harmonic expansion of $p_d(t)$ (Benade & Gans, 1968), along with the non-linear flow equation (Eq. 2.21), an adjusted condition of regeneration is proposed

by Elliot and Bowsher (1982). At the fundamental frequency, this condition is written as follows in the Fourier domain at f_0:

$$\left(CG_d(f_0) - \frac{1}{Z_d(f_0)} - \frac{1}{2R_0}\right) > 0, \tag{2.22}$$

where $R_0 = p_0/U_0$ is the real number characterizing the DC flow resistance and $G_d(f_0)$ and $Z_d(f_0)$ are the complex lip mobility and input impedance of the downstream air column at the fundamental frequency f_0. This condition is hence similar to the Helmholtz condition of regeneration in terms of phase relationship. However, according to this formulation, the amplitude of $CG_d(f_0)$ may have to be raised to overcome the effect of the $1/2R_0$ term, by increasing the blowing pressure for example.

2.1.4 Influence of an upstream resonator on the flow equation

Although Eq. 2.17 provides a reasonable estimation of the volume flow entering the instrument, some refinements can be carried out by revising certain hypotheses. By considering acoustical interactions with the upstream airway and assuming that the jet cross-section area is no longer much smaller than the mouth cross section, the jet velocity entering the mouth v_m is no longer neglected, which leads to the following Bernoulli equation:

$$p_m(t) + \frac{1}{2}\rho v_m(t)^2 = p_{ch}(t) + \frac{1}{2}\rho v_{ch}(t)^2. \tag{2.23}$$

Assuming conservation of the volume flow ($u_m(t) = S_m v_m(t) = u(t) = s_{lip}(t)v_{ch}(t)$), and total dissipation of the kinetic energy of the jet in the mouthpiece ($p_i(t) = p_{ch}(t)$), Eq. 2.23 becomes:

$$p_m(t) - p_i(t) = \frac{1}{2}\rho u(t)^2 \left(\frac{1}{s_{lip}(t)^2} - \frac{1}{S_m^2}\right) \tag{2.24}$$

This formulation has been used to simulate the effect of an upstream resonator in clarinets (Guillemain, 2007).

2.1.5 The vocal-tract resonator

The vocal-tract is a duct extending from the lips to the larynx and about 20 cm long. It is formed by the series combination of the laryngeal cavity, the pharynx and the oral cavity, in parallel with the nasal cavity which communicates with the nasopharynx through the choanae. The nasal cavity may be isolated from the rest of the vocal tract by the soft palate, which happens during swallowing and wind instrument playing. Acoustically, the vocal tract filters the sound arising from the vibration of the vocal folds. The nature of the filtering effect depends on the vocal-tract shape particularly modulated by the tongue. The acoustical influence of the vocal tract has thus been the object of substantial interest in singing voice (Sundberg, 1974, 1975; Joliveau, Smith, & Wolfe, 2004; Garnier, Henrich, Smith, & Wolfe, 2010; Henrich, Smith, & Wolfe, 2011).

Upstream from the lips, the player's vocal tract constitutes an auxiliary resonator whose acoustic properties may participate to the acoustical interactions with the lip-valve system. Analogously to the downstream air column, the resonating character of the vocal tract can be described in terms of its acoustic input impedance Z_u at the mouth:

$$Z_u(\omega) = \frac{P_u(\omega)}{U_u(\omega)}, \tag{2.25}$$

where U_u is the frequency domain representation of the acoustic flow $u_u(t)$ entering the upstream airway.

Assuming continuity of the volume flow at the reed junction (i.e. at the lips) (Benade & Hoekje, 1982), the upstream and downstream volume flows are related as follows:

$$U_u = -U, \tag{2.26}$$

that is the volume flow entering the vocal tract is of the same magnitude and out of phase by 180° with the flow component entering the instrument bore.

This leads to the following expression:

$$\frac{Z_u}{Z_d} = -\frac{P_u}{P_d}. \tag{2.27}$$

From the relation $\Delta P = P_d - P_u$, the total impedance Z loading the lips can be derived:

$$Z = \frac{\Delta P}{U} = \frac{P_d}{U} - \frac{P_u}{U}, \tag{2.28}$$

therefore,

$$Z = Z_d + Z_u. \tag{2.29}$$

In sum, the total impedance seen by the lips results from the series combination of the downstream air column and vocal tract. Note that by taking into account the flow component $u_{lip}(t)$ arising from the longitudinal motion of the lips, the reed acoustic impedance $Z_r = \frac{\Delta P}{U_{lip}}$ can be considered in parallel with the total impedance Z (Elliot & Bowsher, 1982; Fletcher, 1993; Scavone, 2003):

$$Z = \frac{Z_r(Z_d + Z_u)}{Z_r + Z_d + Z_u}. \tag{2.30}$$

However, if Z_r tends to be very large, it can thus be avoided in the parallel combination given by Eq. 2.30 (Benade, 1985; Benade & Hoekje, 1982; Hoekje, 1986).

2.2 Brass instrument respiratory mechanics

In this section, we present the fundamentals of respiratory mechanics and measurement methods relevant to the description of breathing in wind instrument performance. In the following section, as well as in Chapter 6, the choice was made to keep the notations of physical variables in agreement with usual conventions found in the respiratory mechanics literature. Some of them may differ from the notations adopted in Chapters 3, 4 and 5. Among the different processes involved in respiration, the air movement into and out of the lungs will be the primary object of interest in this section.

2.2.1 Physiology and mechanisms of breathing

The respiratory system consists of two main subdivisions: the pulmonary apparatus and the chest wall. The pulmonary apparatus is formed by the lungs and the pulmonary airways including the vocal tract. The lungs are formed by small elastic tissue bags (alveoli), surrounded by the pleura, a two-layered serous membrane structure which transmits pressure variations between the solid and flexible structures. The pulmonary airways, flexible channels streaming air to and from the lungs, encompass the mouth and nose cavities, the pharynx and larynx, the trachea, the bronchi and the bronchioles which subdivide before ending in clusters of alveoli. The chest wall encases the pulmonary apparatus and includes the rib-cage wall (formed by the ribs and cartilages, the sternum, the spine and the clavicle), the diaphragm, the abdominal wall and the abdominal content.

Pulmonary ventilation occurs when air travels from high to low pressure regions. These pressure variations in the pulmonary airways result from passive and active forces applied to the different components of the respiratory system. Passive forces operating on the respiratory system are due to the gravity and the elastic properties of the tissues and structures. Their effect is

further developed in Section 2.2.2. Active forces arise from the contraction of respiratory muscles whose actions are detailed in Section 2.2.3.

Commonly, the chest wall can be considered as a three-compartment system (Agostini & Mead, 1964; Ward, Ward, & Macklem, 1992). The chest wall then consists of the pulmonary or upper rib-cage compartment (mainly reflecting the action of neck and parasternal muscles and the effect of pleural pressure), the abdominal or lower rib-cage compartment (mainly reflecting the action of diaphragm and the effect of pleural and abdominal pressure), and the abdomen compartment (mainly reflecting the action of diaphragm and abdominal muscles). Volume variations of these three subdivisions lead to variations of the volume of the lungs (pulmonary volume) presented in Fig. 2.6. When the lungs are completely filled with air, the volume reached is Total Lung Capacity (TLC). After a full expiration, one reaches Residual Volume (RV). Tidal Volume (TV) refers to the amplitude of quiet breathing cycles, while Vital Capacity (VC) is the difference between TLC and RV and refers to the maximum volume variation available. Consequently, pressures and passive forces vary as a function of the pulmonary volumes of an individual.

2.2.2 Static properties of the chest wall

When respiratory muscles are relaxed under static conditions (relaxation state), the pressure produced by the respiratory system is a function of elastic, surface, and gravitational forces that operate in the lung and the chest wall. The pressure developed by the respiratory system P_{rs} is hence obtained from the difference between alveolar pressure P_{alv} and the body surface pressure considered equal to atmospheric pressure ($P_{rs} = P_{alv} - P_{atm}$). In static conditions, P_{alv} is given by the pressure at the airway opening and can be measured at the mouth or at the nostrils when the other openings are closed. By measuring the mouth pressure P_m during relaxation against obstruction, it is then possible to represent the static pressure-volume relationship of the chest wall at different lung volumes. This curve is represented in Fig. 2.7 where lung volume is indicated as

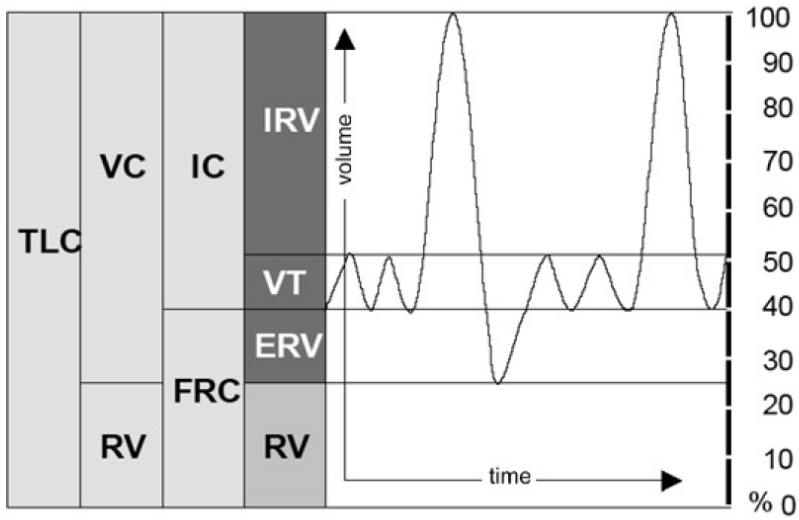

Figure 2.6 Spirometric tracings of static pulmonary volume subdivisions. Total Lung Capacity (TLC), Vital Capacity (VC), Residual Volume (RV), Inspiratory Capacity (IC), Functional Residual Capacity (FRC), Inspiratory Reserve Volume (IRV), Tidal Volume (TV / VT), Expiratory Reserve Volume (ERV) (reprinted from (Aliverti, 1996)).

a percentage of vital capacity (VC) (see Fig. 2.6).

The chest wall and the lungs are placed in series which indicates that the sum of the pressure generated by the two parts equals the respiratory system pressure ($P_{rs} = P_{cw} + P_l$). Given that $P_{rs} = P_{alv}$, it leads to:

$$P_{alv} = P_{cw} + P_l + P_{mus}, \tag{2.31}$$

where P_{mus} accounts for the pressure developed by the recruitment of respiratory muscles.

Furthermore, the pressure exerted by the lungs can be expressed as the difference between the alveolar and pleural pressure P_{pl}:

$$P_l = P_{alv} - P_{pl}, \tag{2.32}$$

and with Eq. 2.31 leads to:

$$P_{pl} = P_{cw} + P_{mus}. \tag{2.33}$$

From Eq. 2.33, P_{mus} may be made equal to zero by relaxing respiratory muscles with closed airways, leading to $P_{cw} = P_{pl}$ during relaxation. Moreover, P_{alv} may be made equal to zero by holding a given lung volume with open airways, leading from Eq. 2.32 to $P_l = -P_{pl}$. Accordingly, the volume-pressure curves of the lung and chest wall can be derived and represented along with the complete respiratory system curve, as shown in Fig. 2.7. In this figure, the applied forces on the chest wall and lungs are illustrated by the side representations at four different volumes (horizontal dashed lines).

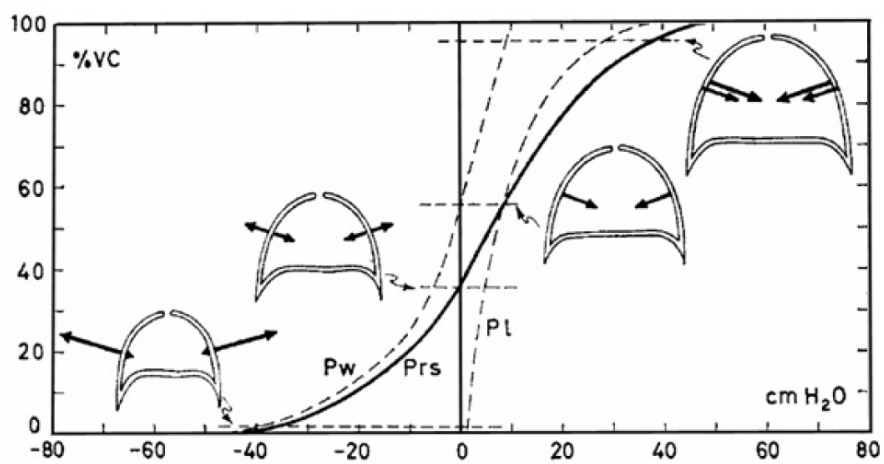

Figure 2.7 Static pressure-volume curves during relaxation in the sitting position: of the lung (P_l), chest wall P_{cw} (here noted P_w) and respiratory system (P_{rs}). The arrows indicate the static forces exerted by the lung and the chest wall at different volumes (horizontal dashed lines) (reprinted from (Agostini & Mead, 1964)).

At the resting volume of the respiratory system (P_{rs}=0), P_{cw} and P_l are equal and opposite: the chest wall recoils outwards and the lungs recoil inward hence operating like two opposing springs. This resting position corresponds to Functional Residual Capacity (FRC). P_l is always positive indicating that the resting volume of the lungs is below 0 % of VC. On the contrary, the

resting volume of the chest wall is around 55 % of VC where ($P_{cw} = 0$). This indicates that above this volume, both the chest wall and lungs recoil inwards.

2.2.3 Respiratory muscles

As stated in Section 2.2.1, respiration is the outcome of the synergistic action of passive and active forces. Active forces arise from the contraction of respiratory muscles which deform the structure of the respiratory system, hence varying the volume of cavities. According to muscle contractility properties and to the resulting effect of contraction on the volume of the lungs, respiratory muscles are classified as either inspiratory or expiratory muscles. Inspiratory muscles produce a force that creates an inward displacement of the air in the respiratory airways, while expiratory muscles generate a force at the origin of an outward displacement of the air. During quiet breathing, for example, inspiration is active (inspiratory muscle contraction) while expiration back to FRC is passive (due to the elastic recoil of the lungs and chest wall). Any movement of the body, as respiration, occurs because of the complex coordination of multiple muscle groups. These muscles work together, or against each other, according to four different functions: agonist, antagonist, synergist and fixator. The following paragraphs summarize the functional anatomy and action of the main respiratory muscles involved in respiration (De Troyer, 1991).

The diaphragm is the only skeletal muscle whose fibers radiate from a central tendon and insert peripherally into solid structures. It consists of an elliptical cylindroid capped by a dome made of tendon and muscles which attach to the bottom of the sternum, to the lower ribs and to the spine. The dome of the diaphragm corresponds primarily to the central tendon, while the cylindrical portion corresponds to the part directly apposed to the inner face of the lower rib cage. When the diaphragm contracts through the phrenic nerves, a caudally oriented (directed towards the floor) force is applied on the central tendon, such that the dome of the diaphragm descends.

This induces two main effects: 1) an expansion of the thoracic cavity along the vertical direction (craniocaudal axis) resulting in a decrease in pleural pressure, and 2) a caudal displacement of the abdominal content (visceral mass) resulting in an increase in abdominal pressure and in outward motion of the ventral abdominal wall. Furthermore, since diaphragm fibers also insert onto the upper margins of the lower six ribs, the cranial orientation of the fibers apposed to the rib cage produces a force oriented cranially during contraction. It hence results in lifting the ribs and rotating them outward. Consequently, the main action of the diaphragm is inspiratory; by increasing thoracic volume and decreasing pleural pressure during contraction, it contributes to inflate the lungs if respiratory airways are open.

Intercostal rib-cage muscles are two thin planes of muscular fibers occupying each of the intercostal spaces. They are categorized into external and internal intercostal muscles because of their surface relationship, the external being superficial to the internal. Due to differences in orientation, contraction of external and internal intercostal muscles produce different net effects on the ribs: external intercostals net effect is to raise the ribs into which the muscles insert, while internal intercostals contraction results in lowering the ribs to which these muscles are attached. Hence, it is commonly admitted that external intercostal muscles produce an inspiratory action whereas internal intercostal muscles operate as expiratory muscles.

Abdominal muscles are the four muscles which constitute the ventrolateral wall of the abdomen. The rectus abdominis is the most ventral of this muscle group and runs caudally from the sternum and lower costal cartilages to the pubis. The external oblique is the most superficial abdominal muscle while the internal oblique lies deeper than the external oblique. The transversus abdominis is the deepest of the muscles of the lateral abdominal wall. These muscles present important functions in flexion and rotation of the trunk and have two main respiratory actions. Firstly, when contracting, they pull the abdominal wall inward and increase the abdominal pressure. This results in displacing the diaphragm cranially (to the top) when it is relaxed, which in

turn, decreases the lung volume and increases pleural pressure. Secondly, these muscles have an effect on the rib cage by potentially pulling the lower ribs caudally (to the bottom) because of their attachment. Overall, abdominal muscles hence behave primarily as expiratory muscles. However, the action of these muscles on the diaphragm enables them to play an important role in inspiration as well: the abdominal pressure transmitted to the lower rib cage because of the zone of apposition of the diaphragm tends to expand this compartment. Furthermore, when forced cranially by an increase in abdominal pressure, the diaphragm is stretched and tends to raise the lower ribs, quite similarly to an active diaphragmatic contraction.

Neck muscles include sternocleidomastoidian and scalene muscles. Sternocleidomastoidian muscles descend from the mastoid process (behind the ear) to the top of the sternum and the medial third of the clavicle. In healthy subjects, they are primarily recruited when ventilation increases substantially or when the inspiratory muscle pump is abnormally loaded (i.e. during wind instrument playing or exercise). The scalenes consist of three bundles running from the lower five cervical vertebrae to the upper surface of the first two ribs. Contrary to sternocleidomastoidian muscles, scalenes are primary muscles for inspiration as their contraction has a determinant effect on the expansion of the rib cage during breathing. Indeed, their action counterbalances the contraction of the diaphragm by preventing the rib cage to collapse. In healthy humans, they are invariably active during inspiration and have a mandatory action during quiet breathing in seated position. In music related studies, the action of neck muscles has particularly been studied in flute playing and singing (Cossette, Sliwinski, & Macklem, 2000; Pettersen & Westgaard, 2004, 2005; Cossette, Monaco, Aliverti, & Macklem, 2008; Cossette, Fabre, Fréour, Montgermont, & Monaco, 2010).

2.2.4 Respiratory pressure measurements

In a mechanical apparatus such as the respiratory system, where motion is translated into volume, forces are expressed in terms of pressures. In combination with volume and flow, pressures are commonly used to derive the mechanical properties of the respiratory system (Section 2.2.2) and the action of respiratory muscles.

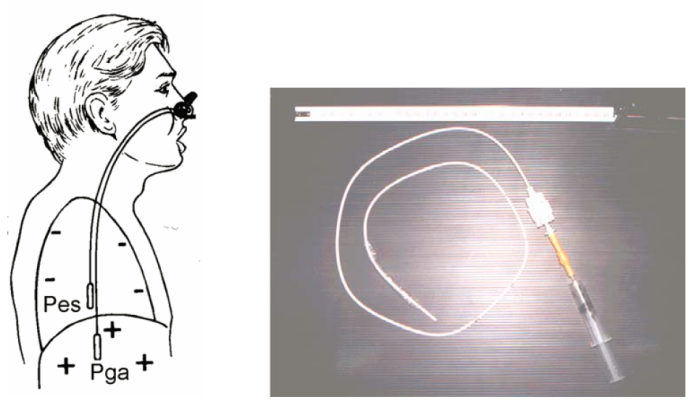

Figure 2.8 Trans-nasal balloon-catheter systems: used for measurement of esophageal and gastric pressures (reprinted from (Aliverti, 1996)).

In the context of brass instrument performance where a significant resistance opposes the output flow, we are interested in four pressure measurements: the mouth pressure P_m driving lip oscillations, the pleural pressure P_{pl} estimated by means of the esophageal pressure P_{es}, the abdominal pressure P_{ab} (pressure within the abdominal cavity) measured by the gastric pressure P_{ga}, and the transdiaphragmatic pressure P_{di} measured as the difference between P_{ga} and P_{es} ($P_{di} = P_{ga} - P_{es}$). Although P_m can be easily monitored by holding in the mouth the extremity of a catheter connected to a pressure transducer, esophageal and gastric pressure measurements require a more invasive methods, making use of trans-nasal balloon-catheter systems swallowed through the nasal cavity and connected to pressure transducers (Milic-Emili, Mead, Turner, & Glauser, 1964) as shown in Fig. 2.8.

In the case of trombone performance, we can consider in a first approximation that the pressure at airway opening equals the atmospheric pressure (no pressure recovery in the mouthpiece of the instrument as discussed in Section 2.1.3) and second, that pressure is homogeneously distributed along the respiratory airways during playing. However, it is possible to investigate the validity of this second hypothesis by observing the value of the transglottal pressure ($P_{gl} = P_{es} - P_m$) during performance. In steady expiratory state, we may consider that this value provides information regarding the degree of abduction of the vocal folds (or glottal resistance), which is likely to occur in wind instrument playing (Mukai, 1992).

2.2.5 Respiratory volume measurements

As described in Section 2.2.2, the lungs and chest wall are placed in series (McCool, 1995). Volume variations of the lungs therefore equal the variation of volume of the chest wall and of the respiratory system:

$$\Delta V_{cw} = \Delta V_l = \Delta V_{rs}. \tag{2.34}$$

Different non-invasive methods have been developed in order to assess ΔV_l from measurement of chest-wall deformations (Wade, 1954; Konno & Mead, 1967; Grimby, Bunn, & Mead, 1968; Zimmerman et al., 1983). Elastic belts and embedded strain gages allow for measurement of the stress induced by chest-wall deformations from which variations of rib-cage and abdomen circumferences can be monitored. Magnetometer sensors positioned on the rib cage and abdomen enable evaluation of the anterio-posterior and lateral dimensions of each compartment. Finally, respiratory inductive plethysmography (RIP) consists in loops of wire, coiled and sewed into elastic belts, and positioned around the rib cage and abdomen. The amplitude of the magnetic flux across the loops is measured and allows the cross-sectional areas of the two compartments

to be monitored (Fig. 2.9). In a first approximation, the variations of chest-wall volumes can

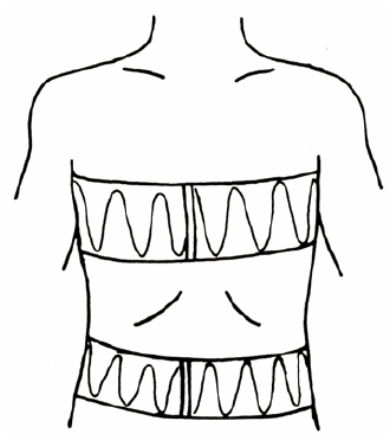

Figure 2.9 Respiratory Inductive Plethysmograhy (RIP). Positioning of the wired elastic belts (reprinted from (Aliverti, 1996)).

be derived from the linear combination of the two belt signals, weighted by coefficients α and β determined empirically:

$$\Delta V_{cw} = \alpha\zeta_{rc} + \beta\zeta_{ab}, \tag{2.35}$$

where ζ_{rc} and ζ_{ab} denote the output voltage from the rib-cage and abdomen belts respectively.

Although these techniques present a non-invasive character while allowing subjects a relative flexibility in movement and postures, they are sensitive to various sources of error, intrinsic to the sensing technique (displacement of the belt, skin contact artifacts). Secondly, they rely on a theoretical representation of the chest wall (commonly two compartment models) requiring calibration of the relative contribution of each compartment. Moreover, despite good agreement with spirometric measurements for stabilized postures and low amplitude breathing patterns, the underlying two degree of freedom model of the chest wall (Eq. 2.35) presents a delimited domain of validity, particularly with respect to chest-wall distortion induced by posture and pressure-

loaded breathing. The addition of a third degree of freedom was shown to significantly improve the measurement of ventilation in variable postural conditions. For instance, a third variable relevant to the thoraco-abdominal dimension (distance between xiphoid and pubic symphysis monitored using magnometers), and weighted by a constant coefficient, can be added to right side of Eq. 2.35 (Smith & Mead, 1986; McCool, Kelly, Loring, Greaves, & Mead, 1986). Alternatively, the dynamic adjustment of α and β in Eq. 2.35 as a function of spinal shape has been proposed (Zimmerman et al., 1983; Peak, Kelly, & McCool, 1990).

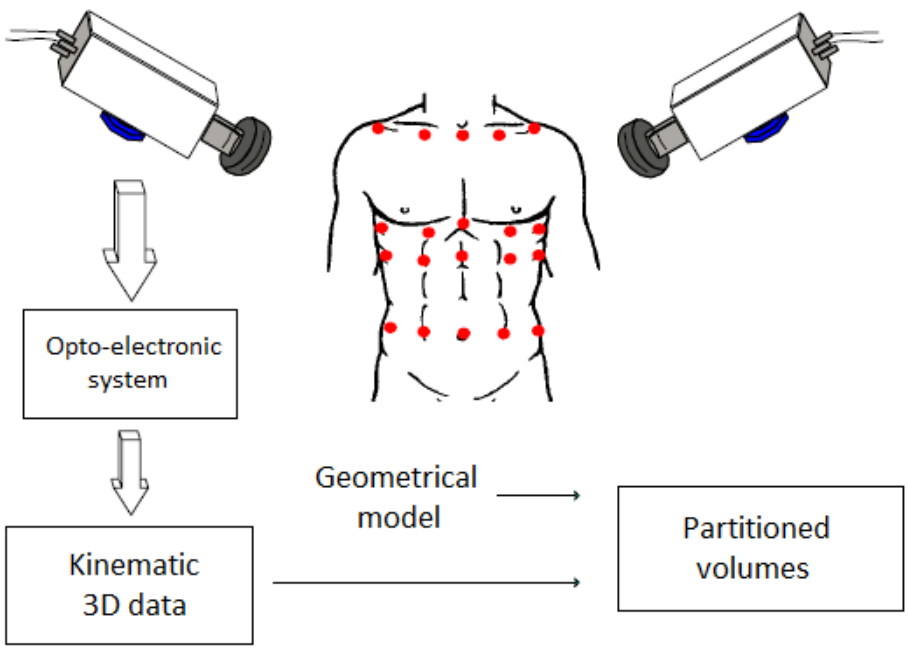

Figure 2.10 Principle of the Opto-Electronic Plethymosgraphy (OEP) method (reprinted from (Aliverti, 1996)).

Recent development of optical methods allows chest-wall volumes to be evaluated in various situations (exercise, supine, music playing) while reducing the influence of errors induced by distortion of the chest wall. The first opto-electronic plethysmograph was proposed by Ferrigno et al. (1994). This method consists in monitoring the 3D-position of reflexive markers placed on anatomical locations on the chest wall, using an opto-electronic motion-capture system. Through

a predefined geometrical model of the chest wall, this allows a 3D mesh to be computed and the volume of individual subdivisions of the chest wall to be quantified. This approach is represented in Fig. 2.10.

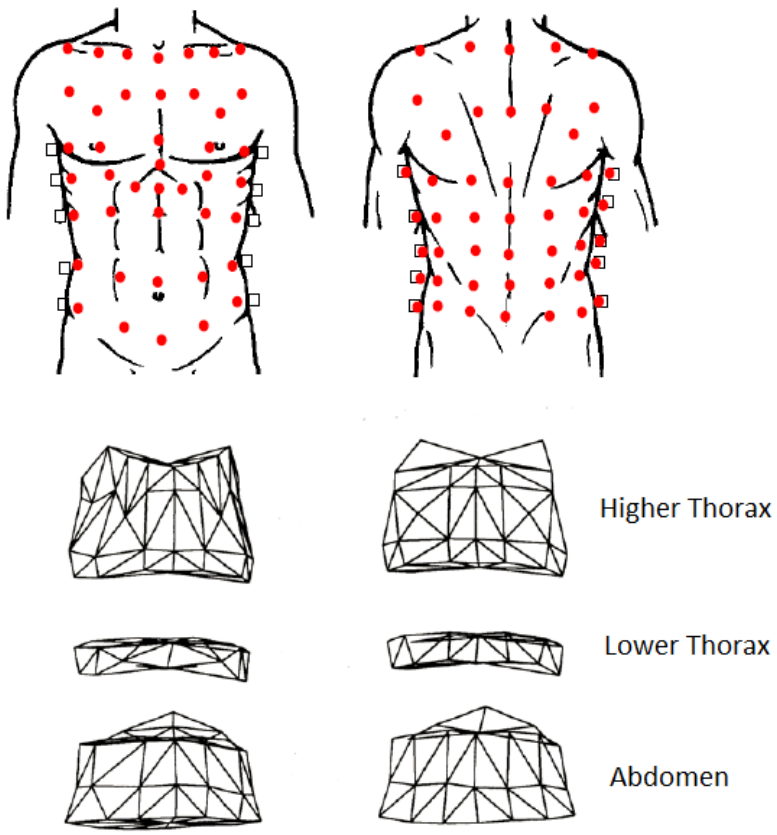

Figure 2.11 89-marker Opto-Electronic Plethysmography setup. Placement of the 89 markers on the chest-wall surface, triangularization of the thoraco-abdominal surface and definition of three compartments corresponding to the pulmonary rib cage, abdominal rib cage and abdominal compartments. (reprinted from (Aliverti, 1996))

In Ferrigno's setup, measurements are based on a mesh subdividing the chest wall into three compartments (upper thorax, lower thorax, and abdomen) by using thirty two passive markers located at specific anatomic landmarks. This mesh consists of a four by four anterior grid and its posterior symmetric. Markers are located at the levels of the second rib, the xiphoid process,

the tenth rib, and the abdominal transversal line. Each compartment is also subdivided into its left and right subpart. By performing triangularization between markers, this mesh results in fifty four tetrahedrons for which individual volume variations are calculated by simple geometrical algebra.

Although this method offers good results in terms of repeatability and consistency with spirometric control measurements, higher accuracy is obtained when calibration is performed for each subject. This suggests a body-specific relationship between OEP measurements and lung volume (obesity is one factor that requires specific calibration for example). Furthermore, the number of un-covered areas may also account for discrepancies observed with spirometric measurements (the abdominal part under the transabdominal line is not covered by markers).

A development of Ferrigno's method was proposed by Cala et al. (1996). Unlike Ferrigno's setup, the thoracic part cranial to the second rib, the abdominal part caudal to the umbilicus, as well as the axillary region are covered by reflective markers. A similar triangularization procedure is applied to the mesh, hence producing a dense 3D grid representing the surface of three chest-wall compartments (Fig. 2.11).

Chest-wall volumes are then calculated from the application of "the Gauss theorem" to the variations of chest-wall surface (Eq. 2.36):

$$\int_V \nabla \vec{F} \, \mathrm{d}V = \int_S \vec{F} \cdot \vec{n} \, \mathrm{d}S. \tag{2.36}$$

where $\vec{F}$ is an arbitrary vector of the 3D space, $\vec{n}$ is a vector normal to the surface S, ∇ is the divergent operator ($\nabla \vec{F} = \frac{\partial \vec{F}}{\partial x} + \frac{\partial \vec{F}}{\partial y} + \frac{\partial \vec{F}}{\partial z}$).

The chest-wall volume is then represented as the sum of the volume of the three chest-wall compartments:

$$V_{cw} = V_{rc,p} + V_{rc,a} + V_{ab}, \tag{2.37}$$

where $V_{rc,p}$ is the volume of the pulmonary rib-cage compartment, $V_{rc,a}$ is the volume of the abdominal rib-cage compartment and V_{ab} is the volume of the abdominal compartment.

Despite its sensitivity to gas compression and blood shifts (Aliverti et al., 2009), this method provides a very low coefficient of variation (smaller than 5 %) compared to spirometric control measurements (Cala et al., 1996), without any need for case-specific calibration.

2.2.6 Pressure developed by respiratory muscles

From the characterization of the relaxation state of the chest wall, as well as the measurement of pressure and volume variations during exercise, the action of respiratory muscles for each of the chest-wall compartments can be quantified. Indeed, in the pressure-volume plane, the net pressure developed by respiratory muscles can be deduced from the horizontal distance between the dynamic pressure-volume loop and relaxation line at a given volume.

This approach was first used by Konno and Mead (1968) in the (P_{ab}, V_{ab}) plane for the assessment of the pressure developed by abdominal muscles. The pressure developed by inspiratory and expiratory rib-cage muscles can be estimated using the same principle in the $(P_{pl}, V_{rc,p})$ plane, where the horizontal distance between the dynamic pressure-volume loop and relaxation curve is corrected by the pressure resulting from the distortion of the pulmonary and abdominal rib-cage compartments away from their relaxation configuration (Kenyon et al., 1997). An illustration of the extraction of the pressure developed by the two groups of muscles during exercise is shown in Fig. 2.12.

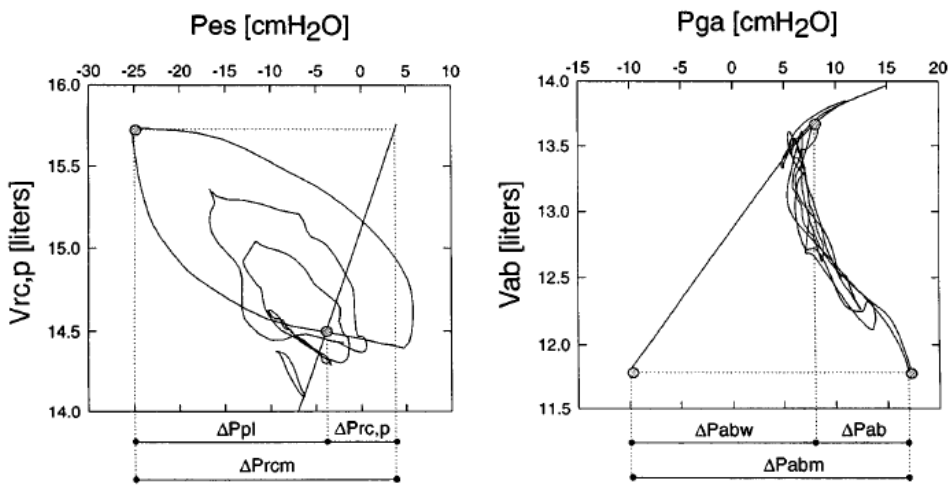

Figure 2.12 Pressure-volume curve during quiet breathing and exercise: *Left*: relationship between esophageal pressure (P_{es}) as an index of pleural pressure (P_{pl}) and volume of the pulmonary rib cage ($V_{rc,p}$) during quiet breathing and exercise at 0, 30, 50 and 70 % of maximum workload. Solid straight line, relaxation pressure-volume curve of the pulmonary rib cage, which gives elastic recoil pressure of pulmonary rib cage ($\Delta P_{rc,p}$) at any volume $V_{rc,p}$. Measurement of pressure generated by rib-cage muscles (ΔP_{rcm}) at any $V_{rc,p}$ is obtained from the horizontal distance between dynamic loop and relaxation line corrected for any restoring force resulting from rib-cage distortion. Points at left of relaxation line are inspiratory; those at right are expiratory. *Right*: relationship between gastric pressure (P_{ga}), used as an index of abdominal pressure (P_{ab}), and volume of abdomen (V_{ab}) during quiet breathing and at various levels of exercise. Solid straight line, relaxation pressure-volume curve of abdomen, which gives its elastic recoil pressure (ΔP_{abw}) at any V_{ab} below functional residual capacity (FRC). Measurement of pressure generated by abdominal muscles (ΔP_{abm}) at any V_{ab} during exercise is obtained from horizontal distance between dynamic loop and relaxation line at that volume. (reprinted from (Aliverti et al., 1997))

Chapter 3

In-vivo Investigation on Vocal-Tract Influence in Trombone Players

In-vivo measurements on musicians are often constrained by the degree of invasiveness of the measurement system. Investigating the acoustical influence of the vocal-tract in wind instrument performance such as woodwinds requires the ability to either measure directly the input impedance of the upstream airway (Fritz & Wolfe, 2005; J. M. Chen, 2009), or estimate the value of Z_u relative to the downstream input impedance at frequencies where acoustic energy is produced (Scavone, Lefebvre, & da Silva, 2008; Guillemain, Vergez, Ferrand, & Farcy, 2010). In both situations, the operation involves measurements of physical quantities in the mouth of the player and/or at the interface with the instrument. In brass instruments, measurements are made even more difficult as the lips constitute the reed themselves and may be very sensitive to any intrusive device possibly disturbing the embouchure. Moreover, invasive measurements in the mouth cavity may interfere with tongue placement or other vocal-tract adjustments, and affect the acoustical properties of the player's vocal-tract during measurements.

The goal of the research presented in this chapter is to develop a measurement method min-

imizing the invasiveness of instrumentation in order to provide experimental results on the influence of the vocal-tract in trombone performance. One particular aim is to characterize how proficient players strategically tune their vocal-tract during specific playing tasks.

A significant number of studies have focused on the influence of vocal-tract resonances in woodwind instruments. Overall, investigations agree on the ability of proficient players to precisely tune vocal-tract resonances in the range of 500–1500 Hz. These adjustments particularly occur when the downstream impedance becomes weak enough so that a vocal-tract resonance may support or even override the effect of the downstream air column. This was particularly observed in saxophones and clarinets during altissimo playing and for special effects such as pitch bending (Fritz & Wolfe, 2005; Scavone et al., 2008; J. M. Chen, Smith, & Wolfe, 2009; Guillemain et al., 2010; J. M. Chen, Smith, & Wolfe, 2011).

Regarding lip-reed instruments, experiments on the didjeridu (Tarnopolsky et al., 2006) showed anti-resonances in the radiated sound induced by vocal-tract resonances. Wolfe et al. investigated the influence of upstream resonances in the didjeridu and trombone performance using an artificial lip reed player (Wolfe, Tarnopolsky, Fletcher, Hollenberg, & Smith, 2003). This system enabled the characteristics of an upstream resonance to be varied (low or high tongue position) while maintaining a fixed reed setting. On both instruments, vocal-tract configuration had an effect on intonation as well as on transitions between two registers; an upstream constriction near the valve was able to increase a little the playing frequency as well as facilitate transition to a higher bore resonance. These results were corroborated by more recent characterizations of the effect of vocal-tract resonances in trumpets (Kaburagi, Yamada, Fukui, & Minamiya, 2011). Different upstream conditions were characterized from MRI imaging of a trumpet player's vocal-tract and tested through numerical simulations (Adachi & Sato, 1996). Vocal-tract configuration especially appeared to influence the minimum blowing pressure, as well as the natural lip frequency at which transitions between registers are observed. Although these studies appear to

confirm a non-negligible influence of the vocal-tract in brass playing, they partly involved analog or numerical simulations of a brass player system and are limited to simple musical tasks, especially in terms of register. Chen et al. performed direct measurements of vocal-tract resonances on trumpet players (J. M. Chen, Smith, & Wolfe, 2012). Although this method allows for direct measurement of vocal-tract input impedance at the lips during performance, results did not show consistent tuning strategies from the players. One objective of the proposed study is therefore to adapt and develop the measurement technique proposed in previous studies (Scavone et al., 2008; Guillemain et al., 2010) for *in-vivo* evaluation of vocal-tract influence in trombones allowing for investigation of a variety of playing tasks.

An important characteristic of brass playing relies on the degree of control from the player on the natural frequency of the lips (see Chapter 2). In woodwind instruments (such as saxophone or clarinet), the reed can be satisfactorily modeled by an inward striking valve (Helmholtz, 1954; Fletcher, 1993). This representation implies that the reed is able to operate over a wide frequency range below its natural frequency. In brass instruments, lip-valves have been shown to be generally better represented by outward striking reed models (Helmholtz, 1954; Fletcher, 1993; F. C. Chen & Weinreich, 1996; Copley & Strong, 1996; Yoshikawa, 1995; Gilbert et al., 1998). Lip valves are able to oscillate only within a narrow frequency range around their natural frequency. This particularly highlights the fact that brass players must be able to adjust the mechanical properties of the lips and hence tune their natural lip frequency in order to excite the air column at a given frequency. This further suggests that vocal-tract tuning in brass performance may be particularly dependent on the nature of the lip-reed mechanism at the given playing frequency (Fletcher, 1993). Therefore, it could be of great interest to consider both amplitude and phase of downstream and upstream system impedances at the frequency of interest. A second objective of this study is thus to adapt the principle of electroglottography (Fabre, 1957) to the monitoring of lip transverse electrical impedance on trombone players in order to enable estima-

tion of the phase of the downstream and upstream impedance at the playing frequency and provide further information on the modalities of the interaction between the downstream air-column, the lips, and the player's upstream airways.

The first section of this chapter presents the theoretical background of the method and restates some basic material introduced in Chapter 2. The second section describes the experimental approach and measurement techniques, including lip electrical impedance measurements. Next, the main section of this chapter presents the results from experiments on a pool of trombone players during different playing tasks, including slurred arpeggios, sustained tones with varying dynamics and pitch bending. Finally, a summary section reiterates the various findings and contributions to the field presented in this chapter.

3.1 Theoretical approach

3.1.1 Upstream to downstream impedance ratio

The assumption of continuity of the volume flow at the lips allows to write Eq. 2.27 repeated here for convenience:

$$\frac{Z_u}{Z_d} = -\frac{P_u}{P_d} \tag{3.1}$$

where u and d subscripts denote upstream and downstream variables. P_d therefore corresponds to the downstream acoustic pressure created in the mouthpiece, and P_u to the upstream acoustic pressure created at the input of the vocal-tract (i.e. in the mouth cavity just upstream from the lips). U_d and $U_u = -U_d$ are the acoustic flows created on the downstream and upstream sides of the lips, and $Z_d = P_d/U_d$ and $Z_u = P_u/U_u$ the input impedance of the downstream air-column and

the player's upstream airway, respectively.

3.1.2 Phase of upstream and downstream impedances

Denoting S_{lip} the frequency-domain alternating lip opening area, the downstream lip mobility G_d is defined as follows:

$$G_d = \frac{S_{lip}}{P_d}. \tag{3.2}$$

G_d is the response of the lip motion to the downstream pressure created in the mouthpiece of the instrument. This expression ignores P_u, the pressure at the input of the vocal-tract, and thus any influence of the upstream airway. Analogously, the upstream lip mobility G_u and the adjusted downstream lip mobility G can be defined as:

$$G_u = \frac{S_{lip}}{P_u} \tag{3.3}$$

$$G = \frac{S_{lip}}{P_d - P_u}. \tag{3.4}$$

G_u is the response of the lip motion to the upstream pressure P_u, ignoring the influence of the acoustic pressure created in the mouthpiece P_d, and G is the response of S_{lip} to the pressure difference across the lips $P_d - P_u$ and therefore takes into account both downstream and upstream interactions.

Under the assumption that the quasi-static mouth pressure p_0 is usually much greater than $p_u(t)$ and $p_d(t)$, the flow equation defined by Eq. 2.14 can be linearized to Eq. 2.18 repeated here for convenience:

$$u_d(t) \simeq \sqrt{\frac{2p_0}{\rho}} \cdot s_{lip}(t). \tag{3.5}$$

This leads to the downstream phase condition of regeneration (PCoR) given by Eq. 2.20 and repeated below:

$$\angle G_d(f_0) + \angle Z_d(f_0) = 0. \tag{3.6}$$

Analogously, two other phase conditions of regeneration can be defined from Eqs. 3.3, 3.4 and 3.5:

$$\angle G_u(f_0) + \angle Z_u(f_0) = \pi, \tag{3.7}$$

$$\angle G(f_0) + \angle Z(f_0) = 0. \tag{3.8}$$

We refer to Eq. 3.7 as the upstream PCoR, and to Eq. 3.8 as the adjusted downstream PCoR, where $Z = Z_d + Z_u$ is the total impedance perceived by the lips.

In sum, Eqs. 3.6, 3.7 and 3.8 give the conditions under which auto-oscillations exist when coupled to both downstream and upstream systems: Eq. 3.6 alone amounts to neglecting acoustical interaction with the upstream airway, Eq. 3.7 alone amounts to neglecting the acoustical coupling with the downstream air column, and finally Eq. 3.8 amounts to considering both upstream and downstream interactions. Under the hypothesis that regeneration occurs on both sides of the lips, Eqs. 3.6, 3.7 and 3.8 show that $\angle G_d$, $\angle G_u - \pi$ and $\angle G$ can therefore be considered as estimates respectively of $\angle Z_d$, $\angle Z_u$ and $\angle Z$ at the fundamental frequency of the sound f_0.

In the low register, our results should be interpreted with care since the complex contact between the lips, as well as lip outward motion may induce a non-negligible non-linearity in the flow equation. However, this should not be the case when the pitch increases and the upward motion of the lips reduces the flow component arising from the lip longitudinal displacement (Copley & Strong, 1996; Adachi & Sato, 1996; Yoshikawa & Muto, 2003). Regarding the effect of collision, as supported by experimental and numerical investigations on vocal-fold vibration (Sidlof, 2007; Mongeau, Franchek, Coker, & Kubli, 1997), we may reasonably consider that given basic similarities in the behaviour of both valve systems, the lip collision during closure does not significantly affect the linear relationship between the volume flow and opening area. During closure, we hypothesize that no volume flow occurs and only residual turbulence is present (Sidlof, 2007). This assumption is supported by the observation of short closed phases in vibrating lips (Bromage, Campbell, & Gilbert, 2010; Hézard, Fréour, Hélie, Caussé, & Scavone, 2013), as well as potential simpler contact during the closed phase as shown by lip electrical impedance measurements (Hézard, Fréour, Hélie, et al., 2013). Furthermore, as supported by Backus and Hunley (1971), as well as Elliot and Bowsher (1982), the small lip opening area in the high register increases the flow resistance of the lip orifice, the latter becoming potentially larger than the downstream impedance in the very high register. Consequently, the volume flow at the lips turns out to be proportional to the lip opening for high playing frequencies.

3.2 Experimental approach

3.2.1 P_d and P_u recordings

A miniature Endevco© pressure transducer (8510-B) was inserted in the cup of the mouthpiece in order to record the downstream acoustic pressure p_d (i.e. at the input of the downstream air-column). A second Endevco© transducer (8507-C) was used to measure the acoustic pressure

at the input of the vocal-tract p_u: the transducer was inserted in a small catheter and the subject asked to maintain the extremity of the catheter in the mouth, above the tongue, as close as possible to the internal wall of the teeth. We can then roughly estimate the distance between the catheter extremity and the lips at around 5 mm, which would cause a group delay of 14 μs, corresponding to a phase shift of about 3.6 degrees at 700 Hz (the maximum sounding frequency). The small diameter of the transducer and catheter (about 2.5 mm) reduced the obstructiveness caused by the transducer. A relative calibration of the downstream and upstream microphones mounted in the catheter was performed over the frequency range of interest. As both transducers measure acoustic and quasi-static pressures, the low frequency (DC) component of the mouth pressure p_0 was extracted by low-pass filtering the upstream transducer signal.

3.2.2 Electrical impedance measurement of the lips

As described in the previous section, our method relies on the evaluation of the phase of the lip opening relative to the phase of the acoustic pressure measured on both sides of the lips. Similar measurements of lip motion were performed on French horn players using a strain gauge attached to the player's upper lip (Yoshikawa, 1995), though this solution was quite invasive for the participant. Moreover, this technique requires a careful calibration in order to correlate the strain gauge signal with the opening and closing phases of the lip motion. Consequently, we propose an alternative approach by measuring the variations of electrical impedance across the lips during playing. This technique is based on the principle of electroglottography developed by Fabre (1957) and extensively applied to the monitoring of vocal-fold vibrations; a high frequency alternate current $i(t)$ is generated between two electrodes located across the larynx and variations of vocal-fold contact area during phonation cause amplitude variations of the alternating tension $\zeta(t)$ recorded at the electrodes. After demodulation of $\zeta(t)$, and according to Ohm's law ($\zeta = Z_{el} \cdot i$), the resulting signal is hence proportional to the varying amplitude of the electri-

cal impedance across the electrodes $Z_{el}(t)$. A somewhat related approach was previously applied on the lips of a didjeridu player by Wolfe and Smith (2008) in order to simultaneously record vocal-fold and lip apertures in didjeridu performance.

In our setup, two electrodes made of silver-plated copper shielding tape were glued on a Kelly plastic mouthpiece of dimensions equivalent to a Vincent Bach 6 1/2 AL (Fig. 3.1). The two electrodes were connected to a commercial electroglottogaph signal conditioner (Voce Vista© [1]) and the resistance of the electrode pair raised in order to fit with the signal conditioner requirements. The resulting tension recorded at the output of the conditioner is therefore proportional to the electrical impedance across the lips Z_{lip}. As in the case of phonation, the oscillations of Z_{lip} are due to periodic variations of the contact area between the lips. Thus, we can reasonably assume that Z_{lip} and S_{lip} oscillate in phase at f_0; when the lips open, the contact area between the lips decreases and Z_{lip} increases; on the contrary when the lips close, Z_{lip} decreases since the contact between the lips becomes larger. Depending on the electroglottograph conditioners used, the output may be presented under the form of a conductance C_{lip} which corresponds to the *open-closed* convention for the representation of the signal. In this case C_{lip} and S_{lip} will simply oscillate out of phase by 180°. Given the purpose of our sensing device, we propose to call it an "electrolabiograph" (ELG). As far as we know, this term was first proposed by Krakow in 1994 for the study of articulatory lip motions in syllables (Krakow, 1994).

In order to measure the latency of the system (delay between actual variations of lip impedance and the output tension from the conditioner), a controllable variable resistance was mounted at the electrodes using a photo FET optocoupler. This calibration procedure enabled estimation of a group delay of 180 μs (see Appendix B). Considering a sampling rate of 44.1 kHz, this latency results in a shift of 8 samples which is not negligible in the context of phase analysis and is therefore taken into account in the analysis.

[1] http://www.eggsforsingers.eu/technology.html

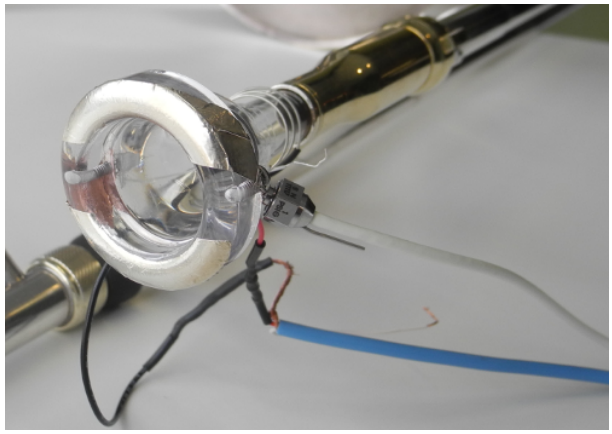

Figure 3.1 Kelly plastic mouthpiece 6 1/2 AL with two silver-plated electrodes mounted on the rim. The downstream microphone is mounted to record the acoustic pressure in the mouthpiece cup.

The electrolabiograph signal, as well as P_d and P_u were recorded using a National Instruments© I/O interface (sampling rate 44.1 kHz). After correction of the latency of the electrolabiograph signal conditioner, $\angle G_d(f_0)$, $\angle G_u(f_0) - \pi$ and $\angle G(f_0)$ are computed by extracting the phase at the f_0 spectral peak from consecutive Fast Fourier Transforms (FFT) of 1024 samples with an overlap of 256 or 512 samples depending on the playing task. Windowing (Hanning window) and zero-padding (by 24000 samples) is performed prior to Fourier transforming in order to increase the frequency sampling of computed spectra and refine the phase estimation at f_0. For each frame, the fundamental frequency is detected through the maximum of the fundamental peak using parabolic interpolation.

3.2.3 Interpretation of the data

Figure 3.2 shows measured values of p_d, p_u, $\angle G_d(f_0)$, $\angle G_u(f_0) - \pi$ and $\angle G(f_0)$ when a subject played an F4 (360 Hz).[1] For convenience, we adopt the following notation: $\angle G_d = \angle G_d(f_0)$, $\angle G_{u-\pi} = \angle G_u(f_0) - \pi$ and $\angle G = \angle G(f_0)$.

[1] In orchestral writing the trombone is generally a non-transposing instrument.

It is worth noting that from the definitions of G_d and G_u, the following relations can be deduced:

$$\begin{aligned}\angle G_d - \angle G_{u-\pi} &= \angle P_u - \angle P_d + \pi \\ &= \angle Z_u - \angle Z_d. \end{aligned} \tag{3.9}$$

Graphically, Eq. 3.9 indicates that the distance between $\angle G_d$ and $\angle G_{u-\pi}$ gives a representation of the distance between $\angle Z_d$ and $\angle Z_u$ at f_0.

Furthermore, the definition of G_d, $G_{u-\pi}$ and G allows to write the following relation:

$$\frac{|\angle G_d - \angle G|}{|\angle G_{u-\pi} - \angle G|} = \frac{|\angle(P_d - P_u) - \angle P_d|}{|\angle(P_d - P_u) - \angle P_u - \pi|} \tag{3.10}$$

We then define ϵ such that $\angle P_d(f_0) = 0$ and $\angle P_u(f_0) = \epsilon - \pi$, calling $p_d(t)$ and $p_u(t)$ the fundamental harmonics of the downstream and upstream pressures of amplitude a_d and a_u respectively:

$$\begin{aligned}\Delta p(t) &= p_d(t) - p_u(t) \\ &= a_d \cos(\omega_0 t) - a_u \cos(\omega_0 t - \pi + \epsilon).\end{aligned}$$

For ϵ small, applying the cosine Taylor series we obtain:

$$\begin{aligned}\cos(\omega_0 t - \pi + \epsilon) &= -\cos(\omega_0 t + \epsilon) \\ &\simeq -\cos(\omega_0 t) + \epsilon \sin(\omega_0 t).\end{aligned}$$

Consequently,

$$\Delta p(t) = (a_d + a_u)\cos(\omega_0 t) - a_u \epsilon \sin(\omega_0 t),$$

which leads to:

$$P_d(f_0) - P_u(f_0) = \Delta P(f_0) = \frac{a_d + a_u}{2} + j\frac{a_u \epsilon}{2}.$$

Therefore, for ϵ small, applying the arctangent Taylor expansion,

$$\begin{aligned} \angle \Delta P(f_0) &= -\text{atan}\left(\frac{a_u \epsilon}{a_d + a_u}\right) \\ &\simeq \frac{a_u \epsilon}{a_d + a_u} \\ &\simeq \frac{\epsilon}{1 + \frac{a_d}{a_u}}. \end{aligned} \tag{3.11}$$

Substituting Eq. 3.11 into Eq. 3.10 leads to:

$$\begin{aligned} \frac{|\angle(G_d(f_0)) - \angle G(f_0)|}{|\angle(G_{u-\pi}(f_0)) - \angle G(f_0)|} &\simeq \left| \frac{\frac{\epsilon}{1+(a_d/a_u)}}{\frac{\epsilon}{1+(a_d/a_u)} + \pi - \epsilon - \pi} \right| \\ &\simeq \left| -\frac{a_u}{a_d} \right| \simeq \left| \frac{Z_u(f_0)}{Z_d(f_0)} \right|. \end{aligned} \tag{3.12}$$

when ϵ is close enough from zero, which implies that $\angle P_d(f_0) - \angle P_u(f_0)$ is close to π. For the measured data presented in this paper, $\angle P_d(f_0) - \angle P_u(f_0)$ ranges between 80 and 180°, which corresponds to an estimation accuracy between 70 and 100 % (as determined by direct comparison of the estimated and exact expressions). Thus, Eq. 3.12 reveals that the relative position between $\angle G$, $\angle G_d$ and $\angle G_{u-\pi}$ is related to the relative acoustical coupling between the lips, the downstream air-column, and the vocal-tract; if the distance between $\angle G$ and $\angle G_d$ is smaller than the distance

between $\angle G$ and $\angle G_{u-\pi}$ (as in Fig. 3.2), this indicates a predominant coupling with the downstream system at f_0, and vice versa. When $\angle G$ is equally spaced from $\angle G_d$ and $\angle G_{u-\pi}$, then both systems provide equal support to lip auto-oscillations.

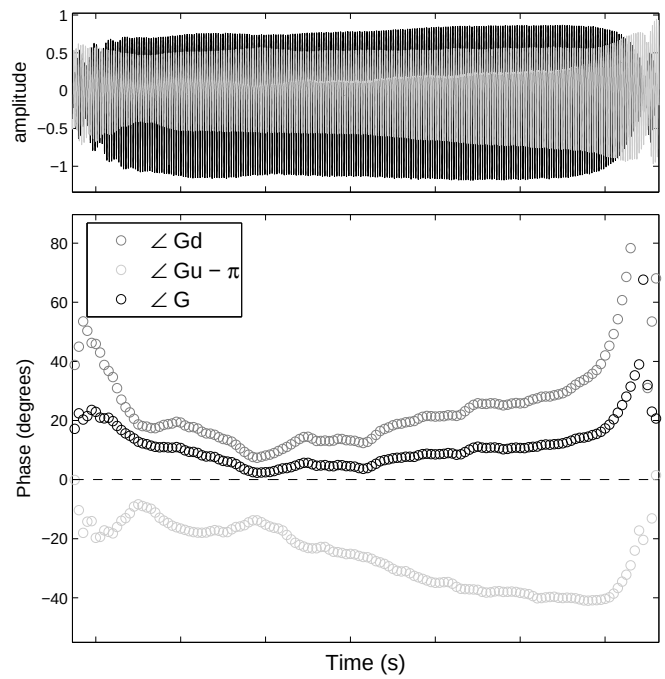

Figure 3.2 Lip mobility estimated for an F4. Top: waveforms of P_d (black), P_u (gray). Bottom: $\angle G_d$ (dark gray), $\angle G_{u-\pi}$ (light gray), and $\angle G$ (black) at f_0 for an F4.

Within the scope of the linear theory of oscillation, we have seen that $\angle G_d$, $\angle G_{u-\pi}$ and $\angle G$ can be considered as estimates of $\angle Z_d(f_0)$, $\angle Z_u(f_0)$ and $\angle Z$ respectively. In the example of Fig. 3.2, the positive nature of $\angle G_d$ infers a negative value of $\angle Z_d$ and thus a capacitive downstream coupling. On the other hand, the negative value of $\angle G_{u-\pi}$ suggests a positive $\angle Z_u$ and therefore an inductive upstream impedance at f_0.

Overall, the data representation proposed in Fig. 3.2 combines time-domain visualizations of three attributes of the regenerative processes at the fundamental frequency of the sound:

1. The dominant regenerative system via the relative amplitude of P_d and P_u (see Eq. 3.1), as well as relative proximities of $\angle G_d$, $\angle G_{u-\pi}$ and $\angle G$, as defined by Eq. 3.12.

2. The degree of "phase tuning" of upstream and downstream systems at the playing frequency via the phase difference between Z_d and Z_u, as defined by Eq. 3.9.

3. An estimate of $\angle Z_d$, $\angle Z_u$ and $\angle Z$ via the values of $\angle G_d$, $\angle G_{u-\pi}$ and $\angle G$.

3.2.4 Player tests

Nine subjects took part in the experiments. Two of them are professional players performing in high level Canadian ensembles and teaching trombone at the Schulich School of Music at McGill University, six are young professional players who perform in classical and jazz ensembles in Montreal, one is an undergraduate student in jazz performance and one is an experienced trombone player. All measurements were performed on the same tenor trombone (King 2B Silver Sonic) and same mouthpiece (Kelly 6 1/2 AL) on which the downstream microphone and electrolabiograph electrodes were mounted. The tuning slide was kept closed and subjects asked to avoid compensating for possible detuning of the instrument (which resulted in playing frequencies slightly above a 440 Hz reference). Participants were given some time to get accustomed to the trombone and mouthpiece setup prior to measurements. The amplitude and phase of the acoustical input impedance of the trombone and mouthpiece with the slide in the closed position are given in Fig. 3.3. The input impedance was measured using a two-microphone impedance measurement system (Macaluso & Dalmont, 2011).

A real-time display of the ELG waveform was provided to the subjects so they could identify when the lip impedance measurement was working or not; for some players, the electrodes needed to be humidified quite often to enable optimum electrical conduction.

Subjects were presented each task prior to execution. Each task was recorded several times

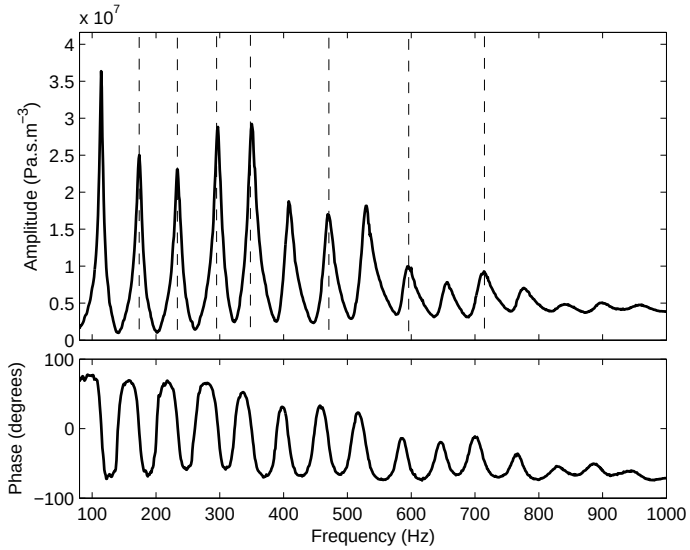

Figure 3.3 Amplitude and phase of the input impedance of the King 2B Silver Sonic tenor trombone and Kelly 6 1/2 AL mouthpiece with the slide in the closed position (the first resonance located below 80 Hz is not measured). Vertical dashed lines indicate the resonances corresponding to the arpeggio series F3-B♭3-D4-F4-B♭4-D5-F5.

until the subjects were satisfied with their performance. At the end of the session, participants were asked to fill out a questionnaire about their trombone performance background and experience. After experiments, all recordings were reviewed by the experimenter. For each subject, the best execution of each task was selected for analysis, based on the sound and ELG signal quality.

3.3 Results from experiments

3.3.1 Arpeggios

The first task involved playing ascending and descending arpeggios in closed position from F3 (175 Hz) to F5 (710 Hz), corresponding to the following tone sequence F3-B♭3-D4-F4-B♭4-D5-F5. The corresponding downstream resonances are indicated in Fig. 3.3. The subjects were asked to slur the tone series (no tonguing articulation between tones). As a first example of

collected data, results obtained from Subject A are presented in Fig. 3.4. Starting from the top of the figure, the first plot represents p_d and p_u waveforms normalized by the p_d maximum, the second represents the temporal evolution of $\angle G_d$, $\angle G_{u-\pi}$ and $\angle G$ at f_0, the third plot represents the evolution of the SPL ratio $\left|\frac{P_u}{P_d}\right|$ in dB at f_0, and the bottom plot the evolution of fundamental frequency f_0 as a function of time.

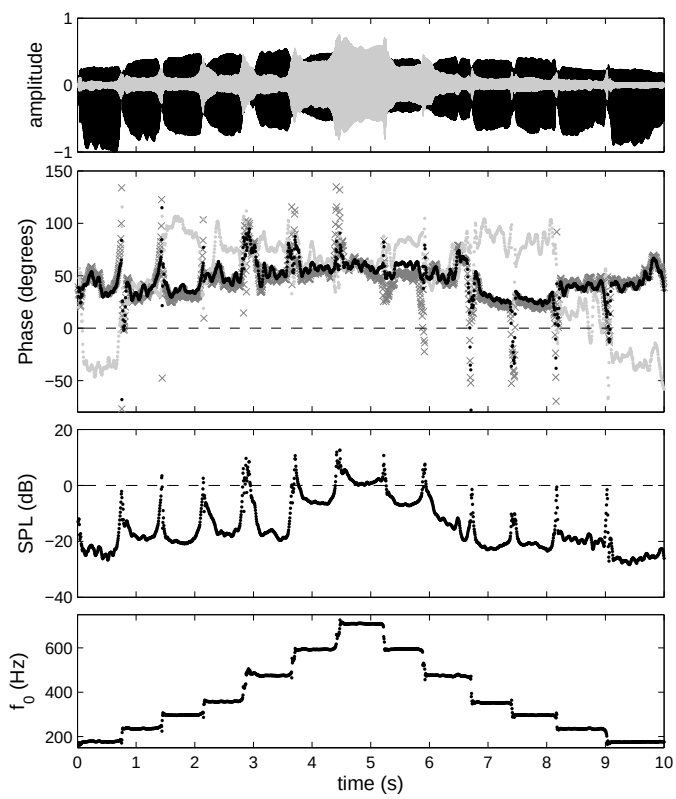

Figure 3.4 Results for Subject A playing ascending and descending arpeggio series: F3-B♭3-D4-F4-B♭4-D5-F5. From top to bottom: waveforms of p_d (black), p_u (gray); $\angle G_d$ (dark gray), $\angle G_{u-\pi}$ (light gray), and $\angle G$ (black) at f_0; SPL ratio in dB of the upstream to downstream pressure; fundamental frequency.

During the sustained portions of the ascending tone series, the ratio $\left|\frac{P_u}{P_d}\right|$ remains low (around -20 dB) until B♭4 (475 Hz). It then reaches a maximum value around 0 dB at the highest tone F5 (710 Hz). Furthermore, tone transitions and onsets are marked by abrupt variations of $\left|\frac{P_u}{P_d}\right|$ with

peak values around 10 dB at the onset of the three highest tones, this effect being less noticeable in the descending arpeggio portion. These first observations show that for the two highest tones, the input impedance of the upstream airways at f_0 becomes close to the magnitude of the downstream input impedance, suggesting a strategic vocal-tract tuning by the player in the high register. The peaks in the $\left|\frac{P_u}{P_d}\right|$ trace at tone transitions also suggest a possible upstream tuning at slurred transitions between tone registers. Although the characteristics of the volume-flow at regime shifts between two tones may significantly deviate from a quasi-static Bernoulli flow model, the duration of these $\left|\frac{P_u}{P_d}\right|$ peaks (above 100 ms) suggest that an increase in $\left|\frac{P_u}{P_d}\right|$ occurs before and after the frequency shift, during a time when steady-state oscillations are established. This potentially indicates occurrences of vocal-tract support at tone transitions. This is further discussed in Section 3.3.4.

Interesting considerations arise from the observation of $\angle G_d$, $\angle G_{u-\pi}$ and $\angle G$. Although $\angle G_d$ and $\angle G$ remain quite stable during the task, significant variations of $\angle G_{u-\pi}$ are observed, from -50° at F3 (175 Hz) to 100° at D4 (295 Hz) and F4 (360 Hz).

No strong hysteresis behaviour is observed between the ascending and descending portions. The negative value of $\angle G_{u-\pi}$ at F3 (175 Hz) suggests a positive value of $\angle Z_u$ and therefore an inductive upstream impedance at f_0. However, all the other tones show a positive value of $\angle G_{u-\pi}$ and thus a capacitive upstream coupling. On the contrary, $\angle G_d$ remains positive for all tones indicating a capacitive downstream impedance at f_0. $\angle G$ seems to overlap with $\angle G_d$ for all notes and with $\angle G_{u-\pi}$ as well for the two highest tones, which is corroborated by the high SPL value of $\left|\frac{P_u}{P_d}\right|$ observed for these two tones. Therefore, the low register is characterized by a dominant downstream coupling, as well as relatively high distance between $\angle Z_d$ and $\angle Z_u$. An increase in pitch seems to correlate with an increase in $\left|\frac{P_u}{P_d}\right|$ as well as a decrease in the distance between $\angle Z_d$ and $\angle Z_u$, suggesting a constructive phase tuning of the downstream and upstream systems at f_0 in the higher register.

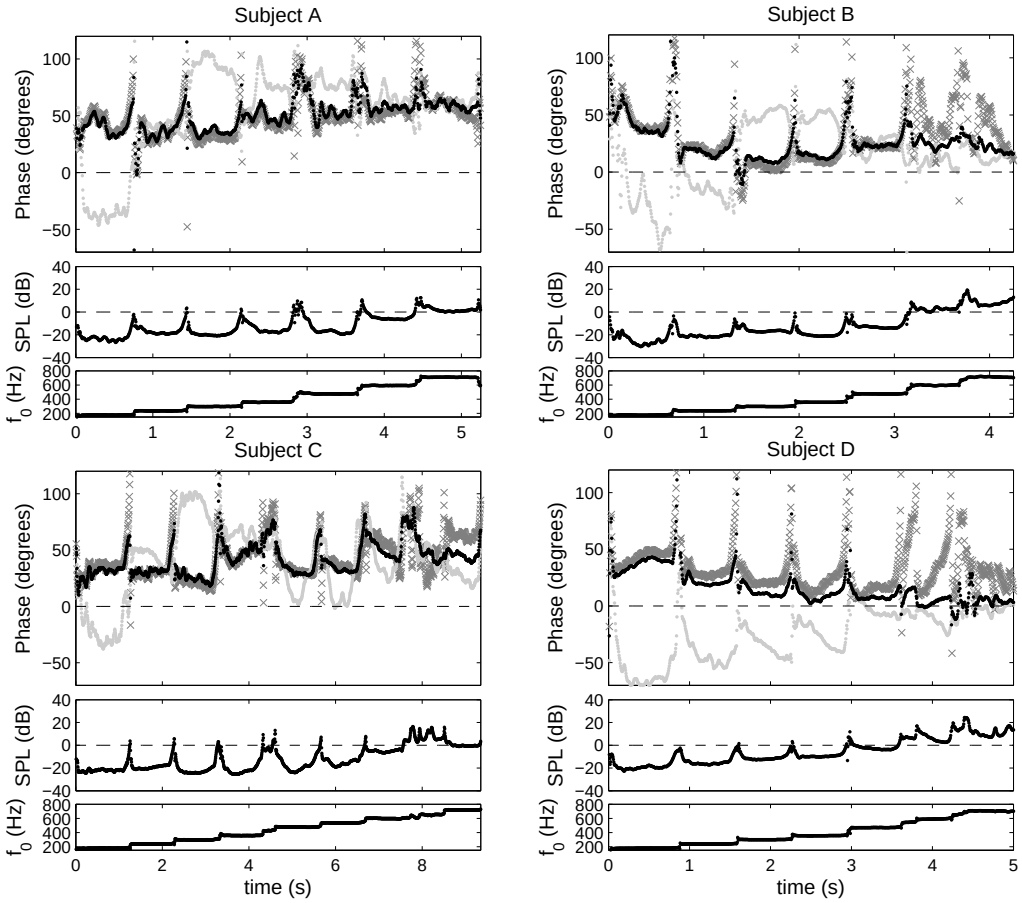

Figure 3.5 Results for Subjects A, B, C and D playing ascending arpeggio series: F3-B♭3-D4-F4-B♭4-D5-F5. From top to bottom: $\angle G_d$ (dark gray), $\angle G_{u-\pi}$ (light gray), and $\angle G$ (black) at f_0; SPL ratio in dB of the upstream to downstream pressure; fundamental frequency.

Figure 3.5 presents results obtained for different participants during the ascending part of the arpeggio series. The left column displays the data from Subject A and Subject C. Note that Subject C played additional overtones (C5 (535 Hz) and E♭5 (640 Hz)) in the tone series. Subject C shows increasing values of $\left|\frac{P_u}{P_d}\right|$ with increase in pitch and a maximum value at E♭5 (not played by Subject A). The values of $\left|\frac{P_u}{P_d}\right|$ at D5 (595 Hz) and F5 (710 Hz) are about the same in both subjects. Analogously to Subject A, the same transitory peak variations of the ratio are observed in Subject C. In both subjects, the abrupt sign change of $\angle G_{u-\pi}$ between the two first

tones is observed. Although $\angle G_{u-\pi}$ stays greater than $\angle G_d$ in Subject A, it becomes smaller than $\angle G_d$ while remaining positive in Subject C from the 5th tone. As in Subject A, $\angle G$ follows the variations of $\angle G_d$ in Subject C, except for the last and highest tone where $\angle G$ lies in between $\angle G_d$ and $\angle G_{u-\pi}$. We observe that $\angle G_d$ shows more variability in Subject C while $\angle G_d$ and $\angle G_{u-\pi}$ are smoothly converging toward the same value with increase in pitch in Subject A.

The right column of Fig. 3.5 displays the data from Subject B and Subject D. In both subjects $\left|\frac{P_u}{P_d}\right|$ values are higher than Subjects A and C in the high register with less pronounced peaks at tone transitions. Subject B shows a change in the sign of $\angle G_{u-\pi}$ at the third tone while $\angle G_{u-\pi}$ stays negative along the entire ascending series for Subject D. In both subjects, $\angle G$ tends to decrease with increase in pitch, as opposed to the tendency observed in Subject A and C. This trend is even more pronounced in Subject D. In Subject A, $\angle G$ and $\angle G_d$ overlap until the two last tones while in Subject D, $\angle G$ smoothly moves from $\angle G_d$ to $\angle G_{u-\pi}$ as the pitch increases. No clear constructive phase tuning of Z_d and Z_u is therefore observed in Subject B and D. Although $\angle G_d$ remains positive in both subjects for the entire task, it shows quite unstable behaviour at the highest tones.

In order to compare experimental results from all the subjects, all extracted variables are averaged over stable sections of each tone. For each subject, stable portions are extracted based on fundamental frequency standard deviation criteria; for a given playing frequency f_0, a section of the tone is considered stable if the standard deviation of f_0 is below a threshold of 4 Hz within the observation window. Using this approach, values of $\left|\frac{P_u}{P_d}\right|$, $|P_d|$, $|P_u|$, p_0, $\angle G_d$, $\angle G_{u-\pi}$ and $\angle G$ are extracted for each tone of the arpeggio series and for each subject.

Figure 3.6 represents the SPL ratio $\left|\frac{P_u}{P_d}\right|$ in dB, as well as dimensionless variables $\gamma_d = \frac{|P_d(f_0)|}{p_0}$ and $\gamma_u = \frac{|P_u(f_0)|}{p_0}$ for all subjects and for each tone of the ascending arpeggio series (1:F3, 2:B♭3, 3:D4, 4:F4, 5:B♭4, 6:D5, 7:F5).

While all the subjects were able to play the ascending tone sequence until B♭4, only the first

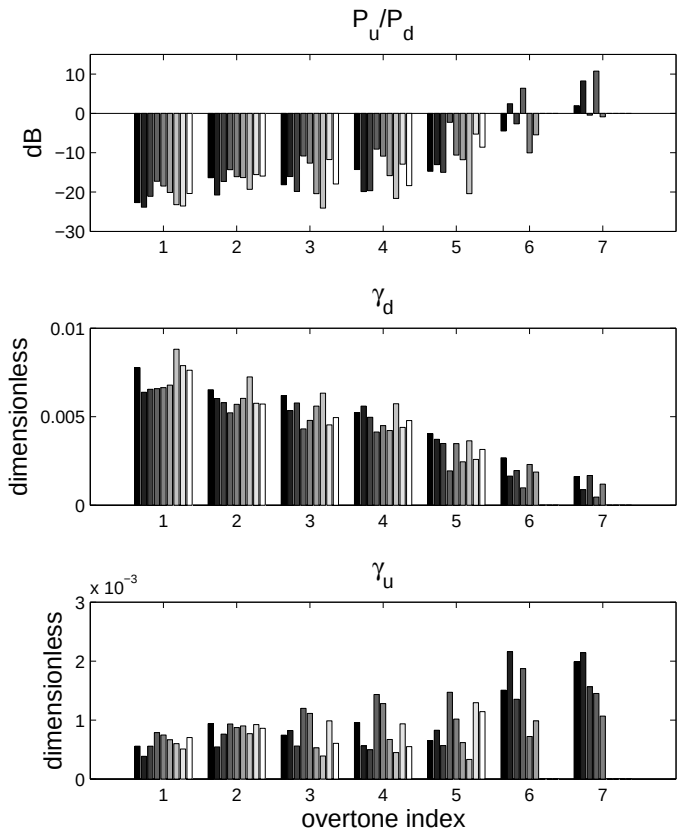

Figure 3.6 SPL ratio in dB of upstream to downstream pressure at f_0, downstream and upstream pressure magnitude at f_0 normalized to the quasi-static blowing mouth pressure as a function of arpeggio index for all subjects (index refers to the ascending series F3-B♭3-D4-F4-B♭4-D5-F5).

six subjects were able to play up to D5 (595 Hz) and only the first five subjects were able to play up to F5 (710 Hz). If we assume that the amplitude of Z_d at f_0 does not differ significantly between subjects despite some small differences in individual playing frequencies, we can reasonably assume that the dimensionless parameter γ_d provides a representation of the mechanical ability of the lips to respond to the static blowing pressure. We therefore use this variable as a descriptor of what can be referred to as the "lip mechanical efficiency".

The low register is marked by negative values of $\left|\frac{P_u}{P_d}\right|$ SPL suggesting predominant influence

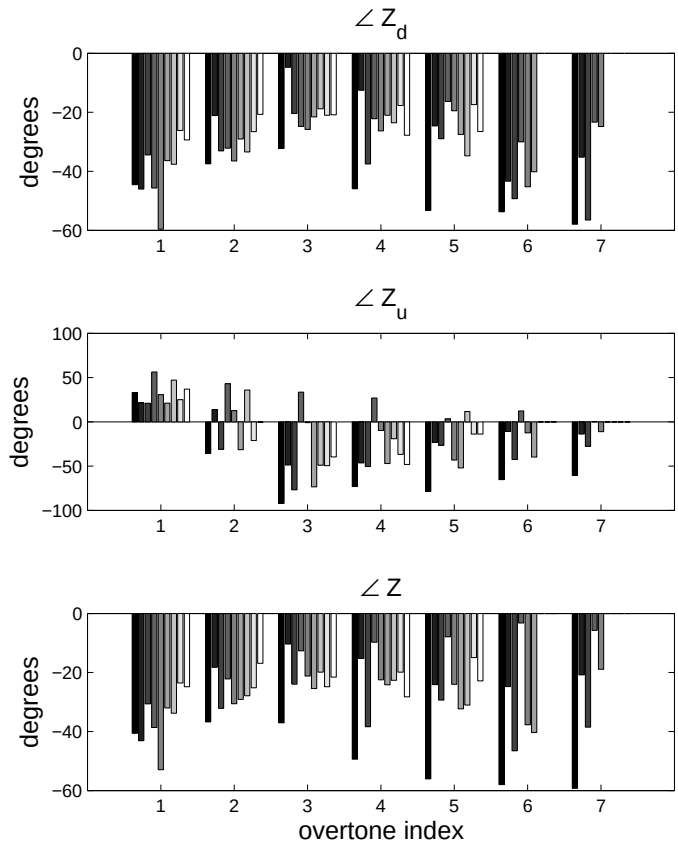

Figure 3.7 Estimated $\angle Z_d$, $\angle Z_u$ and $\angle Z$ at f_0 as a function of arpeggio index for all subjects (index refers to the ascending series F3-B♭3-D4-F4-B♭4-D5-F5).

of the downstream air-column. A clear change is observed at D5 (595 Hz) where Subjects B and D show positive SPL ratios indicating predominant coupling with the vocal tract at the playing frequency. This tendency is confirmed by negative but small values of the SPL ratio in other subjects at D5 (595 Hz). At F5 (710 Hz), Subjects A, B and D exhibit positive SPL ratios whereas Subjects C and E show ratios close to zero. This suggests a significant influence of upstream impedance in all subjects. The values of γ_d decrease with increasing playing frequency, which correlates with a decrease in Z_d amplitude with frequency in brass instruments (as $|Z_d|$ decreases, downstream support becomes weaker and more energy is needed to maintain lip oscillations).

However, the opposite behaviour is observed in γ_u, supporting the hypothesis of a growing amplitude of Z_u at f_0 with increase in pitch.

Estimation of $\angle Z_d(f_0)$, $\angle Z_u(f_0)$ and $\angle Z(f_0)$ from lip mobility measurements are represented in Fig. 3.7. $\angle Z_d(f_0)$ remains negative for all subjects suggesting a compliant downstream input impedance at f_0 along the task. $\angle Z_u(f_0)$ is positive for all subjects at F3 (175 Hz) supporting an inductive upstream impedance at f_0 for the lowest tone. At B♭3 (235 Hz), four subjects show a positive $\angle Z_u(f_0)$. Only Subject D maintains a positive or null $\angle Z_u(f_0)$ value for all tones with $\angle Z_u(f_0) \simeq 0°$ at F5 (710 Hz). Above B♭3 (235 Hz), all other subjects show negative values of $\angle Z_u(f_0)$, except Subject G who shows a positive value at B♭4 (475 Hz). These observations suggest a dominant inductive effect of players' vocal-tract in the low register with a rapid transition to a capacitive upstream coupling with increase in pitch.

Regarding the total impedance applied to the lips, $\angle Z(f_0)$ remains negative for all tones. Inter-subject variability grows with increase in pitch; Subject A shows the smallest values around -60° for the three highest tones, while Subject D shows the greatest values between -8° for B♭4 (475 Hz) and -3° at F5 (710 Hz).

As vocal-tract adjustments appear to occur for high playing frequencies, we now focus our attention on the three highest tones of the arpeggio series.

Figure 3.8 represents a zoomed view of Figs. 3.6 and 3.7 for the last three notes of the arpeggio series (B♭4 (475 Hz), D5 (595 Hz) and F5 (710 Hz)). Looking particularly at $\left|\frac{P_u}{P_d}\right|$, γ_d and γ_u for D5 (595 Hz) and F5 (710 Hz), we observe that Subjects B and D display the higher values of the SPL ratio and lower values of γ_d, indicating that although these two players were able to create high magnitude upstream impedances at f_0, the mechanical efficiency of the lips estimated from the dimensionless parameter γ_d remained low compared to other subjects. This correlation does not apply to γ_u; while the amplitude of Z_d is about the same for all subjects at the playing frequency, the magnitude of Z_u at f_0 significantly differs for each subject as shown by differences

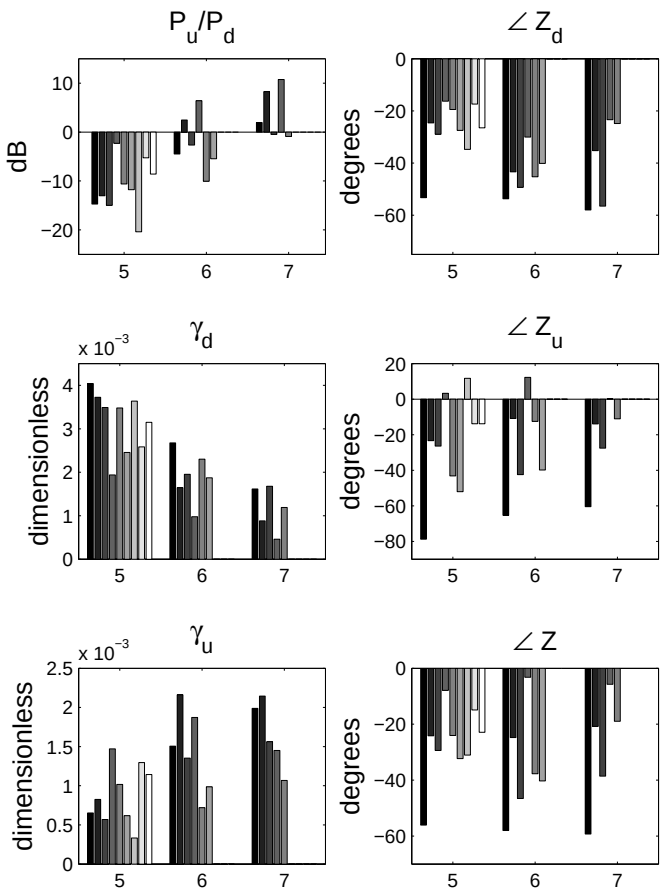

Figure 3.8 SPL ratio in dB of upstream to downstream pressure at f_0, downstream and upstream pressure magnitude at f_0 normalized to the quasi-static blowing mouth pressure, estimated $\angle Z_d$, $\angle Z_u$ and $\angle Z$ at f_0 as a function of arpeggio index for all subjects (index refers to the ascending series B♭4-D5-F5).

in $\left|\frac{P_u}{P_d}\right|$ (high for Subjects B and D, and lower for the others).

It is then interesting to see how these observations correlate with observations on the phase of Z_d, Z_u and Z_d at f_0. As a matter of fact, Subjects A and C show lower values of $\angle Z_d$ and $\angle Z_u$ than Subjects B and D. This may indicate that Subjects A and C were able to create an upstream resonance centered at a lower frequency than Subjects B and D, allowing oscillation to occur at

a lower phase value of $\angle Z_d$. This tuning strategy results in a lower value of $\angle Z$ which means a value of $\angle G$ close to 90°. Therefore, assuming an outward striking model of the lips, one may hypothesize that the tuning strategy for Subjects A and C favors lip oscillations near a mechanical resonance of the lips. We thus distinguish two strategies: 1) strategy of Subjects B and D: high amplitude upstream resonance at f_0 overriding the downstream regenerative influence, and 2) strategy of Subject A and C: careful tuning of the phase of Z_u at f_0 which might better support oscillations near a mechanical resonance of the lips.

Nevertheless, Subject E does not fit clearly in either of the two categories, especially for the highest tone F5 (710 Hz). Indeed, although this subject exhibits values of $\angle Z_d$, $\angle Z_u$ and $\angle Z_u$ similar to Subjects B and D at F5 (710 Hz), Subject E shows a slightly negative $\left|\frac{P_u}{P_d}\right|$ ratio and relatively high γ_d at this playing frequency, as in Subjects A and B.

In order to evaluate whether the observed increase in $\left|\frac{P_u}{P_d}\right|$ with f_0 results from an actual tuning of the vocal-tract or the overall deflection in the magnitude of Z_d resonances with increase in frequency, the value of Z_u is estimated from Eq. 3.1 at the fundamental frequency and first harmonics for each tone of the ascending arpeggio series. It is then possible to characterize the evolution of $|Z_u|$ at particular frequencies appearing in the harmonic structure of specific tones. For instance, the frequency of the first harmonic of B♭3 located around 475 HZ corresponds to the fundamental frequency of B♭4 (475 Hz). Consequently, the magnitude of Z_u around 475 Hz can be calculated at these two steps of the arpeggio sequence and potential changes in $|Z_u|$ identified. The evolution of Z_u magnitude at 475 Hz, 595 Hz and 710 Hz as a function of f_0 is presented in Fig. 3.9 during ascending arpeggios for the subjects able to play up to D5 (595 Hz) (Subjects A to F).

In all subjects able to play over the full range (subjects A to E), the amplitude of Z_u around 710 Hz increases with increase in pitch, supporting the hypothesis of a tuning of the vocal-tract in the higher register. Subject B shows significant variations in $|Z_u|$ around 595 Hz between overtone

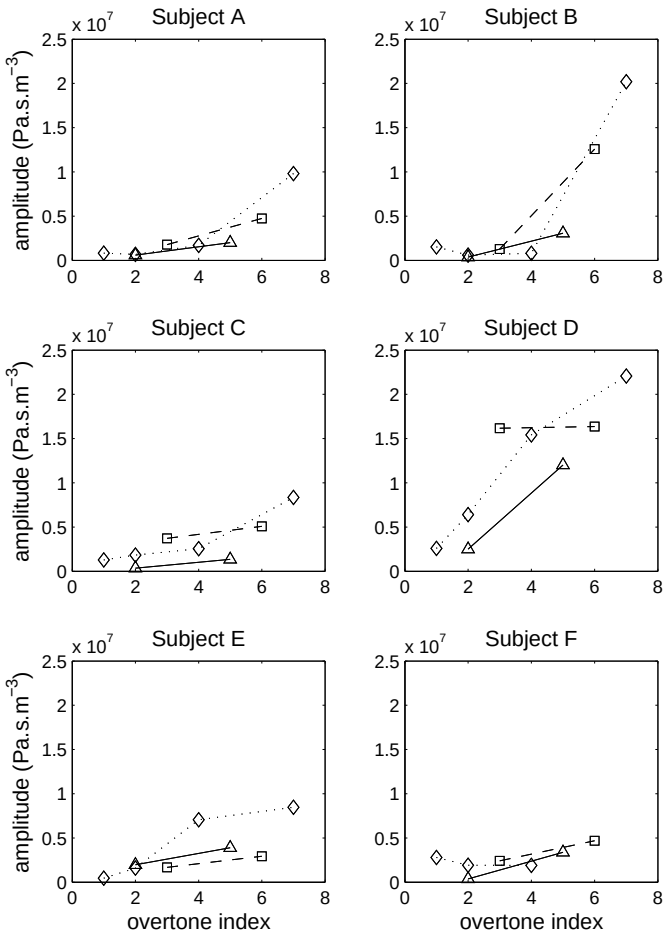

Figure 3.9 Evolution of the magnitude of the upstream input impedance during ascending arpeggios: at 475 Hz (triangle solid line), 595 Hz (square dashed line) 710 Hz (diamond dotted line) as a function of overtone index during ascending arpeggios for subjects A to F (index refers to the ascending series F3-B♭3-D4-F4-B♭4-D5-F5).

3 (D4) and 6 (D5), while Subject C presents a constant but high amplitude of Z_u at 595 Hz and an increase in Z_u amplitude at 475 Hz between overtones 2 (B♭3 at 235 Hz) and 5 (B♭4 at 475 Hz). Moreover, in agreement with the categorization proposed, subjects A and C show similar tuning patterns for the three frequencies observed, while subjects B and D show the highest values of $|Z_u|$ at both 475 Hz and 595 Hz. Subject E presents a tuning trend closer to subjects A and C,

although she is the only one showing lower magnitude of Z_u at 595 Hz. Finally Subject F does not present any significant tuning pattern and could not play the highest tone.

3.3.2 Influence of dynamics

In order to evaluate the influence of loudness on upstream coupling, subjects were asked to play a sustained B♭4 (475 Hz) from *mezzo-piano (mp)*, *crescendo* to the maximum loudness they could comfortably reach and *decrescendo* to *mezzo-piano*. The choice of B♭4 was made since it is high enough to induce significant vocal-tract support and low enough to allow a clear crescendo and decrescendo to be produced comfortably. We propose a representation where $\angle G_d$ and $\angle G_{u-\pi}$ values are mapped onto a color scale extending from -30° to 140° and hence centered around 85°. According to this color scale, dark tonalities will be associated to a capacitive impedance whereas light tonalities will rather suggest an inductive input impedance. The boundary between the color arrays of $\angle G_d$ and $\angle G_{u-\pi}$ correspond to the SPL value of $\left|\frac{P_u}{P_d}\right|$ in dB. Results from Subjects A, B, C, D, E and G are presented in Fig. 3.10. The top color area corresponds to $\angle G_d$ while the bottom area corresponds to $\angle G_{u-\pi}$. The black dashed lines represent the amplitude of $P_d(f_0)$ (considered as an index of loudness). This representation therefore provides a condensed form of vocal-tract tuning parameters presented previously, while allowing overlapping of additional time-domain variables ($|P_d(f_0)|$ in this case).

All subjects show a negative SPL ratio along the tone duration, indicating a predominant coupling with the downstream air-column. In all subjects, $\left|\frac{P_u}{P_d}\right|$ varies significantly with variations in P_d amplitude. All subjects, except B, show a maximum in P_d fitting with a minimum in SPL ratio. In Subject B, both extrema do not exactly match although the SPL ratio shows a low-value plateau around the peak of downstream energy. The lowest minimum value of the SPL ratio is found in Subject C around -40 dB whereas Subject D shows a minimum at -14 dB. The greatest variations of SPL ratio are observed in Subjects B, C and G, for which higher dynamics are

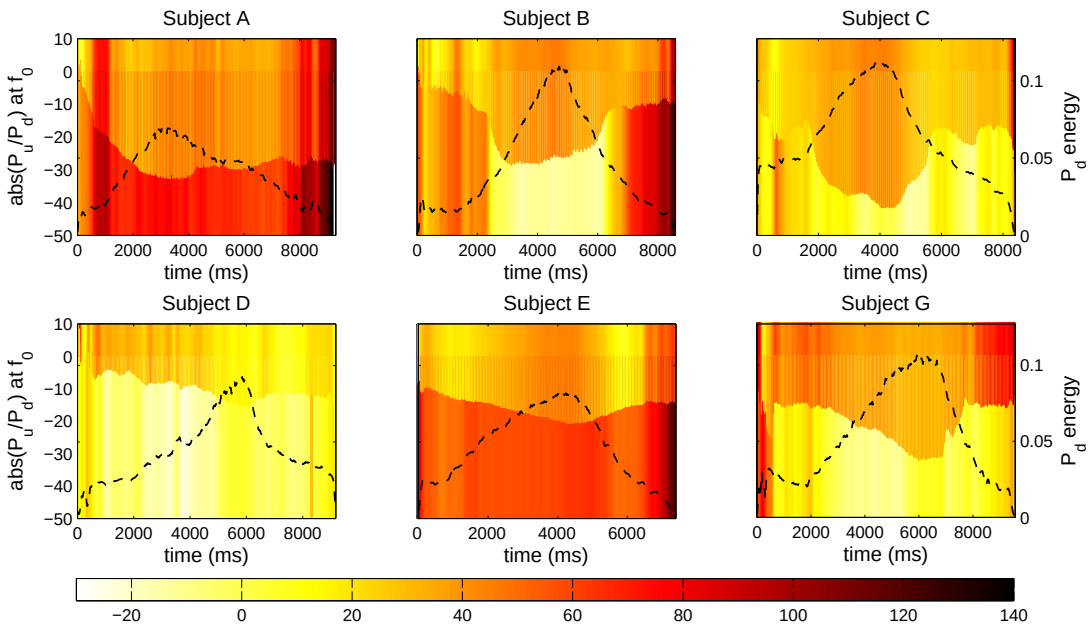

Figure 3.10 Vocal-tract tuning during sustained tones of varying dynamics. SPL ratio in dB of the upstream to downstream pressure (boundary between color areas), $\angle G_d$ (top color area), $\angle G_{u-\pi}$ (bottom color area), P_d amplitude (dashed black line) during sustained B♭4 (475 Hz) played following a *crescendo-decrescendo* dynamic pattern for Subjects A, B, C, D, E and G. Color scale unit: degrees

associated with a plateau of low SPL ratio. This phenomenon is not as visible in Subjects A, D and E.

From color area observations, we notice that $\angle G_d$ remains relatively constant along tone duration for all subjects compared to variations in $\angle G_{u-\pi}$. The values of $\angle G_d$ are quite similar in all subjects (between 20 and 60 degrees) suggesting a capacitive downstream input impedance at f_0. $\angle G_{u-\pi}$ remains positive and constant in Subjects A and E which supports a capacitive vocal-tract impedance along the tone duration. Analogously, $\angle G_{u-\pi}$ remains stable but closer to zero in Subjects D and G suggesting an inductive upstream impedance. More variability in the $\angle G_{u-\pi}$ value is observed in Subject B; Subject C shows small oscillations of $\angle G_{u-\pi}$ along the task while Subject B displays a clear change in $\angle G_{u-\pi}$ around the $|P_d|$ peak value. For this player, vocal-tract impedance varies from a capacitive to an inductive character and the value of $\angle G_{u-\pi}$ seems well

correlated with variations in SPL ratio. To a lesser extent, variations of $\angle G_{u-\pi}$ around the minimum of $\left|\frac{P_u}{P_d}\right|$ are also observed in Subjects C, D, G, and somewhat in E where a smooth variation of both $\angle G_d$ and $\angle G_{u-\pi}$ accompanies variations of loudness and playing frequency.

Overall, these observations suggest two categories of behaviour: 1) a marked decrease in SPL ratio correlated with increase in dynamic, possibly associated with variations in $\angle G_{u-\pi}$ caused by changes in vocal-tract shape, and 2) rather stable upstream impedance, in amplitude and phase, with less marked minimum in SPL ratio at the downstream pressure peak. However, for high amplitude oscillations (as it must be the case at the maximum loudness), it is difficult to formulate strong conclusions from the observation of $\angle G_d$ and $\angle G_{u-\pi}$ since the validity of the linear relation given by Eq. 3.5 may be restricted.

3.3.3 Pitch bending

Although pitch bends are easy to produce on trombones by simply varying the slide length while maintaining a constant blowing condition, bent tones may also be produced by forcing lip oscillations below the frequency of a well sustained tone for a given slide position. This maneuver may be used in order to play for instance an E♭2 (77 Hz) at the 7th position of the slide for which the second input impedance peak is located at the frequency of an E2 (82 Hz). It therefore requires the player to maintain lip oscillations at a frequency not well supported by the downstream air-column. In contrast to woodwind playing, a brass player has a direct control on the mechanical resonance of the lips and may force oscillations away from a resonance of the air-column (F. C. Chen & Weinreich, 1996; Cullen et al., 2000). However, one may also hypothesize that players are capable of producing a significant vocal-tract resonance in the neighborhood of the playing frequency to support lip oscillations during a pitch bend.

In order to investigate this hypothesis, subjects were asked to perform a slow pitch bend starting from a B♭2 at 120 Hz (in closed position of the slide) to the lowest frequency they could

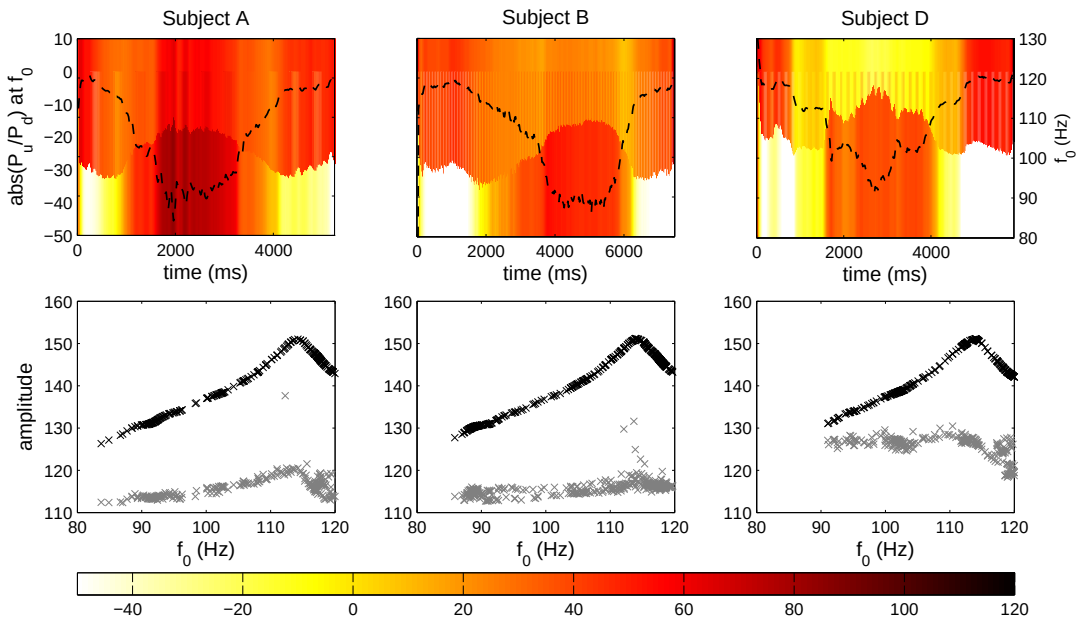

Figure 3.11 Vocal-tract tuning during pitch bending. Top: SPL ratio in dB of the upstream to downstream pressure (boundary between color areas), $\angle G_d$ (top color area), $\angle G_{u-\pi}$ (bottom color area), f_0 (dashed black line) during bending from B♭2 (120 Hz) for Subjects A, B and D. Bottom: magnitude of Z_d and Z_u in dB at f_0 during bending. Color scale unit: degrees

maintain, and then back up to B♭2. Results from Subjects A, B and D (who performed the largest bends) are represented in Fig. 3.11. The frequency range covered by the three subjects is quite identical and extends from 122 Hz to 85 Hz for Subject A, from 122 Hz to 87 Hz for Subject B, and from 122 Hz to 93 Hz for Subject D. Subjects A and B were thus able to bend down to the frequency of an F2 around 90 Hz (a 4th below B♭2), while Subject D bent down to an F2♯ around 95 Hz (a major 3rd below B♭2).

In addition the value of $|Z_u|$ at f_0 is estimated for each subject during the task using Eq. 3.1 and represented in dB in Fig 3.11. In the three subjects, an increase of the ratio $\left|\frac{P_u}{P_d}\right|$ at f_0 is observed when bending down, but this increase seems to be due to the deflection of $|Z_d|$ at f_0 when the pitch is decreased, while Z_u remains constant. Peak values of the ratio are observed around -4 dB in Subject D, -14 dB in Subject B and -16 dB in Subject A. This variation in vocal-tract

support occurs simultaneously with important alterations of $\angle G_{u-\pi}$: $\Delta\angle G_{u-\pi} = 130°$ in Subject A, $\Delta\angle G_{u-\pi} = 110°$ in Subject B, and $\Delta\angle G_{u-\pi} = 110°$ in Subject D. On the contrary, $\angle G_d$ remains more stable in Subjects A ($\Delta\angle G_d = 32°$) and B ($\Delta\angle G_d = 31°$), while it shows more fluctuations alongside f_0 variations in Subject D ($\Delta\angle G_d = 76°$) .

These results suggest that a small contribution of the vocal-tract at f_0 accompanies the lowest frequency part of the pitch bends in all subjects, although this effect does not reflect any significant change in $|Z_u|$ at the playing frequency. Regarding the phase of G_d, the small variations observed in Subjects A and B are inconsistent with the important f_0 deviation that should result in a large variation of $\angle Z_d$ from observation of the trombone impedance curve in Fig. 3.3. Accordingly, we may hypothesize that the assumed linear relationship between the lip opening area and acoustic flow is no longer valid during this bending task. This could be further interpreted as suggesting that players A and B try to maintain a constant lip vibratory mechanism during bending by preserving the phase relationship between S_{lip} and P_d, thus forcing the lips into a particular regime of oscillation. Under this assumption, $\angle G_{u-\pi}$ can no longer be interpreted as an estimate of $-\angle Z_u$.

The interpretation proposed for Subject A and B does not seem to apply to the same extent to Subject D who shows higher variations of $\angle G_d$. This may be correlated with the greater vocal-tract influence observed during bending for this subject. Indeed, appropriate vocal-tract tuning may compensate for the unfavorable downstream coupling and enable the lips to oscillate according to a regime which preserves the linear relationship between lip opening and acoustic flow. This would possibly justify why, in spite of quasi-similar f_0 deviation in the three subjects, the value of $\angle G_d$ observed during bending in Subject D decreases significantly. This is expected from observation of the phase of the input impedance of the trombone in Fig. 3.3, which suggests an increase in $\angle Z_d$ when the playing frequency decreases.

3.3.4 Tone transitions

Since the method proposed allows for a high temporal resolution tracking of $\angle G_d$ and $\angle G_{u-\pi}$, it particularly enables investigation of vocal-tract adjustments at tone transitions. Figure 3.12 shows extracted parameters near the end of a B♭4 (475 Hz) and the beginning of a C5 (535 Hz), therefore highlighting the slur transition between the two tones during the ascending arpeggio series played by Subject B. We notice that at the tone transition, and for a significant amount of time (about 100 ms), the SPL ratio in decibels becomes greater than zero. This is also visible in the p_d and p_u waveforms where a clear boost in p_u amplitude occurs during the transition.

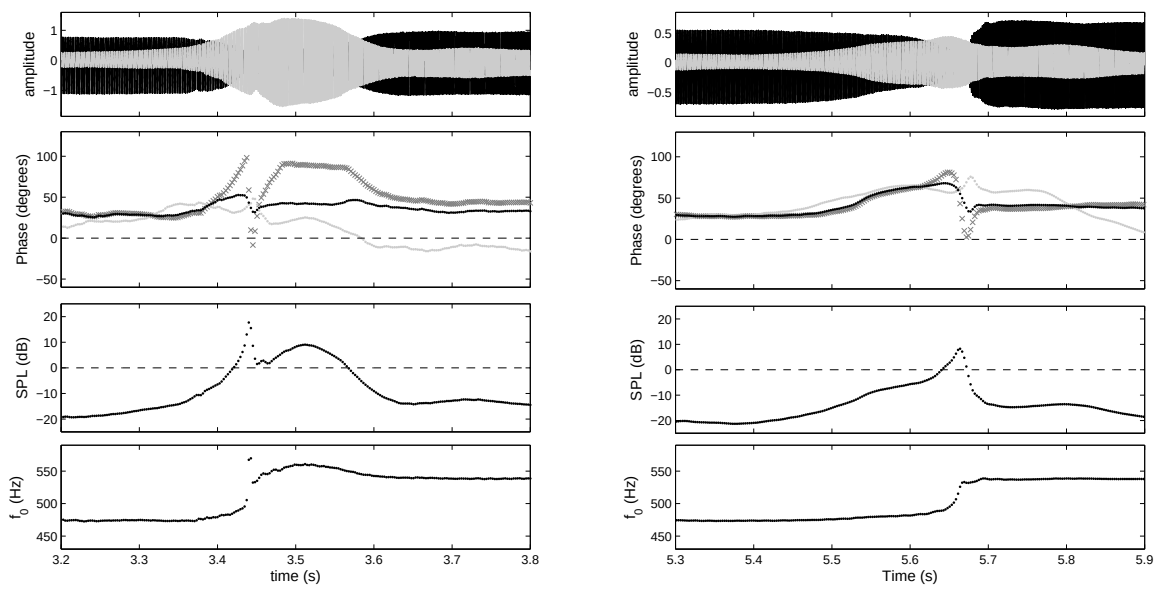

(a) Subject B (b) Subject C

Figure 3.12 Vocal-tract influence at tone transition between B♭4 and C5 for subjects B and C. From top to bottom: waveforms of p_d (black), p_u (gray). $\angle G_d$ (dark gray), $\angle G_{u-\pi}$ (light gray), and $\angle G$ (black) at f_0; SPL ratio in dB of the upstream to downstream pressure; fundamental frequency.

Although the airflow at tone transitions may be turbulent and the continuity of the volume flow not valid at the frequency shift, this $|\frac{P_u}{P_d}|$ bump occurs within a significant amount of time

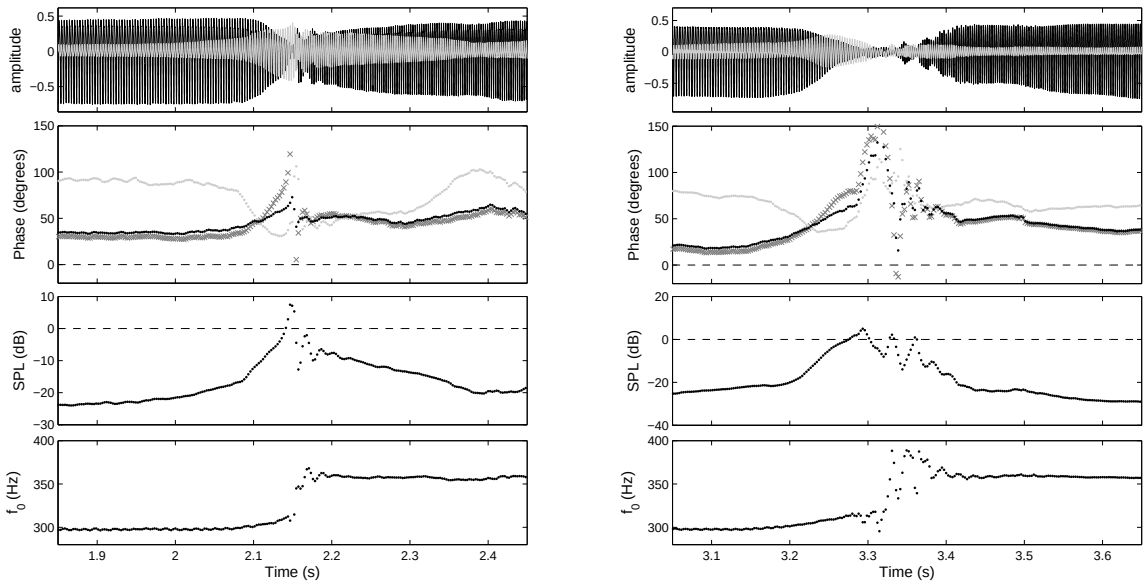

(a) Subject A (b) Subject C

Figure 3.13 Vocal-tract influence at tone transition between D4 and F4 for subjects A and C. From top to bottom: waveforms of p_d (black), p_u (gray). $\angle G_d$ (dark gray), $\angle G_{u-\pi}$ (light gray), and $\angle G$ (black) at f_0; SPL ratio in dB of the upstream to downstream pressure; fundamental frequency.

($\simeq$ 300 ms), well above the time required to reach a steady state of oscillation. We also notice an increase in the SPL ratio before the frequency changes, which suggest an increase in vocal-tract support prior to tone transition. Moreover, $\angle G_{u-\pi}$ shows smooth and continuous variations during this transitory part, whereas $\angle G_d$ shows a discontinuous behaviour.

Regarding $\angle G_d$, this behaviour is logically explained by the sign change in $\angle Z_d$ between two adjacent resonances. On the other hand, the continuous character of $\angle G_{u-\pi}$ may be attributed to a synchronous adjustment of the vocal-tract resonance around f_0 resulting in a smooth phase transition of $G_{u-\pi}$.

Furthermore, this transitory upstream tuning is also visible during slurred transitions at lower frequencies as shown by Figs. 3.13 and 3.14. In Fig. 3.13, an increase in SPL ratio occurs in

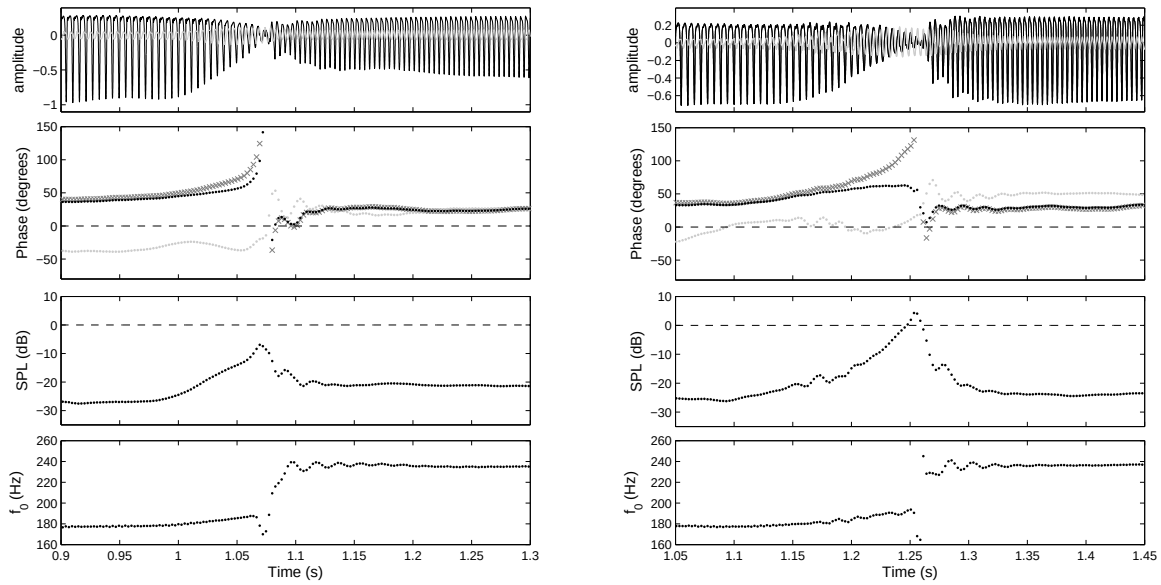

(a) Subject A (b) Subject C

Figure 3.14 Vocal-tract influence at tone transition between F3 and B♭3 for subjects A and C. From top to bottom: waveforms of p_d (black), p_u (gray). $\angle G_d$ (dark gray), $\angle G_{u-\pi}$ (light gray), and $\angle G$ (black) at f_0; SPL ratio in dB of the upstream to downstream pressure; fundamental frequency.

both subjects at the end of the D4 (295 Hz) before the jump to F4 (360 Hz). Even lower in frequency, this phenomenon is also observed for both subjects in Fig. 3.14, where the transitory effect of the vocal tract induces a continuous variation of $\angle G_{u-\pi}$ at the frequency switch between F3 and B♭3. As performers were asked to slur tone transitions (no tonguing articulation), this vocal-tract adjustment might be the result of variations of the vocal-tract geometry inducing no constriction but substantial changes in the upstream impedance. These adjustments may arise from variations of the tongue position, and possibly some laryngeal adjustments or movements. For instance a transitory variation of the glottal area may significantly modify the amplitude of certain vocal-tract resonances (Barney, De Stefano, & Henrich, 2007). Furthermore, movements of the larynx (variations of larynx height) at tone transitions may also contribute to displace

vocal-tract resonances and provide a greater support during regime changes.

3.4 Summary

In this chapter, we have presented a method allowing for evaluation of the relative amplitude of the downstream and upstream input impedance at the playing frequency, as well as an estimation of the phase of the downstream and upstream input impedance at f_0. This approach involves measurements of lip electrical impedance which is assumed to be in phase with lip opening area.

During arpeggio sequences, a significant increase in vocal-tract support is observed in the higher register. A careful observation of the amplitude ratio and absolute phase of the downstream and upstream input impedances for the two highest tones suggests two categories regarding vocal-tract tuning strategies: 1) Z_u amplitude large in comparison with Z_d amplitude and $\angle Z_u$ close to zero at f_0, suggesting a vocal-tract resonance centered at the playing frequency and overriding the effect of the trombone impedance; 2) Z_u amplitude of the same order as Z_d and lower values $\angle Z_u$ phase, suggesting a vocal-tract resonance centered at a lower frequency and allowing lip oscillations at a lower value of $\angle Z$. This last tuning strategy is possibly favorable to an outward striking regime by allowing oscillations to occur close to a mechanical resonance of the lips. This may also contribute to explain why the two players showing these characteristics were able to create higher acoustic downstream energy with lower mouth static pressure. However, this early classification may not apply to some subjects as illustrated by the results obtained for Subject E.

During sustained tones with variations of dynamic, a general trend involving a decrease in vocal-tract support with increase in dynamic is observed. Larger variations in $\left|\frac{P_u}{P_d}\right|$ ratio are observed in subjects showing highest variations in $\angle G_{u-\pi}$, which implies variations in the characteristics of the vocal-tract impedance at f_0 with increase in dynamic. Alternatively, the decrease in vocal-tract support with increase in acoustic energy produced may be explained by non-linear

interactions between harmonics which participate to support lip oscillation and reduce the need for vocal-tract support at f_0.

Pitch bending tasks do not appear to involve any significant vocal-tract support at f_0. The stable phase of G_d observed in two subjects suggests a possible interruption of the assumed linear relationship between lip opening area and the input acoustic flow. A relatively greater vocal-tract support during bending may maintain this linear relationship as shown by significant variations of $\angle G_d$ in one subject.

During slured tone transitions, variations of the amplitude ratio $\left|\frac{P_u}{P_d}\right|$ suggest a transitory vocal-tract influence, at least prior to tone transition, indicating that upstream acoustic support is possibly needed to achieve proper slurs. Smooth variations of $\angle G_{u-\pi}$ at tone transitions also support the hypothesis of a continuous adjustment of a vocal-tract resonance around f_0 during slurs. However, the nature of this transitory vocal-tract coupling should be interpreted with care as the nature of the volume flow at the frequency shift is quite uncertain.

Chapter 4

in-vitro Simulation of Upstream Coupling on an Artificial Player System

In Chapter 3, significant vocal-tract influence in the high register of the instrument was observed. Particularly, an early categorization of the upstream tuning strategy was proposed in light of the results obtained during arpeggios. This highlights the potential importance of phase tuning of the vocal-tract impedance on the behaviour of the lips. In order to clarify the modalities of the acoustical interaction between the vocal-tract and the vibrating lips, it becomes necessary to work under more controlled conditions.

In this chapter, we investigate the nature of the upstream coupling on an artificial player system in order to provide support for analysis of experimental results obtained *in-vivo*. Several artificial player systems have been used in music acoustic research over the last decades. These "blowing machines" have been developed with different degrees of complexity and applied to the excitation of woodwind instruments (Backus, 1985; Idogawa, Kobata, Komuro, & Iwaki, 1993; Mayer, 2003; Fritz, 2004; Ferrand, Hélie, Vergez, Véricel, & Caussé, 2010), as well as to brass instruments where the vibrating lips are typically modeled by a pair of latex tubes filled

with a liquid or fluid element (Gilbert et al., 1998; Vergez, 2000; Richards, 2003; Hélie, Lopes, & Caussé, 2012; Lopes, Hélie, & Caussé, 2003). These systems constitute a basic model of a wind player by combining replicas of the main components involved in the mechanism of sound production. Moreover, these artificial players provide substantial advantages over human subjects such as:

- Control parameters such as the embouchure and the quasi-static mouth pressure can be controlled and maintained constant over a long period of time.
- A number of measurement sensors may be embedded within the system without disturbing the sound production process.
- Some of these systems are now automatized and allow for precise feedback control and monitoring of various physical parameters.
- Such a system is by nature inexpressive, and is therefore not subject to musical interpretations of a given task.

This experimental setup thus potentially enables variations of upstream coupling characteristics independently from embouchure adjustments, which is obviously not possible in human subjects. The influence of different upstream coupling conditions on the behaviour of the lips may therefore be investigated in order to derive the nature of an optimal vocal-tract tuning.

Most recent attempts to incorporate a vocal-tract resonator to an artificial player system were performed on the clarinet (Fritz, Wolfe, Kergomard, & Caussé, 2003; Fritz, Caussé, Kergomard, & Wolfe, 2005) and on the didjeridu and trombone (Wolfe et al., 2003). On the dijeridu and trombone, a system enabled the characteristics of an upstream resonance to be varied (low or high tongue position roughly corresponding respectively to vowels [æ] and [ɪ]) by changing the degree of constriction just upstream from the lips, while maintaining a fixed reed setting. On

both instruments, vocal-tract configuration had an effect on intonation as well as on transitions between two registers. On the clarinet, two vocal-tract configurations corresponding to vowels "aw" and "ee" were realized by assembling plastic rings of different cross-section areas. Although this method allows for simulation of more realistic vocal-tract shapes, the low versatility imposes a reduced number of configurations and makes time-varying manipulation of the vocal-tract impossible. Moreover, the discontinuities at ring junctions may produce aeroacoustical effects interfering with the expected acoustical influence of the vocal-tract.

For this reason, we chose to apply another method based on the injection of an acoustic flux in the mouth cavity of the artificial player, and inspired from previous work by Chen and Weinreich (1996). By properly adjusting the phase and amplitude of the injected signal, we aim at simulating different vocal-tract impedance conditions at the playing frequency using an active control method. This approach was also recently adopted for the study of flute-like instruments (Auvray, Fabre, Lagée, Terrien, & Vergez, 2012).

The first section of this chapter presents the artificial player system as well as the experimental setup and active control protocol developed for the simulation of different upstream acoustical coupling conditions. In a second part, the experimental protocol is described, and results from experiments are presented and discussed in light of the linear theory of oscillation; particular emphasis is put on the analysis of lip mechanical response and linearity of the relationship between the acoustic flow and lip opening.

4.1 Vocal-tract coupling in an artificial player system

4.1.1 Presentation of the artificial player system

This study was performed using the artificial player system developed at IRCAM (Hélie et al., 2012) and presented in Fig. 4.1. This system includes a mouth cavity of cylindrical shape and two

cylindrical artificial lips made of latex and filled with water. The following control commands are available:

- Air flow injected in the mouth cavity controlled by the electrical voltage at the servo valve.
- Volume of water in each lip controlled independently by two actuators.
- Force applied by the lips on the mouthpiece controlled by adjusting longitudinal position of the artificial mouth mounted on a translator, relative to the mouthpiece position.

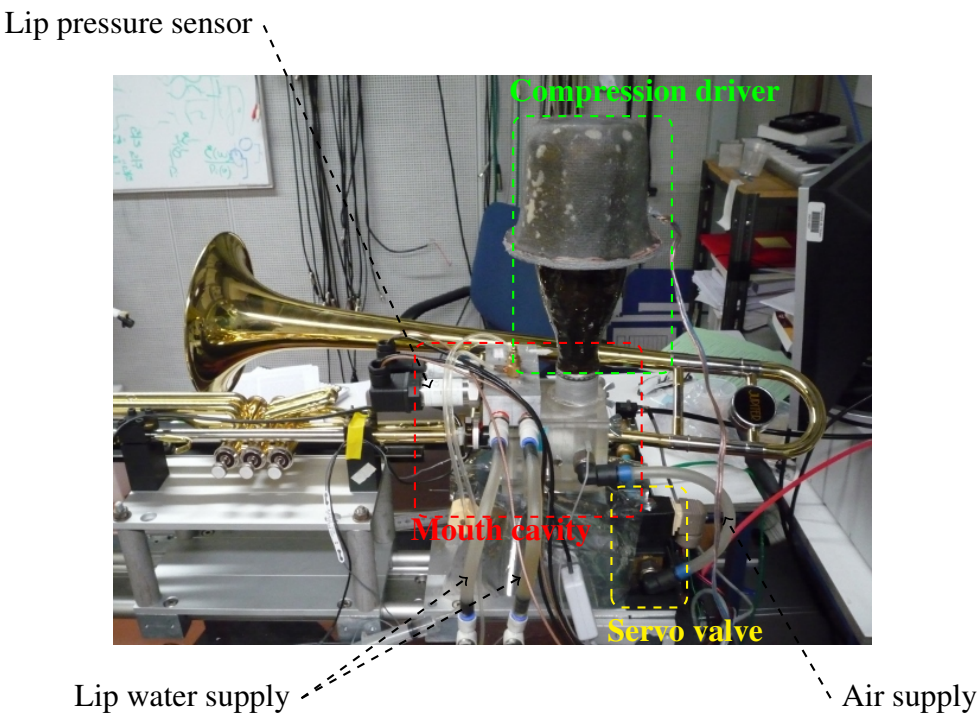

Figure 4.1 IRCAM artificial player system.

Various sensors embedded into the system allow access to the following variables:

- Water pressure in the lips, providing an image of the tension of each lip.

- Force applied by the lips on the mouthpiece.
- Quasi-static mouth pressure.
- Lip opening area measured using a light transmission method as described in previous studies (Vergez & Rodet, 1997; Bromage et al., 2010).

The communication between the control PC, the actuators, and the different sensors is performed through a dSpace© system including an input/output interface working at 1 kHz sampling frequency. This module also includes a digital signal processor that is programmed using a dSpace© software system interfacing with a Matlab-Simulink-RTW© environment (Lopes et al., 2003). This system therefore enables continuous streams of commands and data from the sensors. Feedback control on the actuator commands can be performed, allowing to maintain stable settings during experiments.

4.1.2 Inherent acoustical influence of the mouth cavity

By construction, the mouth cavity presents some acoustical characteristics potentially responsible for an inherent acoustical coupling with the lips. This upstream coupling may occur at frequencies where the amplitude of the upstream acoustic pressure is significant enough in front of the downstream pressure. Alternatively, by comparing the amplitude of the input impedance of the trombone and mouth cavity measured experimentally, we may assess the "default" acoustical influence of the mouth cavity.

The input impedance of the valve trombone used for experiments was measured in the valve position 000 (no valve pressed). Analogously, the input impedance of the mouth cavity was measured at the lips by removing the artificial lips from their enclosure and adjusting the mouth cavity against the impedance probe. Measurements were performed using the commercially available BIAS© measurement system (Widholm et al., 1989) and are presented in Fig. 4.2.

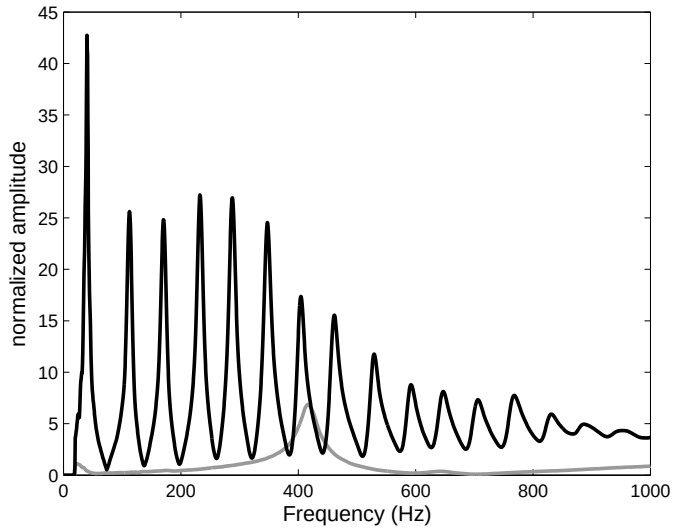

Figure 4.2 Amplitude of the downstream input impedance (black) and upstream input impedance (gray) in the default configuration. The upstream input impedance was measured by Nicolas Lopes using the BIAS© measurement system (Widholm et al., 1989) and mounting the mouth cavity on the probe at the level of the inter-dental orifice.

From Fig. 4.2, an upstream resonance is observed around 400 Hz. The amplitude of this impedance peak being less than half the amplitude of the closest downstream resonance, we consider that the default acoustical coupling with the mouth cavity is overall negligible in comparison with the acoustical feedback from the downstream air-column. We may further infer that, away from this upstream resonance, the acoustic pressure originating from this upstream feedback can be ignored in our active control approach and therefore assume that the mouth cavity behaves like an infinite volume reservoir of null input impedance ($Z_u \simeq 0$). Close to 400 Hz, a non-negligible upstream feedback may occur and a stronger external acoustic signal may be needed during active control to counterbalance the inherent effect of the mouth cavity.

4.1.3 Active control method

Under the assumption of a negligible acoustical feedback from the mouth cavity, a method based on the feedback control of the acoustic pressure created in the mouth cavity is developed. From Eq. 2.27 repeated here for convenience,

$$\frac{Z_u}{Z_d} = -\frac{P_u}{P_d}, \tag{4.1}$$

different conditions of acoustical coupling with the upstream system relative to the downstream system can be simulated at f_0. This is performed by adjusting the amplitude and phase of the pressure at the input of the mouth cavity P_u relative to the pressure at the input of the downstream air-column P_d. This approach hence requires to be able to estimate the amplitude and phase of P_d and P_u at f_0 through short window frames in order to allow for real-time adjustments of the amplitude and phase ratio between Z_u and Z_d. Note that this approach is not necessarily limited to a control at f_0 alone. Indeed, it could be theoretically possible to impose an upstream feedback with several harmonics of the fundamental frequency, but this was not tested in this study.

The overall principle of our active control approach is illustrated in Fig. 4.3. Input signals are the upstream and downstream acoustic pressures measured at the input of the upstream and downstream systems respectively. The output signal is the voltage $\zeta(t)$ at the terminals of a compression driver generating an acoustic flow into the mouth cavity and calculated from Eq. 4.2. The analyzer allows for real-time estimation of the amplitude and phase of P_u and P_d at the fundamental frequency f_0. A PID (proportional integral derivative) controller enables adjustment of $\zeta(t)$ according to the output of the analyzer and input commands from the user. The analyzer and controller blocks are detailed in the following paragraphs.

The spectral analyzer is implemented in programming language Max/MSP. This programming environment allows for the implementation of real-time digital signal processing tools op-

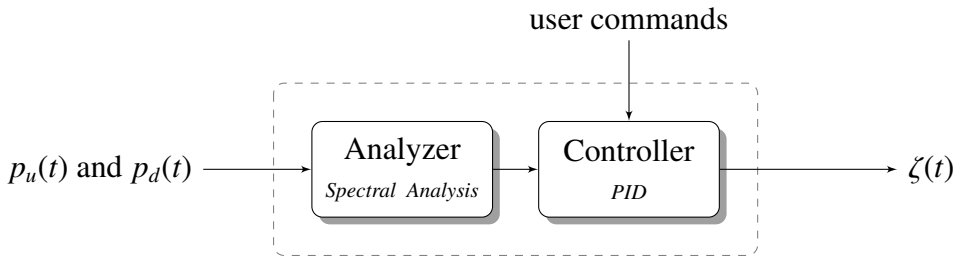

Figure 4.3 Active control method. The input signals are $p_u(t)$ and $p_d(t)$ measured by the upstream and downstream microphones, and the output signal is the electrical voltage at the terminals of the compression driver $\zeta(t)$. The spectral analysis and PID control are implemented using visual programming language Max/MSP.

erating at a high sampling rate suitable for audio applications. One issue concerns the pseudo real-time estimation of the amplitude and phase of $p_u(t)$ and $p_d(t)$ at the fundamental frequency f_0. The solution proposed is illustrated in Fig. 4.4. This method uses 2048-sample Fast Fourier transforms applied to modulated versions of $p_u(t)$ and $p_d(t)$. Calling N the FFT size ($N = 2048$ samples), the frequency step of analysis can then be calculated such as: $\eta = f_s/N$. The extraction of the fundamental frequency is achieved by Max/MSP external *fiddle~* (Puckette, 2012) which computes the value of f_0 over 2048-sample windows from the downstream pressure signal $p_d(t)$. In order to evaluate the phase and amplitude ratio of P_u to P_d at f_0, the spectral resolution needs to be increased around the fundamental frequency peak. This can be achieved by increasing the analysis window size N. Alternatively, the frequency sampling can be increased by applying zero padding to a smaller analysis window. The first approach is not compatible with our requirement of achieving a fast evaluation and is constrained by the boundary value imposed by Max/MSP (4096 samples in Max/MSP 6.1.3 32-bit). The second approach would slow down the process and is not permitted in Max/MSP. To solve this issue, we adopt the following strategy: at each time step, $p_u(t)$ and $p_d(t)$ are both modulated by a cosine signal of frequency $f_0 + \eta$. The modulated signals are then sent at the input of an *fft~* object of window-size 2048 samples and 0% overlap.

The amplitude and phase are extracted from the real and imaginary outputs of the *fft*~ object and stored in two buffers. The modulation applied before the FFT hence results in a displacement of the fundamental frequency peak to the second frequency bin of the computed spectrum (equivalent to ring modulation). The amplitude and phase values at the second bin are then read from the buffers for each computed FFT, at a rate imposed by the *fft*~ object.

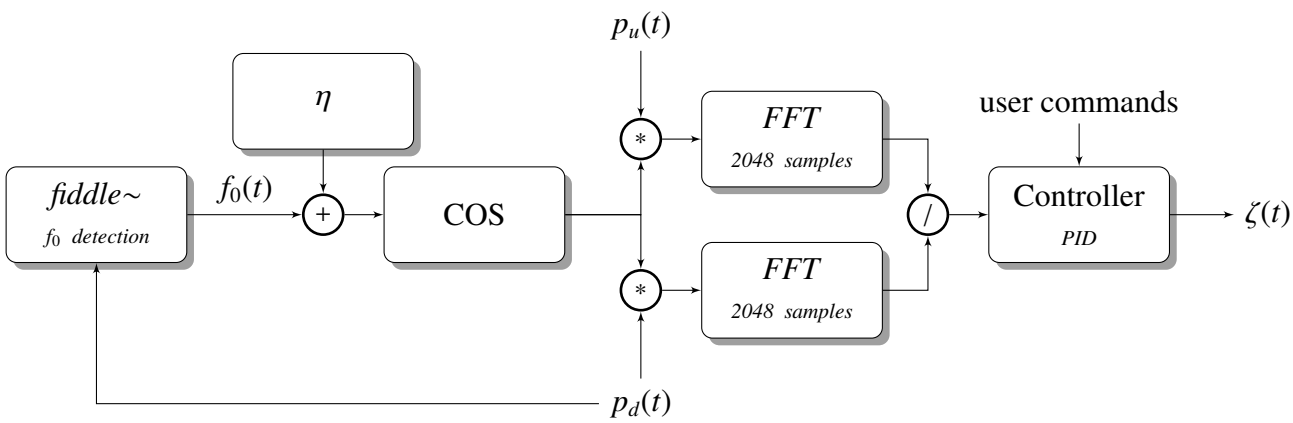

Figure 4.4 Diagram description of the analyzer implemented in Max/MSP.

The output parameter $\zeta(t)$ controlling the electrical voltage at the terminals of the compression driver is calculated from Eq. 4.2:

$$\zeta(t) = A(t) \cdot \cos\left[2\pi f_0(t)t + \phi(t)\right]. \tag{4.2}$$

Parameters $A(t)$ and $\phi(t)$ of the output signal $\zeta(t)$ are calculated from Eqs. 4.5 and 4.6, taking into account the amplitude and phase errors $e_a(t)$ and $e_p(t)$ calculated at each time frame by Eqs. 4.3 and 4.4:

$$e_a(t) = \left|\frac{P_u(f_0)}{P_d(f_0)}\right|_m (t) - \left|\frac{P_u(f_0)}{P_d(f_0)}\right|_c (t), \tag{4.3}$$

$$e_p(t) = \angle\left(\frac{P_u(f_0)}{P_d(f_0)}\right)_m(t) - \angle\left(\frac{P_u(f_0)}{P_d(f_0)}\right)_c(t), \tag{4.4}$$

where m and c subscripts indicate the "measured" and "command" quantities respectively.

Two PID controllers defined by Eqs. 4.5 and 4.6 are implemented using two Max/MSP sub-patches allowing for independent control of the amplitude and phase of the complex ratio P_u/P_d at f_0.

$$A(t) = K_{pa}e_a(t) + K_{ia}\int_0^t e_a(\tau)\,\mathrm{d}\tau + K_{da}\frac{\mathrm{d}}{\mathrm{d}t}e_a(t), \tag{4.5}$$

$$\phi(t) = K_{pp}e_p(t) + K_{ip}\int_0^t e_p(\tau)\,\mathrm{d}\tau + K_{dp}\frac{\mathrm{d}}{\mathrm{d}t}e_p(t), \tag{4.6}$$

The PID coefficients K_{pn}, K_{in} and K_{dn} (where $n = a$ for the amplitude and $n = p$ for the phase) are given in Table 4.1. These values are tuned empirically to allow for a fast response of the system, while maintaining stability and convergence of PID outputs.

PID coefficients	K_{pa}	K_{ia}	K_{da}	K_{pp}	K_{ip}	K_{dp}
Values	0.5	0.06	0	0.5	0.06	0

Table 4.1 PIDs coefficients

4.1.4 Description of the experimental setup

The experimental set-up used for the experiments is described in Fig. 4.5. It involves a downstream pressure transducer (Endevco© 8507C-2) mounted in the mouthpiece cup, an upstream pressure transducer (Endevco© 8507C-5) mounted in the mouth cavity just upstream from the lips, and a compression driver (AURA© 3 inch high-output miniature woofer) mounted on a glass fiber chamber. This enables to reduce the output diameter of the driver, and to connect it

to the mouth cavity. Audio input and output signals are managed by the same audio interface (MOTU©) running at 44.1 kHz. Prior to experiments a relative calibration of the two pressure transducers is performed. The two sensors are mounted on a aluminium tap closing a 30 cm long cylinder of diameter approximately 30 mm. At the other end of the cylinder, a compressor driver is fixed and a sweep generated between 10 Hz and 1 kHz. The amplitude ratio of the upstream to downstream transducer signals is found around 3.65 across the frequency range investigated. This value is then taken into account in the real-time control procedure. Commands of the artificial player are communicated through the dSpace© module working at 1 kHz. During acquisition, the quasi-static mouth pressure, as well as the force applied on the lips are recorded using the dSpace©. Furthermore, since the gain knobs of the I/O audio interface do not enable precise adjustment of the gain of each channel, a Max/MSP subpatch was used before acquisition to calculate correction coefficients for each channel so that the resulting gains applied to input signals are equal.

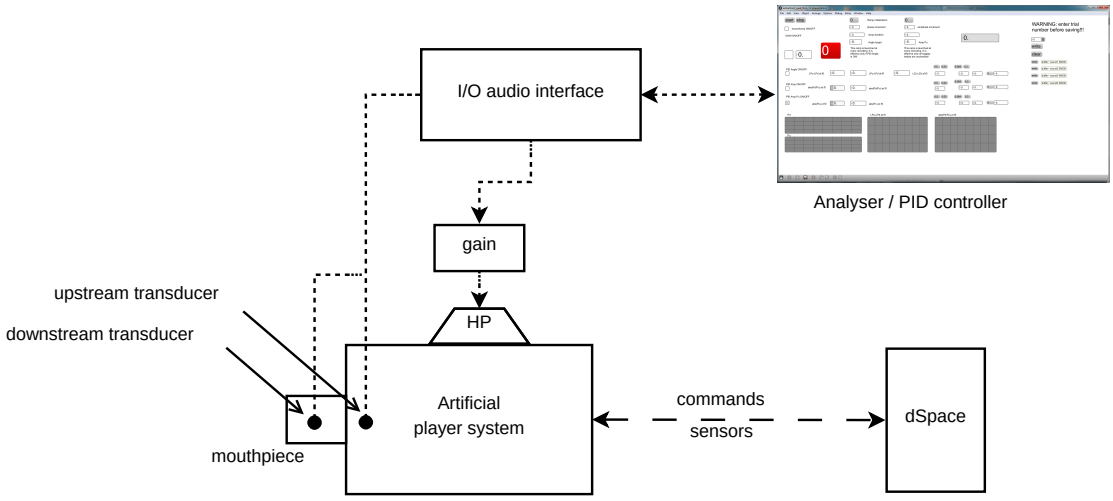

Figure 4.5 Diagram of the experimental setup. Signals from the downstream and upstream pressure transducers are recorded by an audio interface running at 44.1kHz and used for the active control. Commands and data from sensors are managed by a dSpace© module working at 1kHz.

Lip opening is simultaneously monitored using a light transmission method; a LED array fixed at the back of the mouth cavity emits an infrared radiation which is captured by a photo transistor mounted in the mouthpiece of the instrument. Although the relationship between the signal at the transistor output and the lip opening area may be not proportional, we consider that the photo transistor output is in phase with the lip opening area at the fundamental frequency of vibration. This signal is therefore recorded through the audio interface for further analysis.

4.2 Investigation on the effects of the phase at f_0

4.2.1 Experimental protocol

Two acoustic upstream amplitude conditions were simulated. In the first one, the amplitude of the upstream acoustic pressure is controlled so that it remains constant, regardless of variations in the downstream acoustic pressure produced. This first condition aims at maintaining constant the acoustic energy generated on the upstream side of the lips at f_0. In the second condition, the acoustic upstream amplitude is controlled so that the amplitude ratio $\left|\frac{P_u(f_0)}{P_d(f_0)}\right|$ is maintained constant (this second condition accounts for maintaining the amplitude ratio of the upstream to downstream impedances constant along the experiment).

In both conditions, experiments are conducted according to the following sequence:

1. Find a proper control parameter setting (input volume flow, lip tension) to obtain a steady and clear tone without active control.

2. Preset active control parameters to the observed phase difference between $P_u(f_0)$ and $P_d(f_0)$ without active control (which results from the weak acoustical coupling with the mouth cavity).

3. Set a command value for $|P_u(f_0)|$ (constant upstream acoustic energy condition) or for

$\left|\frac{P_u(f_0)}{P_d(f_0)}\right|$ (constant Z_u to Z_d amplitude ratio condition).

4. Turn the active control on.

5. While maintaining a constant amplitude condition, sweep linearly the phase difference $\angle P_u(f_0) - \angle P_d(f_0)$ over a range of 240° in 60 s, which is equivalent to sweeping the phase difference at a rate of 4°/s.

Because vocal-tract influence is expected in the higher register of the instrument as shown by measurements on human subjects (Chapter 3), we try to focus on the highest tones that can be produced by the artificial player without upstream feedback.

4.2.2 Constant acoustic upstream energy condition

Data from a 60-second recording with constant upstream energy condition ($|P_u|$ is a constant) are presented in Fig. 4.6. The sounding frequency is close to 415 Hz (A♭4) corresponding to the seventh resonance of the trombone resonator. It is worth noting that this frequency matches with the location of an impedance peak of the mouth cavity (Fig. 4.2). This resonance may thus contribute to support oscillations of the system at this frequency when active control is turned off. As the pressure transducers capture both acoustic and quasi-static pressures, the quasi-static mouth pressure p_0 is obtained by low-pass filtering the upstream transducer signal.

We first notice that the linear sweep of the phase difference $\angle Z_u - \angle Z_d$ and the constant upstream acoustic energy are well achieved over the first 38 seconds. The system maintains stable oscillations for 38 seconds before entering into a more turbulent regime, certainly due to the destructive phase tuning imposed by the controller and not supported by the lips. At time 46 seconds, active control is stopped and the lip oscillations return to their initial sustained condition.

Regarding the stable sounding section (from 0 to 38 s), we observe that, despite a constant acoustic energy on the upstream side, the linear phase shift induces significant f_0 variations from

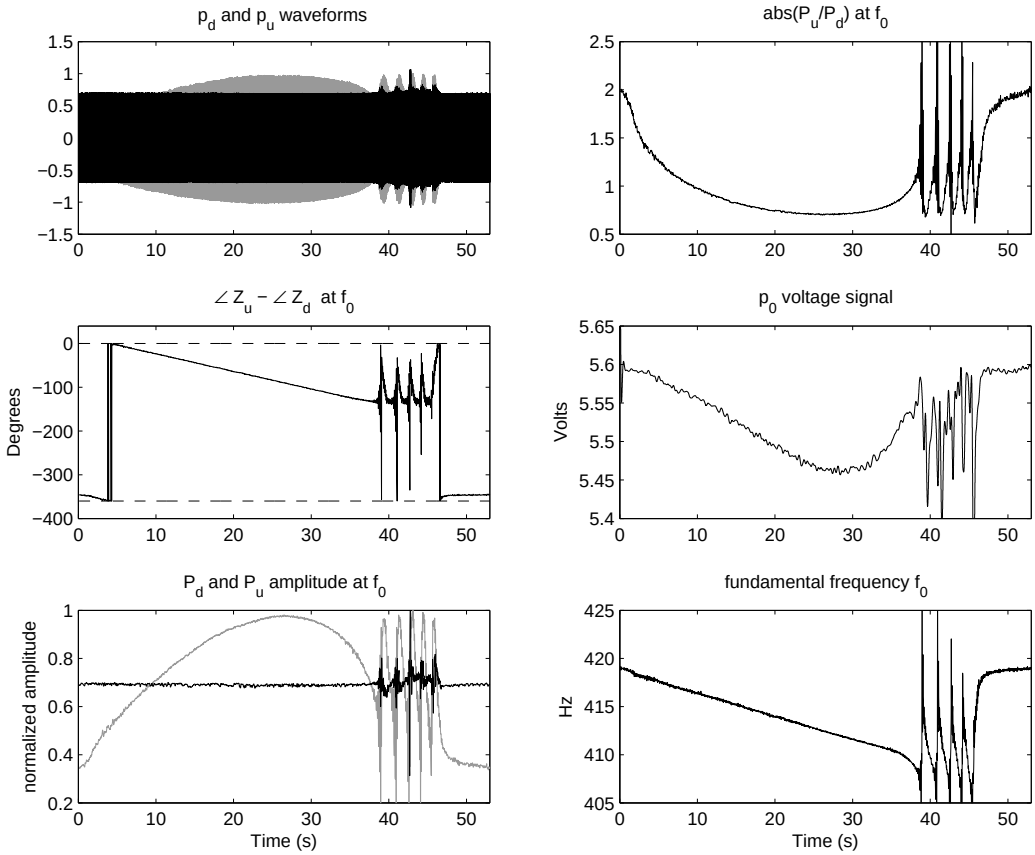

Figure 4.6 Sustained A4♭ with linearly varying phase difference between P_u and P_d at f_0 and amplitude of P_u maintained constant. Left column from top to bottom: P_d (gray) and P_u (black) waveforms; phase difference between Z_u and Z_d at f_0; P_d (gray) and P_u (black) amplitudes at f_0 normalized to the maximum value of P_d. Right column from top to bottom: P_u to P_d amplitude ratio at f_0; quasi-static mouth pressure p_0 (output voltage of the transducer), instantaneous fundamental frequency f_0.

418 Hz to 408 Hz, as well as a maximum of downstream pressure energy at f_0 correlated with a minimum of quasi-static mouth pressure. We note however that the observed decrease in p_0 is about 2.5 % of p_0 maximum value, which makes these variations almost negligible.

These results can be further analyzed with regards to variations of the downstream input impedance Z_d, upstream input impedance Z_u and total series impedance Z at the fundamental

frequency of the sound. From Eq. 4.1, the complex value of Z_u can be derived at frequencies where acoustic energy is observed from the measurement of Z_d. Using the BIAS© measurement system (Widholm et al., 1989), the input impedance of the valve trombone with mouthpiece, normalized by its characteristic impedance Z_c, was measured. The amplitude and phase of Z_d/Z_c are presented in Fig. 4.7.

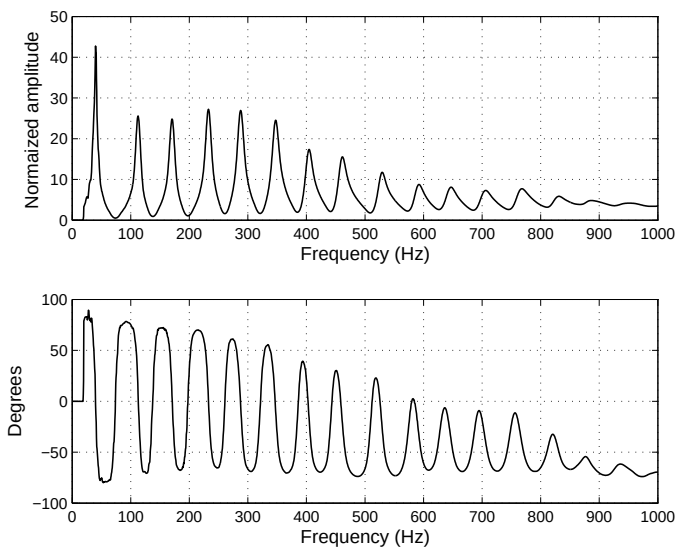

Figure 4.7 Input impedance of the valve trombone. Amplitude (top) and phase (bottom) of the input impedance of the valve trombone (fingering 000) with mouthpiece, normalized to the characteristic impedance Z_c of a cylindrical tube of cross-sectional area equal to the entry cross section of the mouthpiece.

The temporal evolution of the phase and amplitude of Z_d, Z_u and $Z = Z_d + Z_u$ at f_0 are displayed in Fig. 4.8. Variations of the playing frequency observed in Fig. 4.6 (decrease in f_0 with time) results in an increase in Z_d amplitude with time as predicted by Fig. 4.7. The constant upstream acoustic energy condition results in a 'U' shape variation of $|Z_u|$ amplitude at f_0; the magnitude of Z_u is higher than Z_d for the first 9 s, therefore providing the main support to lip oscillations. Past this point, $|Z_u|$ remains below $|Z_d|$ before growing again until the unstable regime at t=38 s. The amplitude of the total impedance Z decreases with time. The linear phase sweep of

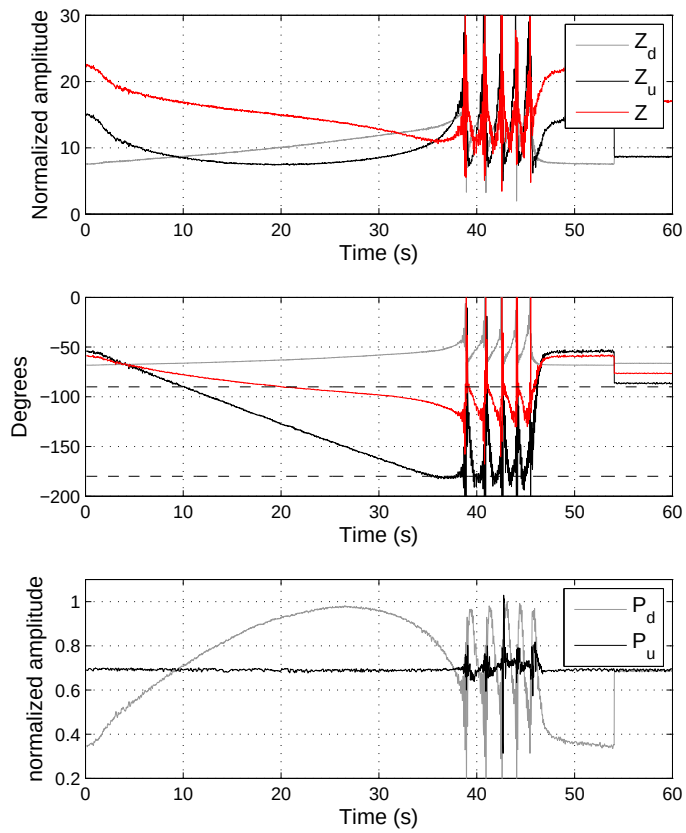

Figure 4.8 Temporal evolution of Z_d, Z_u and Z in the constant upstream energy condition. Amplitude (top) and phase (middle) of Z_d measured experimentally (solid line), as well as Z_u (black) and Z (red) at frequencies where acoustic energy is observed. The two horizontal dashed lines indicate -90 and -180° phase angles. Bottom: P_d (gray) and P_u (black) amplitudes at f_0 normalized to the maximum of P_d.

$\angle P_u - \angle P_d$ results in a linear increase of the distance between $\angle Z_u$ and $\angle Z_d$. Both phase of Z_d and Z_u remain negative during the experiment, indicating a compliant coupling with the downstream and upstream systems. According to Fletcher (1993), these characteristics of the upstream and downstream impedances are favorable to an outward striking mechanism of the lip-valve system. At time t=0 s, $\angle Z_d$ and $\angle Z_u$ are very close and at time t=4 s, Z_d and Z_u are in phase. This constructive phase tuning in the beginning of the experiment contributes to the amplitude of the

total impedance Z. The slight increase of $\angle Z_d$ and significant decrease in $\angle Z_u$ cause a marked decrease of $\angle Z$ with time. We notice that at time t = 20 s, $\angle Z = -90°$. The nature of this point will be further discussed in Section 4.2.5. The lips enter an unstable regime of oscillation when $\angle Z_u$ reaches -180°. The active control forces $\angle Z_u$ towards a phase reversal to +180° that the lip oscillator does not seem to support. This instability may be caused by the transition from a capacitive to an inductive upstream coupling, the latter being unfavorable to the mechanism of lip oscillation. This hypothesis may be drawn in conjunction with the large value of the phase difference between Z_d and Z_u reached when the turbulent regime is initiated. Finally, we observe that the downstream pressure maximum does not match with a $|Z_d|$ peak value. This observation hence suggests that this maximum in downstream pressure may not be due only to an increase in downstream acoustical support but rather to a beneficial phase tuning of Z_u relative to Z_d at f_0.

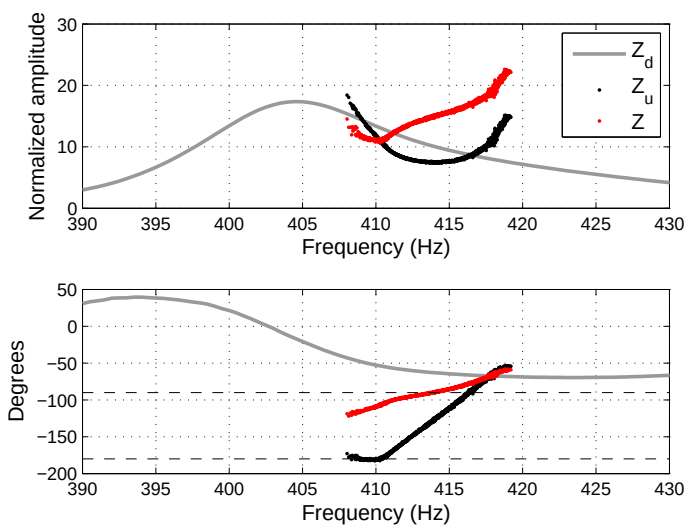

Figure 4.9 Z_d, Z_u and Z in the constant upstream energy condition. Amplitude (top) and phase (bottom) of Z_d measured experimentally (solid line), as well as Z_u (black) and Z (red) at frequencies where acoustic energy is observed. The two horizontal dashed lines indicate -90 and -180° phase angles.

The frequency-domain evolution of data from Fig 4.8 is displayed Fig. 4.9. This representa-

tion clearly shows that oscillations of the lips occur on the right side of a downstream impedance peak, that is on the negative phase side of the corresponding downstream resonance, hence supporting an outward striking behaviour. The 'U' shape variation of the amplitude of Z_u is also appearing in the frequency domain since f_0 varies linearly with $\angle Z_u - \angle Z_d$. As described in the time domain, the emergence of an unstable regime occurs around 410 Hz where $\angle Zu \simeq 180°$.

4.2.3 Constant P_u to P_d amplitude ratio condition

Data from a second experiment with constant unitary $\left|\frac{P_u}{P_d}\right|$ condition are presented in Fig. 4.10. As in previous experiment, stable oscillations are observed until $t \simeq 38$ s where the lips enter an unstable regime. At time 43 seconds, active control is stopped and the lip oscillations return to their initial, sustained condition. The variations of P_d and P_u at f_0 over the stable region show that the active control system was able to follow the amplitude constraints on P_u quite accurately. This is also confirmed by the almost flat unitary amplitude ratio P_u/P_d. However, a slight time lag between P_d and P_u traces is observed, highlighting the intrinsic delay of the active control algorithm. This time lag may be reduced by re-adjusting the PID coefficients K_{pa}, K_{ia} and K_{da}. The variations of f_0 are smaller than in the constant upstream energy condition: f_0 varies from 416.5 Hz to 408 Hz in a less linear fashion than in the previous condition despite an almost identical variation of $\angle Z_u - \angle Z_d$ in both conditions. A maximum of downstream and upstream energy is observed around t = 28 s, matching with a minimum of quasi-static mouth pressure. In this case again, the variation in p_0 represents 2.2 % of the maximum value, which makes these variations negligible.

Regarding the temporal evolution of Z_d, Z_u and Z represented in Fig. 4.11, we observe that Z_d and Z_u amplitudes grow smoothly and almost perfectly overlap until 32 s when $\angle Z_u - \angle Z_d$ becomes very large (>100°). The amplitude of Z is merely constant along the stable oscillation part. As a result of this constant unitary upstream to downstream energy ratio, the phase of Z at f_0

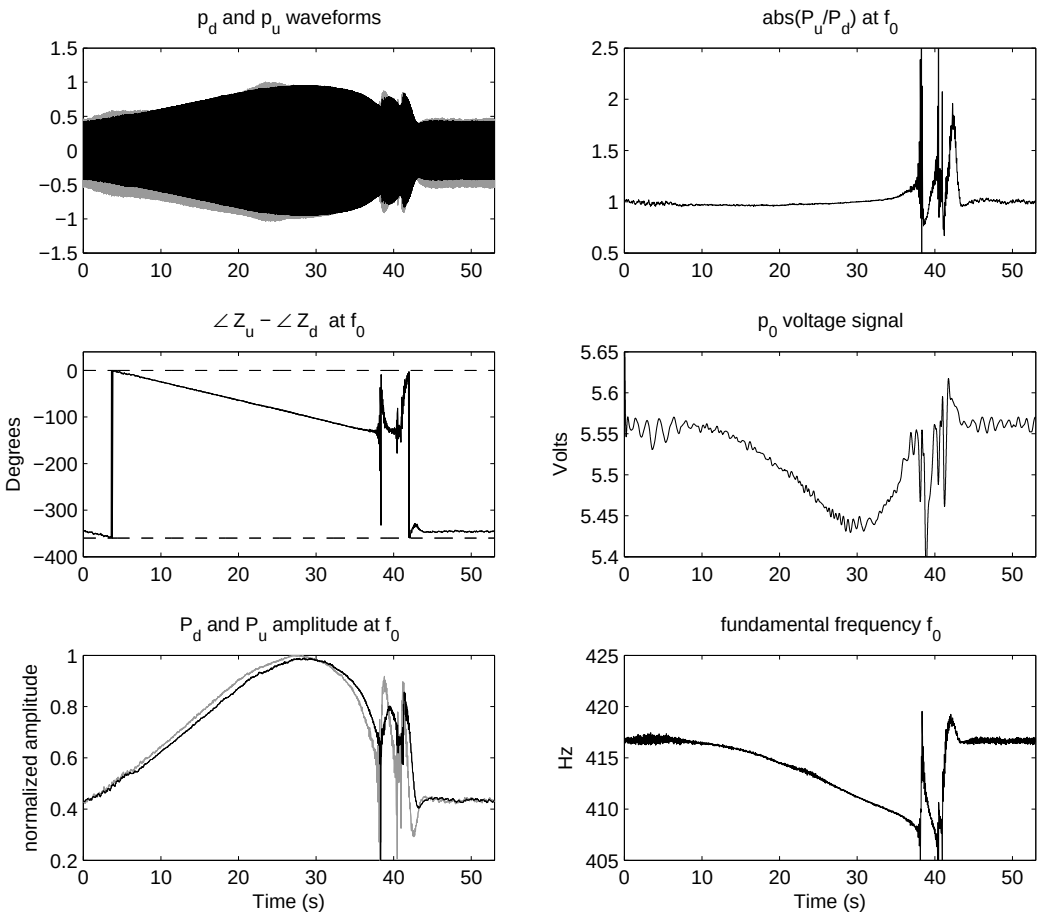

Figure 4.10 Sustained A4♭ with linearly varying phase difference between P_u and P_d at f_0 and amplitude ratio of P_u to P_d maintained constant and equal to unity. Left column from top to bottom: P_d (gray) and P_u (black) waveforms; phase difference between Z_u and Z_d at f_0; P_d (gray) and P_u (black) amplitudes at f_0 normalized to the maximum value of P_d. Right column from top to bottom: P_u to P_d amplitude ratio at f_0; quasi-static mouth pressure p_0 (output voltage of the transducer), instantaneous fundamental frequency f_0.

remains equally spaced from $\angle Z_d$ and $\angle Z_u$ when oscillations are stable. Similarly to the previous experimental condition, $\angle Z$ intersects the -90° line at time t = 18 s. This particular point will be further discussed in Section 4.2.5. We also observe that, in contrast to the previous condition, the unstable regime originates slightly before $\angle Z_u$ reaches -180°. This suggests that this unstable

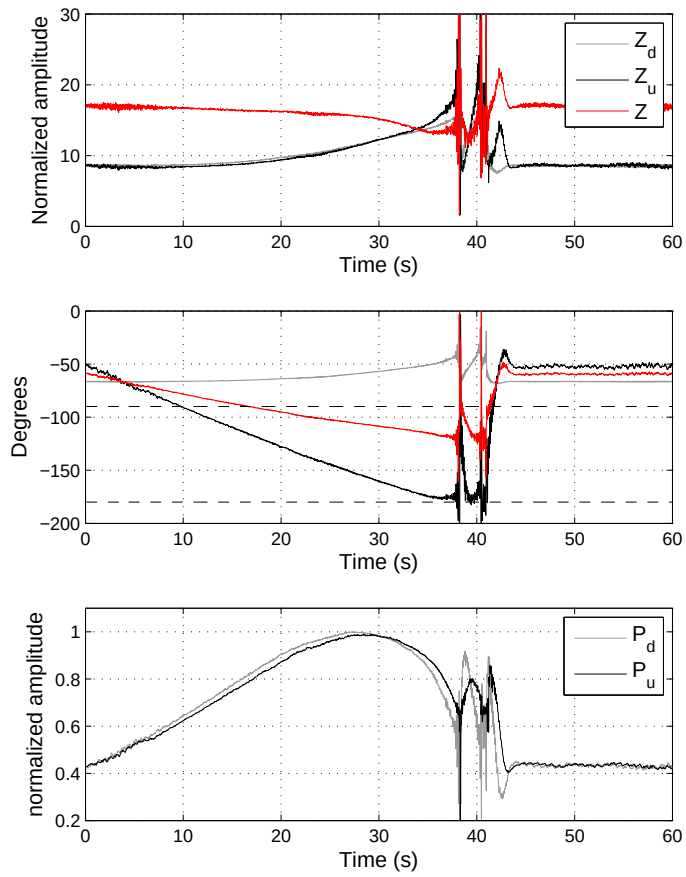

Figure 4.11 Temporal evolution of Z_d, Z_u and Z in the constant amplitude ratio condition. Amplitude (top) and phase (middle) of Z_d measured experimentally (solid line), as well as Z_u (black) and Z (red) at frequencies where acoustic energy is observed. The two horizontal dashed lines indicate -90 and -180° phase angles. Bottom: P_d (gray) and P_u (black) amplitudes at f_0 normalized to the maximum of P_d.

regime is primarily caused by the significant phase difference between Z_u and Z_d, rather than the low value of $\angle Z_u$.

Represented in the frequency domain (Fig. 4.12), the constant Z_u to Z_d amplitude ratio condition (stable between 410 Hz and 416.5 Hz) appears through the overlapping $|Z_d|$ and $|Z_u|$ curves. The decaying amplitude of Z is due to the increasing phase difference $\angle Z_u - \angle Z_d$.

Overall, we observe that both upstream control conditions (i.e. constant amplitude and constant amplitude ratio) cause equivalent effects on the behaviour of the system: a decrease of the playing frequency and variation of the acoustic energy produced, accompanied by small variations of the quasi-static mouth pressure. It is important to remember that during experiments, the electrical voltage at the servo-valve controlling the volume flow entering the mouth cavity was maintained constant. Assuming that the impedance of the air supply system (upstream from the servo valve) is very large compared to the impedance of the artificial mouth (downstream from the valve), we can consider that a constant electrical voltage at the servo valve is equivalent to a constant input flow condition in the mouth cavity. Consequently, the minimum observed in p_0 voltage may result from a minimum of lip resistance or maximum of lip transverse (vertical) displacement.

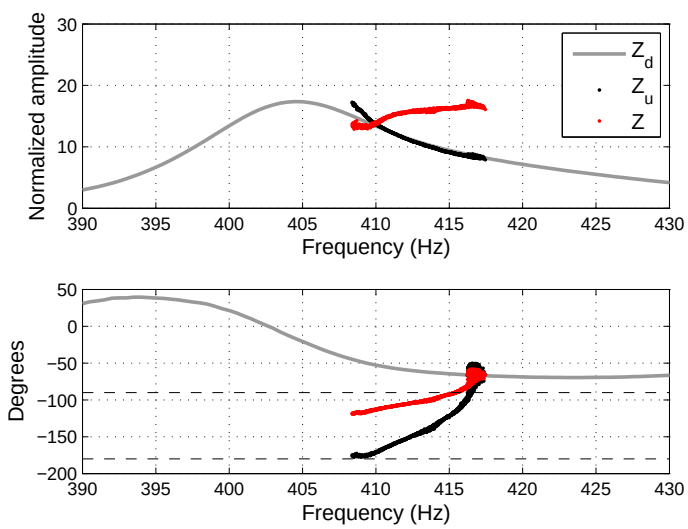

Figure 4.12 Z_d, Z_u and Z in the constant amplitude ratio condition. Amplitude (top) and phase (bottom) of Z_d measured experimentally (solid line), as well as Z_u (black) and Z (red) at frequencies where acoustic energy is observed. The two horizontal dashed lines indicate -90 and -180° phase angles.

4.2.4 Comparison between different upstream levels within the constant upstream energy condition

We have observed that the constant upstream energy condition results in a linear variation of f_0 with $\angle Z_u - \angle Z_d$. In order to investigate the influence of upstream energy amplitude on the linear decay of f_0, we reiterate our experiment with different levels of upstream acoustic energy. We refer to the three upstream levels as the percentage of the higher level produced. Using this convention, results presented in Fig. 4.9 refer to an 85.6% upstream energy level. Figures 4.13 and 4.14 show frequency domain representations of Z_d, Z_u and Z during experiments with 59% and 100% upstream energy level respectively.

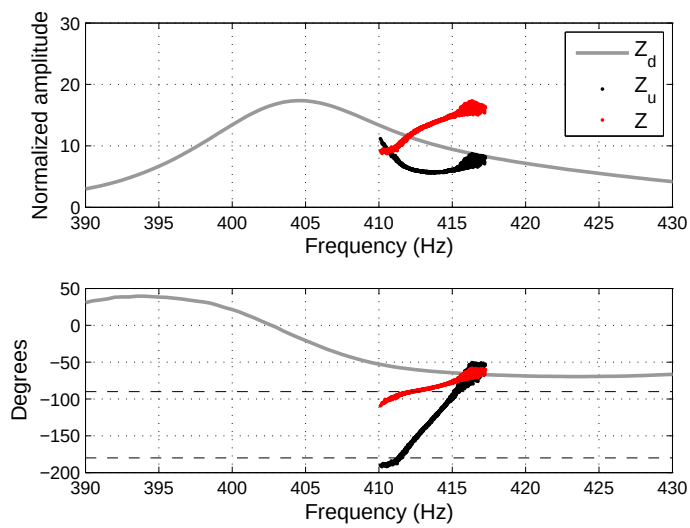

Figure 4.13 Constant acoustic upstream energy condition (upstream level: 59% of the maximum level).

From Figs. 4.13 and 4.14, we observe that increasing P_u amplitude in the constant upstream energy condition increases the range of sounding frequencies. The effect of the different upstream levels on the variations of f_0, p_0 and the downstream acoustic energy (defined as $|P_d(f_0)|$) are summarized in Fig. 4.15. Increasing the amplitude of the upstream signal has a significant

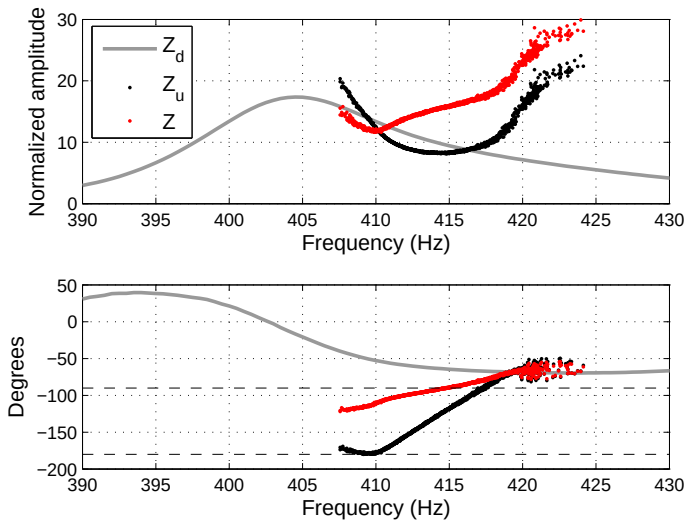

Figure 4.14 Constant acoustic upstream energy condition (upstream level: 100% of the maximum level).

effect on both variations of playing frequency and variations of the downstream acoustic energy produced at f_0. On the contrary, variations of p_0 only reach 3% of the maximum value for the highest upstream level condition.

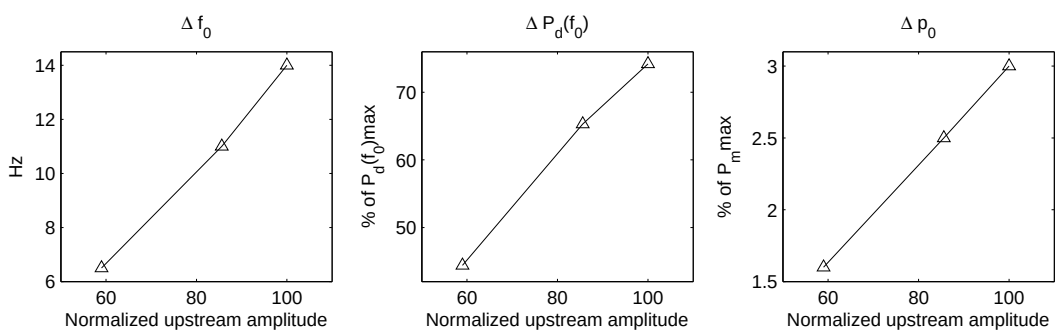

Figure 4.15 Variations of f_0, downstream acoustic energy, and p_0, during active control in three constant upstream energy condition: 59 %, 85 % and 100 % acoustic upstream energy at f_0.

4.2.5 Analysis of the results in light of the linear theory of oscillation

The experimental results presented in the previous section can be further discussed in light of the linear theory of oscillation. From the linearized flow equation given by Eq. 2.18, an adjusted condition of regeneration can be written:

$$\frac{1}{Z} = \sqrt{\frac{2p_0}{\rho}} \cdot G, \tag{4.7}$$

where ρ is the average air density, $Z = Z_d + Z_u$ is the total impedance seen by the lips, and $G = S_{lip}/\Delta P$ is the adjusted lip mobility where S_{lip} denotes the lip opening area and $\Delta P = P_d - P_u$.

From Eq. 4.7, we hence derive the adjusted phase condition of regeneration given by Eq. 3.8, and repeated here for convenience:

$$\angle Z + \angle G = 0. \tag{4.8}$$

In accordance with Eq. 4.8, by lowering the phase of the total impedance Z, the simulated upstream coupling requires the phase of G to be modified and therefore the playing frequency to be displaced. Assuming a one-mode mechanical model underlying the dynamics of the artificial lips, this effect will result in displacing the playing frequency further away or closer to a mechanical resonance of the lips. In turn, this may either reduce or emphasize the amplitude of lip oscillations.

The mechanical response of the lips to the acoustic driving pressure can be formulated such as:

$$H = \frac{S_{lip}}{P_u - P_d} = -\frac{S_{lip}}{\Delta P}, \tag{4.9}$$

which, from the expression of G leads to:

$$\angle G = \angle H - \pi. \tag{4.10}$$

Consequently, from Eqs. 4.8 and 4.10, an estimation of the phase of the mechanical response of the lips $\angle \hat{H}$ can be derived in light of the linearized flow equation (Eq. 4.7):

$$\angle \hat{H} = \pi - \angle Z. \tag{4.11}$$

The phase is a relevant quantity in order to identify the location of lip mechanical resonance. According to the underlying mechanism of the lips, a phase angle of -90° at the resonance is proper to inward striking reeds whereas a phase angle of +90° characterizes an outward striking reed system (see Chapter 2). Following this approach, observations of $\angle \hat{H}(\omega)$ derived from $\angle Z$ in the 85 % constant upstream amplitude condition (Fig. 4.16) suggests the existence of an outward mechanical resonance around 414 Hz where $\angle \hat{H} = +90°$. From the magnitude of the downstream acoustic volume flow U_d calculated from $Z_d = P_d/U_d$ (Fig. 4.17), we notice that the maximum in U_d occurs around 414 Hz, also suggesting a maximum in lip displacement at this frequency.

4.2.6 Comparison between $\angle \hat{H}$ and $\angle H$

In order to evaluate the validity of the linear assumption represented by Eq. 4.7, the phase of the lip mechanical response at the fundamental frequency $\angle H(f_0)$ is calculated from the values of $\angle \Delta P(f_0)$ and $\angle S_{lip}(f_0)$ measured optically. The light transmission method applied to the system allows a signal correlated to the lip opening area to be monitored. We assume that this signal is in phase with S_{lip} at f_0. Using Eq. 4.9, we calculate the phase of $H(\omega)$ at frequencies where acoustic energy is produced. The values of $\angle \hat{H}(f_0)$ and $\angle H(f_0)$ in the 85% constant upstream amplitude condition are represented in Fig. 4.16. We first notice that the two curves follow a similar trend and show similar features (small inflections around 411 Hz and 415 Hz). However, a significant

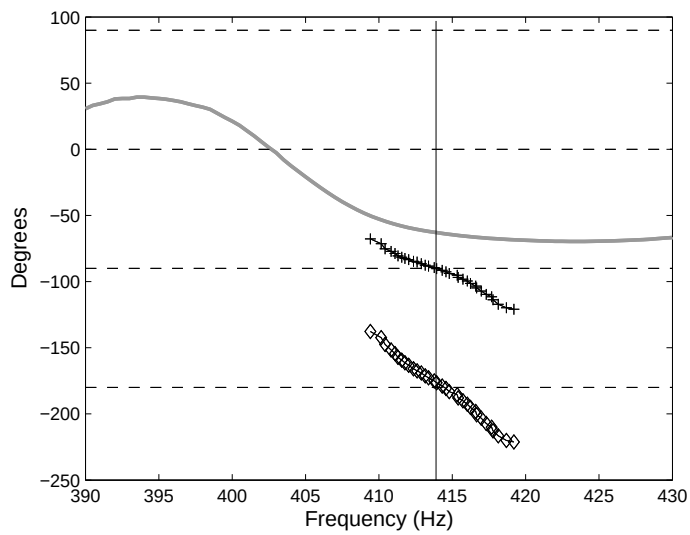

Figure 4.16 $\angle Z_d$ (gray), $\angle \hat{H}$ (crosses), and $\angle H$ (diamonds) during 85 % constant acoustic upstream energy condition. The vertical solid line indicates the frequency at which $\angle \hat{H} = -90°$.

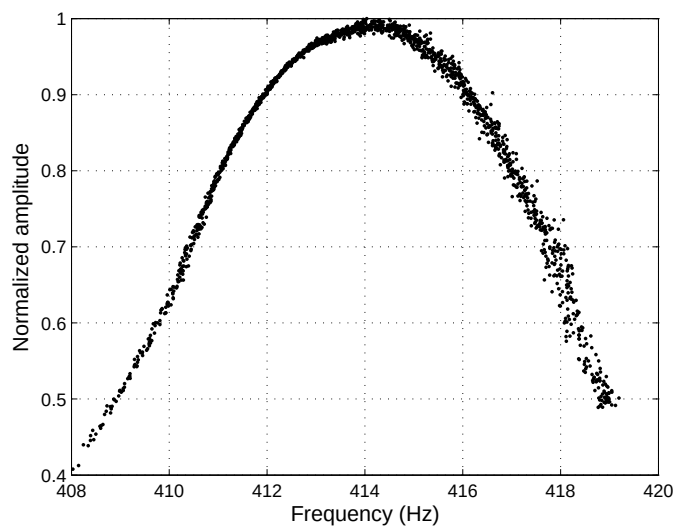

Figure 4.17 Normalized downstream acoustic volume flow U_d as as function of the playing frequency f_0 in the 85 % constant acoustic upstream energy condition.

offset between the phase of $\hat{H}$ and H at f_0 is observed across the frequency range of interest. This phase shift spreads between 100° at 419 Hz and 70° at 409 Hz, suggesting that the acoustical components of the upstream and downstream pressures cannot be neglected in the flow equation.

In order to identify the influence of upstream feedback on the difference observed between $\angle\hat{H}$ and $\angle H$, those two values are compared in the "no active control condition". The amplitude and phase of Z_d, Z_u and Z without active control are presented in Fig. 4.18. The almost-null inherent effect of the mouth cavity results in Z overlapping with Z_d on both amplitude and phase figures. The values of $\angle\hat{H}(f_0)$ and $\angle H(f_0)$ derived from this experiment are shown in Fig. 4.19. At 407.8 Hz, the difference between $\angle\hat{H}$ and $\angle H$ is about 50°, corresponding to a delay of 0.34 ms between S_{lip} and the downstream volume flow U_d. In the 85 % case, 70° are observed between $\angle\hat{H}$ and $\angle H$ at 409.5 Hz, corresponding to a delay of 0.47 ms.

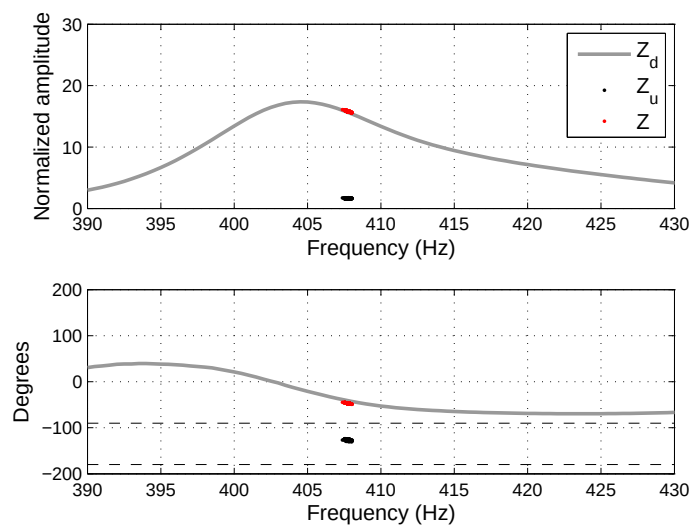

Figure 4.18 Z_d, Z_u and Z without active control. Amplitude (top) and phase (bottom) of Z_d measured experimentally (solid line), as well as Z_u (black) and Z (red) at frequencies where acoustic energy is observed during a sustained tone without active control.

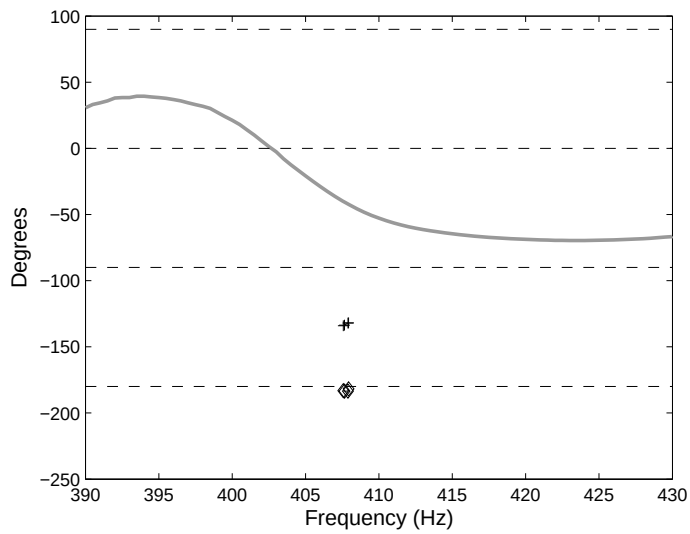

Figure 4.19 $\angle Z_d$ (gray), $\angle \hat{H}$ (crosses), and $\angle H$ (diamonds) without active control.

Results from the 59 % case are presented in Fig. 4.20. We observe that the smaller upstream feedback slightly reduces the difference between $\angle \hat{H}$ and $\angle H$; as an example, at 415 Hz, $\angle \hat{H}$ and $\angle H$ differ by 87.5° in the 59 % condition, corresponding to a delay of 0.56 ms between S_{lip} and U_d. In the 85 % condition, the 89.5° is equivalent to a delay of 0.6 ms at 415 Hz.

Different hypotheses may be formulated in order to explain this significant disagreement between $\angle \hat{H}$ and $\angle H$. Overall, the phase angle difference reveals that S_{lip} lags behind the downstream acoustic flow U_d by more than 70°. Moreover, we observe that even in the presence of a negligible upstream feedback (active control turned off), the difference between $\angle \hat{H}$ and $\angle H$ remains relatively high, suggesting that the upstream acoustic wave has a limited effect on the observed non-linear relationship between S_{lip} and U_d.

The first question to address concerns the possible synchronization issues between the two signal paths. The two signals from the pressure transducer follow identical and parallel pathways in terms of hardware and digital processes. However, the signal from the optical sensor is not processed in the same way in the Max/MSP patch, particularly since it does not need to be

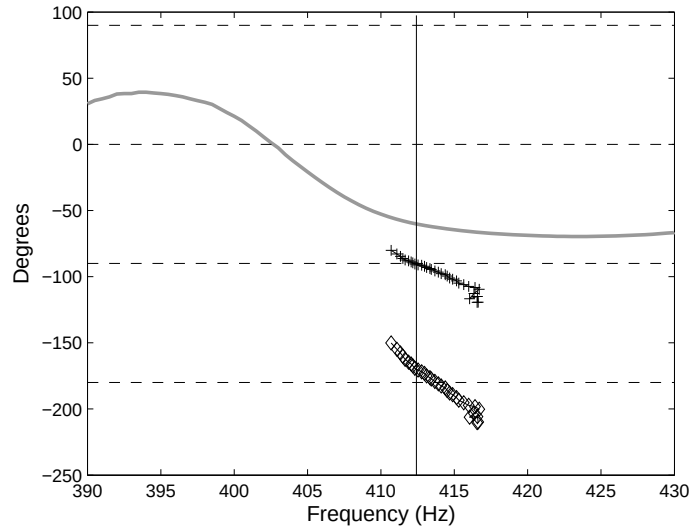

Figure 4.20 $\angle Z_d$ (gray), $\angle \hat{H}$ (crosses), and $\angle H$ (diamonds) during 59 % constant acoustic upstream energy condition. The vertical solid line indicates the frequency at which $\angle \hat{H} = -90°$.

rescaled for the active control procedure. Firstly, the synchronization of the three channels is tested using a common signal. Secondly, synthetic signals are used to investigate possible delays between different pathways in our Max/MSP patch. Although no delay was observed between acoustic pressure and the optical lip signals, some instances of desynchronization between the optical and the two pressure signals were recorded for some patch modifications (linking several *send~* and *receive~* in cascade for example). Even it there is no evidence that the observed delay could be attributed to this defect, these tests highlight the limitations of Max/MSP in providing a robust synchronized acquisition interface. For this reason, a more consistent way to record and prevent synchronization issues should be developed, trying to find an alternative to programming environments such as Max/MSP for which signal processing and precise time locking are not the primary purpose.

Regarding physical causes likely to explain the observed result, we may infer that the artificial lips require less static pressure than human lips to oscillate, making the acoustic components

$p_d(t)$ and $p_u(t)$ not negligible anymore in front of the static component p_0. Additionally, one may point out the possible effect of the longitudinal lip motion responsible for an additional flow component U_{add} ahead of the transverse motion of the lips. However, the ability of this flow component to distort the resulting downstream flow in that extent seems very unlikely. A last hypothesis relies on the potential distortion induced by the optical system of capture which is potentially responsible for a phase distortion of the signal at f_0.

4.3 Summary

In this chapter, we have developed a method to simulate different conditions of acoustical coupling between the lips and the upstream airways on an artificial trombone player system. Using this method, the influence of the amplitude and phase of an upstream resonance near the playing frequency was investigated by applying an active control approach on the fundamental component of the acoustic wave generated in the mouth cavity.

Variations of the phase of Z_u relative to Z_d at f_0 have a significant influence on the playing frequency and on the acoustic energy produced. These results suggest that it is therefore possible to vary the characteristics of the radiated sound (pitch in particular) through vocal-tract adjustments only, and without any change in lip and blowing parameters. Two conditions were investigated where either the upstream acoustic feedback or P_u to P_d amplitude ratio were maintained constant. In both conditions, a peak in downstream energy uncorrelated with $|Z_d|$ maximum was observed, suggesting that this maximum in downstream pressure is not due to an increase of downstream support but rather to a beneficial phase tuning of Z_u relative to Z_d at f_0.

In light of the linear theory of oscillation, results suggest that appropriate upstream tuning allows the playing frequency to be displaced near the resonance frequency of the lip-valve system. Playing near a lip resonance may contribute to increase lip motion and generate a larger acoustic

volume flow into the instrument. However, comparisons with a direct estimation of the phase of the lip mechanical response show significant discrepancies. Overall, the volume flow is found to lead the lip opening area by up to 90° at the fundamental frequency. These observations suggest either a synchronization defect induced by hardware or software processes, a significant distortion of the system of capture of the lip opening, or a particular physical behaviour of the artificial lips. For instance, it is possible that artificial lips require low upstream static pressure, making the linear assumption on the flow equation not valid. They may also significantly oscillate in the longitudinal direction, inducing a volume-flow component ahead of lip opening that contributes to some extent to the observed phenomenon.

Nevertheless, these experimental results support the possibility that a displacement of the playing frequency close to a resonance frequency of the lips can be induced by a specific tuning of the vocal-tract at f_0. In addition, they encourage further evaluation of whether observations of the lip mobility, as performed in trombone players in Chapter 2, provide a reasonable view of the variations of downstream and upstream coupling characteristics at the playing frequency.

Chapter 5

Numerical Simulations of Vocal-Tract Influence on Physical Models of the Lips

In Chapter 4, the influence of an upstream coupling with varying phase and amplitude characteristics at f_0 was found to produce substantial variations in the playing frequency and acoustic energy produced. The maximum of downstream acoustic energy, uncorrelated to a maximum in Z_d amplitude, suggests that an optimal upstream phase tuning allows the playing frequency to be displaced near a mechanical resonance of the lips. To further explore this hypothesis, this experimental approach is transposed to numerical simulations where all parameters of the problem are now controlled.

In this chapter, we investigate numerically the influence of different conditions of upstream coupling on the behaviour of a player-instrument system. Different physical models of the lips are implemented. The downstream resonator is represented in terms of its reflection function derived from the input impedance measurement of the downstream air column. The acoustical influence of the upstream resonator is simulated by injecting acoustic energy upstream from the lips with particular amplitude and phase conditions relative to the downstream acoustic pressure.

Therefore, this approach aims at replicating the experiments conducted on the artificial player system presented in Chapter 4.

Physical modeling has been extensively applied to synthesis of wind instrument sounds. Based on the simulation of the physical mechanisms underlying sound production, this approach can also be employed as a numerical benchmark for the study of the physical behaviour of the instrument and player's control. In brass instruments, particular efforts have been devoted to the development of realistic models of the lip-valve excitation mechanism. Physical representations of lip-reed valves commonly consider the lips as identical and placed symmetrically against the mouthpiece, then reducing the problem to the modeling of one lip.

After Helmholtz's early representation of wind instrument reeds resulting into a classification of valve systems as outward and inward striking valves (Helmholtz, 1954), various refined versions of lip models have been proposed in the literature. Fletcher extended Helmholtz's representation to sideway striking valves and proposed a categorization based on how the valve responds to an increase in the quasi-static pressure on the upstream and downstream sides. Using this convention, an outward striking valve will be represented by the $(+1,-1)$ couple, an inward striking valve by $(-1,+1)$ and a sideway striking valve either by a $(+1,+1)$ or $(-1,-1)$ model (see Chapter 2). The outward, inward and transverse models were studied numerically by Adachi and Sato (1995). Later, the same authors proposed a two-dimensional model of the lips combining the effect of the pressure on the internal, external and channel faces of the lips (Adachi & Sato, 1996). This approach was also replicated by Cullen et al. (2000) for a one-dimensional parametric model likely to be set as a dominant outward or dominant inward striking valve. Cullen et al. also proposed a two-mode (two-mass) model including two coupled oscillators and inspired from vocal-fold models (Cullen, 2000; Richards, 2003).

In this chapter, the influence of upstream coupling is evaluated using simple "outward" or "inward" striking models as proposed by Cullen et al. (2000), as well as a one-mode two-

dimensional model as proposed by Adachi and Sato (1996). The two-dimensional model offers a closer representation of brass player lips by allowing motion in both transverse and longitudinal directions. It hence permits oscillations of the lips to be sustained according to both outward or inward striking regimes.

The dynamics of the player-instrument system are commonly represented by a set of three coupled equations: 1) a mechanical equation representing the dynamics of the lip oscillator (mechanical equation); 2) a flow equation relating the acoustic pressure across the lips to the volume flow generated in the instrument and vocal-tract; and 3) the acoustic equations representing the effect of the linear downstream and upstream resonators. Two possibilities are available to simulate the behaviour of this complete system. Time-domain simulations, presented originally by Schumacher (1981) for the simulation of clarinet sounds, involve the discretization of the differential equations and iterative calculation of individual values of the different variables at each time step. This approach was later applied to the simulation of trumpet sounds (Adachi & Sato, 1995, 1996; Vergez & Rodet, 1997; Kaburagi et al., 2011) where the downstream resonator is represented by its reflection function. Simulations in the frequency domain have been proposed by calculating the spectrum of the periodic steady-state oscillation using an asymptotic method based on the harmonic balance technique. This approach was first proposed by Schumacher (1978) and later applied to brass instruments by Gilbert et al. (1989). Since we are interested in simulating time-varying upstream coupling conditions within the production of one tone, we choose to perform the numerical simulations in the time domain.

Numerical investigations including the effect of vocal-tract resonances in wind instruments have been performed in different ways. Sommerfeldt and Strong (1988) proposed a detailed time-domain simulation of a player-clarinet system involving a six-segment cylindrical tube representation of the player's vocal-tract. Various vocal-tract configurations were explored, some of them producing noticeable changes in the radiated sound spectrum. Fritz et al. proposed an

analytical formulation and frequency-domain simulations of the frequency shift induced by a vocal-tract resonance in clarinets (Fritz et al., 2003). Her work showed significant effect on the playing frequency when an upstream resonance is aligned with a downstream impedance resonance. Scavone investigated the effect of a single resonance on the sound produced by a simple saxophone physical model using the digital waveguide scheme (Scavone, 2003). Simulated effects of the upstream resonance on the spectral content of the mouthpiece pressure were found to be consistent with real playing situations. More recently, Guillemain proposed a refined representation of upstream airways for the simulation of transients on a clarinet model (Guillemain, 2007). In the latter study, the player's vocal-tract was represented by a cylindrical tube including frequency-dependent losses, which aimed at simulating the effect of the first impedance peak of the upstream system. Contrary to previous approaches, the quasi-static pressure was supplied at the entrance of the upstream bore rather than at the reed level, providing a more coherent representation of the physics of the system. Most recently, time-domain simulations including the impedance of the vocal-tract calculated by a transfer matrix method from vocal-tract visualization were performed by Kaburagi et al. (2011). Different upstream conditions were characterized from MRI imaging of a trumpet player's vocal-tract and tested on the numerical model of the lips proposed by Adachi and Sato (1996). Vocal-tract configuration especially appeared to influence the minimum blowing pressure, as well as the transition between adjacent modes.

To further investigate the effect of the upstream system on the behaviour of a player-instrument model, we propose a different approach to what has been previously presented. Our method attempts to replicate the active control method presented in Chapter 4. Therefore, by injecting a disturbing signal of frequency f_0 with controllable amplitude and phase, we aim to simulate varying characteristics of an upstream resonance centered around the playing frequency. In a first part, experiments using this formulation are conducted on two basic outward and inward striking lip models. In a second part, investigations are extended to the case of the two-dimensional

model proposed by Adachi and Sato (1996). The last section of this chapter summarizes the main contributions from these experiments.

5.1 Simple outward and inward striking models

5.1.1 Mechanical equation

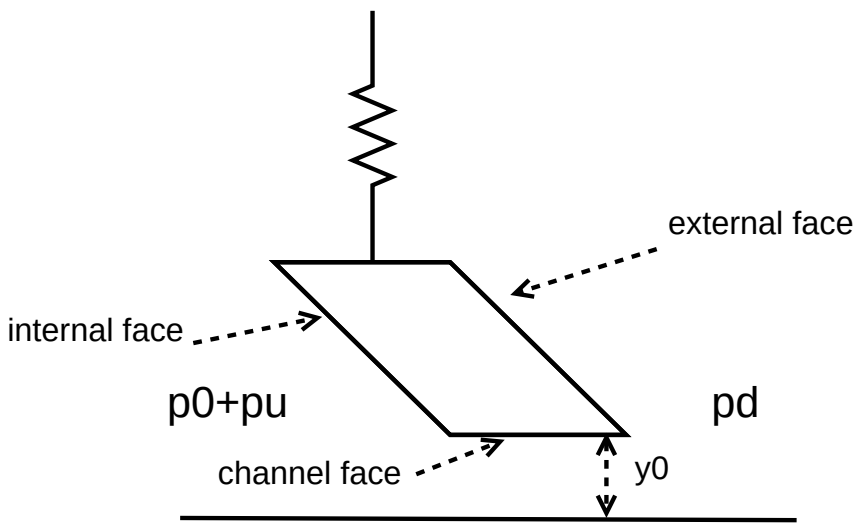

Figure 5.1 One-mass model of the lips.

The mechanical model chosen for the lips is inspired from (Cullen et al., 2000) and presented in Fig. 5.1. The two lips are assumed to be identical and placed symmetrically on the mouthpiece. Each lip is allowed to move along a vertical axis and its vertical position relative to the equilibrium position y_0 is noted y. To simplify the problem, the length of the lip channel is considered close to zero and therefore no interactions are considered between the jet and the channel face. Consequently, an overpressure on the upstream side tends to increase the lip opening area, while an overpressure on the downstream side tends to close it. According to Helmholtz (1954), this model corresponds to an outward striking model of the lips. In accordance with previous

notations, the upstream acoustic pressure (mouth side) arising from the upstream acoustical feedback is noted p_u and the quasi-static mouth pressure p_0. The downstream acoustic pressure (mouthpiece side) arising from the downstream acoustical feedback is noted p_d. As described in Chapter 2, the dynamics of each lip can be represented by the simple second-order oscillator equation:

$$\frac{d^2y}{dt^2} + \frac{\omega_{lip}}{Q_{lip}}\frac{dy}{dt} + \omega_{lip}^2(y - y_0) = \frac{F}{m_{lip}}, \tag{5.1}$$

where ω_{lip} is the lip angular frequency ($\omega_{lip} = 2\pi f_{lip}$), Q_{lip} the quality factor, m_{lip} the mass of one lip and y_0 is the vertical equilibrium position of the lip. F is the vertical component of the force acting on the lip. F is proportional to the pressure difference between mouth and mouthpiece i.e. $F/m_{lip} = (p_0 + p_u - p_d)/\mu$, where μ is the effective mass of the lips, m_{lip}, divided by the effective area of the internal face of the lips; this force therefore supports an outward striking reed behaviour. By substituting F/m_{lip}, Eq. 5.1 becomes:

$$\frac{d^2y}{dt^2} + \frac{\omega_{lip}}{Q_{lip}}\frac{dy}{dt} + \omega_{lip}^2(y - y_0) = \frac{p_0 + p_u - p_d}{\mu}. \tag{5.2}$$

By definition, μ is positive and $p_0 + p_u$ supposedly greater than p_d. The force F/m_{lip} acting on the lips is positive and hence provides work that increases y, and consequently increases the lip opening area. Therefore, by reversing the sign of μ, the effect of F becomes opposite and the lip model is converted into an inward-striking valve.

5.1.2 Flow equation

The lip channel is assumed to have constant width b so that the time-varying lip opening area $s_{lip}(t)$ is estimated by the expression $s_{lip}(t) = 2by(t)$. The volume-flow $u(t)$ through this channel is assumed to be quasi-stationary, frictionless and incompressible. Furthermore, we consider

$s_{lip} << s_{cup}$, with s_{cup} the area of the mouthpiece entryway, and no pressure recovery at the mouthpiece cup. Under these assumptions, $u(t)$ can be expressed as a function of the pressure difference across the lips $p_0 + p_u(t) - p_d(t)$ using a Bernoulli flow model:

$$u(t) = \mathrm{sgn}\left(p_0(t) + p_u(t) - p_d(t)\right) \sqrt{\frac{2\left|p_0(t) + p_u(t) - p_d(t)\right|}{\rho}} \cdot 2b(y(t) + y_0), \tag{5.3}$$

where ρ is the average air density and sgn(x)= +1 if x is positive or null and −1 if x is negative.

5.1.3 Downstream coupling

According to previous studies (Schumacher, 1981; Adachi & Sato, 1995, 1996), the downstream acoustical feedback equation can be expressed as follows:

$$p_d(t) = Z_c u(t) + \int_0^\infty r(\tau)\{Z_c u(t-\tau) + p_d(t-\tau)\}\,\mathrm{d}\tau, \tag{5.4}$$

where $Z_c = \rho c / s_{cup}$ is the characteristic wave impedance of a cylindrical tube of cross-section area s_{cup} and c is the speed of sound. $r(t)$ is the reflection function of the trombone derived from the input impedance Z_d measured experimentally using the experimental setup described in (Lefebvre & Scavone, 2011). As the reliability of the measurements becomes critical below 80 Hz, the real and imaginary parts of Z_d are linearly interpolated to zero below that value. The Fourier transform $R(\omega)$ of $r(t)$ can then be expressed as follows:

$$R(\omega) = \frac{Z_d(\omega) - Z_c}{Z_d(\omega) + Z_c}. \tag{5.5}$$

A quarter-period sinusoidal window is applied to $R(\omega)$ in order to remove the high frequency noise above 12 kHz. After symmetrization of $R(\omega)$ around the Nyquist frequency, $r(t)$ is calculated as the real part of the inverse Fourier transform of $R(\omega)$. Because of the abrupt acoustic

reflection from the mouthpiece, $r(t)$ undergoes a discontinuity at $t = 0$ which is not captured by the discrete calculation. It results in non-zero values of $r(t)$ at times $t < 0$, hence breaking the causality of the reflection function. To address this limitation, a revised causal reflection function $r_c(t)$ is calculated as proposed by Adachi and Sato (1996), taking into account the negative-time components such as:

$$r_c(t) = \begin{cases} r(t) + r(-t), & \text{for } t \geq 0 \\ 0, & \text{for } t < 0 \end{cases}. \tag{5.6}$$

The first 100 ms of $r_c(t)$ are represented in Fig. 5.2.

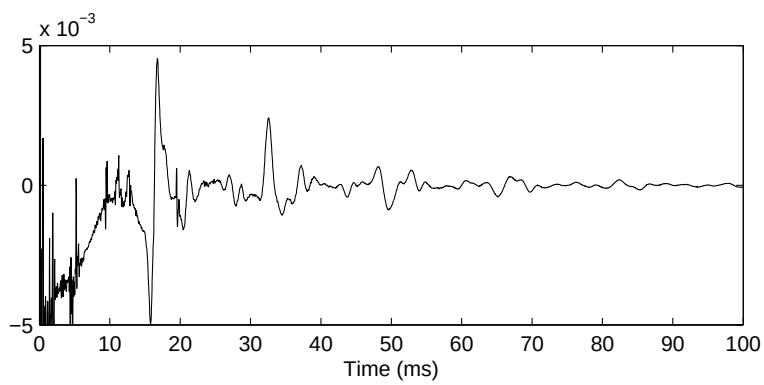

Figure 5.2 Reflection function $r_c(t)$ of a 2B King tenor trombone: calculated from an input impedance measurement (slide in the closed position).

5.1.4 Upstream coupling

Contrary to previous numerical simulations of upstream coupling (Scavone, 2003; Guillemain, 2007), our approach does not rely on the modeling of one or several vocal-tract resonances but only simulates an upstream feedback at f_0. It thus aims at modeling the effects of a single resonance near the playing resonance. Once oscillations are established and sustained with a constant amplitude, the system is disturbed through the injection of a sinusoidal upstream acoustic

pressure $p_u(t)$ of the same instantaneous fundamental frequency as $p_d(t)$. The amplitude of $p_u(t)$ is maintained constant so that the upstream acoustical feedback energy provided to the lips is constant along the tone duration. However, the instantaneous phase of $p_u(t)$ relative to the phase of $p_d(t)$ at f_0 is varied along the tone duration so that the phase difference $\angle Z_u(f_0) - \angle Z_d(f_0)$ varies linearly in time (as depicted by Eq. 2.27). Consequently, this protocol enables a specific investigation of the effect of the upstream impedance phase at f_0, independently from the amplitude of the acoustic energy regenerated on the upstream side of the lips, and independently from the other control parameters. This condition is analogous to the constant upstream energy applied to the artificial player system and described in Chapter 4. This procedure is implemented according to the following looped sequence:

1. After sample $p_d(n)$ has been calculated from Eq. 5.4, a 2nd order resonant filter (center frequency $f_c = f_{lip}$) is applied to vector $-p_d$ through a zero-phase forward and reverse digital IIR filtering process. The resonance bandwidth of the filter is chosen much smaller than the spacing between harmonics of the fundamental. The resulting vector, named p_s, is therefore a sinusoidal waveform of amplitude given by the resonant filter coefficients and out of phase with $p_d(f_0)$ by 180° at f_0.

2. p_s is normalized to its maximum value over its two last periods and scaled by a constant factor C. This step enables the amplitude of acoustic upstream energy to be maintained constant, independently from the amplitude of the downstream pressure produced.

3. $p_u(n)$ is set from the normalized and scaled value of p_s, with a time-shift given by a phase-shift parameter $\Phi(n)$; $p_u(n) = p_s[n-\Phi(n)]$. The phase shift parameter $\Phi(n)$ (implemented as a delay in samples) is an input parameter which thus controls the phase difference between P_d and P_u.

4. $p_u(n)$ is applied as in Eqs. 5.2 and 5.3.

5. The procedure is iterated by one time step.

Consequently, when f_0 is constant and assuming continuity of the volume flow at the lips, this procedure allows the phase difference $\angle Z_u(f_0) - \angle Z_d(f_0)$ to be linearly varied through the array parameter Φ as shown by Eq. 2.27 repeated here for convenience:

$$\frac{Z_u(\omega)}{Z_d(\omega)} = -\frac{P_u(\omega)}{P_d(\omega)}, \tag{5.7}$$

5.2 Time-domain simulations

Simulations are performed using the following parameter values adapted from previous simulations (Cullen et al., 2000): $f_{lip} = 310\,\text{Hz}$, $Q_{lip} = 6$, $\mu = 25\,\text{kg/m}^2$, $b = 10\,\text{mm}$, $y_0 = 0\,\text{mm}$, $s_{cup} = 4.8\,\text{cm}^2$, $\rho = 1.1769\,\text{kg/m}^3$, $c = 347.23\,\text{m/s}$. It is worth mentioning that in the trombone configuration chosen, the fifth and the sixth resonances of the downstream input impedance are around 290 Hz and 350 Hz respectively. It is then clear that the chosen lip resonance frequency f_{lip} is between two acoustic resonances, rather than very close to one, hence allowing oscillations to occur potentially near one or the other downstream resonance.

Time-domain simulations are performed by discretization of the differential equations using the forward Euler method and applying the trapezoidal approximation for the integration in the downstream coupling equation (Eq. 5.4) as performed in (Adachi & Sato, 1996). The sampling frequency is set to 48 kHz.

The quasi-static pressure p_0 is specified using a quarter-period sinusoidal onset of 10 ms, a steady phase at 15 kPa, and a quarter-period sinusoidal decay of 10 ms. The phase shift vector Φ contains values varying linearly from 110 to 240°; the value contained in Φ at index n indicates

the number of shifted samples applied to p_s (in order to obtain p_u value at index n). It therefore refers to the instantaneous phase shift between p_u and p_d waveforms at f_0. The boundary values in Φ are chosen empirically so that the phase shift between p_u and p_d covers the maximal range allowing the system to maintain oscillations. Scaling parameter C is set so that the p_u amplitude is of the same order of magnitude as p_d, hence producing significant effect on the system. Such order of magnitude of $P_u(f_0)/P_d(f_0)$ amplitude ratio are observed in trombone players in the higher register (see Chapter 3). A quarter-period sinusoidal onset envelope is applied to the scaling factor so that the p_u amplitude grows smoothly from zero to C when injected into the system.

Simulations start with no upstream feedback ($p_u = 0$). Once the permanent regime of oscillation is reached (time t_1 determined empirically), upstream coupling is added according to the procedure described in the previous section.

5.3 Results from simulation for the outward striking model

The waveforms of p_d and p_u calculated from a two-second simulation are presented in Fig. 5.3. Around 0.6 s, the upstream feedback is introduced and this results in significant variations in p_d amplitude as the phase difference $\angle P_u - \angle P_d$ varies linearly in time at f_0. This variation is also accompanied by changes in f_0 as shown in Fig. 5.3. At time 1.3 s, a register transition to a lower mode is observed. It results in a smaller slope of the phase shift due to a smaller value of f_0. As for the higher mode, f_0 decays slowly while $\angle P_u - \angle P_d$ is decreased until the end of the tone. Comparing these results with the one obtained using active control on the artificial player system (Fig. 4.6), we observe that the two sets of data share common features: across the two portions of stable oscillations in Fig. 5.3, the downstream waveform goes through an amplitude maximum for a given phase tuning. Furthermore, the linear phase shift results in a linear decay of the play-

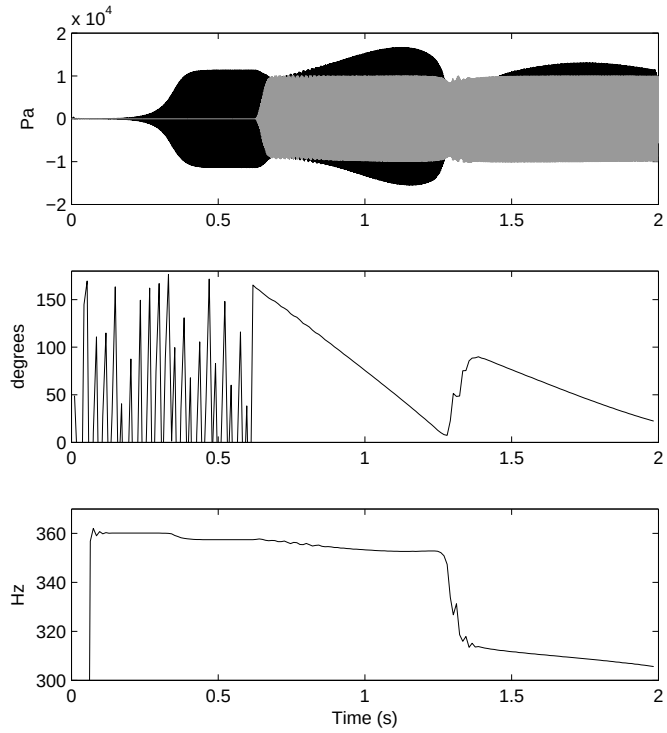

Figure 5.3 Results from a 96000 sample simulation at 48 kHz for an outward striking lip model. From top to bottom: waveforms of p_d (black) and p_u (gray); phase difference between P_u and P_d at the fundamental frequency; fundamental frequency f_0.

ing frequency in both artificial player and numerical model. For the model, this linear behaviour particularly occurs for the lower tone, which is also close to the lip natural frequency f_{lip}.

5.3.1 Lip mobility

Considering only the alternating components of the different variables, the analytical expression of the adjusted lip mobility $G = Y/(P_d - P_u)$ can be written from Eq. 5.2 in the frequency domain as follows:

$$G(\omega) = \frac{-1/\mu}{(\omega_{lip}^2 - \omega^2) + j\frac{\omega_{lip}}{Q_{lip}}\omega}. \tag{5.8}$$

The magnitude and phase of G are represented by solid lines in Fig. 5.4. As predicted by the mechanical model, the outward striking character of the lip-valve system results in a +90° phase shift between Y and ΔP at the resonance.

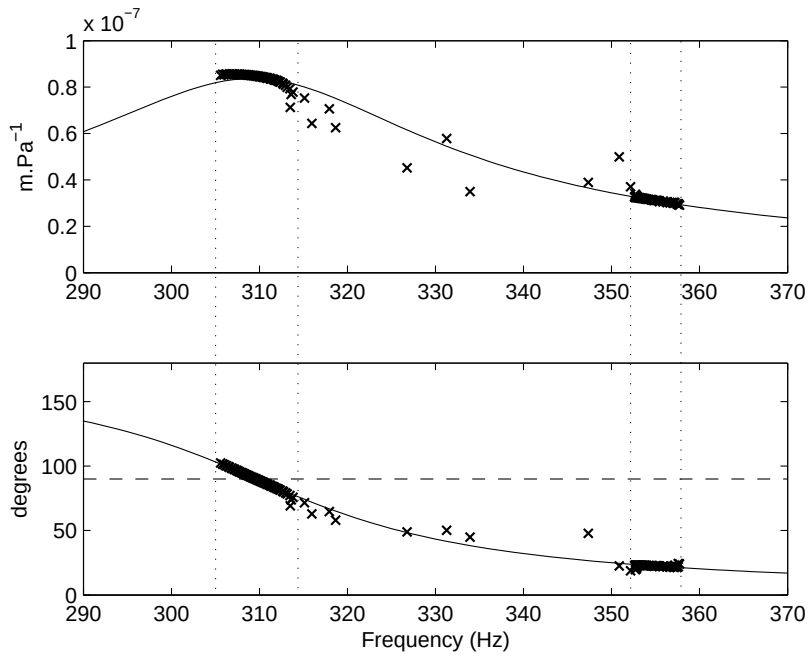

Figure 5.4 Calculated and simulated lip mobility for an outward striking model. Amplitude (top) and phase (bottom) of G: theoretical value (solid line) and calculated from numerical simulations (cross). The horizontal dashed line indicates 90° phase angle. The vertical dotted lines indicate the two regions of stable oscillations corresponding to the two produced tones.

In the same figure, the amplitude and phase of the adjusted lip mobility at f_0 calculated from simulated waveforms of p_d, p_u and y are represented in crosses. As predicted by the model, and over the frequency range where acoustic energy is observed, the amplitude and phase of G estimated from simulations overlap with its theoretical values. In this particular case, variations

of G at f_0 caused by the upstream feedback allow oscillations to occur over a significant frequency range, including the lip natural frequency identified by $\angle G(f_0) = 90°$. This specific tuning point induces a maximum of lip displacement, hence allowing the volume flow to be maximized.

5.3.2 Downstream and upstream input impedances

The influence of downstream and upstream acoustical feedback can be further discussed in terms of input impedances Z_d and Z_u. The total impedance "loading" the lip-valve $Z = U/\Delta P$ can be expressed from Eq. 5.7 as the sum of the downstream and upstream impedances ($Z = Z_d + Z_u$.).

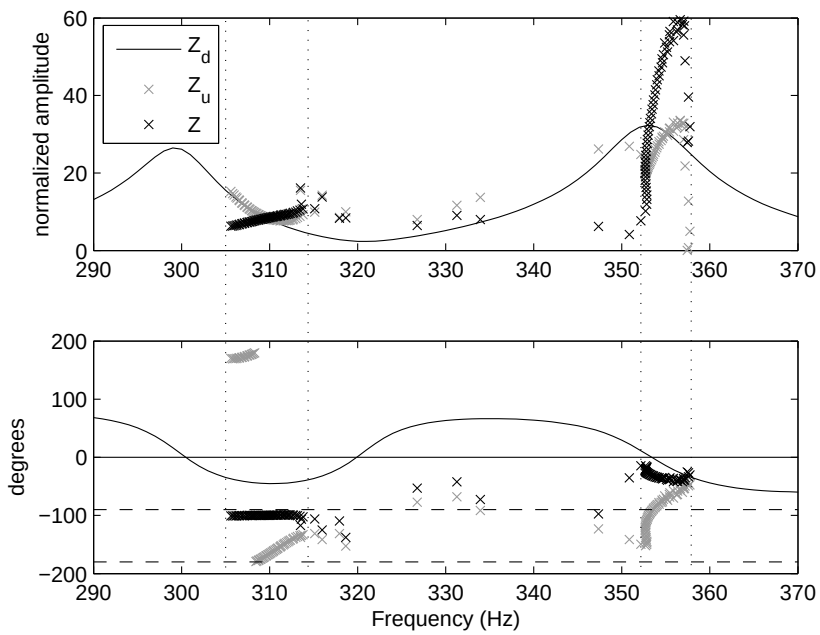

Figure 5.5 Z_d, Z_u and Z during simulations for an outward striking model. Amplitude (top) and phase (bottom) of Z_d obtained from measurements (solid line), as well as Z_u (gray cross) and Z (black cross) at frequencies where acoustic energy is observed. The two horizontal dashed lines indicate $-90°$ and $-180°$ phase angles. The vertical dotted lines indicate the two regions of stable oscillations corresponding to the two produced tones.

Therefore, from experimental measurement of Z_d and analogously to what was performed in

Chapter 4, the complex quantities Z_u and Z can be derived from Eqs. 5.7 and 2.29 at frequencies where acoustic energy is observed. In order to account for truncation of the low frequency and high frequency artifacts in the measured value of Z_d, as well as for the discretization of the downstream feedback equation (Eq. 5.4) during simulations, an updated value of the downstream impedance is computed from the reflection function $r_c(t)$ used for simulation. This procedure involves an unitary impulse volume flow as an input of the simulation scheme, and calculates the resulting downstream pressure from the discretization and trapezoidal approximation performed in Eq 5.4. This corrected value of the downstream input impedance is then calculated as the ratio of the downstream pressure to the input volume flow in the frequency domain. From now on, the notation Z_d refers to this corrected downstream input impedance.

The amplitude and phase of Z_d, as well as amplitude and phase of Z_u and Z calculated from the value of Z_d over the frequency range covered, are represented in Fig. 5.5. For the highest tone produced with upstream support (353–358 Hz region), a decrease in Z_u amplitude is observed with decrease in frequency. This reveals a decrease in the amplitude ratio P_u/P_d at f_0, most probably due to the increase in $|Z_d|$.

The upstream coupling also lowers the value of $\angle Z$. As $\angle Z$ becomes closer to zero, oscillations become unstable and a change of regime occurs to the lower mode around 353 Hz. By looking closer at the frequency region between 352 and 358 Hz (Fig. 5.6), we notice a hysteresis effect at the lower frequency limit; the change in regime occurs around 352.9 Hz when $\angle Z$ is maximized, whereas the lower playing frequency is reached around 352.7 Hz for a larger value of $\angle Z_u - \angle Z_d$ difference. In the region near the lip mechanical resonance (305–315 Hz interval), $|Z_u|$ roughly overlaps with $|Z_d|$, and decreasing values of $\angle Z_u$ force $\angle Z$ towards a low value plateau around -100°.

These observations can be further discussed in light of the linear theory of oscillation. The adjusted phase condition of regeneration under which sustained oscillations are maintained is

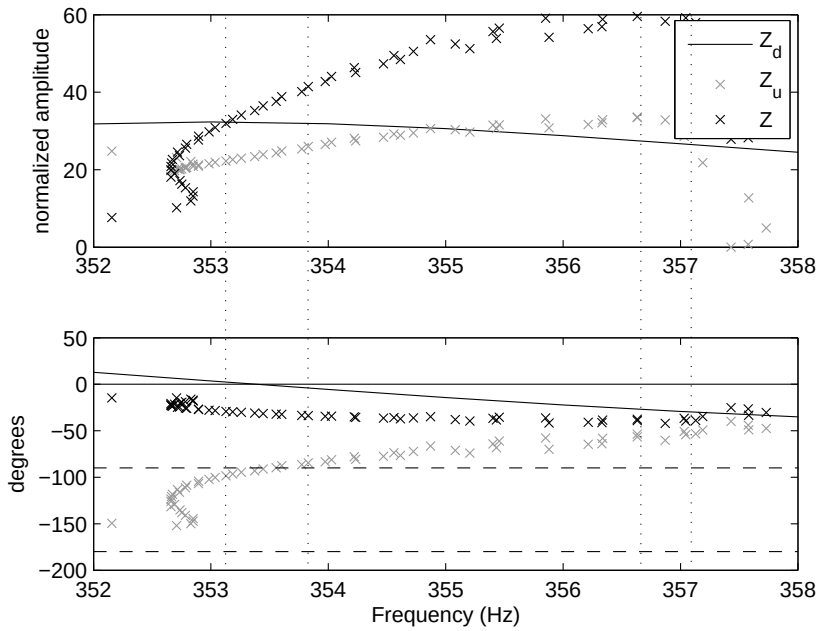

Figure 5.6 Closer view at Fig. 5.5 between 352 Hz and 358 Hz.

given by Eq. 3.8 and repeated here for convenience:

$$\angle Z + \angle G = 0. \tag{5.9}$$

This phase condition relies on the linearisation of the flow equation around the quasi-static pressure p_0 (Eq. 5.3) and therefore assumes that s_{lip} and u oscillate in phase at the playing frequency.

From Eq. 5.9, we observe that injection of upstream acoustic energy allowing $\angle Z$ to reach values below $-90°$ enables $\angle G$ to extend above $90°$. It thus enables oscillations to occur both above and below the lip natural frequency f_{lip}. In the 353-358 Hz region, the lowered value of $\angle Z$ enables oscillations to occur at a lower frequency and hence closer to a maximum in $|Z_d|$. In the 305–315 Hz region, the upstream coupling enables $\angle Z$ to be displaced around -100° and oscillations to occur at the lip natural frequency f_{lip} for which $\angle G = +90°$. In spite of the non-linearity

induced by the downstream and upstream feedback, in the flow equation, Eq. 5.9 successfully explains the displacement of the playing frequency close to the lip resonance caused by appropriate upstream phase tuning conditions.

5.4 Results from simulation for the inward striking model

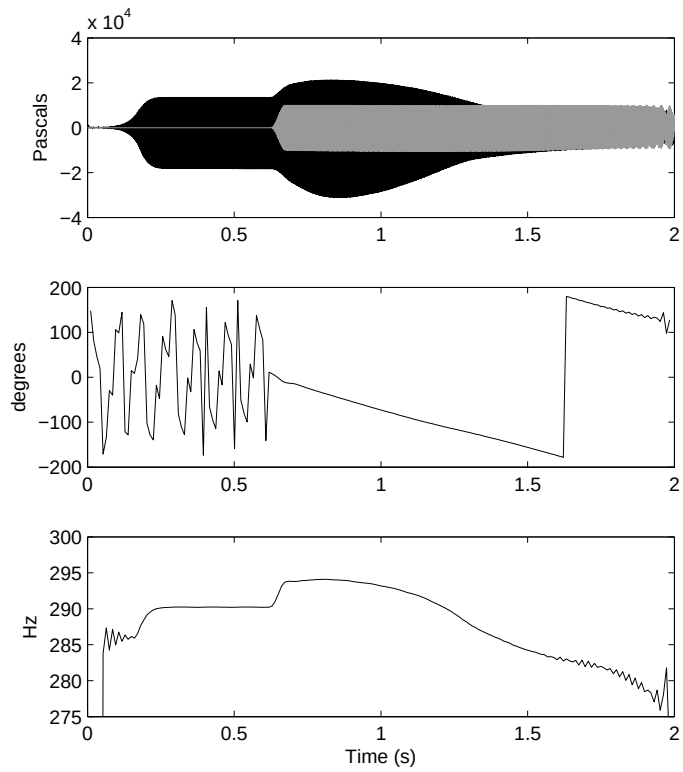

Figure 5.7 Results from a 96000 sample simulation at 48 kHz for an inward striking lip model. From top to bottom: waveforms of p_d (black) and p_u (gray); phase difference between P_u and P_d at the fundamental frequency; fundamental frequency f_0.

An inward striking model of the lips is implemented from Eq. 5.2 by setting the value of μ to -0.04 and setting the equilibrium position of y_0 to 0.5 mm. The negative value of μ results in

a negative term F on the right side of Eq. 5.2. This negative force tends to close the valve when the pressure increases on the upstream side of the lips, and to open it when the pressure rises on the downstream side. The other parameters are unchanged except the equilibrium position y_0 set to 0.5 mm (by construction, this valve requires y_0 to be higher than zero in order to initiate oscillations).

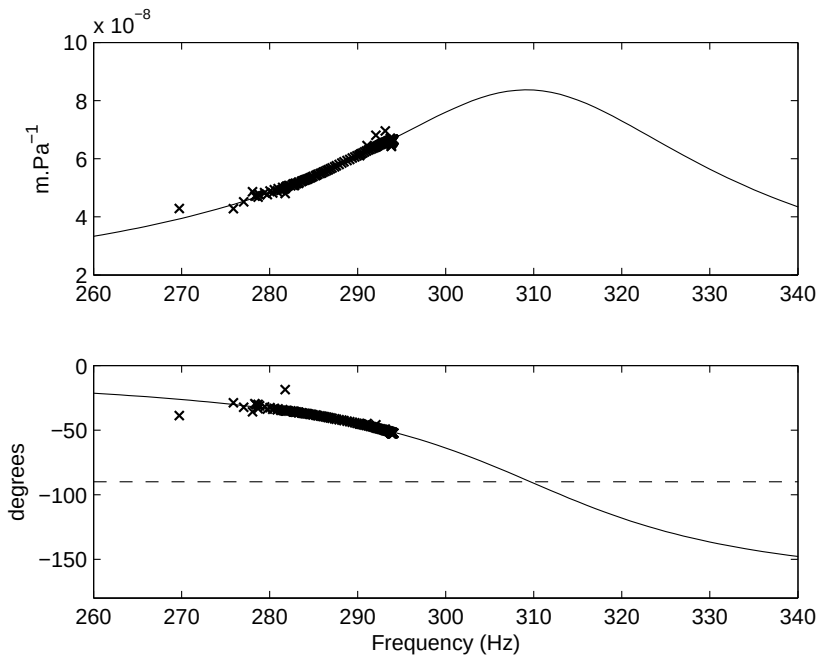

Figure 5.8 Calculated and simulated lip mobility for an inward striking model. Amplitude (top) and phase (bottom) of G: theoretical value (solid line) and calculated from numerical simulations (cross). The horizontal dashed line indicates −90° phase angle.

The waveforms of p_d and p_u calculated from a two-second simulation are presented in Fig. 5.7. As in previous simulations, the upstream feedback is introduced around 0.6 s and results in significant variations in the amplitude of p_d as the phase difference $\angle P_u - \angle P_d$ at f_0 varies linearly in time. This variation is also accompanied by changes in f_0 without any change in register. Contrary to the outward striking model, the variations of f_0 are not linearly correlated to the phase

difference $\angle P_u - \angle P_d$. Injection of the disturbing signal results in a small increase in f_0 before the playing frequency starts to decrease at a variable rate until the end of the tone. Around 1.5 s, small oscillations appear in the phase and frequency signals, as well as in the upstream pressure waveform, probably indicating a limit of stability for the system, as observed in the artificial player experiments (Fig. 4.6).

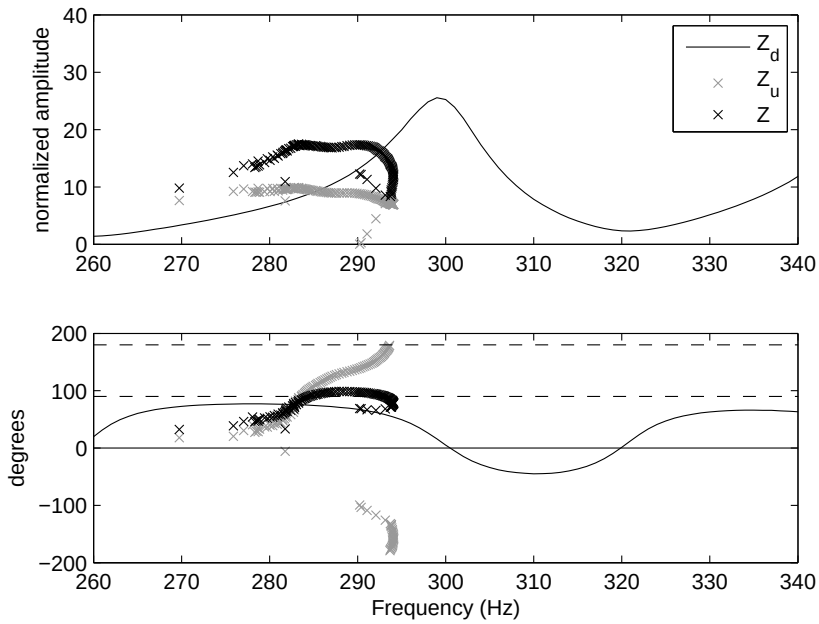

Figure 5.9 Z_d, Z_u and Z during simulations for an inward striking model. Amplitude (top) and phase (bottom) of Z_d obtained from measurements (solid line), as well as Z_u (gray cross) and Z (black cross) at frequencies where acoustic energy is observed. The two horizontal dashed lines indicate 90° and 180° phase angles.

The values of G calculated from simulation results perfectly overlap with the theoretical lip mobility as shown in Fig. 5.8. Contrary to the outward striking model, oscillations occur on the lower frequency side of the lip resonance. The general decrease in playing frequency induced by the phase shift between P_d and P_u hence results in displacing oscillations away from the lip resonance. However, the short increase in f_0 observed at the injection of the perturbation

upstream signal pulls oscillations of the system closer to $|G|$ maximum, which may contribute to explain the significant increase in the amplitude of p_d waveform observed in Fig. 5.7 between 0.6 and 1 s.

Looking at the amplitude and phase of Z_d, Z_u and Z at the playing frequency in Fig. 5.9, we observe that the upstream support allows $\angle Z$ to be raised above 90° in the region where acoustic energy is produced. In light of the linear condition of regeneration (Eq. 5.9), it then allows the phase of the lip mobility G to be decreased closer to the lip resonance. However, from the observation of Figs. 5.8 and 5.9, we observe that the validity of Eq. 5.9 is relatively weak in this case: although $\angle Z$ reaches values above 90°, $\angle G$ only goes down to -50°.

Overall, the combined effect of the growing value of $|G|$ and $|Z_d|$ induced by the increase in playing frequency maximizes lip motion and lip opening area, as well as the amplitude of the acoustic pressure created in the mouthpiece. This results in boosting the amplitude of the acoustic pressure created in the mouthpiece, hence providing optimal efficiency of the sound production process. The effect of the simulated varying upstream coupling should now be investigated on a model allowing both outward and inward striking regimes.

5.5 Two-dimensional lip model

In this section, we investigate the influence of upstream coupling on a more complex and possibly more realistic, model of the lips. A two-dimensional model proposed by Adachi and Sato (1996) is considered and represented in Fig. 5.10. This representation allows motion of the lips in both longitudinal and transverse direction, therefore making possible both outward and upward movements as observed in real lips (Yoshikawa & Muto, 2003; Copley & Strong, 1996). Contrary to simple outward and inward striking models presented previously, this representation presents an important non-linear character arising from the time varying internal and external lip

surface areas. This characteristic is responsible for the ability of the model to operate according to both inward and outward striking regimes.

5.5.1 Mechanical equation

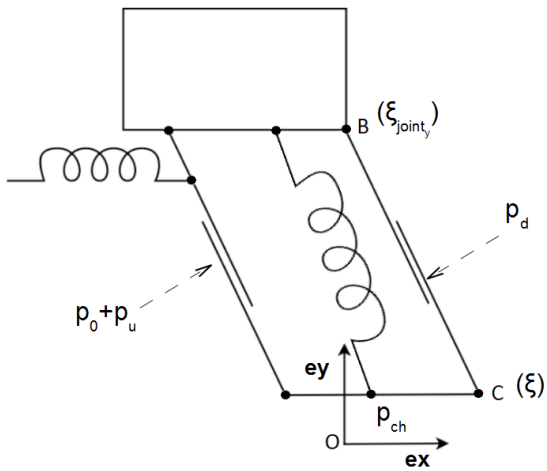

Figure 5.10 Two-dimensional model of the lips.

The mechanical equation is given by Eq. 2.10 and repeated here for convenience:

$$m_{lip}\frac{d^2\xi}{dt^2} + \frac{\sqrt{m_{lip}k}}{Q_{lip}}\frac{d\xi}{dt} = \boldsymbol{F}_{restore} + \boldsymbol{F}_{\Delta p} + \boldsymbol{F}_{Bernoulli}, \tag{5.10}$$

where k is the stiffness factor of the lips, ξ is a two dimensional vector whose coordinates are given by the position of point C in the direct orthonormal system $(0;\boldsymbol{ex};\boldsymbol{ey})$, and ξ_{equil} is the two-dimensional equilibrium vector position.

$\boldsymbol{F}_{restore}$ is the elastic restoring force pointing to ξ_{equil} and arising from the combined action of the two springs of same stiffness (see Fig. 5.10). This force is given by the following expression:

$$\boldsymbol{F}_{restore} = -k(\xi - \xi_{equil}) \tag{5.11}$$

$$= \left[-k(\xi_x - \xi_{equil_x})\right]\mathbf{ex} + \left[-k(\xi_y - \xi_{equil_y})\right]\mathbf{ey}. \tag{5.12}$$

$\boldsymbol{F}_{\Delta p}$ is the external force acting on the internal and external lip faces and due to the pressure difference across the lip valve. It is defined such as:

$$\boldsymbol{F}_{\Delta p} = s(p_0 + p_u - p_d)\mathbf{n} \tag{5.13}$$

$$= [s(p_0 + p_u - p_d) \cdot \cos\theta]\,\mathbf{ex} + [s(p_0 + p_u - p_d) \cdot \sin\theta]\,\mathbf{ey} \tag{5.14}$$

$$= \left[-b(p_0 + p_u - p_d)(\xi_y - \xi_{joint_y})\right]\mathbf{ex} + \left[b(p_0 + p_u - p_d)(\xi_x - \xi_{joint_x})\right]\mathbf{ey}, \tag{5.15}$$

where $\mathbf{n}$ is a unitary vector normal to the internal lip face and oriented toward positive horizontal-axis values, s is the time-varying effective area of the internal and external lip faces, and θ is the angle between BC and the vertical axis defined by $\boldsymbol{ey}$.

The length of the lip channel (lip thickness) is no longer neglected and $\boldsymbol{F}_{Bernoulli}$ is the force acting on the lip channel face and generated by the Bernoulli pressure:

$$\boldsymbol{F}_{Bernoulli} = bdp_{ch}\mathbf{ey}, \tag{5.16}$$

where d is the thickness of one lip and p_{ch} is the pressure in the lip channel.

The mathematical expressions of the three force components can be projected onto the horizontal and vertical axis. Two equations governing the evolution $\xi(t)$ in the horizontal and vertical directions are then derived from Eq. 5.10:

$$m_{lip}\frac{d^2\xi_x}{dt^2} + \frac{\sqrt{m_{lip}k}}{Q_{lip}}\frac{d\xi_x}{dt} = -k(\xi_x - \xi_{equil_x}) + b(p_0 + p_u - p_d)(\xi_{joint_y} - \xi_y) \tag{5.17}$$

$$m_{lip}\frac{d^2\xi_y}{dt^2} + \frac{\sqrt{m_{lip}k}}{Q_{lip}}\frac{d\xi_y}{dt} = -k(\xi_y - \xi_{equil_y}) + b(p_0 + p_u - p_d)\xi_x + bdp_{ch}. \tag{5.18}$$

We notice that $\xi_{joint_x} = 0$ and hence does not appear in Eq. 5.18.

Assuming that the jet cross-section area is much smaller than the input section of the mouthpiece, the velocity in the mouthpiece is considered negligible. Furthermore, we assume total dissipation of the kinetic energy of the jet in the mouthpiece. The pressure in the mouthpiece can then be considered equal to the pressure on the lip channel.

$$p_{ch} = p_d. \tag{5.19}$$

From the expression $\omega_{lip} = \sqrt{\frac{k}{m_{lip}}}$, lip parameters m_{lip} and k are expressed as a function of f_{lip} according to the following formulas (Adachi & Sato, 1996):

$$m_{lip} = 1.5/((2\pi)^2 f_{lip})\text{kg} \tag{5.20}$$

$$k = 1.5 f_{lip}\text{N/m}. \tag{5.21}$$

5.5.2 Lip mobility calculation

In order to calculate the analytical expression of the lip mobility $G(\omega)$ for this model, both horizontal and vertical components of ξ are decomposed into their static (DC) and alternating (AC) components: $\xi_x = \xi_x^{dc} + \xi_x^{ac}$ and $\xi_y = \xi_y^{dc} + \xi_y^{ac}$. By only considering the DC components of the variables involved, and ignoring the DC component of the downstream pressure, Eqs. 5.17

and 5.18 can be written under the following matrix form:

$$\begin{pmatrix} \xi_x^{dc} \\ \xi_y^{dc} \end{pmatrix} = \frac{1}{\left(\frac{k}{2}\right)^2 + (bp_0)^2} \begin{pmatrix} \left(\frac{k}{2}\right)^2 \xi_{equil_x} + \frac{k}{2} bp_0(\xi_{joint_y} - \xi_{equil_y}) \\ \left(\frac{k}{2}\right)^2 \xi_{equil_y} + \frac{k}{2} bp_0 \xi_{joint_x} + (bp_0)^2 \xi_{joint_y} \end{pmatrix}. \tag{5.22}$$

Analogously, considering only the AC components of the variables involved, application of the Fourier transform to Eqs. 5.17 and 5.18 leads to the following frequency-domain matrix equation:

$$\begin{pmatrix} \frac{k}{2}\gamma^{-1}(\omega/\omega_{lip}) & bp_0 \\ -bp_0 & \frac{k}{2}\gamma^{-1}(\omega/\omega_{lip}) \end{pmatrix} \begin{pmatrix} \xi_x^{ac}(\omega) \\ \xi_y^{ac}(\omega) \end{pmatrix} = \begin{pmatrix} -b\xi_{joint_y} \\ -b\xi_x^{dc} + bd\frac{p_{ch}(\omega)}{P_d(\omega) - P_u(\omega)} \end{pmatrix} (P_d(\omega) - P_u(\omega)), \tag{5.23}$$

where $\omega_{lip} = 2\pi f_{lip}$, $\gamma(\Omega) = \frac{1}{1-\Omega^2 + j(\Omega/Q)}$ and the influence of the quadratic term $\xi_y^{ac}(P_u - P_d)$ is considered as negligible and is omitted. From the projection of Eq. 5.23 on the $\boldsymbol{ex}$ axis, the following expression of ξ_x^{ac} can be derived:

$$\xi_x^{ac}(\omega) = \frac{-2b}{k\gamma^{-1}(\omega/\omega_{lip})} \left(\xi_{joint_y}(P_d(\omega) - P_u(\omega)) - p_0 \xi_y(\omega)\right). \tag{5.24}$$

Injecting Eq. 5.24 into Eq. 5.23 projection on the $\boldsymbol{ey}$ direction, we derive the following expression for the lip mobility $G(\omega)$:

$$G(\omega) = \frac{\xi_y^{ac}(f)}{\Delta P(\omega)} = (2b) \frac{(d\frac{1}{1-P_u(\omega)/P_d(\omega)} - \xi_x^{dc}) - 2b\xi_{joint_y} p_0 \left[\gamma(\omega/\omega_{lip})/k\right]}{1 + \left[2bp_0 \left[\gamma(\omega/\omega_{lip})/k\right]^2\right]} \frac{\gamma(\omega/\omega_{lip})}{k}, \tag{5.25}$$

where ξ_x^{dc} is derived from Eq. 5.22 projected on $\boldsymbol{ex}$ axis:

$$\xi_x^{dc} = \frac{\left(\frac{k}{2}\right)^2 \xi_{equil_x} + \frac{k}{2} b p_0 (\xi_{joint_y} - \xi_{equil_y})}{\left(\frac{k}{2}\right)^2 + (b p_0)^2}. \tag{5.26}$$

In the case of a neglected acoustic effect of the upstream airways ($P_u/P_d = 0$), the factor d in the first term of the numerator in Eq. 5.25 becomes equal to unity and we obtain the expression of the lip mobility as proposed by Adachi and Sato (1996):

$$G(\omega) = \frac{\xi_y^{ac}(f)}{\Delta P(\omega)} = (2b) \frac{(d - \xi_x^{dc}) - 2b\xi_{joint_y} p_0 \left[\gamma(\omega/\omega_{lip})/k\right]}{1 + \left[2b p_0 \left[\gamma(\omega/\omega_{lip})/k\right]^2\right]} \frac{\gamma(\omega/\omega_{lip})}{k}. \tag{5.27}$$

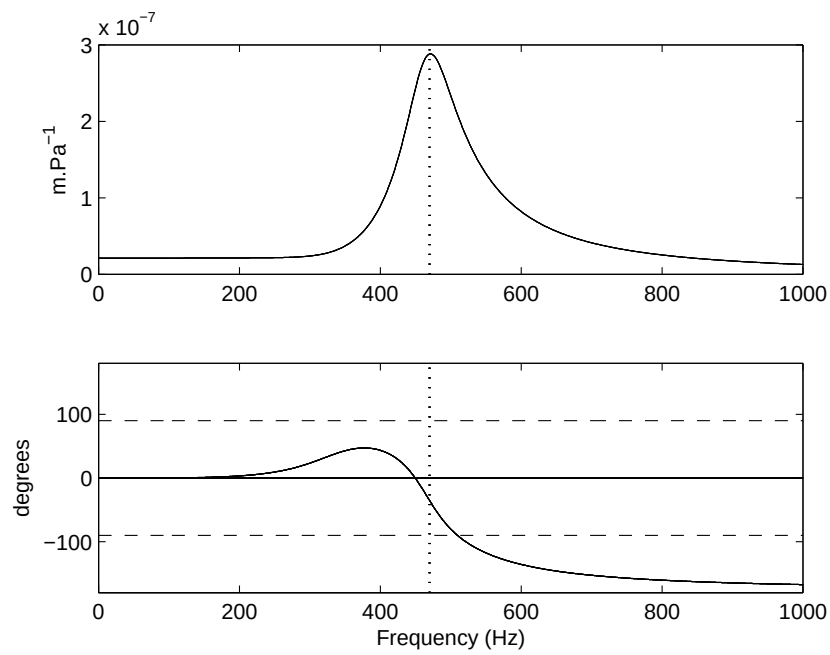

Figure 5.11 Lip mobility for a two-dimensional lip model. Amplitude (top) and phase (bottom) of G. The horizontal dashed lines indicate −90° and +90° phase angle.

The theoretical value of G is calculated from Eq. 5.27, corresponding to Eq. 5.25 where the term $\frac{1}{1-P_u/P_d}$ is omitted to make the calculation possible. This simplification constitutes an approximation that may contribute to produce significant disagreement with values of G calculated

from simulations, but remains relevant to illustrate the nature of this particular lip-valve system.

The theoretical values of G calculated from Eq. 5.27 from 0 to 1 kHz are represented in Fig. 5.11. Contrary to purely "inward" or "outward" striking models previously reported, the phase of G takes positive and negative values around the resonance frequency (f_{lip} =470 Hz). Therefore, it predicts the ability of the model to oscillate according to both outward and inward striking regimes.

5.5.3 Flow equations

In this model, the volume flow $u(t)$ is calculated as the sum of two flow components: 1) the Bernoulli flow given by Eq. 5.3 and resulting from the pressure difference across the lips, and 2) a flow component $u_{lip}(t)$ induced by the longitudinal motion of the lips and equivalent to the volume swept by the lips per unit of time (Adachi & Sato, 1996).

$$u_{lip}(t) = b\left[\xi_x(t)\frac{d\xi_y}{dt} - (\xi_y(t) - OB)\frac{d\xi_x}{dt}\right]. \tag{5.28}$$

5.5.4 Simulation results

Numerical simulations are performed using the same conditions of downstream and upstream feedback as presented in Sections 5.1.3 and 5.1.4. Discretization of the differential equations and the trapezoidal approximation are performed similarly to Section 5.2, and the sampling frequency is set to 48 kHz. The different parameters of the mechanical and flow equations are set to the following values: $f_{lip} = 470$ Hz, $Q_{lip} = 3$, $b = 10$ mm, $d = 4$ mm, $\xi_{joint_y} = 4$ mm $\xi_{equil_x} = 2$ mm, $\xi_{equil_y} = 0.3$ mm, $s_{cup} = 4.8\,\text{cm}^2$, $\rho = 1.1769\,\text{kg/m}^3$, $c = 347.23$ m/s. This leads to $m_{lip} = 80.8$ mg from Eq. 5.20 and $k = 705$ N/m from Eq. 5.21. Finally, the phase shift vector Φ is set to vary between 110 and 230 samples.

When the lips are in contact ($s_{lip} = 0$), Adachi and Sato proposed a supplementary restoring

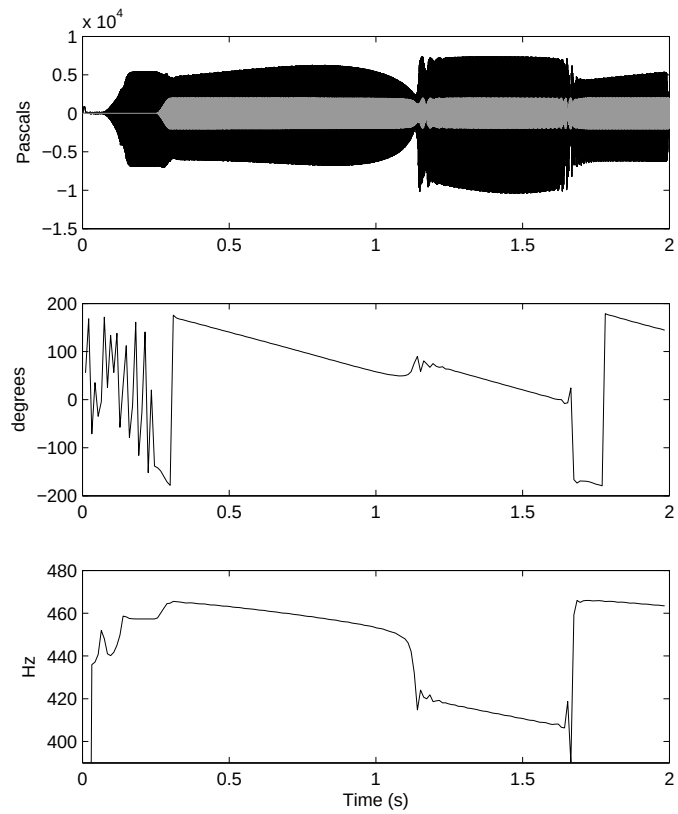

Figure 5.12 Results from a 96000 sample simulation at 48 kHz for a two-dimensional lip model. From top to bottom: waveforms of p_d (black) and p_u (gray); phase difference between P_u and P_d at the fundamental frequency; fundamental frequency f_0.

force accounting for the collision between the lips, and triggered by the condition $\xi_y < 0$. Additionally, the viscous loss due to the collision of the lips were taken into account by updating Q to a value smaller than 1 during the closed phase (i.e. when $s_{lip} = 0$) (Adachi & Sato, 1996). Likewise, Vergez and Rodet proposed to add an extra stiffness coefficient and damping coefficient during the closed phase (Vergez & Rodet, 1997), likely to be dynamically adjusted during the progressive closure (Vergez & Rodet, 2001). For simplicity, we do not take into account these adjustments and only set $\xi_y = 0$ when the $s_{lip} = 0$, which results in re-initialization of ξ_y to zero

whenever complete closure of the lip valve occurs.

Time-domain simulation results are presented in Fig. 5.12. Contrary to previous simulations, the amplitude of $p_u(t)$ is set through coefficient C to a smaller value since this lip model appears to be more sensitive to an upstream acoustical perturbation. Despite the small amplitude of $p_u(t)$, the linear sweep of the phase difference $\angle Z_u - \angle Z_d$ at f_0 results in significant variations of the fundamental frequency with a transition to a lower mode between 1.2 and 1.6 s. Along with variations in f_0, the acoustic downstream energy varies noticeably during sound production.

The amplitude and phase of the lip mobility G calculated from Eq. 5.27 (solid line) and from simulations (cross) are represented in Fig. 5.13.

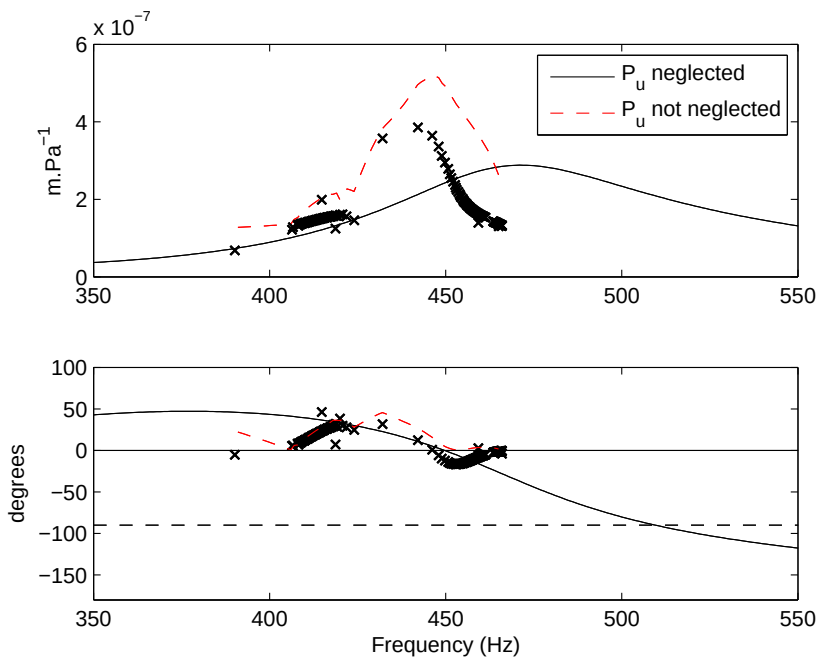

Figure 5.13 Calculated and simulated lip mobility for a two-dimensional lip model. Amplitude (top) and phase (bottom) of G: theoretical value (solid line), theoretical value corrected by the upstream coupling (dashed red), and values calculated from numerical simulations (cross). The horizontal dashed line indicates $-90°$ phase angle.

Results from simulations weakly agree with the theoretical value of G, although $\angle G$ estimated from simulations lies in the region of values defined by the analytical expression of the lip mo-

bility. Regarding the amplitude, values obtained from the time-domain simulation particularly disagree with the theoretical value in the 450–470 Hz region. These discrepancies may be attributed to the approximations performed in the analytical calculation (Eq. 5.27) where the static component of the downstream pressure was neglected in Eq. 5.22, the quadratic term $\xi_y^{ac}(P_u - P_d)$ was omitted in Eq. 5.23, and the influence of the upstream acoustic pressure is not considered.

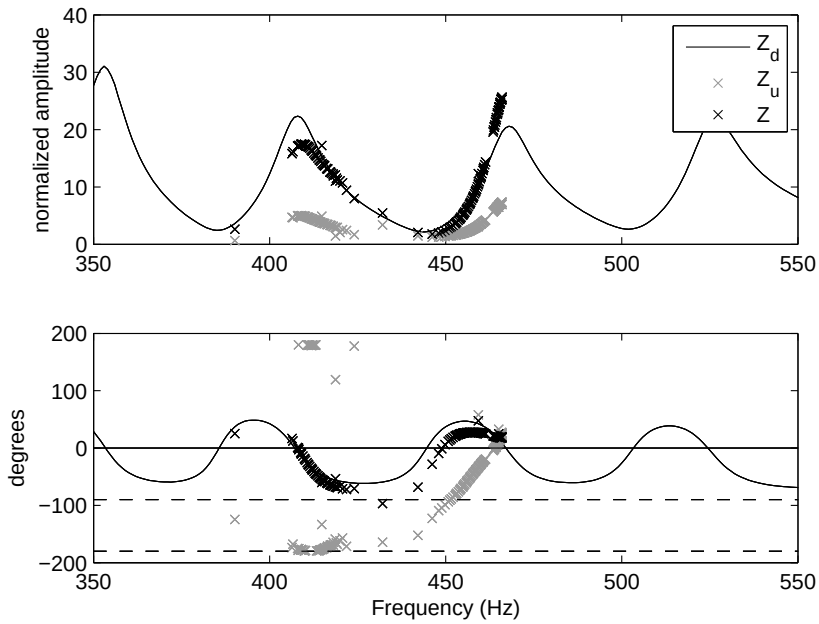

Figure 5.14 Z_d, Z_u and Z during simulations for a two-dimensional lip model. Amplitude (top) and phase (bottom) of Z_d obtained from measurements (solid line), as well as Z_u (gray cross) and Z (black cross) at frequencies where acoustic energy is observed during simulations. The two horizontal dashed lines indicate 90° and 180° phase angles.

However, both simulation and theoretical results agree to predict the change in sign of $\angle G$, indicating a transition from an inward to outward striking regime of oscillation when going down in frequency. In order to visualize the influence of the upstream coupling on the analytical expression of G, the amplitude and phase of the lip mobility calculated from Eq. 5.25 is represented at frequencies where energy is produced in Fig. 5.13 (red dashed line). The complex values of

P_u/P_d obtained from simulations are hence taken into account in the calculation. Results from simulation are in better agreement with this corrected evaluation of the lip mobility, especially for the phase where simulation results overlap well in the 405–420 Hz region. Regarding the amplitude, the hypothesis of a maximum in lip mobility amplitude around 445 Hz suggested by simulation results is confirmed by the corrected values of $|G|$.

Looking at the amplitude and phase of Z_d, Z_u and Z in Fig. 5.14, we observe that the small magnitude of Z_u compared to Z_d (resulting from the low amplitude of p_u) induces a small effect on the value of $\angle Z$. Consequently, Z is strongly correlated to Z_d in amplitude and phase. Despite this small upstream influence, significant variations in f_0 occur, as observed in Figs. 5.12 and 5.13. The linear theory of oscillation provides a reasonable prediction of the relationship between $\angle G$ and $\angle Z$; the positive sign of $\angle Z$ over the 450–470 Hz range correctly agrees with the negative sign of $\angle G$ over the same frequency interval, while the negative sign of $\angle Z$ over the 405–420 Hz range is in agreement with the positive character of $\angle G$ over the same interval. Over the frequency range where acoustic energy is produced, the phase difference between Z and $-G$ at f_0 stays between -40° and 20°, as shown in Fig. 5.15.

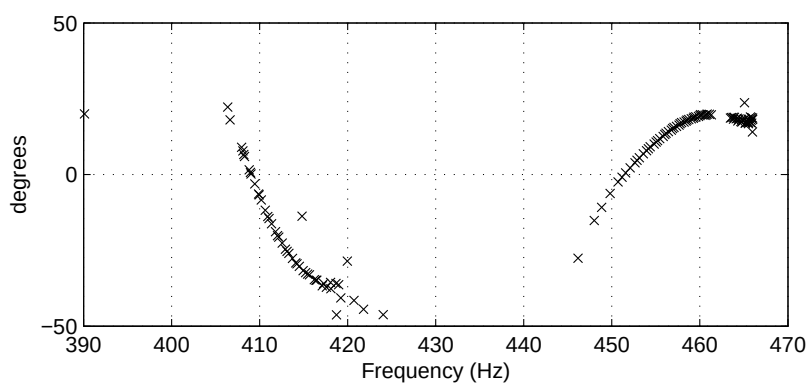

Figure 5.15 Phase difference between Z and $-G$ at the fundamental frequency f_0.

By varying the playing frequency, control of the upstream coupling with a fixed lip setting allows a transition from a dominant inward (or upward) to a dominant outward striking behaviour.

Near 450 Hz, the high amplitude of G provides support to lip oscillations, allowing sound to be produced despite the low value of $|Z|$. Above 450 Hz and below 420 Hz, oscillations are only possible for higher values of $|Z|$, closer to a downstream impedance peak, most probably as a consequence of the lower magnitude of G in this frequency range.

5.6 Summary

In this chapter, we have investigated the effect of different upstream phase tuning conditions on different physical models of the lips. Numerical simulations have been performed in the time domain and involved discretization of the three sets of equations governing the dynamics of the system. To simulate the effect of an upstream coupling with the vibrating lips, a similar approach to that presented in Chapter 4 was implemented by adding an acoustic component with given amplitude and phase characteristics to the quasi-static mouth pressure.

We focused on the influence of the phase difference between Z_d and Z_u at f_0, independently from their relative amplitude. Analogously to results obtained from experiments on an artificial trombone player system (see Chapter 4), linear variation of the phase of Z_u relative to Z_d at f_0 induces significant variations in the playing frequency, as well as in the acoustic energy produced. In the case of simple one-dimensional lip models, the variations of the total impedance Z, caused by the varying nature of the upstream coupling, displaces the amplitude and phase of G over its theoretical value. This induces a maximum of lip motion around the mechanical resonance of the lips. Along with variations in the playing frequency, the combined effect of an increase in $|G|$ and $|Z_d|$ induces a maximum of downstream acoustic energy produced on the downstream side and hence an optimal efficiency of the system. Furthermore, despite the non-linear relationship between the acoustic flow U and lip opening area S_{lip}, the observation of $\angle G$ appears to provide a reasonable prediction of $\angle Z$ variations in the context of the linear theory of oscillation. This

further reinforces the confidence for the analysis conducted from *in-vivo* measurements with regard to the determination of the nature of the downstream and upstream couplings (capacitive or inductive) at the playing frequency.

In the case of a two-dimensional lip model, the influence of upstream acoustic energy appears to be very strong on the behaviour of the system. The effect of a linear variation of the phase of Z_u relative to Z_d at f_0 results in great changes in the playing frequency, producing variations in the acoustic energy generated, as well as a switch from an inward to outward striking mechanism of oscillation. Overall, these results lend support to the hypothesis that vocal-tract tuning may be used independently from other parameters (lip tension, mouth pressure) to perform fine tunings of the playing frequency, to increase the efficiency of the lip-valve mechanism, an even to achieve a register change. Similarly to one-dimensional models, the linear theory of oscillation enables a reasonable prediction of the variations of phase of the total impedance from the observation of the lip mobility.

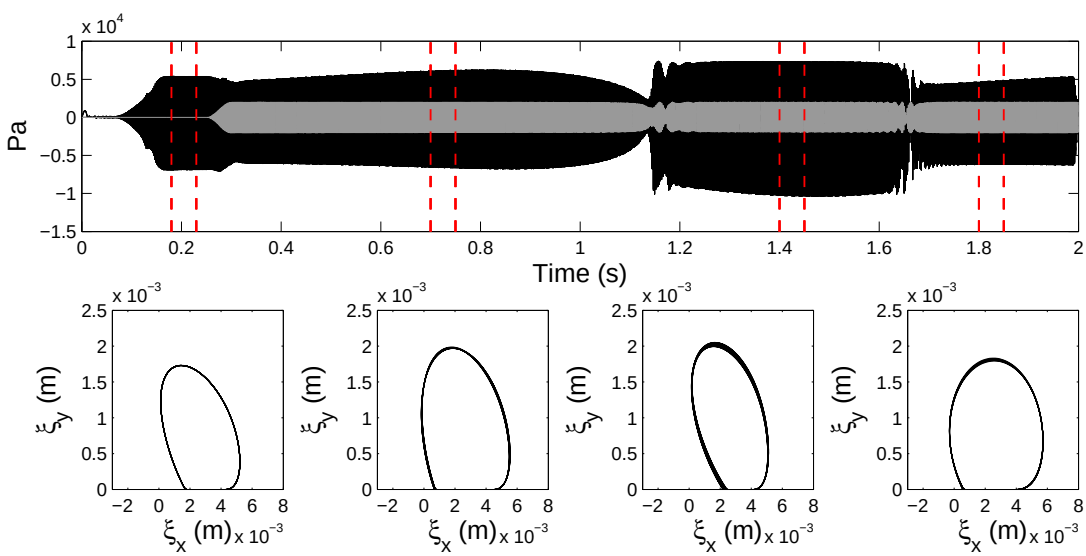

Figure 5.16 Influence of the upstream coupling on the two-dimensional lip motion. Results from a 96000 sample simulation at 48 kHz for a two-dimensional lip model. From top to bottom: waveforms of p_d (black) and p_u (gray); 2-dimensional lip motion in the $(\boldsymbol{ex}, \boldsymbol{ey})$ plane at different time steps indicated by the vertical red dashed lines.

Nevertheless, some refinements could be taken into account in our model. First, some improvements in the estimation of the reflection function could be performed by minimizing the influence of distortions in the measured trombone input impedance as suggested by Gazengel et al. (1995). More attention could be also paid to the lip contact. In particular, a refined modeling of the collision involving an extra stiffness and damping during the closed phase could be considered (Adachi & Sato, 1996; Vergez & Rodet, 1997, 2001).

Finally, comparisons between the two-dimensional model and real or artificial lips may also be explored with regards to lip displacement. The transverse displacement of the lip tip (C point) is represented at different steps of the simulation in Fig. 5.16. Interestingly, oscillations occurring on the negative phase side of Z_d between 1.17 and 1.63 s (outward striking behaviour) are characterized by a smaller horizontal displacement and a rather upward striking motion. On the contrary, the horizontal motion is emphasized for the two adjacent regions where a dominant inward striking regime of oscillation is predicted from the observation of $\angle Z$. These observations may be attributed to the fixed geometrical parameters of the model, in particular to the lip thickness parameter b which controls the effect of the Bernoulli force applied on the lip channel face.

Chapter 6

Respiratory Control in Trombone Performance

In Chapters 3, 4 and 5, we have investigated the control of acoustic pressures at the interface between the player and instrument, as well as their influence on the excitation mechanism. Our results suggest that the vocal tract constitutes an important resonating element, whose influence can be controlled to substantially interact with the sound production process in certain circumstances (notably in the high register and at slurred transitions). Furthermore, we may speculate that by providing support to lip oscillations, vocal-tract influence may alter the conditions on adjacent parameters such as the quasi-static mouth pressure. Subsequently, we may assume that the regulation of acoustic and static pressures are intimately related, as they both arise from a coherent physiological control. We then wish to clarify the management of the quasi-static mouth pressure in trombone performance, and further understand whether the respiratory control of static pressures interconnects with the acoustical control of the usptream airways.

A growing interest has been devoted to investigations of respiratory control in music performance. Earlier contributions in the study of respiration in wind instruments have been proposed

by Bouhuys (1964) and Berger (1965, 1968) who performed a variety of measurements on different wind players. In Bouhuys' study, recordings included quasi-static mouth pressure and expiratory volume flow, CO_2 concentration, thorax displacements, and electrocardiogram (Bouhuys, 1964). Quasi-static volume flow was assessed by an indirect method consisting in subtracting residual volume (RV), measured using a nitrogen-clearance method, from the vital capacity (VC) after playing a sustained tone from 100 % VC. Bouhuys also observed the respiratory patterns of sustained tones in the chest-wall volume / lung pressure plane for different instruments, suggesting the possible co-activation of inspiratory muscles during playing in order to counterbalance the elastic recoil of the chest wall. This assumption, first suggested by Roos (1936), was later confirmed by Cossette et al. (2008) in flautists.

Later work by Bouhuys involved measurement of volume flow through body plethysmography as shown in Fig. 6.1 (Bouhuys, 1968). In this study, pleural and mouth pressures were also recorded during singing, whistling and trombone performance. The power produced by the player, as well as embouchure resistance were derived from mouth pressure and volume flow measurements. Results demonstrate a non-linear relationship between mouth pressure and air flow with increase in loudness. Interestingly, comparisons between the mouth and alveolar pressures revealed a partial transmission of the pleural pressure to the oral cavity, suggesting a non-homogeneous distribution of the pressure along the respiratory airways (from the lung to the oral cavity). These results hence suggest possible laryngeal adjustments responsible for the pressure difference observed across the glottis. This hypothesis is supported by Griffin et al. (1995) who reported different laryngeal manipulation according to different conditions of breath support in singers, as well as by different studies investigating laryngeal pharyngeal adjustments in wind instruments (King, Ashby, & Nelson, 1989; Mukai, 1992; Rydell, Karloson, Milesson, & Schalén, 1996; Dejonckere, Orval, Miller, & Sneppe, 1983). Therefore, laryngeal control (particularly at the level of the glottis) may significantly influence a coupling between respiratory mechanisms

and the control of the acoustical properties of the vocal tract.

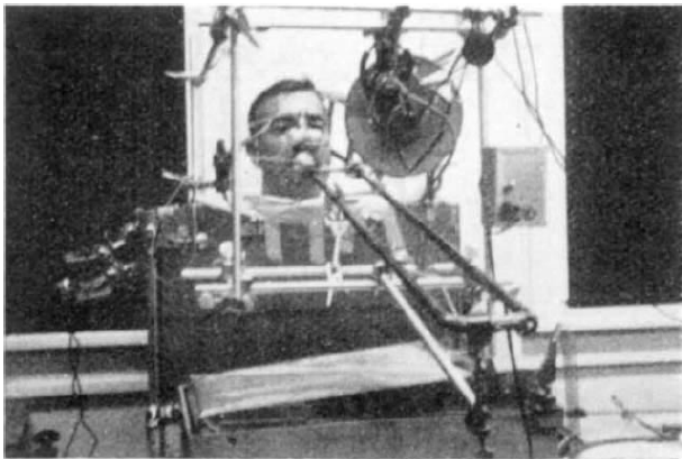

Figure 6.1 Bouhuys' experiment on a trombone player using a body plethysmograph (reprinted from (Bouhuys, 1969)).

Experimental investigations have focused on quantitative description of chest-wall displacement in music performance. Early results were reported by Bouhuys who measured thorax movements using a pneumograph (Bouhuys, 1964). More recently, Cossette et al. (2000) evaluated variations of antero-posterior and lateral distances of the rib cage and abdomen in flute performance. These recordings allowed for characterization of chest-wall distortion relative to the relaxation state. Different kinematic patterns were observed according to subjects, along with a high consistency in the control of the mouth pressure across subjects. Later, the use of an opto-electronic plethysmograph (OEP), allowing to dissociate contributions from three chest-wall compartments, was combined to electromyography (EMG) and pressure measurements in the mouth cavity during flute performance (Cossette et al., 2008). In that study, a quantitative evaluation of "breath support" (associated with high quality of playing) was performed on a pool of flute players. Results highlighted a significant activation of non-diaphragmatic inspiratory muscles (scalenes and sternocleidomastoids) while expiring during playing. This co-activation, in response to the elastic recoil of the chest wall and to the activation of expiratory muscles,

clearly denotes the fine role of inspiratory muscles in precisely regulating mouth pressure during breath support. In contrast, a “no breath support” condition was characterized by performance at lower volumes, no recruitment of inspiratory muscles and by a higher contraction of expiratory muscles.

In this chapter, we aim to combine Cossette’s latter two approaches (OEP and EMG) in order to provide a characterization of respiratory dynamics in trombone performance and particularly investigate the contribution from different respiratory muscle groups. In brass instruments, the quasi-static pressure in the mouth constitutes a crucial control parameter influencing the dynamics of the lip-reed system and the characteristics of the air flow across the lips. A first objective is to understand the mechanisms underlying the control of mouth pressure with respect to pressure regulation in the respiratory system achieved by respiratory muscles. A second objective is to investigate the nature of a possible coupling between the acoustical tuning of upstream airways and the control of respiratory pressure. From a larger perspective, we intend to provide insights regarding the possible interactions between regulation of acoustic pressure in the vocal-tract and respiratory pressures, by closely observing breathing mechanisms during performance.

In a first part, the experimental method is described with particular emphasis on the characterization of relaxation curves of the different chest-wall compartments. In a second part, playing control parameters extracted from measurements are observed during standard musical tasks involving independent variations of pitch and loudness. In a third part, the dynamics of the chest wall are analyzed and discussed with respect to the control of the static pressure in the mouth. Finally, the last section of this chapter summarizes the main contributions from this study.

6.1 Materials and methods

6.1.1 Opto-electronic measurement of chest-wall deformations: kinematics measurements

The chest wall is subdivided into three compartments whose volumes are monitored independently: the pulmonary rib cage (RC_p) corresponding to the the region of the rib cage which encompasses the lungs and whose volume is noted $V_{rc,p}$, the abdominal rib cage (RC_a) corresponding to the diaphragm-apposed part of the rib cage of volume $V_{rc,a}$, and the abdominal compartment (AB) of volume V_{ab}. The total chest-wall volume V_{cw} is then defined by Eq. 6.1 as the sum of the volume contribution from the three compartments:

$$V_{cw} = V_{rc,p} + V_{rc,a} + V_{ab}. \tag{6.1}$$

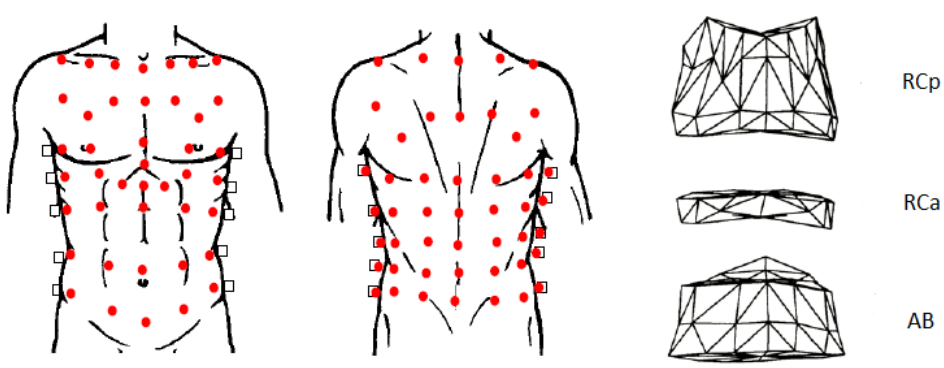

Figure 6.2 Marker positions and chest-wall compartments for optical analysis in standing position. Chest-wall compartments: upper thorax or lung-apposed pulmonary rib cage (RC_p), lower thorax or diaphragm-apposed abdominal rib cage (RC_a), abdomen (AB) (Aliverti, 1996).

The deformations of the three chest-wall compartments are monitored by opto-electronic plethysmography (OEP)[1] which consists of nine infrared cameras running at 60 Hz and tracking the 3D coordinates of 89 hemispherical reflective markers (diameter 10 mm) in a calibrated

[1] SMART E-System©, BTS bioengineering, Milan, Italy

space. These markers are applied on the front and back areas of the chest wall along seven rows between the clavicle and the iliac crest (Aliverti, 1996) as shown in Fig. 6.2. This marker setup allows creation of a digital mesh of the chest wall. It then enables the volume of each compartment to be derived through application of the Gauss theorem as described by Cala et al. (1996).

Figure 6.3 Experimental setup for recording of the radiated sound.

During acquisition, obtrusion of the camera range by the adjacent equipment may cause partial disappearance of one marker. In this case, the position of the missing marker is interpolated by linear extrapolation from the position of two neighbouring markers.

In order to avoid having the instrument to obstruct the view of the cameras fronting the subject, the trombone slide was replaced by a flexible plastic tube of approximately the same diameter and the same length as the slide in closed position. A Bach 11C mouthpiece was fixed to one extremity, and the other end was attached to the bell section of the instrument. In this way, the bell section could be placed outside the camera views (Fig. 6.3), while the player only had to hold the mouthpiece attached to the tube with one hand (Fig. 6.4). Furthermore, this solution

allows the acoustical response of the instrument to be maintained close to a “normal” instrument. The acoustic input impedance measured at the mouthpiece entry of the trombone with the slide in closed position and with the slide replaced by a plastic tube are represented in Fig. 6.5.

These measurements were performed using the experimental setup described in (Macaluso & Dalmont, 2011). We observe that the two input impedances follow a similar trend in amplitude and phase. The slightly lower length of the plastic tube induces a noticeable displacement of the resonances towards lower frequencies. The amplitude at the resonances is also reduced in the plastic tube condition, most probably because of larger losses induced by the soft walls. Moreover, these variations may also be induced, to some extent, by the changes in radiativity pattern and reflexions at the bell due to the bed (the trombone bell section could not be mounted vertically due to some microphone fixture constraints). Despite these discrepancies with the original instrument, the main features of the acoustical response are preserved, hence allowing quasi-normal playing condition.

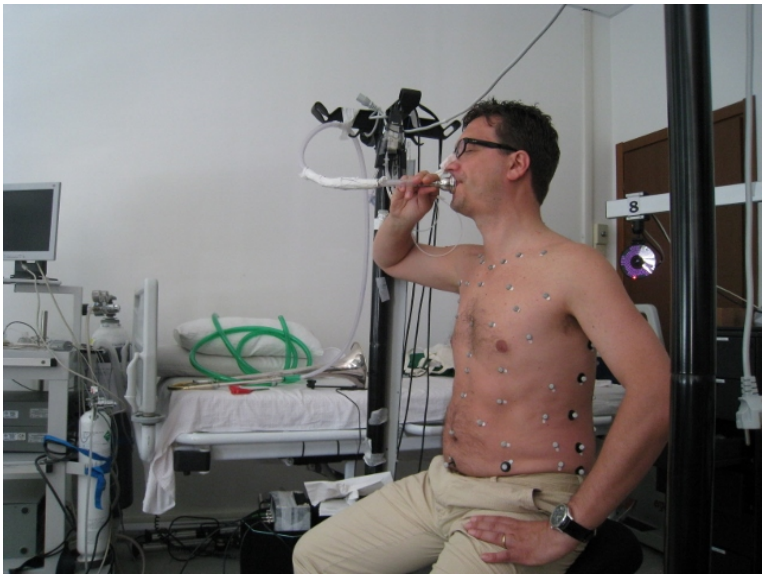

Figure 6.4 Experimental setup.

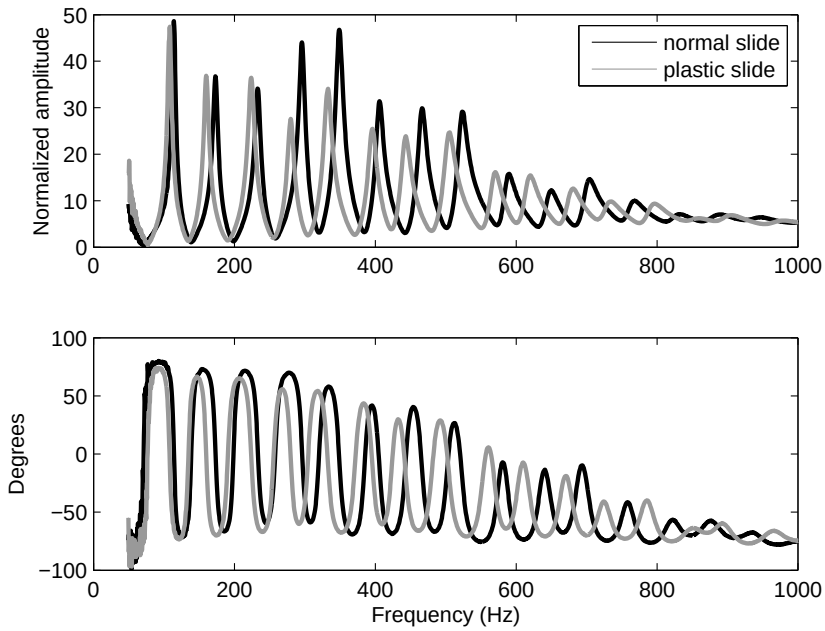

Figure 6.5 Input impedance of a tenor trombone and modified instrument used for experiments. Amplitude and phase of the input impedance normalized to the characteristic impedance of a King 2B Silver Sonic tenor trombone and Bach 11C mouthpiece with the slide in the closed position (black) and of the same trombone with the slide replaced by a flexible plastic tube (gray).

6.1.2 Respiratory pressure measurements

Three pressure signals were measured directly at different levels: the esophageal pressure (P_{es}) as an estimate of the pleural pressure (P_{pl}), the gastric pressure (P_{ga}) as an estimate of the abdominal pressure (P_{ab}), and the mouth pressure (P_m). The three pressure signals recorded are quasi-static signals with no acoustic component and were recorded relative to atmospheric pressure. The esophageal and gastric pressures were measured using conventional transnasal balloon-catheter systems (Milic-Emili et al., 1964). The gastric balloon was placed in the stomach and the esophageal balloon about 10 cm above the diaphragm (Baydur, Behrakis, Zin, & Milic-Emili, 1982). The mouth pressure was recorded using a catheter that the subject was instructed to hold with his free hand so that the extremity of the catheter was placed above the tongue

along the air stream. The three catheters were connected to pressure transducers calibrated prior to experiments. Signals from pressure transducers were digitalized using the acquisition board embedded in the OEP system and sampled at 960 Hz.

From these three pressure measurements, two variables can be derived: the transdiaphragmatic pressure (P_{di}) and the transglottal pressure (P_{gl}) whose expressions are given as follows:

$$P_{di} = P_{ab} - P_{pl} = P_{ga} - P_{es} \tag{6.2}$$

$$P_{gl} = P_{sub} - P_m \simeq P_{es} - P_m. \tag{6.3}$$

where P_{sub} is the subglottal pressure just behind the glottis. In Eq. 6.3, it is assumed that the esophageal pressure provides a decent estimation of P_{sub} (Lieberman, 1968; Schutte, 1992).

6.1.3 Radiated sound measurement

The radiated sound pressure was recorded about 10 cm from the bell of the instrument using an AMT P800 microphone. The signal was channeled to both the OEP system running at 960 Hz and an external acquisition unit (Alesis MicLink XLR-USB interface cable) running at 44.1 kHz for precise analysis. The fundamental frequency and acoustic power generated at the bell were derived from the acoustic signal using the YIN algorithm (de Cheveigné & Kawahara, 2002).

6.1.4 Flow measurement

The quasi-static volume flow going in and out from the lungs can be estimated from OEP volume data. The variations of volume of the chest wall are assumed to only result from volume variations of the lungs. Therefore the volume flow Q_l induced during breathing can be evaluated as follows:

$$Q_l = -\frac{\mathrm{d}V_{cw}}{\mathrm{d}t} - \frac{1}{\rho c^2}\left[P_{es}\frac{\mathrm{d}V_{cw}}{\mathrm{d}t} + V_{cw}\frac{\mathrm{d}P_{es}}{\mathrm{d}t}\right], \tag{6.4}$$

where ρ is the average air density, c is the speed of sound in air and P_{es} is assumed to be an estimate of the pressure in the lungs. According to Eq. 6.4, expiratory flow is positive and inspiratory flow negative. The second term in Eq. 6.4 is a correction factor taking into account volume variations of the chest wall induced by air compressibility (Cossette et al., 2010). In order to reduce the noise resulting from the differentiation, V_{cw} and P_{es} are filtered before calculation of Q_l using a third-order low-pass filter (cut-off frequency: 2 Hz).

6.1.5 Relaxation curves

As described in Chapter 2, the relaxation curve of the chest-wall compartment provides an empirical relationship between pressure and volume along which respiratory muscles are completely relaxed. The distance to the relaxation curve during exercise in the pressure-volume plane enables assessment of the net pressure developed by respiratory muscles for each of the compartments.

In order to determine the relaxation curve of the upper rib-cage and abdominal compartments, a relaxation maneuver was performed. This task consists in relaxing against a resistance imposed at the mouth output, starting from Total Lung Capacity (TLC) and exhaling to Residual Volume (RV). An example of the temporal evolution of $V_{rc,p}$, $V_{rc,a}$, V_{ab} and V_{cw} is shown in Fig. 6.6 (approximately between 100 and 128 seconds). Before computing the analytical expressions of the relaxation curves, the DC component of $V_{rc,p}$ and V_{ab} is removed so that both vectors are centered around zero and noted $\Delta V_{rc,p}$ and ΔV_{ab} respectively. The evolution of P_{ga}, P_{es} and P_{di} during the same time frame is shown in Fig. 6.7.

Pulmonary rib-cage relaxation curve: The relaxation curve of the pulmonary rib-cage com-

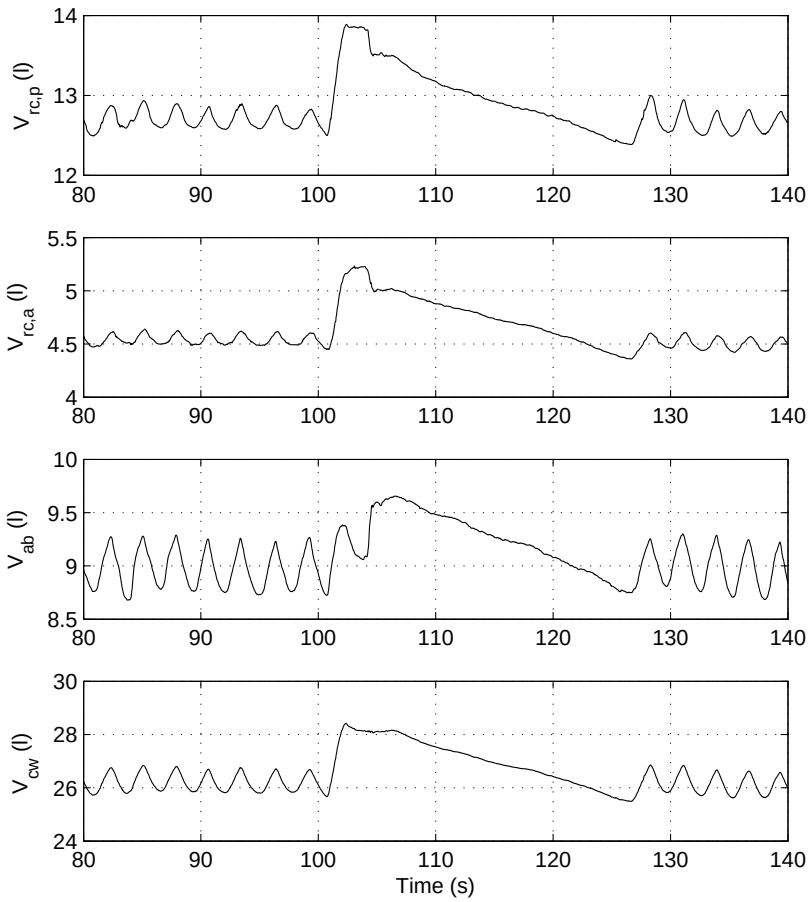

Figure 6.6 Chest-wall volumes during quiet breathing and a relaxation maneuver. From top to bottom: pulmonary rib-cage volume ($V_{rc,p}$), abdominal rib-cage volume ($V_{rc,a}$), abdominal volume (V_{ab}), chest-wall volume (V_{cw}). Volumes are expressed in liters.

partment is computed from the expiration phase of the relaxation maneuver as shown in Fig. 6.8 (Aliverti et al., 2002). A second-order polynomial interpolation is applied in the $(P_{es}, \Delta V_{rc,p})$ plane over the expiration section of the maneuver. The analytical expression of rib-cage relaxation curve is therefore written as follows:

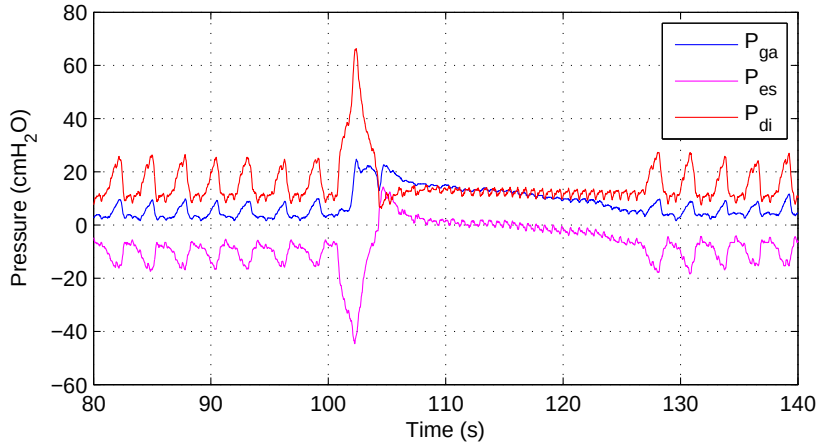

Figure 6.7 Respiratory pressures during quiet breathing and a relaxation maneuver. Gastric pressure (P_{ga}) (blue), esophageal pressure (P_{es}) (magenta), transdiaphragmatic pressure (P_{di}) (red).

$$\Delta V_{rc,p} = \alpha P_{es}^2 + \beta P_{es} + \gamma, \tag{6.5}$$

where α, β and γ are the three constant coefficients calculated from the second-order regression.

Abdominal relaxation curve: the relaxation curve for the abdominal compartment is computed from the quiet breathing section (quiet breathing only involves respiratory muscle recruitment during inspiration) recorded before a relaxation maneuver as illustrated by Fig. 6.9. This procedure is performed according to the following sequence: 1) re-sampling of four consecutive quiet breathing cycles onto a 0 to 100% temporal scale; 2) averaging of the four re-sampled cycles; 3) linear interpolation on the first half of the expiration phase in the $(\log(P_{ga}), \Delta V_{ab})$ space (Aliverti et al., 2002).

Since relaxation maneuvers are performed in a slightly different position than during music performance, the abdominal relaxation curve calculated from the relaxation maneuver data is slightly shifted compared to a relaxation curve calculated from quiet breathing before a musical task. However, quiet breathing during musical tasks was often not as regular as during prelim-

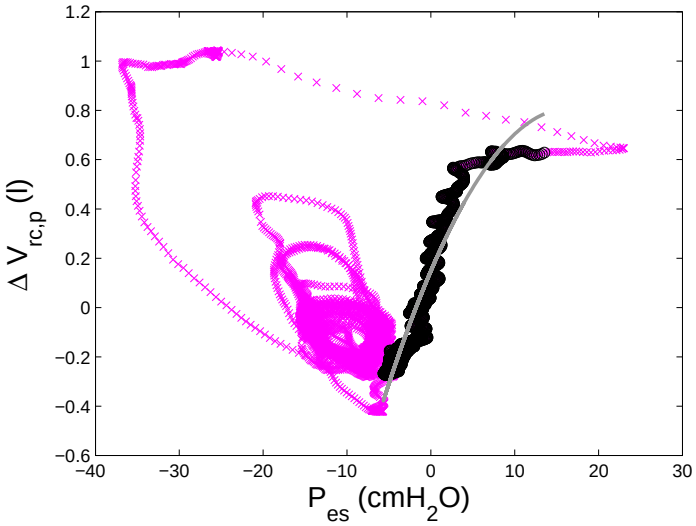

Figure 6.8 Rib-cage relaxation curve. Relaxation curve (gray line), relaxation maneuver preceded by quiet breathing (magenta cross), section of the maneuver used for interpolation (black circle).

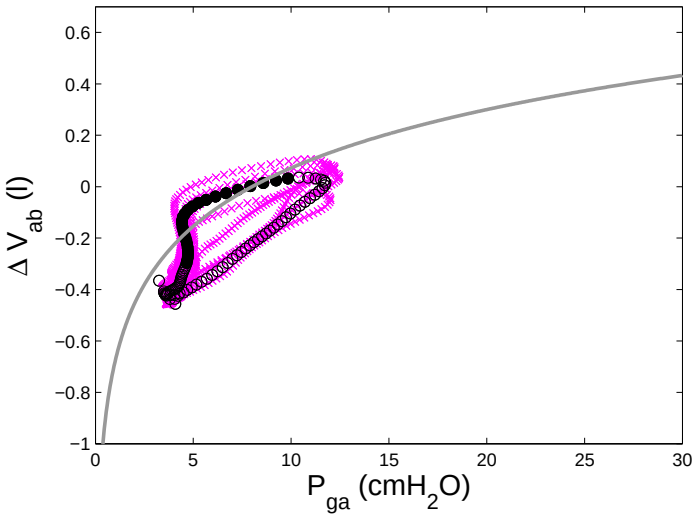

Figure 6.9 Abdominal relaxation curve. Relaxation curve (gray line), quiet breathing cycles used for calculation (magenta cross), averaged quiet breathing cycle (circle), section of the average quiet breathing cycle used for interpolation (filled circle).

inary relaxation maneuvers, most probably because of the perturbation induced by the protocol and equipment. In order to compensate for this offset, the relaxation curve (calculated from a quiet breathing segment during the relaxation maneuver) is adjusted to an end-expiration point extracted from a quiet breathing cycle preceding a musical task. The location of this point is determined by the maximum of V_{cw} over the selected cycle, extracted through parabolic interpolation. Noting $(P_{ga,ref}, \Delta V_{ab,ref})$ the coordinates of the end-expiration point in the $(P_{ga}, \Delta V_{ab})$ plane, the expression of the adjusted abdominal relaxation curve is written as follows:

$$\Delta V_{ab} = \gamma \log\left(\frac{P_{ga}}{P_{ga,ref}}\right) + \Delta V_{ab,ref}. \tag{6.6}$$

where γ is a coefficient calculated from the linear regression at step 3.

The pressure developed by respiratory muscles is calculated by departures of dynamic pressure-volume loops during exercise from relaxation curves (Aliverti et al., 1997). In the $(P_{es}, \Delta V_{rc,p})$ plane, the position of the pressure-volume loops relative to the pulmonary relaxation curve provides a quantitative estimation of the net pressure developed by the contraction of rib-cage muscles ($P_{i,rc}$ if it contributes to inspiration, and $P_{e,rc}$ if it contributes to expiration). Since rib-cage muscles include both inspiratory and expiratory muscles, the dynamic loop is likely to be displaced on both sides of the relaxation curve during exercise (see Fig. 2.12). In the $(P_{ab}, \Delta V_{ab})$ plane, the relative position of the pressure-volume loops provides an estimation of the pressure developed by contraction of abdominal muscles ($P_{e,ab}$). Since abdominal muscles are expiratory muscles showing only a negligible contribution to inspiration, pressure-volume dynamic loops during exercise are expected to occur only on the right side of the abdomen relaxation curve (see Fig. 2.12).

Diaphragm activity is measured by the pressure produced during activation and given by $P_{di} = P_{ga} - P_{es}$. Although P_{di} remains a good estimator of diaphragm activity, passive stretching

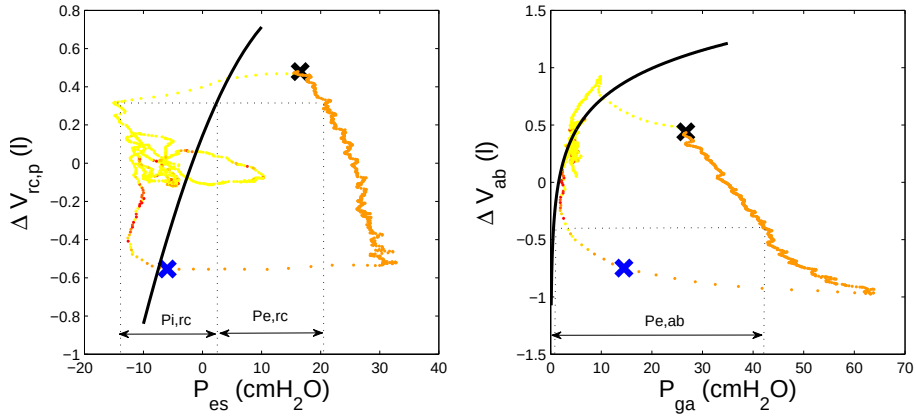

Figure 6.10 Rib-cage and abdominal pressure-volume curves during a sustained B♭3. Left: relationship between esophageal pressure (P_{es}) as an index of pleural pressure (P_{pl}) and volume variations of the pulmonary rib cage ($\Delta V_{rc,p}$), the color scale indicates the playing frequency (yellow refers to no sound). Solid black line, relaxation curve of the pulmonary rib cage. Measurement of the pressure generated by rib-cage muscles ($P_{i,rc}$ and $P_{e,rc}$) at any value of $\Delta V_{rc,p}$ is given by the horizontal distance between the dynamic loop and relaxation line at that volume. Points on the left of the relaxation curve are inspiratory ($P_{i,rc}$) and points on the right are expiratory ($P_{e,rc}$). Right: relationship between gastric pressure (P_{ga}) as an index of abdominal pressure (P_{ab}) and volume variations of the abdomen (ΔV_{ab}), the color scale indicates the playing frequency (yellow refers to no sound). Solid black line, relaxation curve of the abdomen. Measurement of the pressure generated by abdominal muscles ($P_{e,ab}$) at any value of ΔV_{ab} is given by the horizontal distance between the dynamic loop and relaxation line at that volume. Points on the right of the relaxation line are expiratory. The black and blue cross indicate tone onset and offset respectively. Orange and red points after tone offset are artifacts from the f_0 estimation.

of the diaphragm induced by high abdominal muscle recruitment may cause an increase in P_{di} that does not reflect any active contraction of the diaphragm.

An example of dynamic loop during a sustained B♭3 with constant dynamic is shown in Fig. 6.10. The color scale indicates the playing frequency f_0 as provided by the YIN algorithm where yellow refers to 0 Hz (no sound). In this example, the subject was asked to maintain a tone at a constant and comfortable dynamic as long as possible.

From this representation, the pressure developed by rib-cage and abdominal muscles can be derived at each time step by calculating the horizontal distance of the pressure-volume loop to the

pulmonary and abdomen relaxation curves. Graphically, we observe that the main contribution to inspiration comes from rib-cage muscles. During playing, the pressure-volume relationship follows a linear relationship with negative slope in both compartments. The smaller slope for the rib-cage compartment indicates less pressure variations during tone production. On the contrary, abdominal muscles provide an increasing expiratory pressure with decrease in volume. Both muscle groups generate an expiratory action during tone production, with the abdominal muscles contributing the most.

6.1.6 Power and resistance

Additional physiological parameters are considered, the embouchure resistance (R_e) and glottal resistance (R_g) in Ohms (Ω) calculated over the expiration phases respectively as the ratio of the pressure difference across the lips to the expiratory volume flow, and the ratio of the pressure difference across the glottis to the expiratory volume flow (Q_l). We consider that the quasi-static component of the mouthpiece pressure is negligible so the pressure difference across the lips is given by the mouth pressure P_m. Moreover, the subglottal pressure is estimated using the esophageal pressure P_{es} which leads to the following expressions:

$$R_g = \frac{P_m}{Q_l} \tag{6.7}$$

$$R_e = \frac{P_{es} - P_m}{Q_l}. \tag{6.8}$$

Analogously, the input power at the mouth Pw_m in Watts can be calculated as the product of the expiratory flow in m^3/s with the mouth pressure in Pascals (Pa):

$$Pw_m = Q_l \cdot P_m. \tag{6.9}$$

6.1.7 Data visualization

All recorded and extracted parameters are represented as a function of time during a sustained B♭3 in Fig. 6.11. This representation offers a complementary view to the pressure-volume diagram presented in Fig. 6.10 while allowing fast and easy visualization of the temporal evolution of physiological data. As predicted by the pressure-volume representation (Fig. 6.10), expiratory pressure developed by rib-cage and abdominal muscles increases along the production of the tone while the mouth pressure remains constant. The diaphragm is active at inspiration just before tone onset and drops very fast to baseline. Transdiaphragmatic pressure remains close to baseline during sound production indicating no active contraction of the diaphragm. A slight increase in P_{di} is observed around the end of tone, due to passive stretching of the diaphragm at low abdominal volumes. The end of the tone is also marked by a positive glottal resistance, while embouchure resistance remains constant. This late increase in glottal resistance may reflect a reduction of glottal opening occurring at the very end of expiration, close to Residual Volume (RV).

6.1.8 Protocol

One experienced trombone player (the author if this thesis) served as a subject for this experiment. The subject has about 10 years of training and experience in professional ensembles in France and Canada. Experiments involved two preparatory respiratory tasks and three musical tasks. The two preparatory tasks included a vital capacity maneuver allowing to assess the respiratory function of the subject, as well as a relaxation maneuver described in the previous part. For these two tasks, the the subject was instructed to breath through a pneumotach (Hans Rudolf 0-160 l/min) in order to monitor respiratory flow independently from OEP recording. The first music task consisted of isolated sustained tones at a comfortable dynamic in an ascending

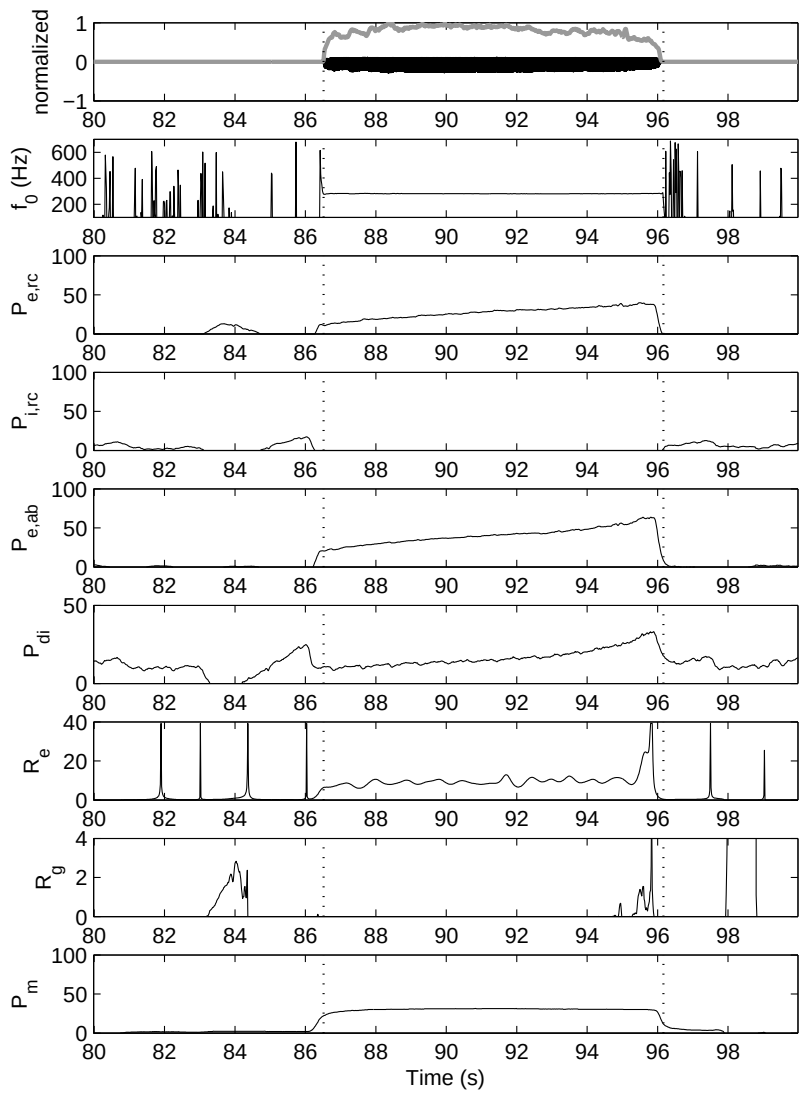

Figure 6.11 Time-domain data representation during a sustained B♭3. From top to bottom: waveform of the radiated sound pressure (black) and normalized acoustic sound power at the bell (gray), fundamental frequency of the sound (f_0) in Hz, expiratory pressure developed by rib-cage muscles ($P_{e,rc}$), inspiratory pressure developed by rib-cage muscles ($P_{i,rc}$), expiratory pressure developed by abdominal muscles ($P_{e,ab}$), transdiaphragmatic pressure (P_{di}), embouchure resistance (R_e) and glottal resistance (R_g) in MΩ, mouth pressure (P_m). Vertical dotted lines indicate tone onset and offset. Pressures are indicated in cmH_2O unit.

sequence corresponding to the arpeggio series played with the slide in closed position: B♭2; F3; B♭3; D4; F4; B♭4; D5; F5. The second task consisted in playing the same isolated tone sequence while varying the dynamic of each tone from *mp* to *ff* back to *mp*. Finally, the last task consisted in playing ascending and descending arpeggio series with slurred transition (no tonguing) at comfortable dynamic between B♭2 and F5.

6.2 Playing control parameters in stable pitch and loudness conditions

We first focus our attention on the characteristics of playing control parameters with respect to playing frequency and dynamic during sustained tones. Analysis is conducted according to the following sequence: 1) tone onsets and offsets are detected using a threshold criteria on the acoustic power signal calculated from the radiated sound using YIN, 2) the value of the following playing control parameters, mouth pressure P_m, volume flow Q_l, embouchure resistance R_e, glottal resistance R_g, power input at the mouth Pw_m, and amplitude of the trombone acoustic input impedance (or downstream input impedance) at the fundamental frequency $Z_d(f_0)$ are averaged over the duration of each tone. This operation results in one value of each of these parameter for each tone played in the first task. The results are presented as a function of the playing frequency f_0 in Fig. 6.12.

The results corroborate previous findings (Bouhuys, 1964, 1965, 1968; Elliot & Bowsher, 1982; Fletcher & Tarnopolsky, 1999). Under a constant dynamic constraint, the static pressure in the mouth, the embouchure resistance and the input power at the mouth increases with frequency, while the expiratory volume flow decreases with increase in f_0. The relationship between P_m and f_0 is particularly linear, as observed by Fletcher and Tarnopolsky in trumpets (Fletcher & Tarnopolsky, 1999). The averaged mouth pressure ranges between 14 and 62 cmH_2O (1.4 and 6.1 kPa), while averaged embouchure resistance is comprised between 4 and 27 MΩ. Minimum

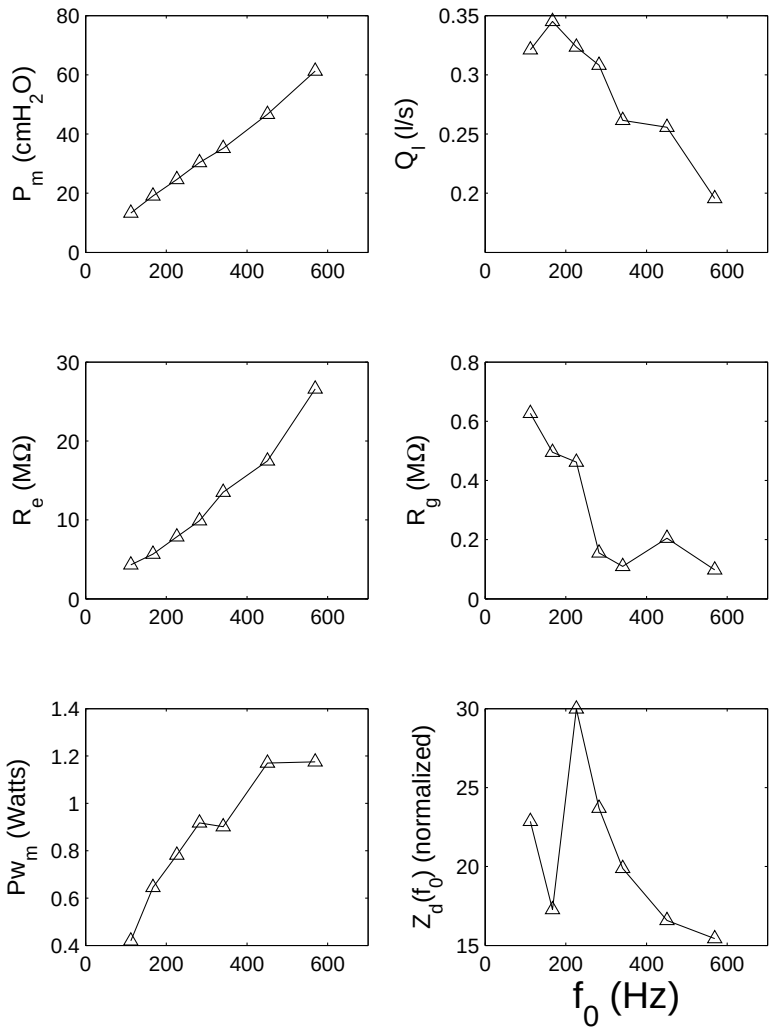

Figure 6.12 Averaged control parameters as function of the fundamental frequency. Mouth pressure P_m, volume flow Q_l, embouchure resistance R_e, glottal resistance R_g, power input at the mouth Pw_m, and amplitude of the trombone acoustic input impedance at the fundamental frequency $Z_d(f_0)$ averaged along the duration of sustained tones.

averaged volume flow is observed at 0.2 l/s and maximum at 0.35 l/s. The averaged glottal resistance is very small compared to the averaged embouchure resistance and tends to decrease with pitch. However, this observation should be taken carefully; in all tones, R_g is null along the tone duration and takes positive values only at the very end of the tone. Thus, averaging the value R_g over the tone duration may not be adequate in this context. Finally, it is worth noticing that the value of $Z_d(f_0)$ follows consistently the amplitude of the peaks in Z_d as shown in Fig. 6.5. Particularly, the amplitude of the fourth resonance is reduced compared to the neighbouring peaks (Fig. 6.5), which results in a low value of $Z_d(f_0)$ for the second tone played at 170 Hz (Fig. 6.12).

A second series of analysis is conducted on the second task according to the following sequence: 1) tone onsets and offsets are detected using a threshold criteria on the acoustic power signal calculated from the radiated sound, 2) the value of the mouth pressure P_m and volume flow Q_l are averaged over ten-sample windows (167 ms) resulting in vectors describing the smoothed evolution of P_m and Q_l over the duration of each note. The values corresponding to each playing frequency are represented in the (Q_l, P_m) plane in Fig. 6.13, together with lines of equal input power ($P_m \cdot Q_l$ constant) and equal embouchure resistance (P_m/Q_l constant).

The results obtained are comparable to previous findings (Bouhuys, 1968), which provide support to our protocol. Minimum flow occurs at minimum dynamic around 0.1 l/s and maximum flow is observed for the lowest tone and maximum loudness at 0.8 l/s. Minimum mouth pressure is observed at 8 cmH_2O for the lowest tone (f_0=114 Hz) and minimum dynamic, and maximum pressure around 65 cmH_2O for the highest playing frequency (f_0=450Hz) at maximum loudness. At all frequencies, a clear hysteresis behaviour is induced by the change in amplitude of the radiated sound. The largest input power ($\simeq$ 1.5 Watts) occurs for the lowest playing frequencies at high dynamic. Increase in pitch results in higher embouchure resistance, as well as lower input power. In the (Q_l, P_m) plane, the playing area defined for each tone by the positions of data points tends to move from the lower part of the plane (low R_e and large Pw_m range) to the top left corner

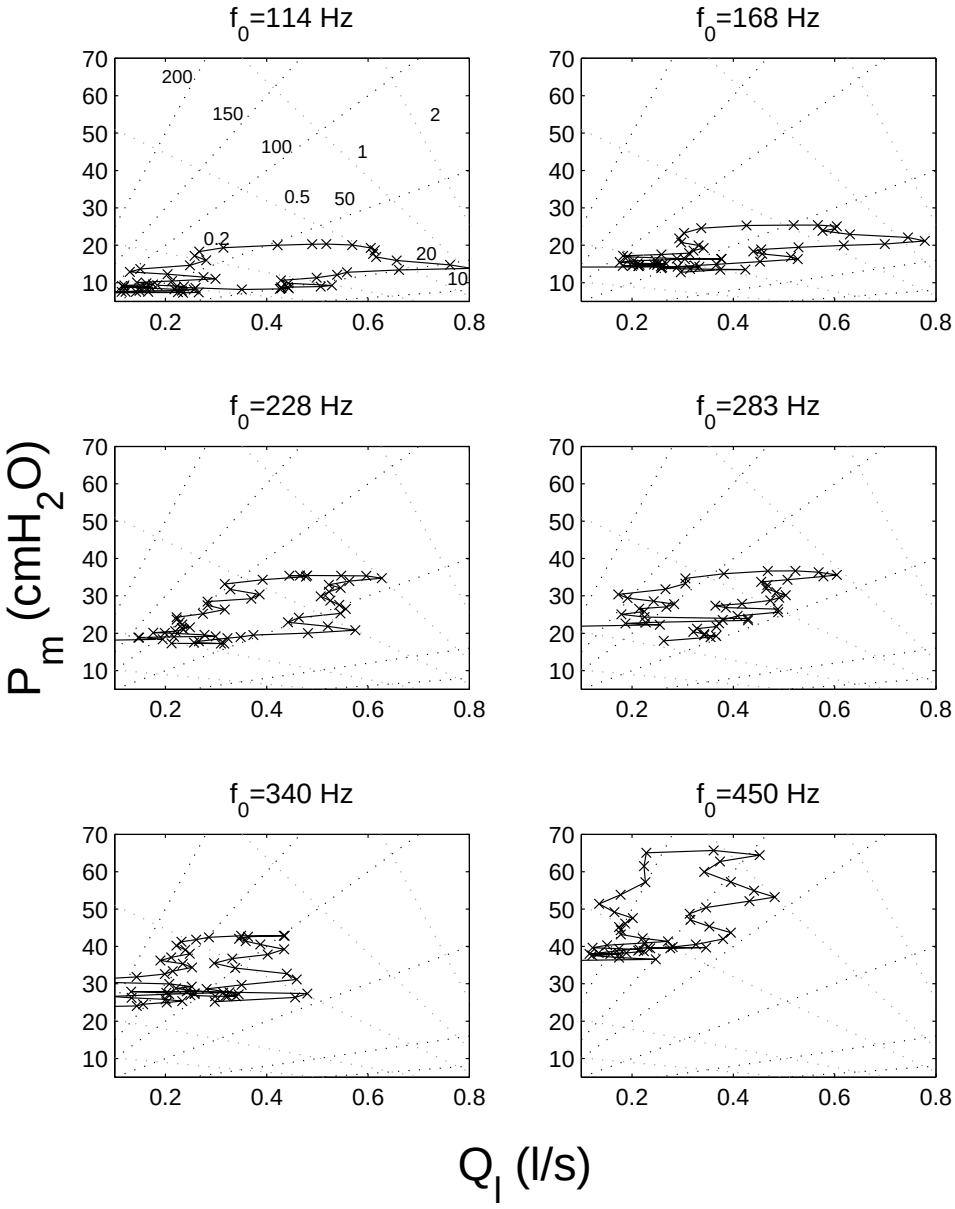

Figure 6.13 Pressure-flow relationship during sustained tones with increasing and decreasing dynamic (from *pp* to *ff* and back to *pp*). Mouth pressure P_m as a function of volume flow Q_l averaged over 10-sample windows. Black dotted lines indicates lines of equal embouchure resistance in cmH_2O.s.l^{-1} (P_m/Q_l constant), gray dotted lines indicate lines of equal input power in Watts ($P_l \cdot Q_l$ constant).

(high R_e and small Pw_m) with increase in playing frequency.

6.3 Chest-wall dynamics

In this part, we investigate the action of respiratory muscles on the management of pressure within the respiratory system during the three tasks presented previously. As discussed, in Section 6.1.5, the pressure developed by respiratory muscles can be deduced from the distance of pressure-volume loops to the relaxation curves of the pulmonary rib-cage and abdominal compartments. Analogously, we introduce a third two-dimensional space: (P_{es},V_{cw}), where the pressure induced by all chest-wall respiratory muscles is determined in reference to the chest-wall relaxation curve. The chest-wall relaxation curve is determined by a second-order polynomial fit on the relaxation phase in the (P_{es}, V_{cw}) plane, similarly to the pulmonary rib cage. This representation gives an overall view of the relaxation characteristics of the chest wall.

6.3.1 Sustained tones

Pressure-volume loops for sustained tones from B♭2 to F4 are presented in Fig. 6.14. The corresponding time-domain quantities are displayed in Fig. 6.15. From pressure-volume diagrams (Fig. 6.14), we observe a rather linear relationship between volume and pressure for the rib cage and abdomen during sound production (expiratory phase). Larger volume and pressure variations are observed for the abdominal compartments. No overlap is observed between each tone in the pressure-volume planes.

From the time-domain representation in Fig. 6.15, we notice a linear increase in the net expiratory pressure developed by rib-cage and abdominal muscles, while the mouth pressure remains constant. Transdiaphragmatic pressure is close to baseline (P_{di} baseline: minimum P_{di} during quiet breathing at 10 cmH_2O) at tone onset and slightly increases with time. This behaviour does

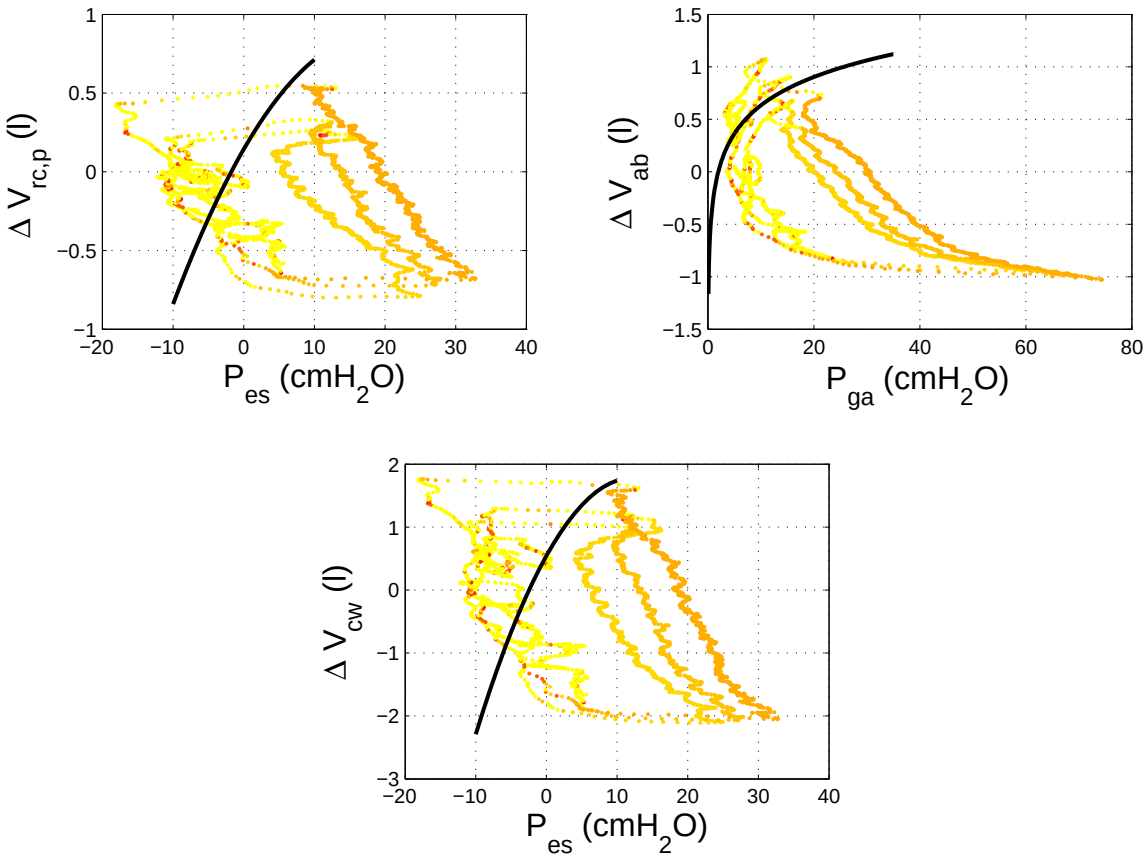

Figure 6.14 Pressure-volume loops during sustained B♭2, F3 and B♭3. Top left: relationship between esophageal pressure (P_{es}) as an index of pleural pressure (P_{pl}) and volume variations of the pulmonary rib cage ($\Delta V_{rc,p}$). Solid black line, relaxation curve of the pulmonary rib cage. Top right: relationship between gastric pressure (P_{ga}) as an index of abdominal pressure (P_{ab}) and volume variations of the abdomen (ΔV_{ab}). Solid black line, relaxation curve of the abdomen. Bottom, relationship between esophageal pressure (P_{es}) as an index of pleural pressure (P_{pl}) and volume variations of the chest wall (ΔV_{cw}). Solid black line, relaxation curve of the chest wall. The color scale indicates the playing frequency (light yellow refers to no sound).

not necessarily reflect an active contraction of the diaphragm, but may rather indicate a passive stretching due to significant decrease in the volume of the abdominal compartment and the important contraction of abdominal muscles. Embouchure resistance R_e is relatively constant over the duration of the tones, while the glottal resistance R_g increases only at the very end of each

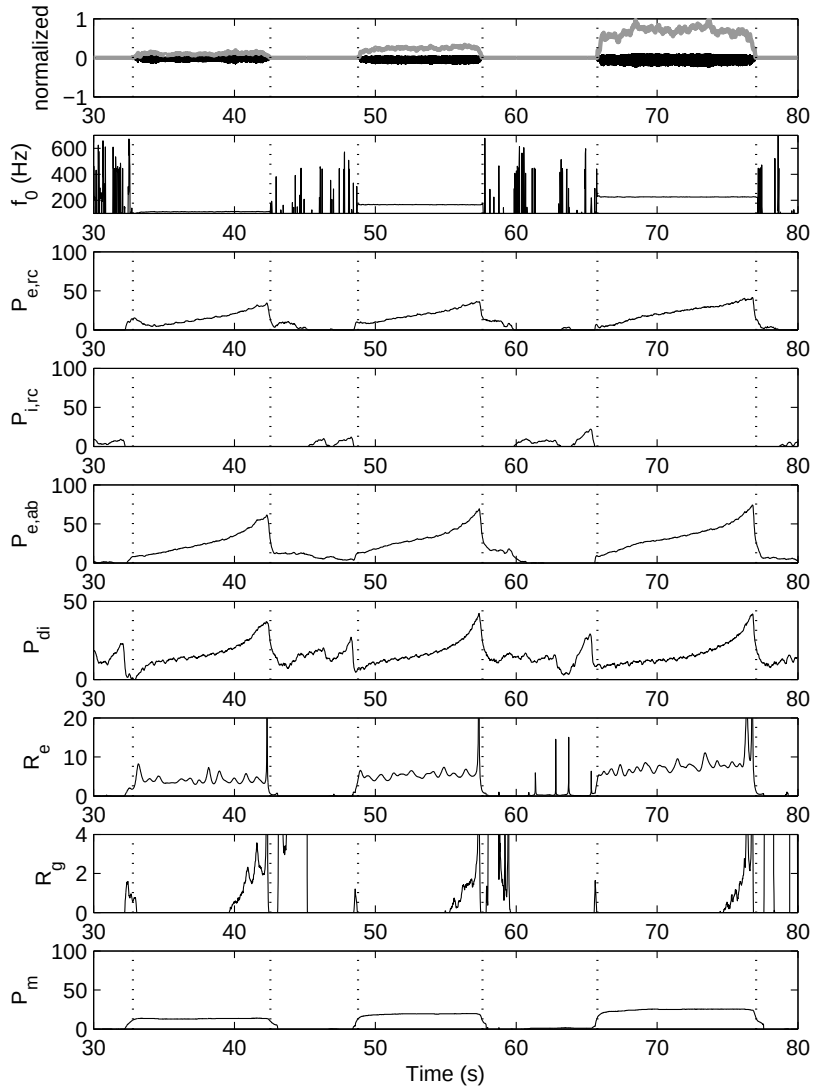

Figure 6.15 Time-domain parameters during sustained B♭2, F3 and B♭3. From top to bottom: waveform of the radiated sound pressure (black) and normalized acoustic sound power at the bell (gray), fundamental frequency of the sound (f_0) in Hz, expiratory pressure developed by rib-cage muscles ($P_{e,rc}$), inspiratory pressure developed by rib-cage muscles ($P_{i,rc}$), expiratory pressure developed by abdominal muscles ($P_{e,ab}$), transdiaphragmatic pressure (P_{di}), embouchure resistance (R_e) and glottal resistance (R_g) in MΩ, mouth pressure (P_m). Vertical dotted lines indicate tone onset and offset. Pressures are indicated in cmH_2O units.

tone in conjunction with P_{di} peak value.

Overall, similar patterns are obtained from B♭3 to D5. Results collected in this frequency range are presented in Figs. A.1 and A.2 (Appendix A pp. 190 and 191). Some additional conclusions may however be formulated in light of this data. Overall, the slope of the pressure-volume line during playing decreases with increase in pitch, indicating smaller volume variations as playing frequency rises. This corroborates the results shown in Fig. 6.12, which demonstrates a decrease in expiratory volume flow with increase in playing frequency. Results from Fig. A.1 also emphasize some other features: in particular the increase of the pressure developed by respiratory muscles and increase of starting volumes with increase in playing frequency.

6.3.2 Varying loudness

Pressure-volume loops for sustained tones from D4 to B♭4 are presented in Fig. 6.16. The corresponding time-domain quantities are displayed in Fig. 6.17. As in previous tasks, all instances seem to follow a very stereotypic pattern; the increase and decrease in mouth pressure (following the increase and decrease in loudness) is reflected in the three pressure-volume loops shown in Fig. 6.16. In the pressure-volume plane (Fig. 6.16), a two-step sequential evolution of the upper rib cage and abdominal volumes appears: a first step involves a strong and rapid decay in V_{ab}, while V_{rc} decreases slowly; this is followed by a second step where V_{rc} decreases at a higher rate while V_{ab} remains almost constant. This sequential and asymmetrical pattern in the (P_{es}, V_{rc}) and (P_{ga}, V_{ab}) planes results into a relatively symmetrical loop in the (P_{es}, V_{cw}) plane inducing a decrease of chest-wall volume at a constant rate. Overall, each tone is marked by a sequential and hierarchical pattern involving an initial decrease in abdominal volume that transfers to the rib-cage compartment when the abdominal volume becomes too small (close to RV).

In the time domain (Fig. 6.17), we observe that the net expiratory pressure developed by rib-cage muscles seems to follow more closely the evolution of P_m, while the net expiratory

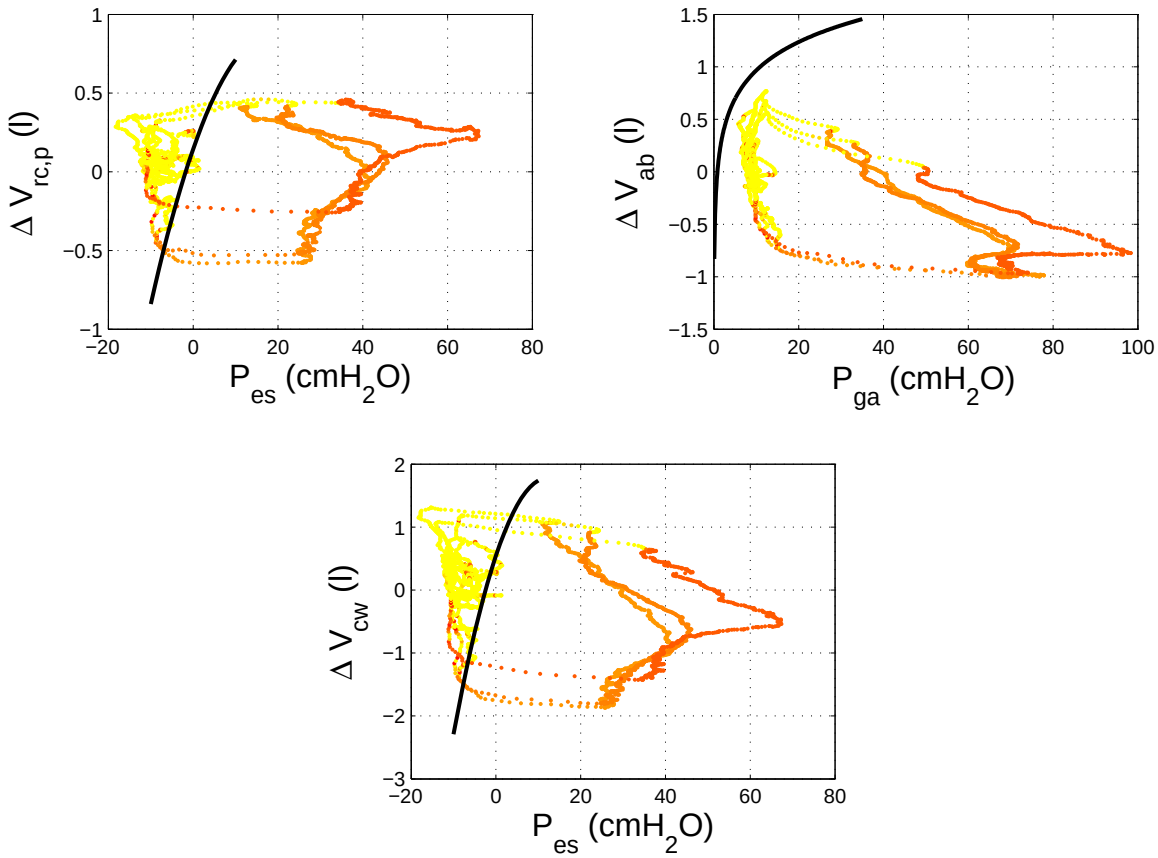

Figure 6.16 Pressure-volume loops during sustained D4, F4 and B♭4 played with increasing and decreasing dynamics. Top left: relationship between esophageal pressure (P_{es}) as an index of pleural pressure (P_{pl}) and volume variations of the pulmonary rib cage ($\Delta V_{rc,p}$). Solid black line, relaxation curve of the pulmonary rib cage. Top right: relationship between gastric pressure (P_{ga}) as an index of abdominal pressure (P_{ab}) and volume variations of the abdomen (ΔV_{ab}). Solid black line, relaxation curve of the abdomen. Bottom, relationship between esophageal pressure (P_{es}) as an index of pleural pressure (P_{pl}) and volume variations of the chest wall (ΔV_{cw}). Solid black line, relaxation curve of the chest wall. The color scale indicates the playing frequency (light yellow refers to no sound).

pressure developed by abdominal muscles overall increases with time. This characteristic is particularly true for D4 and F4 (two first tones in Fig. 6.17), where the correlation between $P_{e,ab}$ and P_m seems weaker than in other tones. This suggests that for these two tones, the abdominal compartment behaves as pressure generator providing a uniformly growing pressure, while the

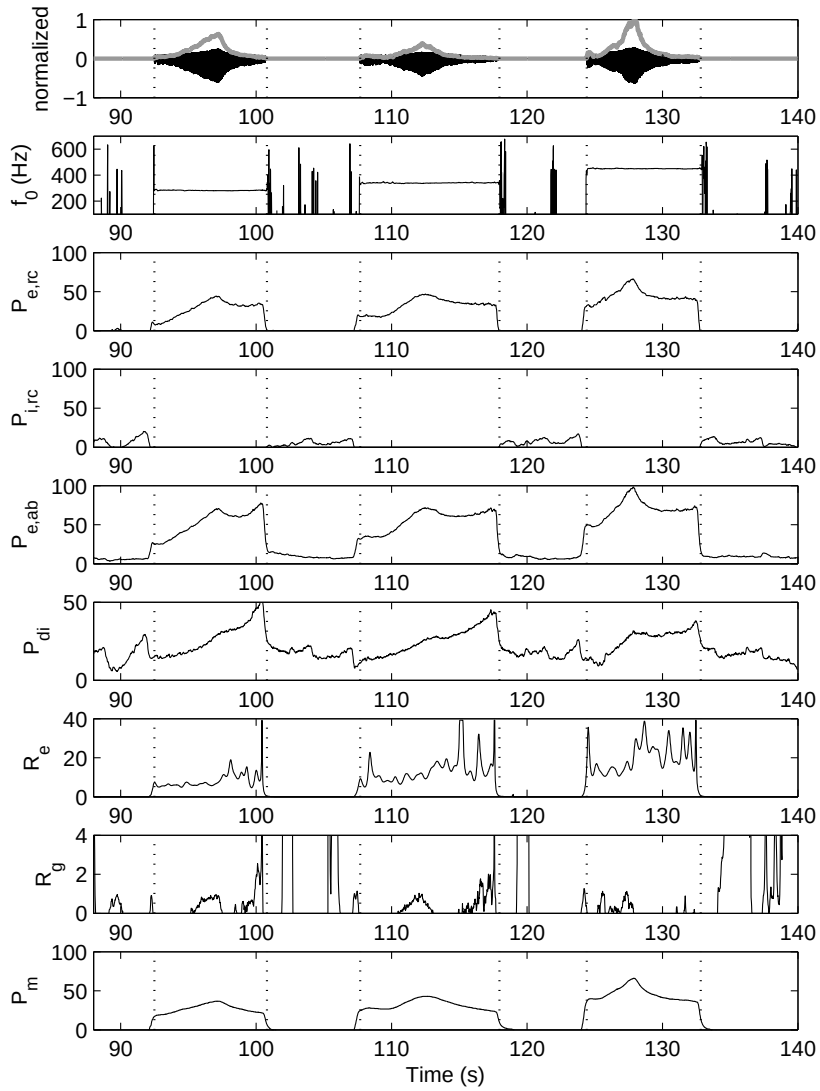

Figure 6.17 Time-domain parameters during sustained D4, F4 and B♭4 played with increasing and decreasing dynamics. From top to bottom: waveform of the radiated sound pressure (black) and normalized acoustic sound power at the bell (gray), fundamental frequency of the sound (f_0) in Hz, expiratory pressure developed by rib-cage muscles ($P_{e,rc}$), inspiratory pressure developed by rib-cage muscles ($P_{i,rc}$), expiratory pressure developed by abdominal muscles ($P_{e,ab}$), transdiaphragmatic pressure (P_{di}), embouchure resistance (R_e) and glottal resistance (R_g) in MΩ, mouth pressure (P_m). Vertical dotted lines indicate tone onset and offset. Pressures are indicated in cmH_2O units.

rib-cage compartment acts as a pressure modulator, adjusting the mouth pressure to the desired value. As in previous tasks, $P_{e,ab}$ is also characterized by an abrupt increase at the end of each tone. This behaviour may reflect the need for a strong abdominal recruitment at low lung volumes in order to generate the appropriate mouth pressure. This effect is less marked in the high register (for the two highest tones). However the reasons for these differences remain uncertain. Possibly, an active contraction of the diaphragm may participate to increase abdominal pressure at the end of certain tones. Moreover, the small bump observed in P_{di} in Fig. 6.17, and which coincides with the maximum in P_m (maximum loudness), implies a possible active contraction of the diaphragm likely to reduce the effect of $P_{e,ab}$ on the pressure in the lungs.

Embouchure resistance R_e is relatively stable along the duration of each tone and does not seem to follow significantly the variation of dynamic, except for the last tone. On the contrary, R_g becomes significant at the maximum of sound energy and at the end of the tones, except for the last one. This potentially indicates a resistance transfer between the lips and the glottis at high dynamic levels, potentially in order to maintain R_e constant and substitute to mechanical constraints on the lips. The late increase in R_g may contribute to maintain the levels of P_{es} and P_{ga} at low volumes, and possibly participate to adjust vocal-tract acoustical resonances around the playing frequency by reducing glottal opening (Barney et al., 2007). Again, R_g seems relatively correlated to the evolution of P_{di}, whose justification remains uncertain. The value of P_{di} close to baseline suggests an optimal mechanical coupling between the abdominal and rib-cage compartments, hence allowing efficient transmission of the abdominal pressure to the pleural pressure.

Overall, these observations can be extrapolated to lower frequency tones. Indeed, relatively similar behaviours are observed from B♭3 to B♭4 as shown by Figs. A.3 and A.4 (Appendix A pp. 192 and 193).

6.3.3 Varying pitch

The pressure-volume loop for an ascending and descending arpeggio series from B♭2 to F5 back to B♭2 (arpeggio series: B♭2, F3, B♭3, D4, F4, B♭4, D5, F5) is presented in Fig. 6.18. The corresponding time-domain quantities are displayed in Fig. 6.19. In this exercise, the sequential coordination of the rib-cage and abdominal compartments is even more apparent: during the ascending pitch section, $V_{rc,p}$ is constant and even slightly increasing, while V_{ab} significantly decreases; on the contrary, during the descending pitch phase, $V_{rc,p}$ decreases drastically while V_{ab} remains constant as P_{ga} decreases. The late effect of an increase in $P_{e,ab}$ is also present and involves a small decay in V_{ab}.

This small increase in $V_{rc,p}$ in the ascending pitch phase reflects an expanded upper chest condition, where the musician maintains a large upper rib-cage volume. The reasons for this particular pattern may reflect different control strategies during the ascending and descending parts. In the time domain (Fig. 6.19), we observe that $P_{e,rc}$ and $P_{e,ab}$ follow a similar evolution, with a higher level of pressure developed by abdominal muscles, possibly contributing to an increase in $V_{rc,p}$ through a transfer of pressure from the abdominal to rib-cage compartment. We further hypothesize that the sequential control of chest-wall volumes aims to maintain a balanced distribution of the pressure generated by abdominal and rib-cage muscles along the tone duration. Possibly, we may conclude that abdominal compression is beneficial for the production of a high level of pressure in the ascending pitch part, while rib-cage compression offers a better control of the pressure on the descending part. This sequential activation results in a very symmetrical loop in the (P_{es}, V_{cw}) as observed in task 2 (Fig. 6.18). Finally, the sound onset in the $(P_{es}, V_{rc,p})$ and (P_{es}, V_{cw}) planes occurs very close to relaxation curves, indicating a relaxed state of the chest wall and rib cage at the beginning of the task.

Similarly to Fig. 6.12, R_e consistently follows the evolution of f_0. Glottal resistance R_g takes

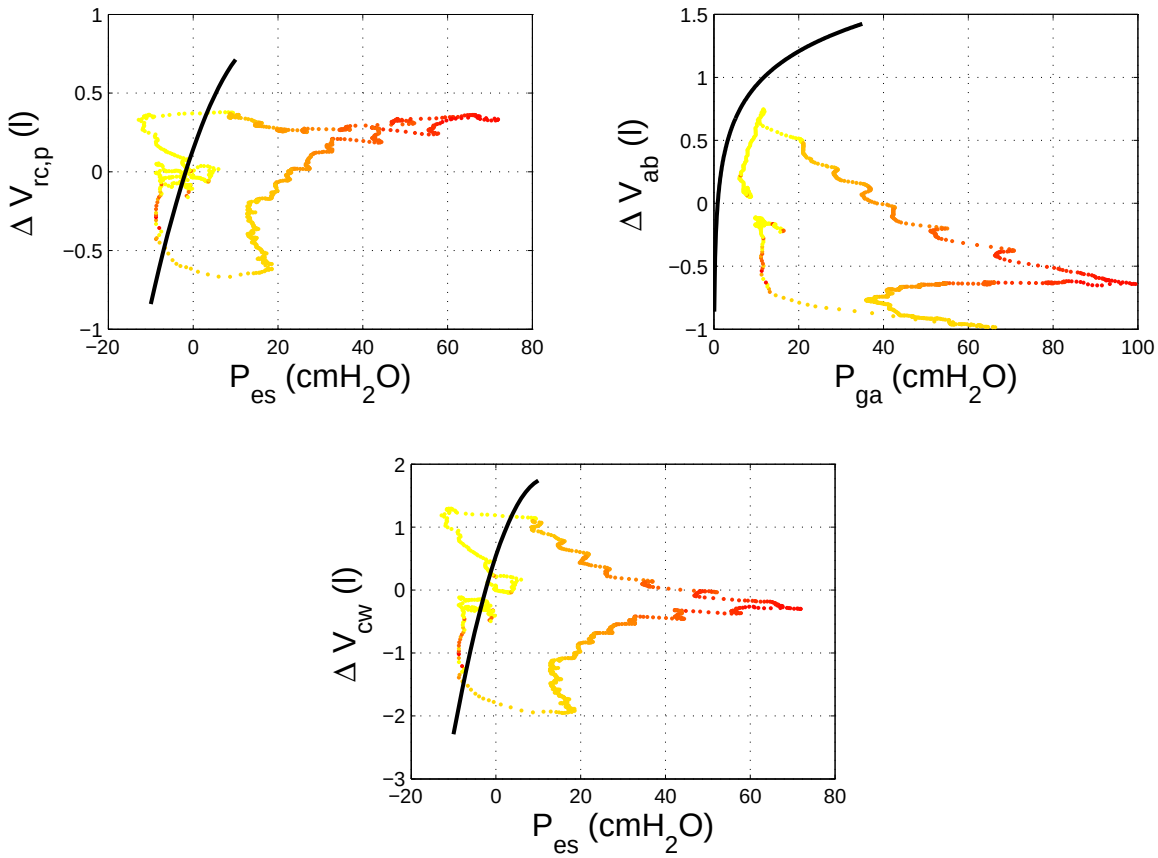

Figure 6.18 Pressure-volume loops during ascending and descending arpeggios (arpeggio series: B♭2, F3, B♭3, D4, F4, B♭4, D5, F5). Top left: relationship between esophageal pressure (P_{es}) as an index of pleural pressure (P_{pl}) and volume variations of the pulmonary rib cage ($\Delta V_{rc,p}$). Solid black line, relaxation curve of the pulmonary rib cage. Top right: relationship between gastric pressure (P_{ga}) as an index of abdominal pressure (P_{ab}) and volume variations of the abdomen (ΔV_{ab}). Solid black line, relaxation curve of the abdomen. Bottom, relationship between esophageal pressure (P_{es}) as an index of pleural pressure (P_{pl}) and volume variations of the chest wall (ΔV_{cw}). Solid black line, relaxation curve of the chest wall. The color scale indicates the playing frequency (light yellow refers to no sound).

positive value for the highest tones at the end of the ascending pitch phase around 70 seconds in Fig. 6.19. Again, assuming that R_g denotes a reduction of glottal opening, this observation may be consistent with an acoustical tuning of the vocal tract as a support to lip oscillations in the high register (cf. Chapter 3). The high value of R_g at the end of the tone sequence (between

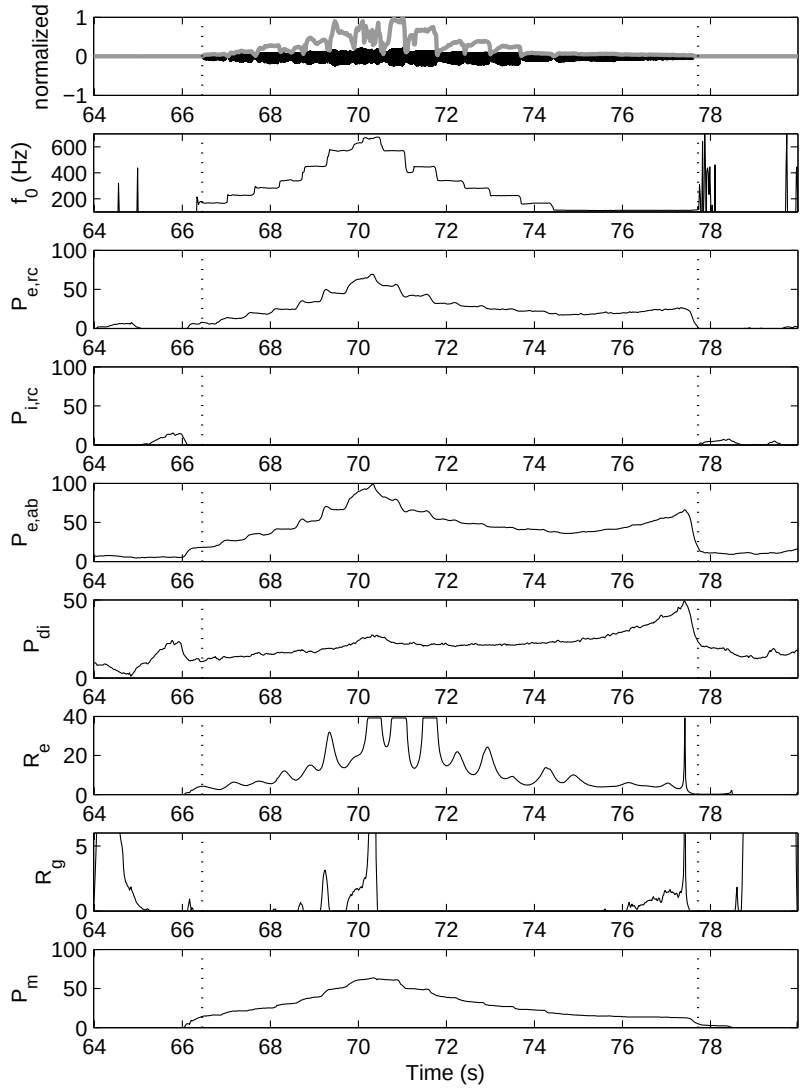

Figure 6.19 Time-domain parameters during ascending and descending arpeggios. From top to bottom: waveform of the radiated sound pressure (black) and normalized acoustic sound power at the bell (gray), fundamental frequency of the sound (f_0) in Hz, expiratory pressure developed by rib-cage muscles ($P_{e,rc}$), inspiratory pressure developed by rib-cage muscles ($P_{i,rc}$), expiratory pressure developed by abdominal muscles ($P_{e,ab}$), transdiaphragmatic pressure (P_{di}), embouchure resistance (R_e) and glottal resistance (R_g) in MΩ, mouth pressure (P_m). Vertical dotted lines indicate tone onset and offset. Pressures are indicated in cmH_2O units.

76 and 78 seconds in Fig. 6.19) is consistent with observations in previous tasks; it may reflect either an acoustical adjustment of the vocal-tract or a flow resistance, allowing a given level of pressure in the rib cage and abdomen to be maintained. This last hypothesis is supported by the simultaneous increase in P_{di}. Although it can be attributed to passive stretching of the diaphragm caused by a high level of abdominal pressure, this may also indicate an active contraction in order to maintain a given level of abdominal pressure (but hindering pressure transmission to the upper compartments).

6.3.4 Chest-wall dynamics and playing control parameters

In this section, we further focus our attention on the correlations between chest-wall dynamics and the control of quasi-static mouth pressure. In task 2, variations of the loudness of each tone involves significant variations in the mouth pressure P_m. This logically confirms that at a given playing frequency, P_m has a direct effect on the acoustic energy radiated outside the instrument. In task 3, variations of playing frequency with no constraints on the loudness also involves significant variations in P_m. This further confirms that P_m participates in the control of the fundamental frequency of the sound when the dynamic is constant. It is then interesting to observe how this control of P_m is performed by respiratory muscles in both situations.

The evolution of the net expiratory pressure produced by rib-cage and abdominal muscles during sustained tones played with varying dynamics is represented in Fig. 6.20 as a function of the mouth pressure P_m. For both muscle groups, the phase of increasing loudness (corresponding to an increase in P_m) is characterized by a linear relationship between the net pressure produced by respiratory muscles and the resulting mouth pressure. This relationship is distorted in the descending loudness part where the correlation with P_m becomes particularly non-linear for the abdominal compartment. This hysteresis effect tends to disappear with increase in pitch and an overall linearisation of the relationship between net expiratory pressures and P_m is visible for the

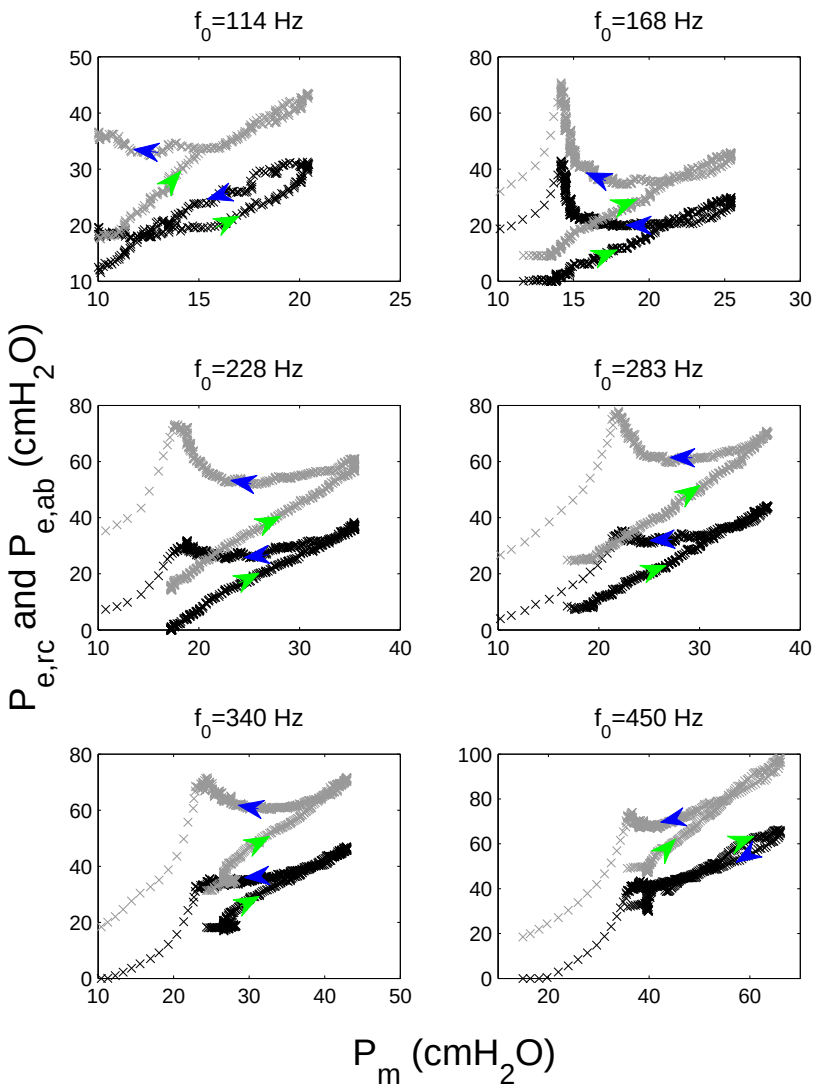

Figure 6.20 Relationship between the mouth pressure P_m and the net expiratory pressure developed by respiratory muscles during sustained tones with varying dynamics (*crescendo-decrescendo*). Pressure developed by rib-cage muscles (black cross) and abdominal muscles (gray cross). Green arrows indicate the *crescendo* and blue arrows the *decrescendo* phases.

highest tone. Furthermore, $P_{e,rc}$ and $P_{e,ab}$ follow a parallel trajectory revealing a synchronized control of the expiratory pressure developed by both compartments.

Analogously, the evolution of the net expiratory pressure produced by rib-cage and abdominal muscles during task 3 as a function of P_m is represented in Fig. 6.21. The linear relationship with the mouth pressure is emphasized in this case, although some distortion appears at the end of the task for the abdomen. A smaller hysteresis effect is observed between the ascending and descending pitch phases. Similarly, the net pressure developed by both muscle groups follows a very similar and parallel trajectory. This observation supports the hypothesis of an accurate regulation of the pressure developed by rib-cage and abdominal muscles, resulting into the sequential variations of the chest-wall volumes observed in previous sections.

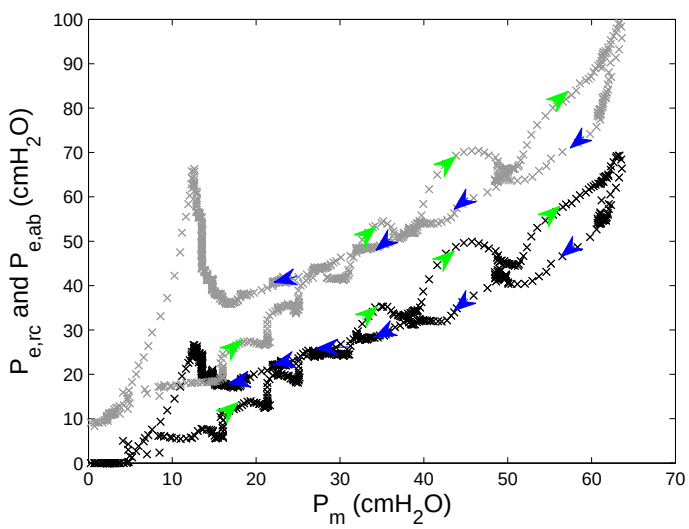

Figure 6.21 Relationship between the mouth pressure P_m and the net expiratory pressure developed by respiratory muscles during ascending and descending arpeggios. Pressure developed by rib-cage muscles (black cross) and abdominal muscles (gray cross). Green arrows indicate the ascending and blue arrows the descending arpeggio phases.

Looking at the evolution of the net expiratory pressure produced by rib-cage and abdominal muscles during task 3 as a function of f_0 in Fig. 6.22, we observe a striking linear relationship for both compartments. It is important to remember that this task was performed with no loudness constraint, resulting in variable radiated energy according to f_0. Therefore, if a constraint had

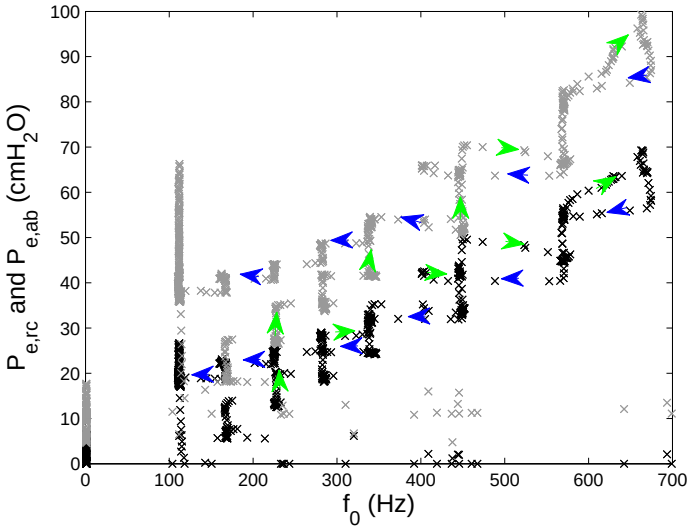

Figure 6.22 Relationship between the mouth pressure f_0 and the net expiratory pressure developed by respiratory muscles during ascending and descending arpeggios. Pressure developed by rib-cage muscles (black cross) and abdominal muscles (gray cross). Green arrows indicate the ascending and blue arrows the descending arpeggio phases.

been given on the sound level produced, the variation in $Z_{in}(f_0)$ would have possibly required different levels of mouth pressure. Hence, these results suggest a predominant feedback control applied on the internal respiratory pressures rather than on sound intensity. We may further infer that a linear mental representation of the arpeggio series from the player, projects into a linear control of the mouth pressure relative to the playing frequency (Fig. 6.22). This relation may then be further translated into a linear control of respiratory muscles (Fig. 6.21).

6.4 Discussion in light of previous studies

Considering that results from only one subject are reported in this chapter, it is not possible to draw general conclusions out of our observations. Nevertheless, we may provide some elements of discussion by confronting our results with respiratory investigations conducted in other

instruments.

In flute playing, different co-ordinations of respiratory muscles were observed in three players, despite a consistent regulation of the mouth pressure P_m and embouchure aperture across subjects (Cossette et al., 2000). In the same study, various sequential deflections of chest-wall volumes were also observed during sustained tones: a) through an initial decrease of the rib-cage volume followed by deflection of the abdominal volume, b) an initial decrease of the abdominal volume followed by a decrease of the rib-cage volume, or c) simultaneous deflection of both compartments. The second strategy corroborates the sequential variation of chest-wall volumes observed in our data. According to Cossette et al. (2000), the first pattern suggests a gradual relaxation of inspiratory muscles, while the second sequence suggests a coactivation of non-diaphragmatic inspiratory muscles and the third sequence an activation of the diaphragm simultaneously to the expiratory muscles. The sequential variation of chest-wall volumes observed in trombone playing may be explained by a similar theory: despite a need for higher pressure in the trombone, inspiratory muscles are recruited at the beginning of expiration in order to maintain a high rib-cage volume. In the case of the trombone it potentially provides higher capability of generating expiratory pressures from the rib cage.

These patterns were further explored in (Cossette et al., 2008), where electromyographic (EMG) recordings of neck and abdominal muscles where performed. This study aimed at quantitatively assess the subjective interpretation of “breath support” and “no breath support” conditions in flautists. The recruitment of antagonist inspiratory muscles to counterbalance the elastic recoil of the chest wall was confirmed in the “breath support” condition. According to the author, this allows the rib cage to be held at a high volume and regulate the expiratory flow arising from the elastic recoil of the chest wall and of the lungs. Consequently, the author speculates that expiratory muscles, particularly abdominal muscles, become available for other types of control, such as fine adjustments of the mouth pressure required for precise tasks (stacatti, vibrato,

etc.). In light of these interpretation, we may infer that the high rib cage condition observed at the beginning of sustained tones with varying dynamic and arpeggios in our subject reveals a low activation of expiratory rib-cage muscles as well. Contrary to the flute, we speculate that this allows a fine regulation/modulation of the mouth pressure by rib-cage expiratory muscles (modulator), while abdominal muscles act as the main pressure generator. Furthermore, given the higher levels of pressure involved in trombone performance compared to flute playing, this high rib-cage volume observed in trombones may also result from the high esophageal pressure induced by strong abdominal muscle contraction and a relaxed diaphragm (which provides an optimal pressure-coupling between both compartments). Therefore, the expansion of the rib cage observed, particularly in the arpeggios (Fig. 6.18), supports the hypothesis of relaxed expiratory rib-cage muscles during the first part of the tone. Neck muscles (sternocleidomastoids and scalenes) may also contribute to maintain the upper rib cage elevated. This could be validated by recording EMG activity of these muscle groups. A complementary interpretation is that the weak rib-cage expiratory recruitment in the beginning of the tone reflects a "saving strategy" intending to preserve energy for the last part of the tone. It is also important to note that flute playing according to Cossette et al. (2000) required the flautists to use between 80 and 95 % of their vital capacity. Most of the tasks performed by our trombone player started around Functional Residual Capacity (FRC) or a bit above, which is far from being representative of the full vital capacity.

Despite occasional occurrences of diaphragm activation for specific technique playing (vibrato and staccati), Cossette et al. (2000) reported no diaphragmatic activation to counterbalance the elastic recoil of the chest wall and expiratory muscular activity in flute. This corroborates our results where P_{di} is found close to baseline in almost all exercises. The elevation of P_{di} at the end of the tones is an accordance with a passive stretching of the diaphragm occurring at low abdominal volumes as observed in flutes (Cossette et al., 2000). Furthermore, in trombone where the mouth pressure levels are higher than in flute, a low P_{di} value infers a high transmission of the

abdominal pressure to the lungs, consequently an optimal coupling between both compartments and a maximal effect of abdominal musculature on the driving mouth pressure.

Nevertheless, some instances of diaphragmatic recruitment observed, along with increase in glottal resistance R_g, may be prone to further interpretation. Sundberg et al. (1989) observed in singers correlations between diaphragmatic activity and contraction of the cricothyroid (CT) muscles acting on the tension of the vocal folds. Particularly, it was found that diaphragmatic activity emphasizes a tracheal pull effect (caudal force exerted on the trachea when diaphragm contracts) and widens the anterior gap between the cricoid and thyroid cartillages, thus slackening the vocal folds and decreasing pitch. In response to this perturbation, an increase in CT EMG activity was observed to maintain a constant pitch. In the context of our study, we may infer that diaphragmatic contractions (which origins are unclear) may have an effect on laryngeal configuration, hence producing some laryngeal muscle contractions causing a reduction of the glottal opening area. Although this statement remains at the stage of a speculation, the effect of diaphragm activity on the larynx should be a crucial subject of interest, since it may influence the vocal-tract geometry and therefore its acoustical properties.

In another study, Iwarsson and Sundberg observed correlations between lung volume and vertical position of the larynx in singers (Iwarsson & Sundberg, 1998). High lung volumes induced by high inspiratory muscle recruitment were correlated with low laryngeal position. According to the author, this is most probably due to the mechanical linkage between respiratory structures and the larynx, especially the tracheal pull induced by diaphragmatic recruitment during deep inspirations. These additional elements provide support to the hypothesis of a link between diaphragm activity and laryngeal configuration in trombone performance. This also corroborates the small increase in P_{di} observed around the highest tones in Fig. 6.19 where the glottal resistance is high and vocal-tract support is likely to be significant as shown in Chapter 3. One hypothesis is that the diaphragm induces some laryngeal adjustments through a tracheal pull and thus participates

to modify the acoustical properties of the vocal tract. Moreover, since the lung volume may have an effect on laryngeal height, it should then influence the length and shape of the vocal tract, and potentially its acoustical properties.

6.5 Summary

In this chapter we have presented an experimental setup for the investigation of chest-wall dynamics and respiratory control during trombone performance. This protocol utilizes a state-of-the-art optical acquisition technique (OEP) for the assessment of respiratory volumes and airflow during exercise. The monitoring of mouth-cavity, esophageal and gastric pressures allow the estimation of muscle activity by groups, diaphragm recruitment, as well as embouchure and glottal resistance. Although only the results from one subject are presented, self-consistent respiratory patterns are observed during musical tasks of varying loudness and pitch. These patterns are characterized by a sequential decay of abdominal and rib-cage volumes where the rib-cage volume is maintained high and the abdomen strongly deflected in the beginning of the tone. The relation is reversed for the second part of the tone. This pattern, suggests a relaxation of expiratory rib-cage muscles, either to save energy, or to allow a fine regulation of the mouth pressure by rib-cage muscles.

The net pressure developed by abdominal rib-cage muscles was found to follow parallel pathways in all tasks, with more pressure developed by abdominal muscles. Furthermore, diaphragmatic activity was found always close to baseline, indicating a relaxed diaphragm during playing. Transdiaphragmatic pressure is significantly raised at the end of long tones and arpeggio series, most probably as a result of a passive stretching of the diaphragm induced by high abdominal pressures. However, some occurrences of tonic diaphragmatic contractions were observed, especially at maximum loudness during *crescendo-decrescendo* exercises and at the highest tones

of arpeggio series. This activity also correlates with an increase in glottal resistance, suggesting a possible effect on laryngeal configuration. The hypothesis that diaphragm contraction has a non-negligible influence on the configuration and muscular activity of the larynx is reinforced by previous findings in singers (Sundberg et al., 1989; Iwarsson & Sundberg, 1998). It may also be inferred that neck muscles, likely to be recruited to maintain a high rib-cage volume during expiration, have a non-negligible effect on laryngeal configuration. These insights should throw the basis of further investigations on the correlations between respiration and the control of the acoustical properties of the vocal tract during performance.

Finally, in addition to the quasi-linear relationship between the mouth pressure P_m and playing frequency f_0 observed in arpeggios, the net pressure developed by rib-cage and abdominal muscles was found to vary linearly (and with no significant hysteresis) with P_m and f_0. This is observed in spite of the varying sound amplitude and magnitude of the trombone input impedance at f_0 along the arpeggio sequence. Since no constraints were imposed to the subject in terms of loudness, these observations may imply motor control strategy based on a linear representation of the relationship between f_0 and P_m, or f_0 and the pressure developed by respiratory muscles in arpeggios. This assumption raises our attention to the fundamental question of feedback in music performance. In particular, it points out the issue of the influence of the sensorimotor perception of respiration on the learning and control of sound production in wind instruments.

Conclusion and Future Work

The work presented in this thesis was undertaken with the aim to improve our understanding of the player-instrument interaction and control in brass performance. First, an experimental setup was developed in order to allow the characteristics of the upstream and downstream input impedances to be evaluated at the playing frequency. This approach provides a great temporal resolution, while maintaining a relatively low degree of invasiveness for the player. In light of experiments conducted on a pool of trombone players, the amplitude of the vocal tract input impedance at the playing frequency was found to increase with pitch, and equal or even override the regenerative effect of the downstream air column for the highest tones. Therefore, vocal-tract support seems required for the production of high tones at which the amplitude of the instrument input impedance is low. This support appears to result from a tuning of the amplitude of the vocal-tract impedance near the fundamental frequency when playing from the low to high register. Although pitch bendings do not seem to involve any acoustical support from the upstream airways, noticeable influence was observed during slurred tone transitions suggesting a complementary action of the vocal tract, taking over the regenerative effect of the trombone during a change of register. Furthermore, significant variation in the influence of the vocal tract was observed as a function of dynamic: the decreased upstream influence at high sound amplitudes may be related to the effect of higher harmonics on the support of lip auto-oscillations. It may also arise from a decrease in the control of upstream airway geometry, due to the constraints induced

by high static pressure along the respiratory airway.

Additionally, *in-vivo* measurements suggest that vocal-tract phase tuning at f_0 may be a determining aspect of an optimized tuning of the upstream airway. This hypothesis was first studied on an artificial player system by driving the mouth cavity with an external signal and simulating different conditions of upstream coupling at the fundamental frequency (active control method). Varying the phase of the upstream disturbing signal independently from its amplitude had an effect on both the playing frequency and acoustic energy produced. These observations suggest an ability of a player to alter the playing frequency without changing embouchure parameters by only adjusting the characteristics of a vocal-tract resonance near f_0. In light of a linear theory of oscillation, these results also suggest that an accurate tuning of the vocal-tract impedance at the playing frequency may allow oscillations to occur very close to a resonance frequency of the lip-valve system, hence emphasizing the motion of the lips.

This hypothesis was further investigated on different physical models of the lips through time-domain simulations. Linear variation of the phase difference between the upstream and downstream impedances was found to induce significant variations of playing frequency (including change of register), as well as changes in the acoustic energy produced. Despite the non-linearity induced by the downstream and upstream acoustic feedback, the linearisation of the flow equation around the quasi-static mouth pressure appears to successfully explain the variations of playing frequency observed. It further supports the hypothesis that an appropriate phase tuning of the vocal tract impedance at f_0 contributes to optimize the sound production process, especially by allowing lip oscillations to occur near the lip resonance. An optimal control may hence be achieved by maximizing the amplitudes of the lip mobility and downstream input impedance at the playing frequency. Applied to a two-dimensional lip model, similar displacements of the playing frequency are observed, also illustrating the ability of an upstream coupling to influence a transition from an inward to outward striking mechanism.

Finally, the regulation of respiratory pressures investigated in one trombone player highlights the sequential recruitment of abdominal and rib-cage muscles, as well as the optimization of the mechanical linkage between both compartments by the passive diaphragm. Some instances of diaphragmatic recruitment are however observed and may possibly correlate with variations in laryngeal configurations. Analogously, the recruitment of inspiratory non-diaphragmatic muscles as the instercostals and neck muscles (allowing the rib cage to be maintained at a relatively constant volume for a longer period of time during expiration) may have an effect on laryngeal configuration and consequently on the acoustic characteristics of the vocal tract.

Future Work

The *in-vitro* experimental approach presented in this thesis partly relies on the assumption of synchrony between the lip electrical impedance signal and opening area of the lips. The validity of this hypothesis needs to be further examined using synchronized high speed imaging of lip opening for example (Hézard, Fréour, Hélie, et al., 2013). Careful analysis of electrolabiograph (ELG) waveforms may also provide complementary information regarding lip vibration mechanisms (Hézard, Fréour, Caussé, Hélie, & Scavone, 2013).

In this thesis, $in-vitro$ and numerical simulation results suggest that variations of the playing frequency can be controlled by the acoustic interaction with the vocal tract only. These conclusions should be further investigated on other types of lip models (two-mass model) and by taking into account additional details (lip collision, dynamic geometry) in order to better approximate the behaviour of real lips. Although it is very difficult to isolate vocal-tract from embouchure influence on the playing frequency, these conclusions should be verified experimentally on real players and the contribution of the vocal tract quantified during tuning of high tones at which the magnitude of Z_d is relatively small.

Moreover, the assessment of the phase difference between the lip opening area and the acoustic pressure across the lips should be validated or fixed on the artificial player system. Although the choice was made to use Max/MSP for the control and acquisition of acoustic signals in Chapter 4 (for sampling frequency purposes), other environments may provide more robust platforms for the precise analysis of phase relationships between these acoustic signals. A precise estimation of the phase of the lip mobilities on the robot will enable to evaluate more precisely the relationship between lip opening area and acoustic flow at the lips. This will particularly enable the active control method to be applied to the identification of lip mechanical resonances during playing conditions.

Nevertheless, the active control setup developed shows a robust behaviour to both adjustments of the phase and amplitude of the upstream acoustic signal. This approach may therefore be useful to facilitate tone production in the high register, the control of which is often an issue on artificial player systems. Making such a system more robust and improving its playability may open up applications in terms of compositional work and on-stage performances that are always limited by the complexity of such a musical device.

The respiratory study presented in this thesis should provide the basis for further investigation on the respiratory control of sound production in brass instruments. Notably, more subjects should be considered to investigate the variety of possible strategies. Although our conclusions regarding a potential coupling between vocal-tract acoustics and respiratory control are relatively speculative, neck-muscle electromygraphic activities, as well as downstream and upstream acoustic pressure measurements could be added to the protocol to further investigate the correlations between vocal-tract acoustical tuning and the activity of respiratory muscles.

Finally, it would be of primary interest to adapt the method developed in this thesis to a music performance and training context. In particular, the development of a real-time feedback environment allowing some acoustical attributes of the vocal tract to be visualized can be of great

interest for musicians and pedagogues. A first prototype has been developed following this thesis work. This should be the object of a collaboration with musicians for the development of new tools for studio teaching and practice.

Appendix A

Respiratory Pressure-Volume and Time-Domain Curves During Musical Tasks

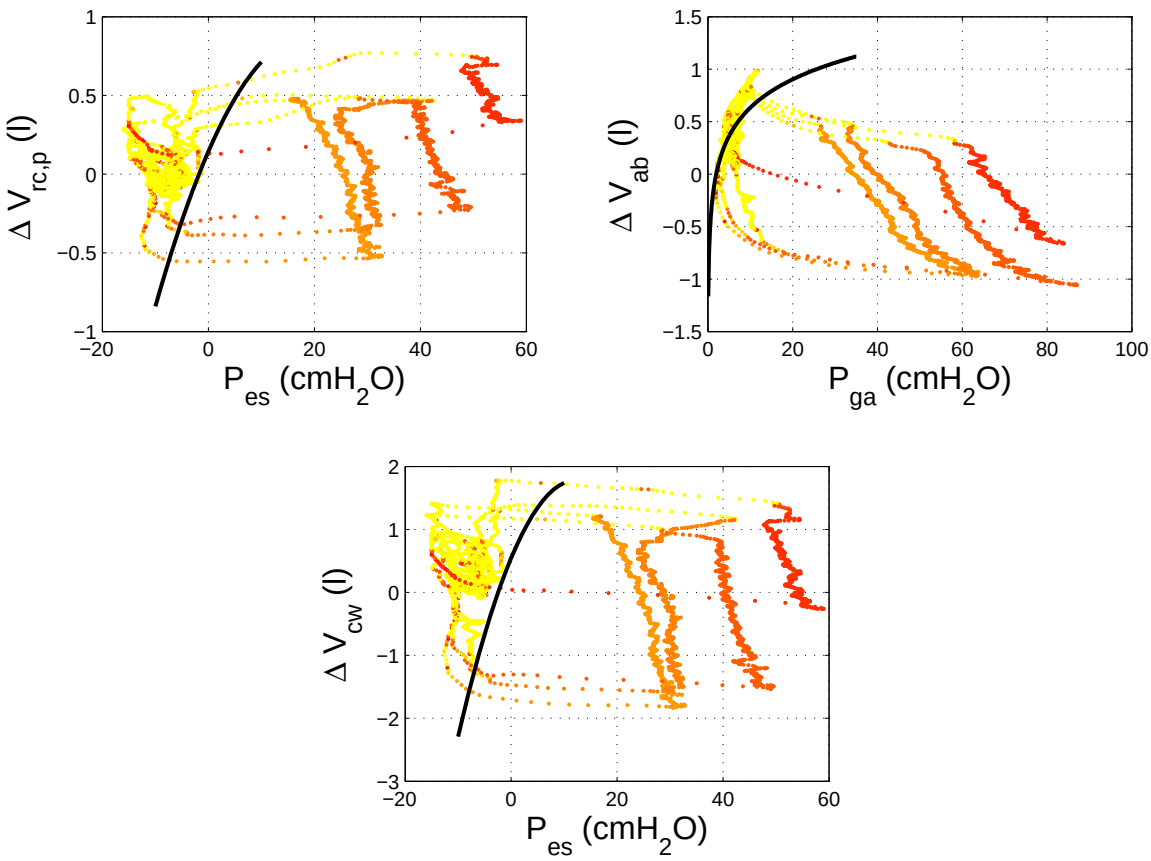

Figure A.1 Pressure-volume loops during sustained D4, F4, B♭4 and D5. Top left: relationship between esophageal pressure (P_{es}) as an index of pleural pressure (P_{pl}) and volume variations of the pulmonary rib cage ($\Delta V_{rc,p}$). Solid black line, relaxation curve of the pulmonary rib cage. Top right: relationship between gastric pressure (P_{ga}) as an index of abdominal pressure (P_{ab}) and volume variations of the abdomen (ΔV_{ab}). Solid black line, relaxation curve of the abdomen. Bottom, relationship between esophageal pressure (P_{es}) as an index of pleural pressure (P_{pl}) and volume variations of the chest wall (ΔV_{cw}). Solid black line, relaxation curve of the chest wall. The color scale indicates the playing frequency (light yellow refers to no sound).

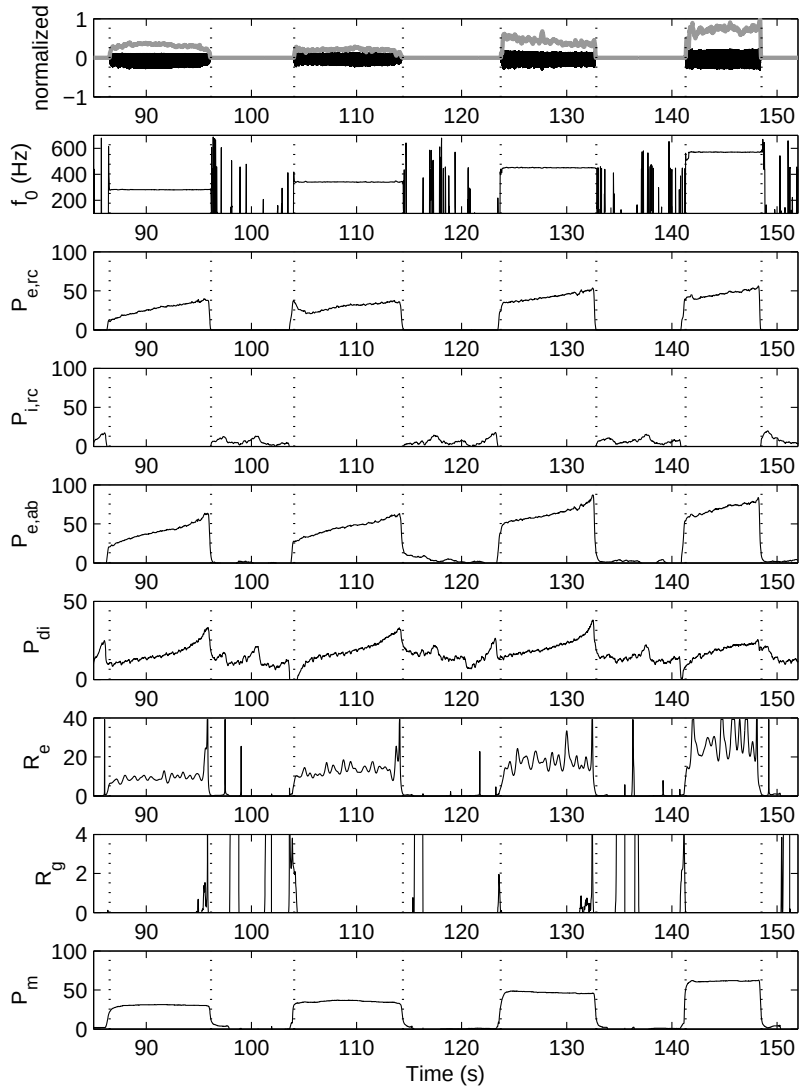

Figure A.2 Time-domain parameters during sustained D4, F4, B♭4 and D5. From top to bottom: waveform of the radiated sound pressure (black) and normalized acoustic sound power at the bell (gray), fundamental frequency of the sound (f_0) in Hz, expiratory pressure developed by rib-cage muscles ($P_{e,rc}$), inspiratory pressure developed by rib-cage muscles ($P_{i,rc}$), expiratory pressure developed by abdominal muscles ($P_{e,ab}$), transdiaphragmatic pressure (P_{di}), embouchure resistance (R_e) and glottal resistance (R_g) in MΩ, mouth pressure (P_m). Vertical dotted lines indicate tone onset and offset. Pressures are indicated in cmH_2O units.

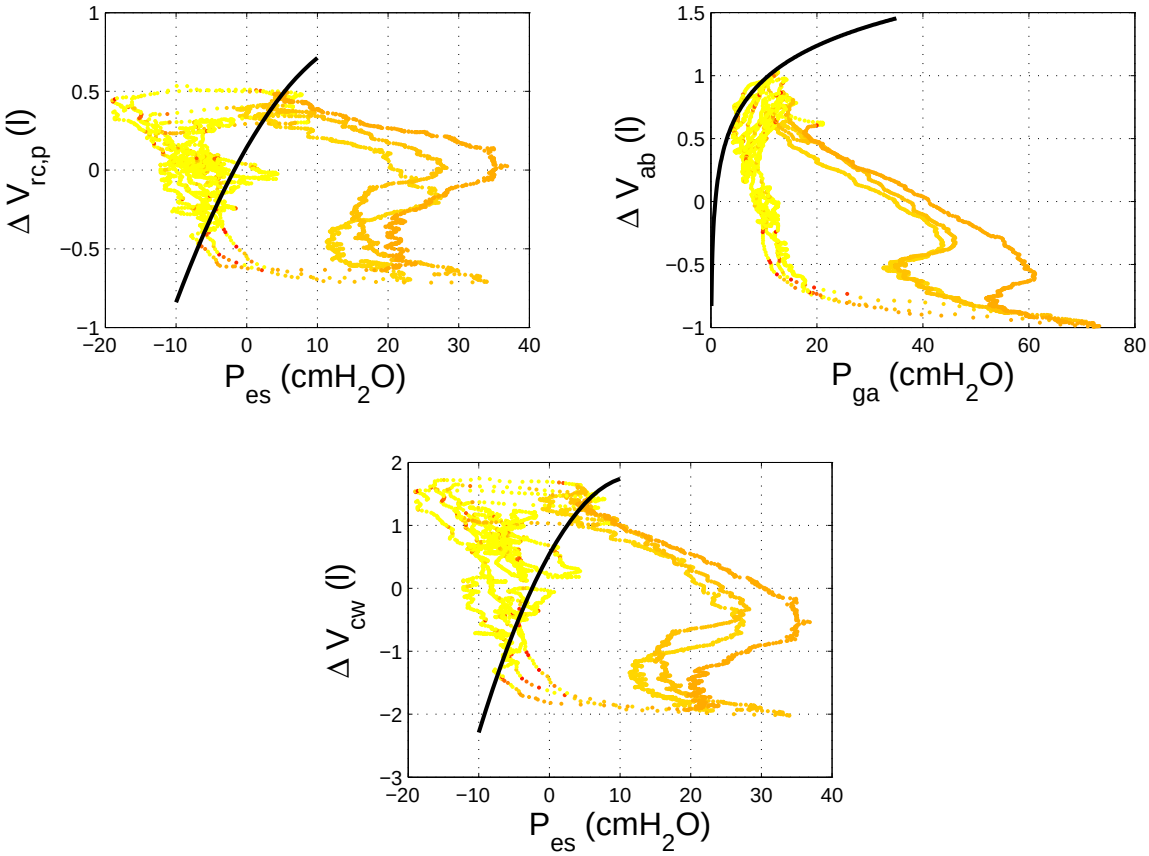

Figure A.3 Pressure-volume loops during sustained B♭2, F3 and B♭3 played with increasing and decreasing dynamic. Top left: relationship between esophageal pressure (P_{es}) as an index of pleural pressure (P_{pl}) and volume variations of the pulmonary rib cage ($\Delta V_{rc,p}$). Solid black line, relaxation curve of the pulmonary rib cage. Top right: relationship between gastric pressure (P_{ga}) as an index of abdominal pressure (P_{ab}) and volume variations of the abdomen (ΔV_{ab}). Solid black line, relaxation curve of the abdomen. Bottom, relationship between esophageal pressure (P_{es}) as an index of pleural pressure (P_{pl}) and volume variations of the chest wall (ΔV_{cw}). Solid black line, relaxation curve of the chest wall. The color scale indicates the playing frequency (light yellow refers to no sound).

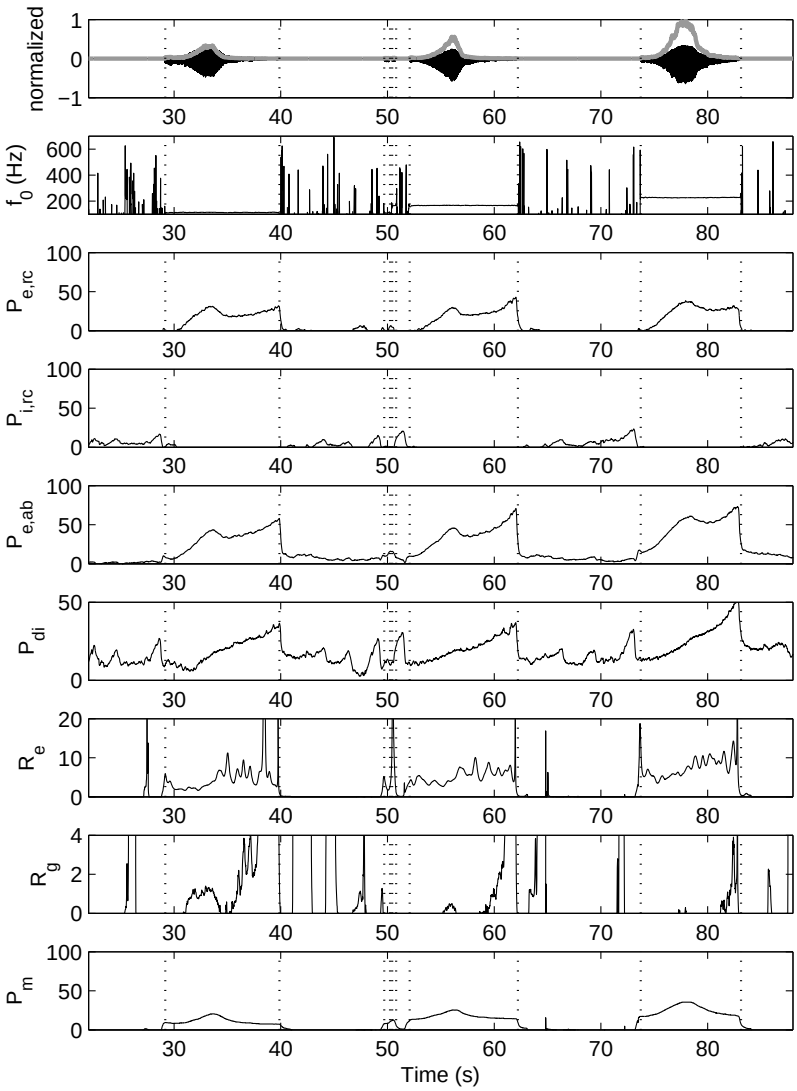

Figure A.4 Time-domain parameters during sustained B♭2, F3 and B♭3 played with increasing and decreasing dynamics. From top to bottom: waveform of the radiated sound pressure (black) and normalized acoustic sound power at the bell (gray), fundamental frequency of the sound (f_0) in Hz, expiratory pressure developed by rib-cage muscles ($P_{e,rc}$), inspiratory pressure developed by rib-cage muscles ($P_{i,rc}$), expiratory pressure developed by abdominal muscles ($P_{e,ab}$), transdiaphragmatic pressure (P_{di}), embouchure resistance (R_e) and glottal resistance (R_g) in MΩ, mouth pressure (P_m). Vertical dotted lines indicate tone onset and offset. Pressures are indicated in cmH_2O units.

Appendix B

Measurement of the Latency of the Electrolabiograph Signal Conditioner

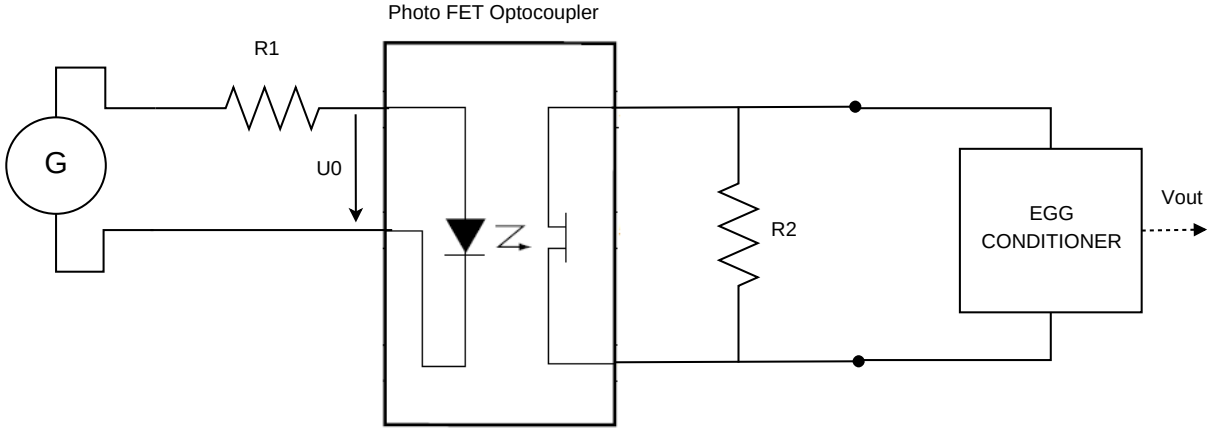

Figure B.1 Circuit diagram for the measurement of the latency of the VoceVista signal conditioner.

In order to evaluate the latency of the ELG signal conditioner (Voce Vista EGG conditioner), a circuit allowing the resistance at the electrodes to be varied is built. The diagram of this circuit is presented in Fig. B.1. It involves a photo FET optocoupler (used as a remote variable resistor) driven by an alternating square current whose frequency is varied between 50 and 1000 Hz. The

tension U_0 is proportional to the variations of resistance imposed at electrodes. U_0 and the output tension from the signal EGG signal conditioner V_{out} are measured using a National Instrument acquisition card (sampling rate: 51.2 kHz).

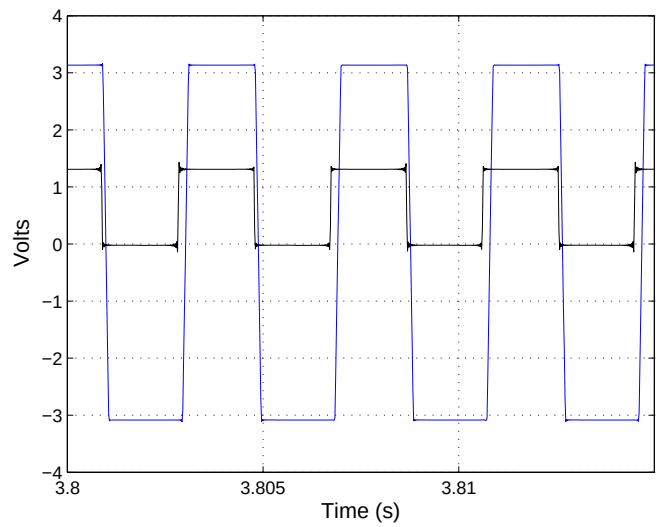

Figure B.2 Calibration measurements. Electrical tensions U_0 (black) and V_{out} (blue).

A group delay of 180 μs is observed between V_{out} and U_0. This delay is independent of the frequency, as shown by the linear phase shift induced between both signals as a function of the frequency of the driving tension U_0 (Fig. B.3).

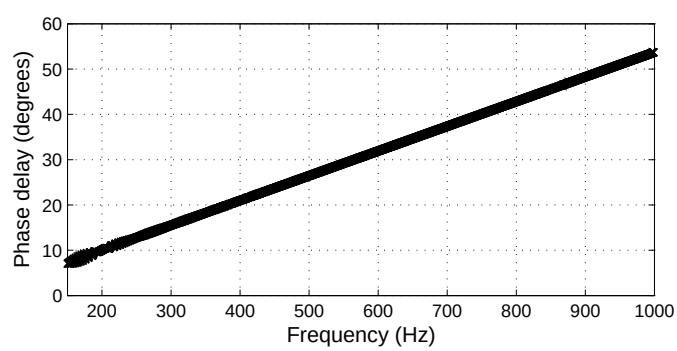

Figure B.3 Phase difference between V_{out} and U_0 as function of the frequency of the driving tension.

References

Adachi, S., & Sato, M. A. (1995). Time-domain simulation of sound production in the brass instrument. *Journal of the Acoustical Society of America*, *97*(6), 3850-3861.

Adachi, S., & Sato, M. A. (1996). Trumpet sound simulation using a two-dimensional lip vibration model. *Journal of the Acoustical Society of America*, *99*(2), 1200-1209.

Agostini, E., & Mead, J. (1964).

In W. O. Fenn & H. Rahn (Eds.), *Handbook of physiology, section 3: Respiration* (p. 387-409). Wahington, DC: American Physiological Society.

Aliverti, A. (1996). *Metodi e tecniche innovative per lo studio della meccanica respiratoria*. Unpublished doctoral dissertation, Politecnico di Milano, Milan, Italy.

Aliverti, A., Bovio, D., Fullin, I., Dellacà, R. L., Lo Mauro, A., Pedotti, A., & Macklem, P. T. (2009). The abdominal circulatory pump. *PLoS ONE*, *162*(5), e5550. doi:10.1371/journal.pone.0005550.

Aliverti, A., Cala, J., Duranti, R., Ferrigno, G., Kenyon, C. M., Pedotti, A., ... Yan, S. (1997). Human respiratory muscle actions and control during exercise. *Journal of Applied Physiology*, *83*, 1256-1269.

Aliverti, A., Iandelli, I., Duranti, R., Cala, J. S., Kayser, B., Kelly, S., ... Macklem, P. T. (2002). Respiratory muscle dynamics and control during exercise with externally imposed expiratory flow limitation. *Journal of Applied Physiology*, *92*, 1953-1963.

Auvray, R., Fabre, B., Lagée, P.-Y., Terrien, S., & Vergez, C. (2012). Influence of the fluctuations of the control pressure on the sound production in flute-like instruments. In *Proc. Acoustics 2012 Nantes Conference* (p. 1634-1638).

Backus, J. (1985). The effect of player's vocal tract on woodwind instrument tone. *Journal of the Acoustical Society of America*, *78*(1), 17-20.

Backus, J., & Hundley, T. C. (1971). Harmonic generation in the trumpet. *Journal of the Acoustical Society of America*, *49*, 509-519.

Barney, A., De Stefano, A., & Henrich, N. (2007). The effect of glottal opening on the acoustic response of the vocal tract. *Acta Acustica united with Acustica*, *93*, 1046-1056.

Baydur, A., Behrakis, P. K., Zin, W. A., & Milic-Emili, J. (1982). A simple method for assessing the validity of the esophageal balloon technique. *American Review of Respiratory Disease*, *126*, 788-791.

Benade, A. H. (1976). *Fundamental of musical acoustics*. Oxford University Press, New York.

Benade, A. H. (1985).

In I. R. Titze & R. C. Scherer (Eds.), *Vocal fold physiology, biomechanics, acoustics, and phonatory control* (p. 425-452). Denver Center for the Performing Arts, Denver, CO.

Benade, A. H., & Gans, D. J. (1968). Sound production in wind instruments. *Annals of the New York Academy of Sciences*, *155*, 247-263.

Benade, A. H., & Hoekje, P. (1982). Vocal tract effects in wind instrument regeneration. *Journal of the Acoustical Society of America*, *71*(S1), S91.

Berger, K. (1965). Respiratory and articulatory function in wind instrument performance. *Journal of Applied Physiology*, *20*(6), 1217-1221.

Berger, K. (1968). Electromyographic recording during wind instrument performance. *Annals of the New York Academy of Sciences*, *155*(1), 297-302.

Bouhuys, A. (1964). Lung volumes and breathing patterns in wind-instrument players. *Journal*

of Applied Physiology, *19*, 967-975.

Bouhuys, A. (1965). Sound-power production in wind instruments. *Journal of the Acoustical Society of America*, *37*(3), 453-456.

Bouhuys, A. (1968). Pressure-flow events during wind instrument playing. *Annals of the New York Academy of Sciences*, *155*(1), 264-273.

Bouhuys, A. (1969). Physiology and musical instruments. *Nature*, *221*, 1199-1204.

Bromage, S. (2007). *Visualisation of the lip motion of brass instrument players, and investigations of an artificial mouth as a tool for comparative studies of instruments*. Unpublished doctoral dissertation, University of Edinburgh, Edinburgh, United Kingdom.

Bromage, S., Campbell, M., & Gilbert, J. (2010). Open areas of vibrating lips in trombone playing. *Acta Acustica united with Acustica*, *96*, 603-613.

Cala, J., Kenyon, C. M., Ferrigno, G., Carnevali, P., Aliverti, A., Pedotti, A., . . . Rochester, D. F. (1996). Chest wall and lung volume estimation by optical reflectance motion analysis. *Journal of Applied Physiology*, *81*, 2680-2689.

Campbell, M. (2004). Brass instruments as we know them today. *Acta Acustica united with Acustica*, *90*, 600-610.

Chaigne, A., & Kergomard, J. (2008). *Acoustique des instruments de musique*. Belin, Paris.

Chen, F. C., & Weinreich, G. (1996). Nature of the lip reed. *Journal of the Acoustical Society of America*, *99*(2), 1227-1233.

Chen, J. M. (2009). *Vocal tract interactions in woodwind performance*. Unpublished doctoral dissertation, University of New South Wales, Sydney, Australia.

Chen, J. M., Smith, J., & Wolfe, J. (2009). Pitch bending and glissandi on the clarinet: Roles of the vocal tract and partial tone hole closure. *Journal of the Acoustical Society of America*, *126*(3), 1511-1520.

Chen, J. M., Smith, J., & Wolfe, J. (2011). Saxophonists tune vocal tract resonances in advanced

performance techniques. *Journal of the Acoustical Society of America*, *129*(1), 415-426.

Chen, J. M., Smith, J., & Wolfe, J. (2012). Do trumpet players tune resonances of the vocal tract? *Journal of the Acoustical Society of America*, *131*(1), 722-727.

Copley, D. C., & Strong, W. J. (1996). A stroboscopic study of lip vibrations in a trombone. *Journal of the Acoustical Society of America*, *99*(2), 1219-1226.

Cossette, I., Fabre, B., Fréour, V., Montgermont, N., & Monaco, P. (2010). From breath to sound: Linking respiratory mechanics to aeroacoustic sound production in flutes. *Acta Acustica united with Acustica*, *96*, 654-667.

Cossette, I., Monaco, P., Aliverti, A., & Macklem, P. T. (2008). Chest wall dynamics and muscle recruitment during professional flute playing. *Respiratory Physiology and Neurobiology*, *160*(2), 187-195.

Cossette, I., Sliwinski, P., & Macklem, P. T. (2000). Respiratory parameters during professional flute playing. *Respiration Physiology*, *121*(1), 33-44.

Cullen, J. S. (2000). *A study of brass instrument acoustics using an artificial reed mechanism, laser doppler anemometry and other techniques*. Unpublished doctoral dissertation, University of Edinburgh, Edinburgh, United Kingdom.

Cullen, J. S., Gilbert, J., & Campbell, D. M. (2000). Brass instruments: Linear stability analysis and experiments with an artificial mouth. *Acta Acustica*, *86*, 704-724.

de Cheveigné, A., & Kawahara, H. (2002). Yin, a fundamental frequency estimator for speech and music. *Journal of the Acoustical Society of America*, *111*(4), 1917-1930.

Dejonckere, P. H., Orval, F., Miller, R., & Sneppe, R. (1983). Mécanisme oscillatoire de la glotte dans le jeux de cor. *Brass Bulletin*, *41*, 28-35.

De Troyer, A. (1991).

In R. Crystal, J. West, B. P.J., N. Cherniack, & E. Weibel (Eds.), *The lung: Scientific foundations* (p. 869-882). New York: Reaven Press.

Elliot, S. J., & Bowsher, J. M. (1982). Regeneration in brass instruments. *Journal of Sound and Vibration*, *83*(2), 181-217.

Fabre, P. (1957). Un procédé électrique percutané d'inscription de l'accolement glottique au cours de la phonation: Glottographie de haute fréquence. *Bulletin de l'Académie Nationale de Médecine*, 66-69.

Ferrand, D., Hélie, T., Vergez, C., Véricel, B., & Caussé, R. (2010). Bouche artificielles asservies: étude de nouveaux outils pour l'analyse du fonctionnement des instruments á vent. In *Proc. 10ème Congrès Français d'Acoustique.* Lyon, France.

Ferrigno, G., Carnevalli, P., Aliverti, A., Molteni, F., Beulcke, G., & Pedotti, A. (1994). Three-dimensional optical analysis of chest wall motion. *Journal of Applied Physiology*, *77*, 1224-1231.

Fletcher, N. H. (1993). Autonomous vibration of simple pressure-controlled valve in gas flows. *Journal of the Acoustical Society of America*, *93*(4), 2172-2180.

Fletcher, N. H., & Tarnopolsky, A. (1999). Blowing pressure, power and spectrum in trumpet playing. *Journal of the Acoustical Society of America*, *105*(2), 874-881.

Fordhman, J. (2005). Albert mangelsdorff, german jazz trombonist noted for stunning solo improvisations. *The Guardian*. Retrieved from http://www.theguardian.com/news/2005/jul/28/guardianobituaries.arts

Fritz, C. (2004). *La clarinette et le clarinettiste : influence du conduit vocal sur la production du son*. Unpublished doctoral dissertation, Université Paris 6, Paris, France.

Fritz, C., Caussé, R., Kergomard, J., & Wolfe, J. (2005). Experimental study of the influence of the clarinettist's vocal tract. In *Proc. Forum Acusticum 2005.* Budapest, Hungary.

Fritz, C., & Wolfe, J. (2005). How do clarinet players adjust the resonances of their vocal tracts for different playing effects? *Journal of the Acoustical Society of America*, *118*(5), 3306-3315.

Fritz, C., Wolfe, J., Kergomard, J., & Caussé, R. (2003). Playing frequency shift due to the interaction between the vocal tract of the musician and the clarinet. In *Proc. Stockholm Music Acoustics Conference 2003* (p. 263-266).

Garnier, M., Henrich, N., Smith, J., & Wolfe, J. (2010). Vocal tract adjustments in the high soprano range. *Journal of the Acoustical Society of America*, *127*(6), 3771-3780.

Gazengel, J., Gilbert, N., & Amir, N. (1995). From the measured input impedance to the synthesis signal: where are the traps? *Acta Acustica*, *3*, 445-472.

Gilbert, J., Kergomard, J., & Ngoya, E. (1989). Calculation of the steady-state oscillations of a clarinet using the harmonic balance technique. *Journal of the Acoustical Society of America*, *86*(1), 39-41.

Gilbert, J., Ponthus, S., & Petiot, J. F. (1998). Artificial buzzing lips and brass instruments: Experimental results. *Journal of the Acoustical Society of America*, *104*(3), 1627-1632.

Griffin, B., Woo, P., Colton, R., Casper, J., & Brewer, D. (1995). Physiological characteristics of the supported singing voice. a preliminary study. *Journal of Voice*, *9*, 45-56.

Grimby, G., Bunn, J., & Mead, J. (1968). Relative contribution of rib cage and abdomen to ventilation during exercise. *Journal of Applied Physiology*, *24*, 159-166.

Guillemain, P. (2007). Some roles of the vocal tract in clarinet breath attacks: Natural sounds analysis and model-based synthesis. *Journal of the Acoustical Society of America*, *121*(4), 2396-2406.

Guillemain, P., Vergez, C., Ferrand, D., & Farcy, A. (2010). An instrumented saxophone mouthpiece and its use to understand how an experienced musician plays. *Acta Acustica united with Acustica*, *96*, 622-634.

Hélie, T., Lopes, N., & Caussé, R. (2012). Open-loop control of a robotized artificial mouth for brass instruments. *Journal of the Acoustical Society of America*, *131*(4), 3470.

Helmholtz, H. L. F. (1954). *On the sensations of tone*. New York: Dover Publications, Inc.

Henrich, N., Smith, J., & Wolfe, J. (2011). Vocal tract resonances in singing: Strategies used by sopranos, altos, tenors, and baritones. *Journal of the Acoustical Society of America*, *129*(2), 1024-1035.

Hézard, T., Fréour, V., Caussé, R., Hélie, T., & Scavone, G. P. (2013). Synchronous multimodal measurements on lips and glottis: comparison between two human-valve oscillating systems. *Acta Acustica united with Acustica*. (Manuscript under revision)

Hézard, T., Fréour, V., Hélie, T., Caussé, R., & Scavone, G. P. (2013). Synchronous visualization of multimodal measurements on lips and glottis: Comparison between brass instruments and the human voice production system. *Journal of the Acoustical Society of America*, *133*(5), 3417.

Hirschberg, A. (1995).

In *Mechanics of musical instruments* (chap. 7). Springer Verlag.

Hoekje, P. (1986). *Intercomponent energy exchange and upstream/downstream symmetry in nonlinear self sustained oscillations of reed instruments*. Unpublished doctoral dissertation, Case Western Reserve University, Cleveland, Ohio, USA.

Idogawa, T., Kobata, T., Komuro, K., & Iwaki, M. (1993). Nonlinear vibrations in the air column of a clarinet artificially blown. *Journal of the Acoustical Society of America*, *93*(1), 540-551.

Iwarsson, J., & Sundberg, J. (1998). Effects of lung volume on vertical larynx position during phonation. *Journal of Voice*, *12*(2), 159-165.

Joliveau, E., Smith, J., & Wolfe, J. (2004). Vocal tract resonances in singing: The soprano voice. *Journal of the Acoustical Society of America*, *116*(4), 2434-2439.

Kaburagi, T., Yamada, N., Fukui, T., & Minamiya, E. (2011). A methodological and preliminary study on the acoustic effect of a trumpet player's vocal tract. *Journal of the Acoustical Society of America*, *130*(1), 536-545.

Kenyon, C. M., Cala, S. J., Yan, S., Aliverti, A., Scano, G., Duranti, R., ... Macklem, P. T. (1997). Rib cage mechanics during quiet breathing and exercise in humans. *Journal of Applied Physiology*, *83*, 1242-1255.

King, A. I., Ashby, J., & Nelson, C. (1989). Laryngeal function in wind instruments: The brass. *Journal of Voice*, *3*(1), 65-67.

Konno, K., & Mead, J. (1967). Measurement of the separate volume changes of rib cage and abdomen during breathing. *Journal of Applied Physiology*, *22*, 407-422.

Konno, K., & Mead, J. (1968). Static volume-pressure characteristics of the rib cage and the abdomen. *Journal of Applied Physiology*, *24*, 407-422.

Krakow, R. A. (1994). *Nonsegmental influences on velum movement patterns: Syllables, sentences, stress, and speaking rate* (Tech. Rep. No. SR-117/118). Haskins Laboratories Status Report on Speech Research.

Lefebvre, A., & Scavone, G. P. (2011). A comparison of saxophone impedances and their playing behaviour. In *Proc. Forum Acusticum 2011* (p. 539-544). Aalborg, Denmark.

Lewis, L. (2010). *About us.* Retrieved from http://www.embouchures.com/About.htm

Lieberman, P. (1968). Direct comparison of subglottal and esophageal pressure during speech. *Journal of the Acoustical Society of America*, *43*(5), 1157-1164.

Lopes, N., Hélie, T., & Caussé, R. (2003). Control of an artificial mouth playing a trombone and analysis of sound descriptors of experimental data. In *Proc. Stockholm Music Acoustics Conference 2013* (p. 521-528).

Macaluso, C. A., & Dalmont, J. P. (2011). Trumpet with near-perfect harmonicity: Design and acoustic results. *Journal of the Acoustical Society of America*, *129*(1), 404-414.

Mayer, A. (2003). Riam (reed instrument artificial mouth) a computer controlled excitation device for reed instruments. In *Proc. Stockholm Music Acoustics Conference 2003.*

McCool, F. D. (1995).

In C. Roussos (Ed.), *Thorax* (p. 1049-1067). New York: Marcel Dekker, Inc.

McCool, F. D., Kelly, K. B., Loring, S. H., Greaves, I. A., & Mead, J. (1986). Estimates of ventilation from body surface measurements in unrestrained subjects. *Journal of Applied Physiology*, *61*, 1114-1119.

Milic-Emili, J., Mead, J., Turner, J. M., & Glauser, E. M. (1964). Improved technique for estimating pleural pressure from esophageal balloons. *Journal of Applied Physiology*, *19*, 207-211.

Mongeau, L., Franchek, N., Coker, C., & Kubli, R. A. (1997). Characteristics of a pulsating jet through a small modulated orifice, with application to voice production. *Journal of the Acoustical Society of America*, *102*(2), 1121-1133.

Mukai, M. S. (1992). Laryngeal movements while playing wind instruments. In *Proc. International Symposium on Musical Acoustics* (p. 239-242). Tokyo, Japan.

Newton, M. J., Campbell, M., & Gilbert, J. (2008). Mechanical response measurements of real and artificial brass player lips. *Journal of the Acoustical Society of America*, *123*(1), EL 14-EL20.

Peak, D., Kelly, K. B., & McCool, F. D. (1990). Postural effects on measurements of tidal volume from body surface displacements. *Journal of Applied Physiology*, *68*, 2482-2487.

Pettersen, V., & Westgaard, R. H. (2004). Muscle activity in professional classical singing: A study on muscles in the shoulder, neck and trunk. *Logopedics Phoniatrics Vocology*, *29*, 56-65.

Pettersen, V., & Westgaard, R. H. (2005). The activity patterns of neck muscles in professional classical singing. *Journal of Voice*, *19*(2), 238-251.

Puckette, M. (2012). *fiddle~ max/msp external.* Retrieved from http://crca.ucsd.edu/~tapel/software.html

Richards, O. (2003). *Investigation of the lip reed using computational modelling and experi-*

mental studies with an artificial mouth. Unpublished doctoral dissertation, University of Edinburgh, Edinburgh, United Kingdom.

Roos, J. (1936). The physiology of playing the flute. *Archives néerandaises en phonétique expérimentale*, *12*, 1-26.

Rydell, R., Karloson, M., Milesson, A., & Schalén, L. (1996). Laryngeal activity during wind instrument playing: Video endoscopic documentation. *Logopedics Phoniatrics Vocology*, *21*, 43-48.

Scavone, G. P. (2003). Modeling vocal-tract influence in reed wind instruments. In *Proc. Stockholm Music Acoustics Conference 2003* (p. 291-294).

Scavone, G. P., Lefebvre, A., & da Silva, A. R. (2008). Measurement of vocal-tract influence during saxophone performance. *Journal of the Acoustical Society of America*, *123*(4), 2391-2400.

Schumacher, R. T. (1978). Self sustained oscillations of the clarinet: An integral equation approach. *Acustica*, *40*, 298-309.

Schumacher, R. T. (1981). Ab initio calculations of the oscillation of a clarinet. *Acustica*, *48*, 71-85.

Schutte, H. K. (1992). Integrated aerodynamic measurements. *Journal of Voice*, *6*, 127-134.

Sidlof, P. (2007). *Fluid-structure interaction in human vocal folds*. Unpublished doctoral dissertation, Charles University in Prague, Prague, Czech Republic.

Smith, J. C., & Mead, J. (1986). Three degree of freedom description of movement of the human chest wall. *Journal of Applied Physiology*, *60*, 938-934.

Sommerfeldt, S. D., & Strong, W. J. (1988). Simulation of a player-clarinet system. *Journal of the Acoustical Society of America*, *83*(5), 1908-1918.

Sundberg, J. (1974). Articulatory interpretation of the “singing formant”. *Journal of the Acoustical Society of America*, *55*(4), 838-844.

Sundberg, J. (1975). Formant technique in a professional female singer. *Acustica*, *32*, 89-96.

Sundberg, J., Leanderson, R., & von Euler, C. (1989). Activity relationship between diaphragm and cricothyroid muscles. *Journal of Voice*, *3*(3), 225-232.

Tarnopolsky, A. Z., Fletcher, N. H., Hollenberg, L., Lange, L., Smith, J., & Wolfe, J. (2006). Vocal tract resonances and the sound of the australian didjeridu (yidaki) i. experiment. *Journal of the Acoustical Society of America*, *119*(2), 1194-1204.

Vergez, C. (2000). *Trompette et trompettiste : un systeme dynamique non lineaire a analyser, modeliser et simuler dans un contexte musical*. Unpublished doctoral dissertation, Université Paris 6, Paris, France.

Vergez, C., & Rodet, X. (1997). Comparison of real trumpet playing, latex model of lips and computer model. In *Proc. International Computer Music Conference 1997.*

Vergez, C., & Rodet, X. (2001). Trumpet and trumpet player: Model and simulation in a musical context. In *Proc. International Computer Music Conference 2001.*

Wade, O. L. (1954). Movements of the thoracic cage and diaphragm in respiration. *Journal of Physiology*, *124*, 193-212.

Ward, M., Ward, J., & Macklem, P. T. (1992). Analysis of human chest wall motion using a two-compartment rib cage model. *Journal of Applied Physiology*, *72*, 1338-1347.

Widholm, G., Pichler, H., & Ossmann, T. (1989). Bias, a computer-aided test system for brass wind instruments. In *Proc. 87th AES Convention.*

Wolfe, J., & Smith, J. (2008). Acoustical coupling between lip valves and vocal folds. *Acoustics Australia*, *36*(1), 23-27.

Wolfe, J., Tarnopolsky, A. Z., Fletcher, N. H., Hollenberg, L. C. L., & Smith, J. (2003). Some effects of the player's vocal tract and tongue on wind instrument sound. In *Proc. Stockholm Music Acoustics Conference 2003* (p. 307-310).

Yoshikawa, S. (1995). Acoustical behavior of brass player's lips. *Journal of the Acoustical*

Society of America, *97*(3), 1929-1939.

Yoshikawa, S., & Muto, Y. (2003). Lip-wave generation in horn players and the estimation of lip-tissue elasticity. *Acta Acustica united with Acustica*, *89*, 145-162.

Zimmerman, P. V., Connellan, S. J., Middleton, H. C., Tabona, M. V., Goldman, M. D., & Pride, N. (1983). Postural changes in rib cage and abdominal volume-motion coefficients and their effect on the calibration of a respiratory inductance plethysmograph. *The American Review of Respiratory Disease*, *127*, 209-214.